# RITTER ENABLED CATALYTIC ASYMMETRIC HALOAMIDATION AND MECHANISTIC STUDIES FOR INTERMOLECULAR HALOFUNCTIONALIZATION

By

Daniel C. Steigerwald

A DISSERTATION

Submitted to
Michigan State University
in partial fulfillment of the requirements
for the degree of

Chemistry—Doctor of Philosophy

2021

**ABSTRACT**

RITTER ENABLED CATALYTIC ASYMMETRIC HALOAMIDATION AND
MECHANISTIC STUDIES FOR INTERMOLECULAR HALOFUNCTIONALIZATION

By

Daniel C. Steigerwald

This thesis presents the development of an efficient catalytic asymmetric olefin haloamidation method and mechanistic investigations of intermolecular halofunctionalization reactions. It guides the reader through the challenges of catalytic asymmetric olefin halofunctionalization and presents how our group has used a mechanistically conscious approach to solve these problems to achieve high enantiocontrol over a stereodefined carbon-halogen bond.

Chapter 1 focuses on the development of a catalytic asymmetric Ritter-type haloamidation of olefins. The stereodefined vicinal haloamine moiety is highly valuable; however, catalytic asymmetric variations have not realized the same success as analogous haloetherification and dihalogenation reactions. We utilize *Halenium Affinity* to examine the core difficulties of haloaminations and design a competent nucleophile for this transformation. Chapter 2 gives the reader a more accurate mechanistic understanding of intermolecular olefin halofunctionalizations. This reaction is often depicted as a stepwise mechanism with the formation of a haliranium ion that is then intercepted by a nucleophile to provide the difunctionalized product. Preliminary mechanistic evidence suggests a spectrum of concerted vs. stepwise mechanisms dependent on the alkene, halenium ion, halenium donor, and nucleophile.

## ACKNOWLEDGMENTS

# TABLE OF CONTENTS

# LIST OF TABLES

# LIST OF FIGURES

# KEY TO SYMBOLS AND ABBREVIATIONS

‡        Transition State

[α]       Specific Rotation

°C       Degree Celsius

Δ        Change

1°        Primary

Å        Angstrom

Ar       Aryl

BINOL    1,1′-Bi-2-naphthol

cal       Calorie

$CDCl_3$    Deuterated Chloroform

$CHCl_3$    Chloroform

$Cs_2CO_3$   Cesium Carbonate

d        Days

DBDMH   1,3-Dibromo-5,5-Dimethylhydantoin

DCDMH   1,3-Dichloro-5,5-Dimethylhydantoin

DCM      Dichloromethane

DHQ      Dihydroquinine

DHQD    Dihydroquinidine

DMAP    4-Dimethylaminopyridine

DMC      Dimethylcyanamide

| | |
|---|---|
| DMSO | Dimethylsulfoxide |
| *dr* | Diastereomeric Ratio |
| *ee* | Enantiomeric Excess |
| *ent* | Enantiomer |
| *es* | Enantiospecificity |
| ESI | Electrospray Ionization |
| Et | Ethyl |
| EtOAc | Ethyl Acetate |
| EtOH | Ethanol |
| g | Gram |
| H | Enthalpy |
| h | Hour |
| *HalA* | Halenium Affinity |
| HCl | Hydrochloric Acid |
| HFIP | 1,1,1,3,3,3-Hexafluoro-propan-2-ol |
| HOMO | Highest Occupied Molecular Orbital |
| HRMS | High Resolution Mass Spectrometry |
| Hz | Hertz |
| *i*-Pr | Isopropyl |
| *J* | Coupling Constant |
| K | Kelvin |
| kcal | Kilocalorie |

| | |
|---|---|
| KIE | Kinetic Isotope Effect |
| LiCl | Lithium Chloride |
| ln | Natural Logarithm |
| LUMO | Lowest Unoccupied Molecular Orbital |
| M | Molar |
| Me | Methyl |
| MeCN | Acetonitrile |
| MeOH | Methanol |
| mg | Milligram |
| MHz | Megahertz |
| min | Minutes |
| mL | Milliliter |
| mmol | Millimole |
| MS | Molecular Sieves |
| $Na_2S_2O_3$ | Sodium Thiosulfate |
| $Na_2SO_4$ | Sodium Sulfate |
| *NAAA* | Nucleophile Assisted Alkene Activation |
| NAPH | Naphthalene |
| NBA | N-bromoacetamide |
| NBP | N-bromophthalimide |
| NBS | N-bromosuccinimide |
| NBSac | N-bromosaccharin |

| | |
|---|---|
| NCP | N-chlorophthalimide |
| NCS | N-chlorosuccinimide |
| NCSac | N-chlorosaccharin |
| $NEt_3$ | Triethylamine |
| NIS | N-iodosuccinimide |
| $NK_1$ | Neurokinin 1 |
| $NO_2$ | Nitro |
| Ns | Nosyl |
| PHAL | phthalazinediyl |
| q | quartet |
| $R_f$ | Retention Factor |
| *rr* | Regioisomeric Ratio |
| RT | Retention Time |
| rt | Room Temperature |
| S | Entropy |
| $SiO_2$ | Silicon Dioxide |
| t | Time |
| TBSCl | Tert-Butyldimethylsilyl Chloride |
| tBu | Tert-Butyl |
| TCCA | Trichloroisocyanuric Acid |
| TFE | 2,2,2-Trifluoroethan-1-ol |
| THF | Tetrahydrofuran |

| | |
|---|---|
| TLC | Thin Layer Chromatography |
| δ | Chemical Shift |
| $\mu$L | Microliter |

# Chapter I  Ritter Enabled Catalytic Asymmetric Chloroamidation of Olefins

## I-1  Introduction
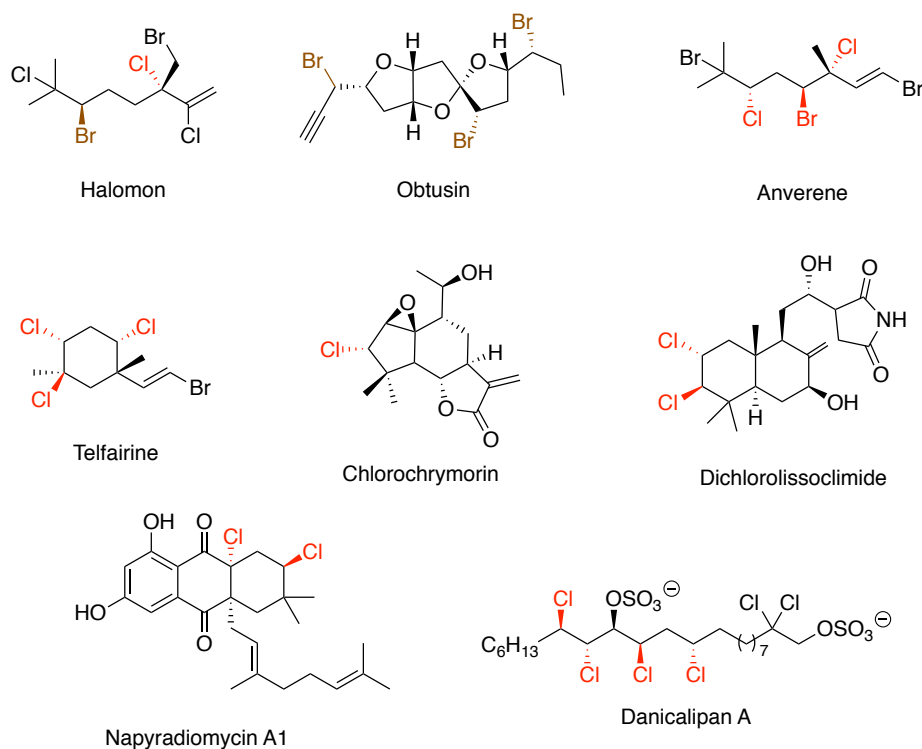


**Figure I-1:** Natural products containing stereodefined carbon halogen bonds

The carbon carbon double bond is one of the most important motifs in organic chemistry. The olefin's importance stems from its versatility; the olefin is a slate for key reactions, such as epoxidation,[1-4] aziridination,[4-5] dihydroxylation,[6] aminohydroxylation,[7-9] hydrogenation,[10-11] and more. It is important to note that within these difunctionalization reactions, there is the potential for the generation of two new stereocenters and that asymmetric methodology has been developed for the aforementioned reactions. The asymmetric variations of such reactions have been a useful starting point to install chirality

for asymmetric total syntheses.[12] Interestingly, halofunctionalizations, which are among the first reactions introduced in sophomore organic chemistry, had not succumbed to catalytic asymmetric variations until the last decade. The realization of asymmetric halofunctionalization can establish a starting point in the synthesis of complex molecules as the stereodefined carbon halogen bond is prevalent in valuable natural products (Figure I-1)[13-16] and can serve as a lynchpin for downstream functionalizations.[17] The incorporation of a stereodefined heteroatom vicinal to the halogen provides an additional layer of versatility with the potential to incorporate oxygen, halogen, nitrogen, and carbon nucleophiles.

## I-2   Racemization Processes of Halonium Ions

The mechanistic comprehension of halofunctionalization mechanisms is critical to the design of novel halofunctionalization reactions, especially intermolecular enantioselective halofunctionalizations. The traditional stepwise mechanistic hypothesis for halofunctionalizations suggests reactions proceed through a haliranium ion such as **I-1** which incites racemization processes such as olefin to olefin halenium transfer (Figure I-2a) and the opening to the beta-halocarbenium ion **I-4** (Figure I-2b). Thus, the face selectivity for the initial halenium transfer to the alkene is not necessarily the face selectivity observed in the difunctionalized product. The configurational and chemical stability of these intermediates is even more problematic with intermolecular

halofunctionalizations, which do not benefit from proximity-driven rate enhancement which may result in longer lived haliranium ions (Figure I-2c).
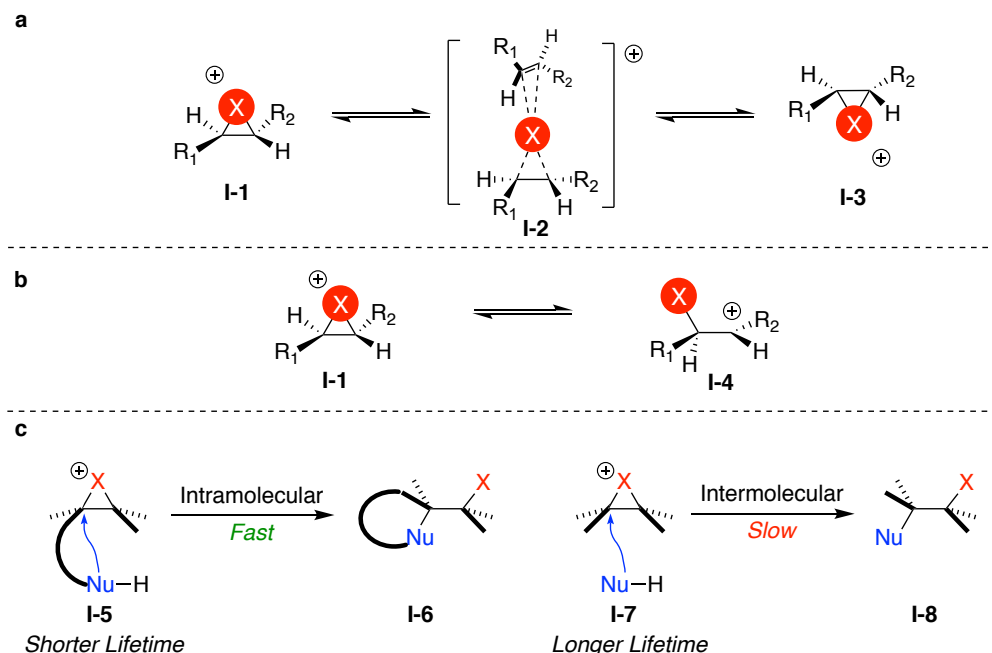


**Figure I-2:** Racemization processes for haliranium ions (a) Olefin to olefin halenium transfer (b) Opening of the haliranium in to the β-halocarbenium ion (c) Enhanced problematic nature of haliranium ions in asymmetric intermolecular functionalizations

## I-2-1   Racemization via Olefin to Olefin Halenium Transfer

Early studies by Brown[18] demonstrated the existence of olefin-to-olefin halonium ion transfer and, in 2010, Denmark[19] investigated olefin to olefin bromenium transfer as a potential racemization process (Figure I-3). This study hinged on the formation of enantioenriched bromiranium ions and the products' stereospecificity when trapped by a nucleophilic partner. They were able to generate the $C_2$ symmetric bromiranium ion **I-10** in-situ via the anchimerically assisted ionization of **I-9**. With no excess olefin in solution (Figure I-3b), the bromiranium ion is trapped by the acetate ion to provide **I-11** with full

enantiospecificity. This indicates stereospecific formation of the bromonium ion and with no racemization events occurring without additional olefin. However, under the same reaction conditions but with one equivalent of **I-12**, **I-11** is formed with a significant loss of enantiospecificity (30% *es*) (Figure I-3b). This experiment displays the intrinsic difficulties involved with enantioselective bromofunctionalizations. The analogous experiments with chloronium ions were also performed and yielded orthogonal results to the bromonium experiments (Figure I-3c). The process of ionization to form the chloronium ion as well as the trapping with acetate proceeded with full enantiospecificity, indicating that olefin to olefin racemization is not present in this system. Though proceeding through a chloronium ion intermediate may appear to be an appealing process to obviate racemization, the authors did note that the chloroacetate products were produced in reduced yields. The authors attribute this inverse relationship between chemical and stereochemical stability via bromine and chlorine's relative electronegativities. The greater electronegativity of chlorine leads to more positive charge on the carbon, leaving it more susceptible to nucleophilic attack as well as elimination reactions. Conversely, bromine's greater positive charge facilitates the π-complex required for olefin-to-olefin transfer. This data serves as an example that enantioselective halofunctionalizations initiated by different halenium ions will provide unique challenges.
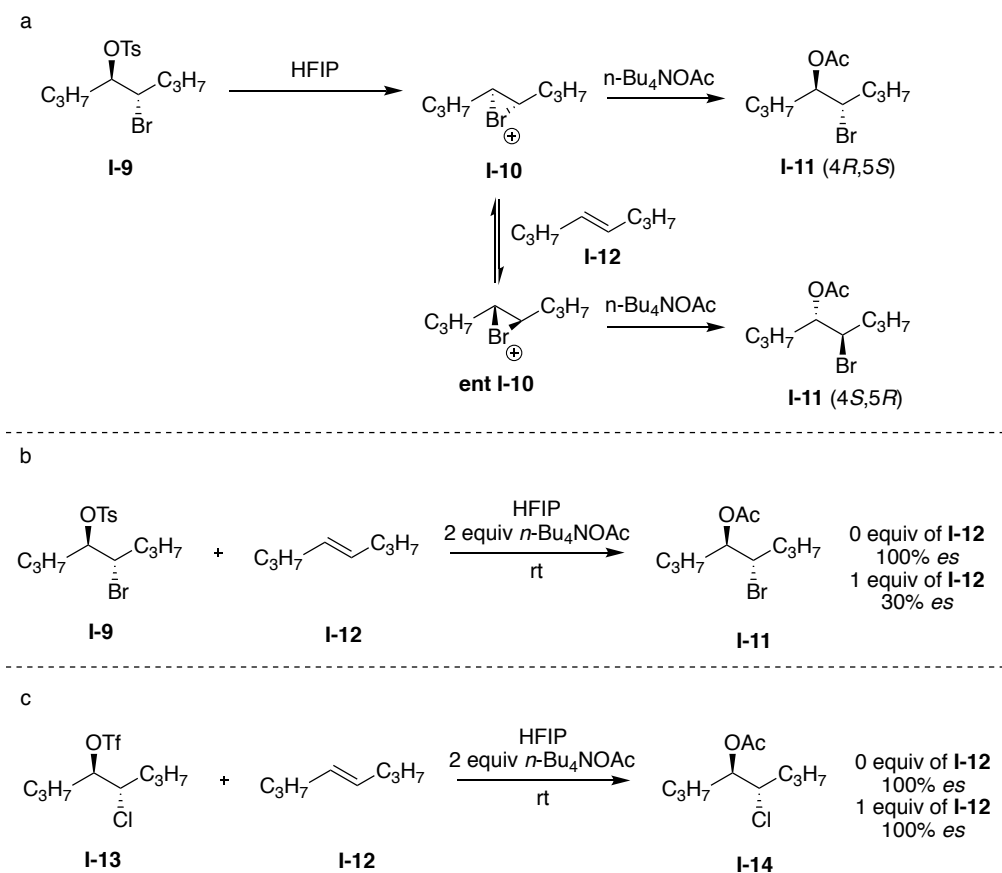
**Figure I-3:** a) Mechanistic overview of olefin-to-olefin transfer as a racemization process (b) Propensity of bromonium ions to racemize in the presence of excess olefin (c) Stereochemical stability of chloronium in the presence of excess olefin
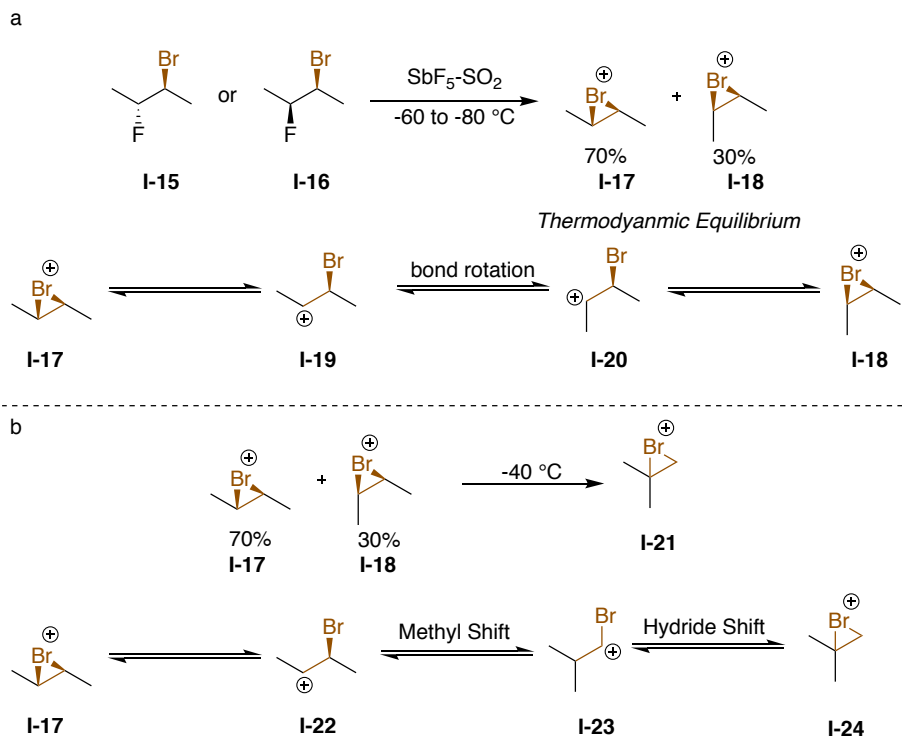
**Figure I-4:** (a) The propensity of long lived haliranium ions to open to the β-halocarbenium ion with diastereomeric consequences (b) Potential rearrangements associated with haliranium ions

## I-2-2 Isomerization to the β-Halocarbenium Ion

Olah's use of super acids[20] to generate various halonium ions shed light on other potential issues involved with haliranium ion pathways. Upon exposure of either bromofluoride diastereomer **I-15** or **I-16** with $SbF_5$-$SO_2$ they obtained the same 70%-30% ratio of **I-17** : **I:18** (Figure I-4a). While the authors explicitly stated that the non-stereospecific solvolysis might generate the haliranium ion, they also suggested that this might result from the opening to the β-halocarbenium ion **I-19** with ensuing bond rotation and closure to form haliranium ion **I-18**, the diastereomer of **I-17**. Further displaying the instability of bromiranium ions, upon warming to -40 °C, both **I-17** and **I-18** underwent hydride and methyl sifts to yield **I-24** (Figure I-4b). Ohta and co-workers[21] observed similar β-

halocarbenium ions and alkyl shifts in their NMR studies of deuterated halogenated substrates. Not only will β-halocarbenium ions lead to deteriorated yields and diastereoselectivity due to rearrangement, but they may also lead to a lowered enantioselectivity due to two successive openings with bond rotations (Figure I-5).
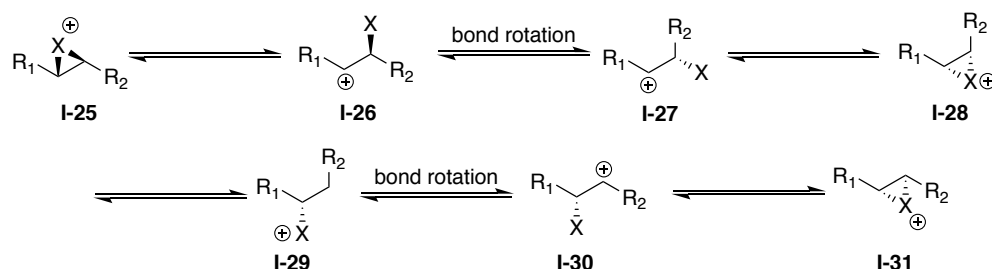


**Figure I-5:** Racemization via β-Halocarbenium Ion

## I-3   Mechanistic Comprehension of Halofunctionalizations

### I-3-1   Halenium Affinity

The synthetic utility and ubiquitous nature of carbon halogen bonds makes electrophilic halofunctionalization a key tool in organic synthesis. While this chemistry is widely employed, much of the progress relies on trial and error. In the context of the synthesis of more complex molecules, there are often multiple potential halenium acceptors. This translates into difficulties in predicting chemoselectivity, which can complicate synthetic strategies. In order to address this limitation, our lab introduced the *Halenium Affinity* (*HalA*)[22] concept as a quantitative descriptor of the thermodynamic affinity of various functional groups to halenium ions. This method was demonstrably successful in providing the correct prediction of halenium acceptor *HalA*. The equations for the calculation of a neutral acceptor (equation 1) or anionic acceptor (equation 2) are displayed below.

7

Neutral acceptor: $\Delta H_{rxn}(X^+ + :LB \rightarrow X\text{-}LB^+)$      Equation 1

Anion acceptor: $\Delta H_{rxn}(X^+ + :LB^- \rightarrow X\text{-}LB)$      Equation 2

The *HalA* values discussed in this text are in kcal/mol at T = 298.15 K as derived computationally in equation 3.

$$HalA = -\Delta E_{(elec)} - \Delta ZPE - \Delta E'_{(vib)} + \frac{5}{2}RT \quad \text{Equation 3}$$

With a computational method in hand, the halenium affinities of various chlorenium donors were calculated and compared to each other to probe the validity of *HalA*. *HalA* predicts that a Lewis base with the higher *HalA* will abstract a chlorenium ion from a donor with a lower *HalA* (of its corresponding Lewis base). An NMR competition experiment between tetra-n-butyammonium succinimidate acceptor (Figure I-6b, *HalA* (Cl) = 194.0) and DCDMH donor (Figure I-6c *HalA* (Cl) of Lewis base = 181.1 kcal/mol) was performed to probe the validity of the *HalA* calculations. The succinimide anion possesses a higher halenium affinity than the chlorohydantoin anion and thus should abstract the chlorenium ion from the DCDMH donor. This proposition is supported by the chemical shifts of the 1:1 mixture of DCDMH and tetrabutylammonium succimidate (Figure I-6d) in which the methylene protons of the succimidate (H$_a$) which would lie at about 2.3 ppm if anionic (Figure I-6b) shift upfield to the same chemical shift of NCS (Figure I-6a). Consequently,

the methyl protons of the DCDMH donor experience a upfield shift indicating transfer of

the chlorenium ion.
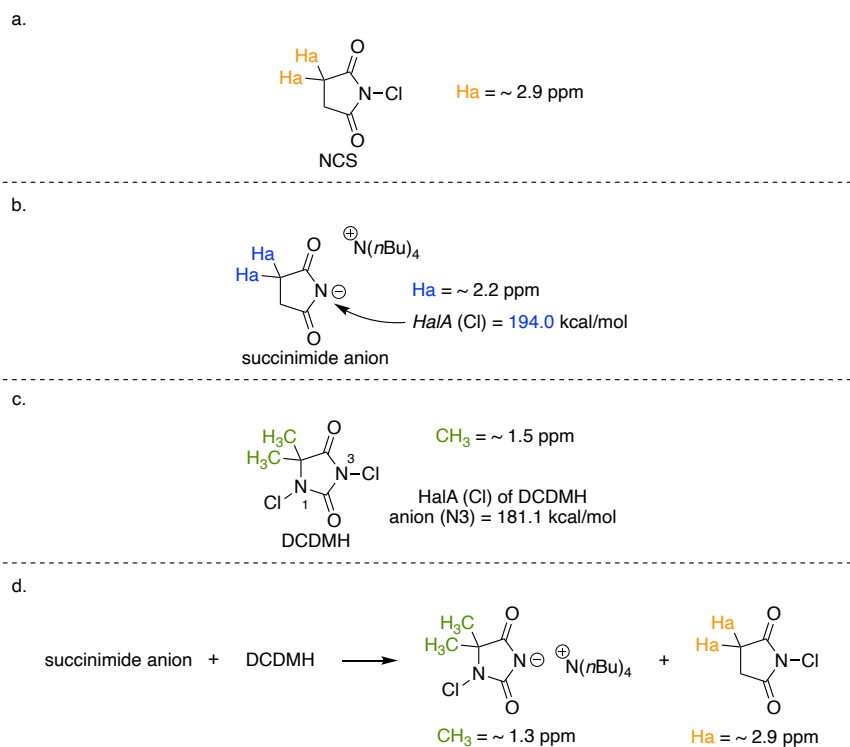


**Figure I-6:** (a) 1H NMR of NCS (b) $^1$H NMR of succinimide anion (c) $^1$H NMR of DCDMH (d) $^1$H NMR of succinimide anion DCDMH mixture that results in the abstraction of chlorenium to form NCS

The comprehension of *HalA* in the context of a molecule with multiple competitive

Lewis basic functionalities enables the prediction of chemoselectivity of reactions (Figure

I-7). For example, molecule **I-32** contains two potential sites for halogenation: the

aromatic ring (*HalA* = 181.5 kcal/mol), which leads to the chlorination of the aromatic ring,

or the aryl alkene (*HalA* = 179.3 kcal/mol), which leads to the carbocyclization product.

As predicted by *HalA*, exposure of **I-32** to chlorenium source DCDMH yields the

electrophilic aromatic chlorination reaction product **I-33**. Modification of the electronic

nature of the aromatic ring via the removal of methoxy electron donors led to the

attenuation of the *HalA* of the aromatic ring in substrate **I-34** (*HalA* = 164.5 kcal/mol, about

15 kcal/mol less than the alkene) thus rendering the alkene the functionality with the highest *HalA* within the molecule and providing the carbocyclization product **I-35**.[22]



HalA (Cl) values in Kcal/mol (B3LYP/6-31G*)
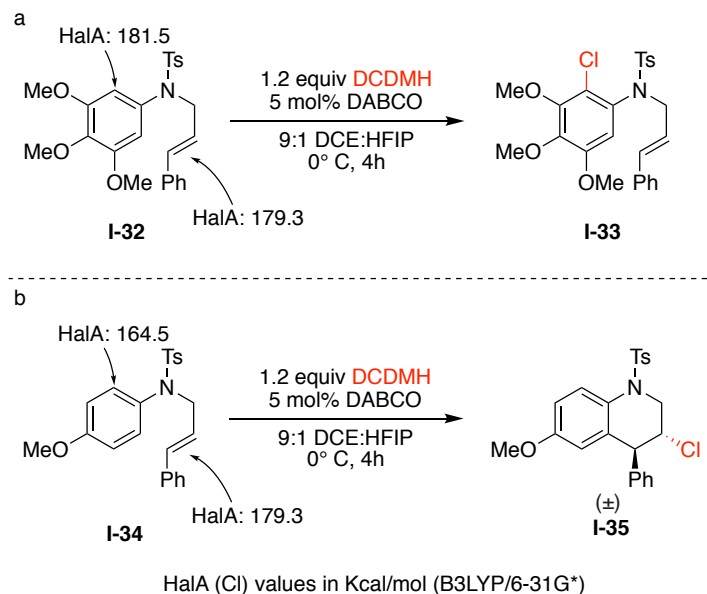
**Figure I-7:** Predictive ability of Halenium affinity in chemoselectivity (a) Aromatic ring with high halenium affinity undergoing chlorination (b) Aromatic ring with attenuated halenium affinity undergoes a carbocyclization

## I-3-2   Nucleophile Assisted Alkene Activation

Recently our group disclosed studies on the intramolecular Nucleophile Assisted Alkene Activation (*NAAA*).[23] This is a mechanistic revelation that challenges the traditional stepwise halofunctionalization mechanism by asserting, with strong experimental evidence, that intramolecular halofunctionalizations often proceed through an asynchronous concerted mechanism driven by an interaction between the HOMO of the nucleophile and LUMO of the alkene, thus increasing the *HalA* to the extent that transfer of the halenium ion to the alkene can occur. This is demonstrated via the conformer dependent *HalAs* of **I-45** (Figure 1-8a). In the stepwise reaction path

10

proceeding through a carbocation (Figure I-8b) the halenium affinity of the unactivated **I-45** alkene is 167.4 Kcal/mol. Conversely, in the nucleophile assisted reaction pathway C (Figure I-8C) the *HalA* of **I-45** is increased to 173.3 kcal/mol. Thus, with a higher *HalA*, the coiled conformer **I-45** reacts faster. Additionally, viewed in the context of an asymmetric halofunctionalization, a concerted addition of both the nucleophile and halenium ion in *NAAA* circumvents racemization processes involved with haliranium ions.
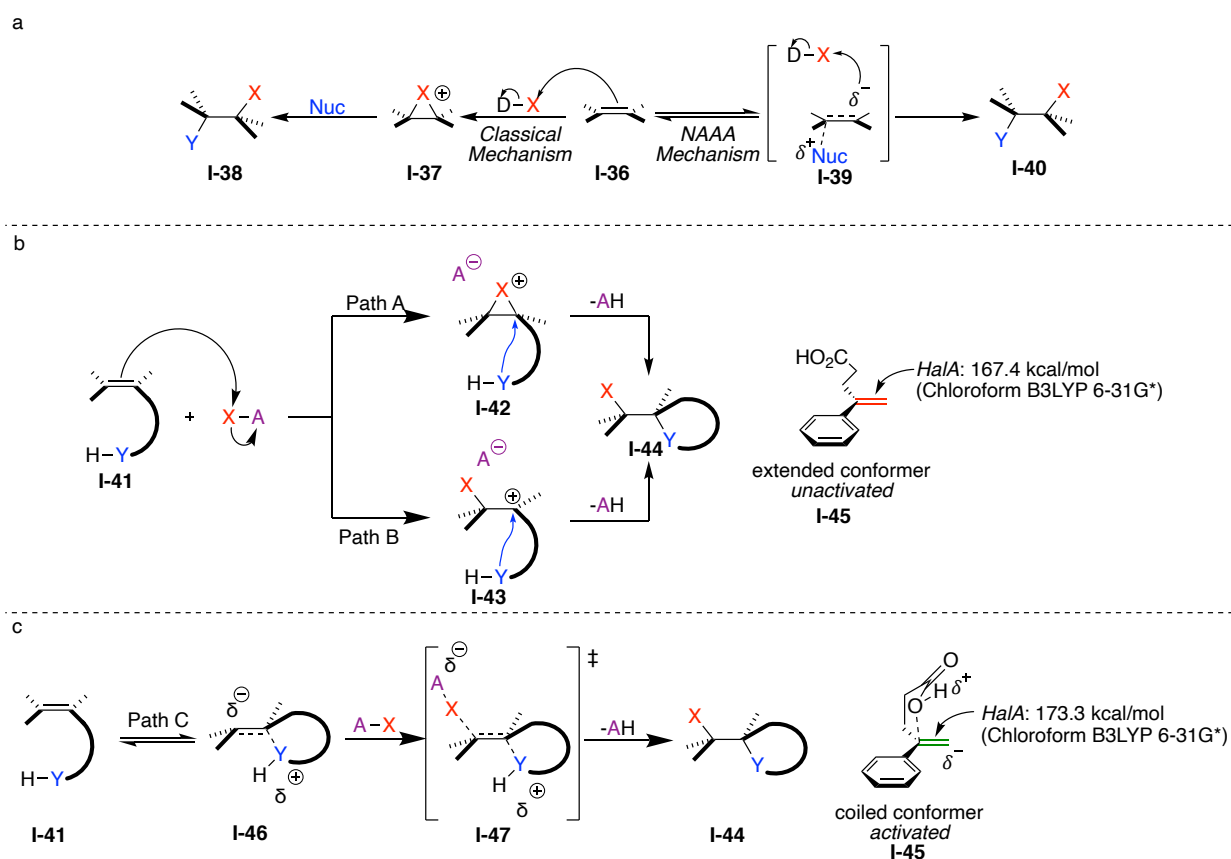


**Figure I-8:** (a) Contrasting classical and nucleophile assisted halofunctionalizations (b) Reaction pathway for a classical halofunctionalization and the halenium affinity of the alkene in this mechanism (c) Reaction pathway for a *NAAA* halofunctionalization and *HalA* in this mechanism

11

## I-3-2-1 Experimental Evidence for Nucleophile Assisted Alkene Activation

Dr. Kumar Ashtekar's elegant experiments provided support for *NAAA*. The next section will be a brief discussion of the most convincing experiments supporting this controversial mechanism. While the following experiments provide evidence for the existence of *NAAA*, it is critical to recognize that it is a mechanistic spectrum of
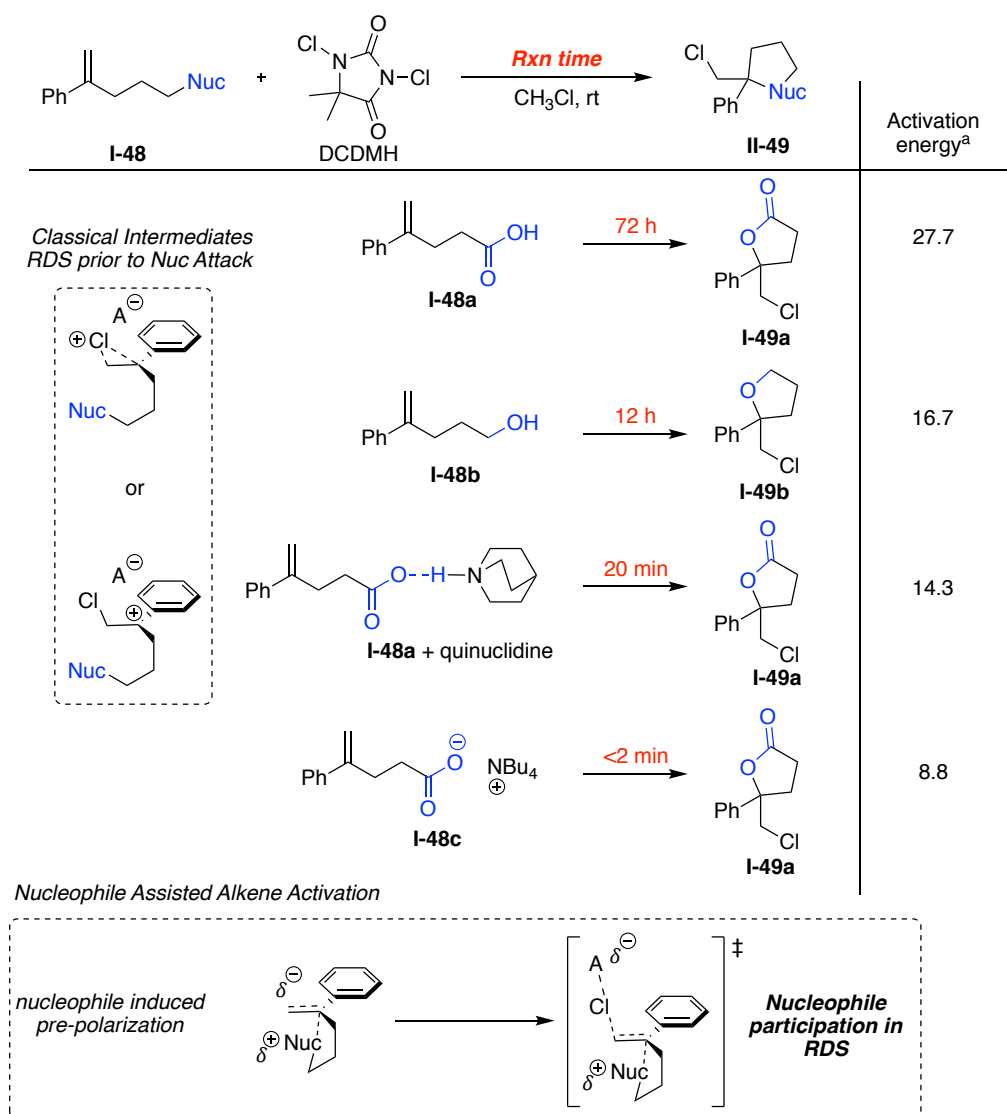


**Figure I-9:** Influence of nucleophilicity on reaction rate

possibilities, both the *NAAA* and traditional stepwise reaction pathways can occur depending on the olefin, halenium donor, and nucleophile.

The traditional halofunctionalization mechanism depicts the rate-determining step as the haliranium ion formation. This implies the nucleophile plays no role, therefore if the nucleophile is not involved in the rate-determining step, then modulation of the nucleophilicity should have no effect on the reaction rate (Figure I-8b). To explore the possibility of a nucleophile assisted mechanism, Dr. Ashtekar synthesized substrates with tethered nucleophiles possessing a range of nucleophilicities (Figure I-9). Carboxylic acid **I-48a** is the weakest nucleophile, therefore it provides the least assistance and the most sluggish reaction. Progression to stronger nucleophiles such as alcohol **I-48b** or basic additives with **I-48a** correlate with an increased reaction rate, indicating that the nucleophile is involved in the rate-determining step. The variation of reaction rates is supported with computational data indicating a lower activation energy with a stronger nucleophile.

NMR spectroscopy probed the possibility of an asynchronous transition state via a pre-polarized nucleophile. Here, the tethered nucleophiles that displayed varied reaction rates were synthesized and their respective NMR spectra were observed (Table I-I). In line with rate observation, stronger nucleophiles, such as **I-50c**, provided more shielding (electron density) to Ha while deshielding Hb. The enhanced electron density of the alkene results from the HOMO of the nucleophile interacting with the LUMO of the alkene. This raises the halenium affinity of the alkene and increases the reaction rate.

**Table I-1:** $^1H$ and $^{13}C$ resonances of Z-styrylic alkene upon modulation of electronic of a remotely tethered nucleophile

Ha $_{\delta-}$ $_{\delta+}$Hb
Ph
Nuc

**I-50**
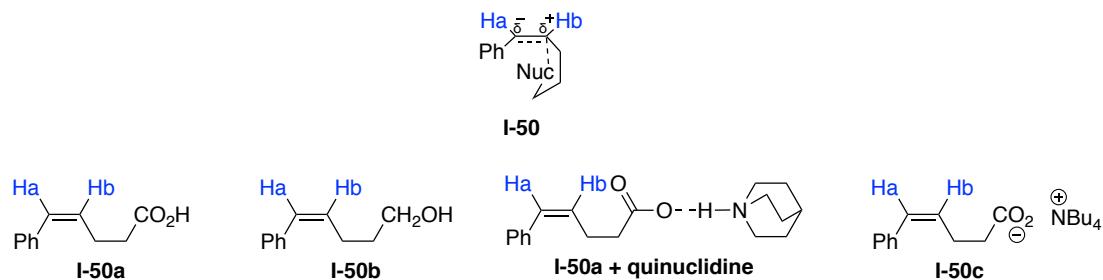
| Entry | Substrate | δ $^1H_a$ (ppm) | δ $^1H_b$ (ppm) | δ $^{13}C$-$H_a$ (ppm) | δ $^{13}C$-$H_b$ (ppm) |
|-------|-----------|-----------------|-----------------|------------------------|------------------------|
| 1 | I-50a | 6.48 | 5.62 | 130.4 | 129.8 |
| 2 | I-50b | 6.44 | 5.66 | 129.4 | 132.0 |
| 3 | I-50a + quinuclidine | 6.34 | 5.66 | 128.6 | 132.6 |
| 4 | I-50c | 6.30 | 5.73 | 127.8 | 133.7 |

Kinetic isotope effects were critical in differentiating between potential mechanistic pathways (Figure I-10). If proceeding through a stepwise fashion, the halolactonizations of **I-51** and **I-53** are expected to proceed through the tertiary benzylic halocarbenium ion.[22] If the formation of this intermediate is the rate determining step, then no $^{13}C$ is expected at the benzylic carbon. The chlorolactonization of **I-51** displays a KIE of 1.011 indicating hybridization state change of that carbon in the transition state and thus the nucleophile's involvement in the rate determining step. To display the $^{13}C$ KIE of a stepwise pathway electron rich **I-53** was subjected to the same conditions and yielded a KIE of 1.001 at the benzylic center, indicating a carbocationic reaction pathway without assistance from the nucleophile. This difference in KIE between these two substrates is a direct observation of an *NAAA* in an alkene with lower *HalA* (**I-51**) requiring *NAAA* to enable the abstraction of a halenium ion and a non-*NAAA* pathway with an electron-rich alkene that does not

require further *HalA* enhancement from the nucleophile to abstract the halenium ion from

the donor.
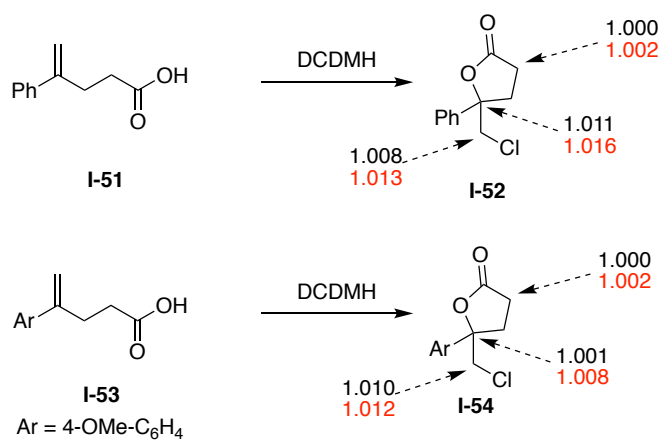


**Figure I-10:** $^{13}C$ natural abundance KIE studies of chlorolactonizations

# I-4 Development of Catalytic Asymmetric Halofunctionalizations

## I-4-1 Intramolecular Catalytic Asymmetric Halofunctionalizations

Cognizant of the intrinsic chemical and confirmational instabilities haliranium ions pose, our group first explored catalytic asymmetric halocyclization. The proximity-driven rate enhancement or *NAAA* would limit the haliranium ion lifetime, thus lessening the potential for racemization processes. In 2010 Dr. Whitehead disclosed the first catalytic
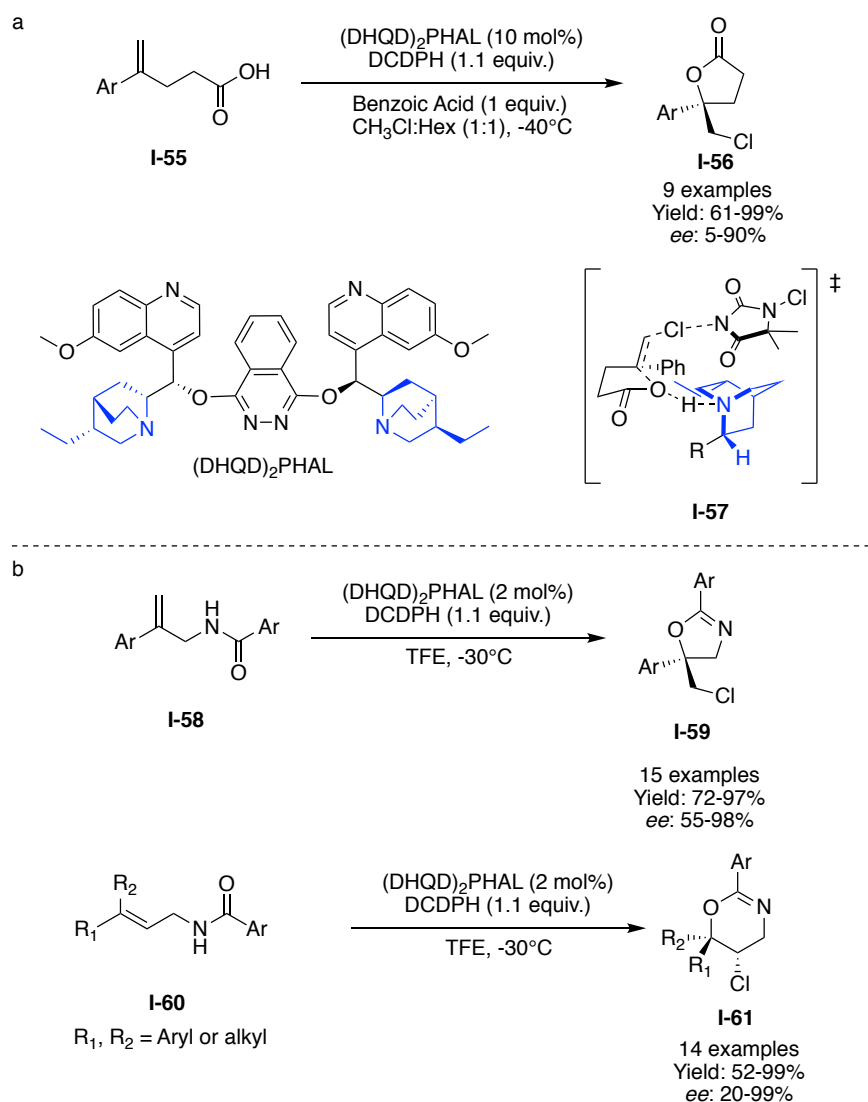


**Figure I-11:** (a) Catalytic asymmetric chlorolactonization with proposed mechanism (b) Catalytic asymmetric amide halocyclizations

asymmetric chlorolactonization employing cinchona alkaloid dimer (DHQD)$_2$PHAL as a catalyst and N-halohydantoins as halenium sources (Figure I-11A).[24] This reaction is tolerant of most electronic perturbations of the aryl ring of **I-55**, providing enantioselectivities in excess of 80% *ee* for the majority of substrates. Highly electron rich substrates such as the 4-methoxy phenyl substrate provides severely deteriorated enantioselectivity. The reduction in enantiocontrol is attributed to the substrate's high halenium affinity that possibly does not require *NAAA* or the catalyst to transfer the chlorenium ion to the alkene. Mechanistic studies suggest an *NAAA* mechanism for the catalytic reaction with the quinuclidine of (DHQD)$_2$PHAL functioning to activate the acid nucleophile. Dr. Jaganathan expanded this chemistry to include amide halocyclizations (Figure I-11B). By altering the substituents on the alkene, both the 5-exo (**I-58**) and 6-endo (**I-60**) products were attainable. Like the chlorolactonizations, this reaction was highly tolerant to most alkenes but suffered a reduction of enantioselectivity with the most electron-rich substrates.[25-26]

### I-4-2   Intermolecular Catalytic Asymmetric Halofunctionalizations

In 2015 Dr. Soltanzadeh disclosed the stereoselective intermolecular haloetherification of allyl-amides(Figure I-12).[27] Employment of (DHQD)$_2$PHAL, DCDMH, and a methanol nucleophile proved to be optimal in the highly enantioselective transformation of Z and E olefins of aliphatic and aromatic substitution to their corresponding chloro-ether products (Figure I-12a). This methodology was not limited to chlorenium reagents as NBS provided the bromoether product in high yield and enantioselectivity (Figure I-12b).[28]

This work expanded the prior art in the field as it provided strong regiochemical catalyst control over unactivated alkenes that contain minimal electronic bias (Table I-2). Relative to halocyclization reactions, control of regioselectivity is more challenging in intermolecular haloetherifications that do not benefit from regioselective bias due to ring closure kinetics. Dr. Soltanzadeh discovered that (DHQD)$_2$PHAL is significant in determining the regiochemical outcome of the reaction, improving the regio-isomeric ratio (**I:65** to **I:66**) to 24:1 for the catalyzed reaction as opposed to 4:1 without the catalyst. Interestingly, (DHQD)$_2$NAPH reversed the regio-isomeric ratio back to 4:1 (Table I-2).

**a**

(DHQD)$_2$PHAL (10 mol%)
DCDMH (2.0 equiv.)

Nucleophile:MeCN (3:7)
(0.01 M), -30 °C

**I-62**
R$_1$, R$_2$ = aryl or alkyl
R$_3$ = alkyl, H, or acyl

**I-63a**
22 examples
Yield: 49-93%
*ee*: 50-99%

**b**

(DHQD)$_2$PHAL (10 mol%)
NBS (2.0 equiv.)

Nucleophile:MeCN (3:7)
(0.01 M), -30 °C

**I-62**
R$_1$, R$_2$ = alkyl
R$_3$ = Me or H

**I-63b**
4 examples
Yield: 51-92%
*ee*: 70-99%
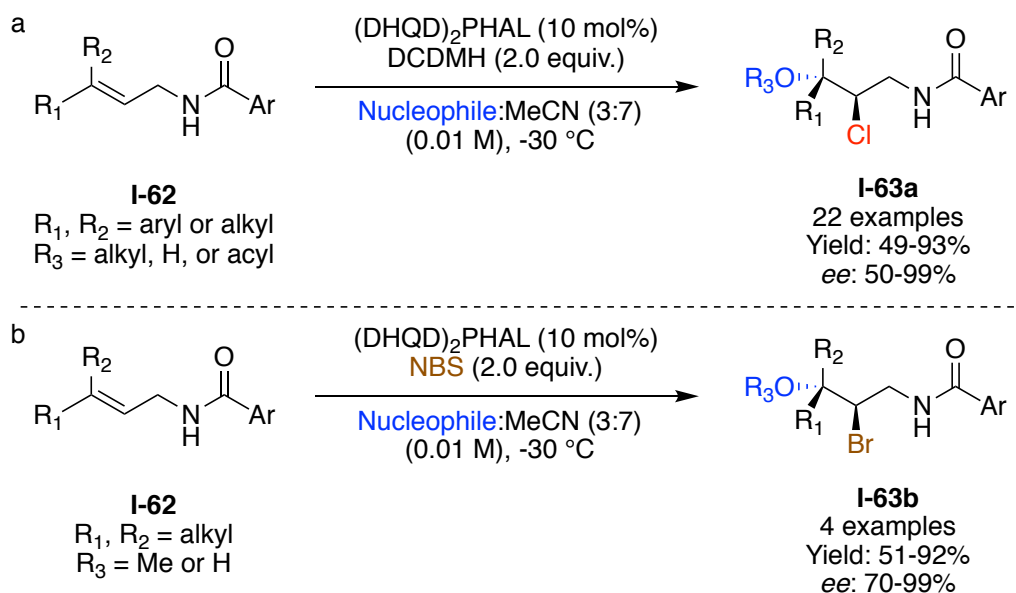
**Figure I-12:** (a) Catalytic asymmetric intermolecular chloroetherification scope (b) Catalytic asymmetric intermolecular bromoetherification scope

This may be attributed to substrate phthalazine hydrogen bonding through the N-H of the amide or enhancing structural rigidity of the catalyst.

**Table I-2:** Catalyst control of *regiochemistry* for haloetherification reactions
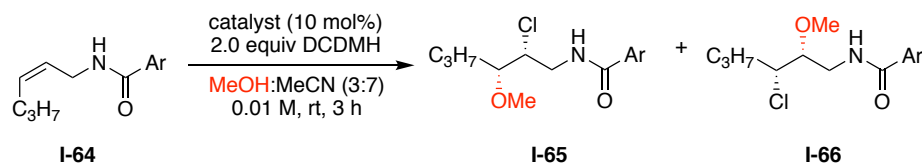


| Entry | Catalyst | rr (**I-65**:**I-66**) |
|-------|----------|------------------------|
| 1 | None | 4:1 |
| 2 | (DHQD)₂PHAL | 24:1 |
| 3 | (DHQD)₂NAPH | 4:1 |

(DHQD)₂NAPH
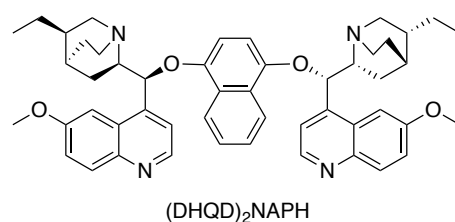
Mechanistic studies led by Dr. Sarkar elucidated an unorthodox catalytic transformation. The order of each reagent was determined through detailed *Reaction Progress Kinetic Analysis* and *Variable Time Normalized Analysis* developed by Blackmond and Burns. The elucidation of the order of each reagent sheds light on the rate-determining step and off-cycle processes of the catalytic cycle. It was determined that the reaction was first order in substrate and methanol nucleophile suggesting that it is involved in the rate-determining step and zeroth order in DCDMH. The zeroth-order suggests saturation with the chlorohydantoin and the catalyst. Interestingly, the reaction was also zeroth order in the catalyst at molar equivalents greater than 0.01, indicating that the catalyst is not involved in the rate-determining step. Considering the observed orders, Dr. Sarkar proposed a catalytic cycle with the rate-determining pre-catalytic step to form the activated alkene with complexation of the substrate with methanol. Once in this reactive conformation, the substrate reacts with the chiral DCDMH (DHQD)₂PHAL

complex to provide the chloro-ether product in high yield, regioselectivity, and enantioselectivity. The transfer of from chlorenium to DCDMH and (DHQD)₂PHAL to form **I-67** presents a catalytic system with potentially broad applicability as a chiral source of chlorenium. Additionally, kinetic data elucidating a first order of methanol and an inverse KIE support a concerted mechanism (Figure I-13b). A concerted mechanism obviates racemization processes and allows for the inclusion of unactivated alkenes in an intermolecular halofunctionalization process.
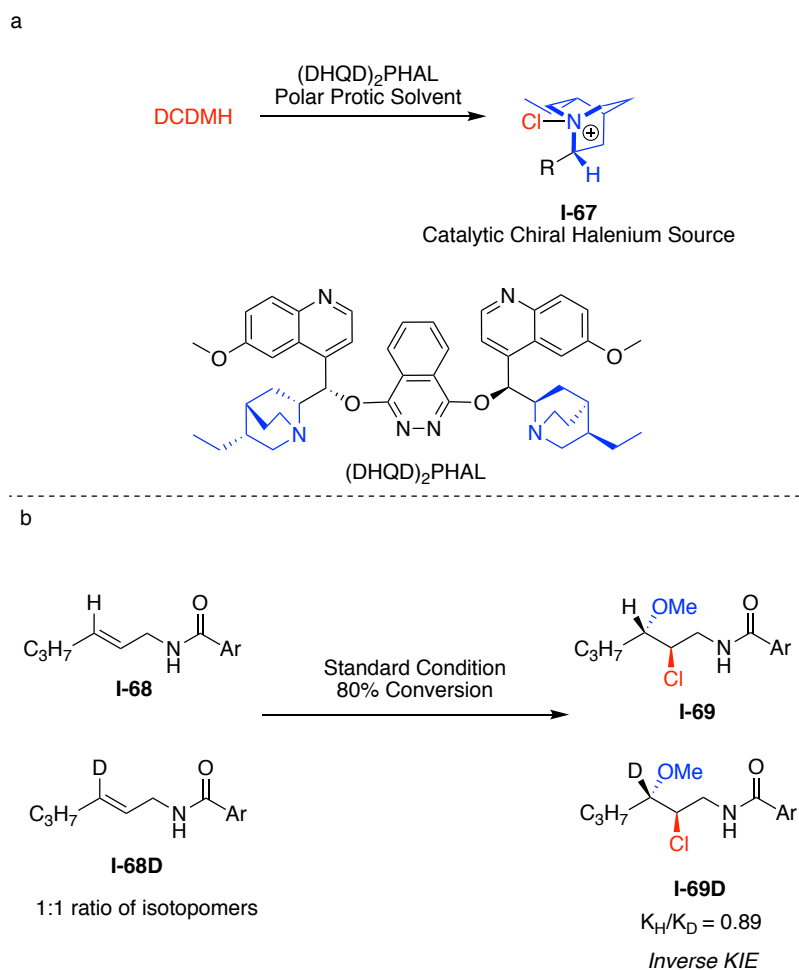


**Figure I-13:** (a) Transfer of chlorenium from DCDMH to (DHQD)₂PHAL to form chiral halenium source (b) KIE experiment suggesting a concerted nucleophile assisted mechanism

## I-5   Catalytic Asymmetric Haloamination of Olefins

The catalytic asymmetric haloamination of olefins is a desirable tool for synthetic chemists. The installation of the enantiopure carbon halogen bond provides a ubiquitous moiety found in many natural products and an important handle for downstream stereospecific reactions (Figure I-14a). Additionally, the stereodefined carbon nitrogen bond is common in many compounds of biological and synthetic significance (Figure I-14b).
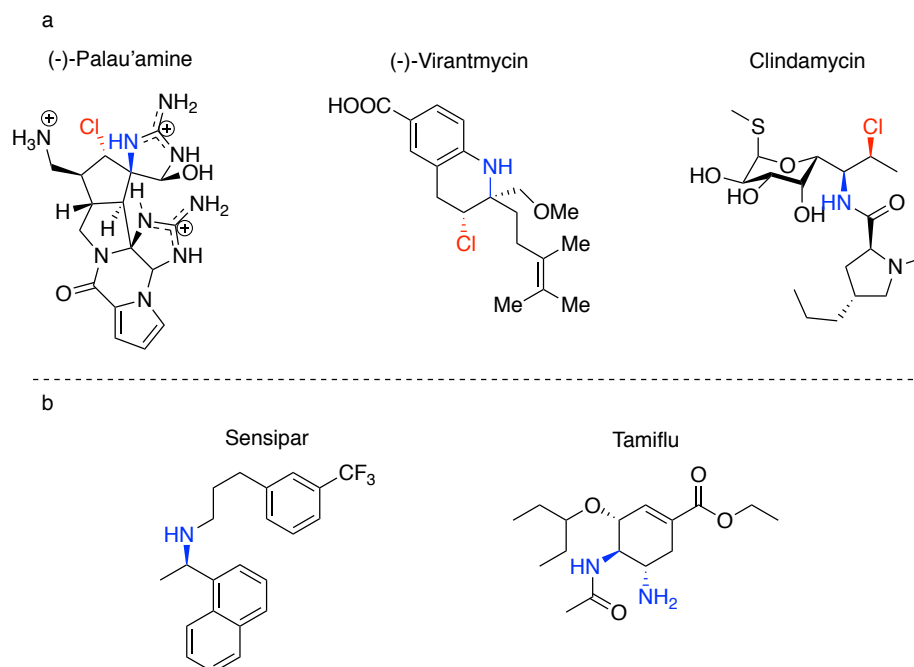


**Figure I-14:** (a) Biologically significant molecules that contain a chiral vicinal chloramine (b) Stereodefined amines in small molecule pharmaceuticals

While this reaction's desire is clear, intermolecular asymmetric haloamination reactions have not afforded the same success that related halofunctionalization reactions with halogen and oxygen nucleophiles provide. The key difference between these nucleophilic species is their respective halenium affinities. A sampling of halenium

affinities is shown in the table below (Figure I-15a). The halenium affinity of alcohols, representative of oxygen nucleophiles, falls below the range of alkenes and, as a result, does not compete with alkene **I-70** for halenium ions permitting the formation of haloether product **I-71**. Conversely, amines have a halenium affinity higher than alkenes and under analogous haloamination conditions the amine nucleophile out competes the alkene **I-70** for the capture of the halenium ion.[22] This results in the retainment of the allyl-amide starting material and the formation of **I-73** and **I-74** as a kinetic trap via hydrogen halogen exchange between the two nitrogen atoms.
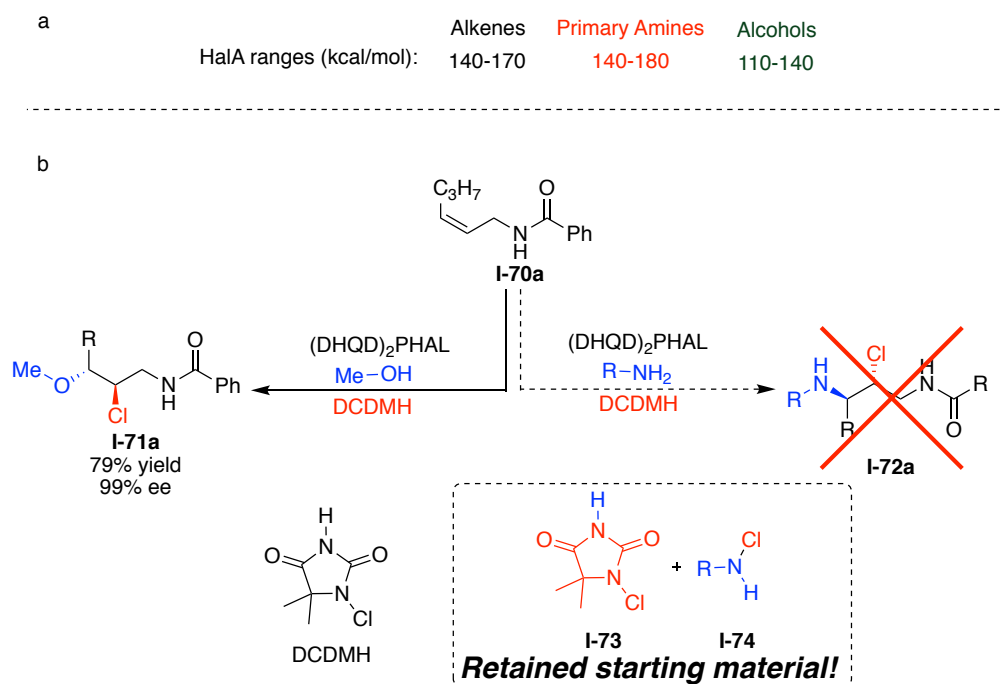


**Figure I-15:** (a) Sampling of potential nucleophiles for halofunctionalizations (b) The role of halenium affinity in the control of the reaction pathway

Many groups have leveraged an elegant "pro-nucleophile" approach to construct vicinal haloamines utilizing a nitrogen-based halenium source (Section I-5-2). While this is a clever method to circumvent the quenching of the halenium source by the nucleophile,

it hinges on the olefin's capability to fully abstract the halenium ion from the halenium source. This subsequently produces a haliranium or β-halocarbenium ion that is trapped by the nitrogen-based counter anion to yield the difunctionalized product. The drawback to this chemistry is that a halenium ion's abstraction via the olefin to form putative haliranium or β-halocarbenium ion intermediates is a kinetically difficult stepwise process. This often requires either a highly reactive alkene, halenium source, or catalyst. These procedures frequently employ bromenium or iodenium reagents as their respective haliranium intermediates are more stable to mitigate the chemical instability of these high-energy intermediates. This stepwise pro-nucleophile mechanistic pathway differs from other halofunctionalizations that enable an *NAAA* pathway that helps assist the transfer of halenium ions to unactivated olefins.

## I-5-1 Literature Precedent for Intramolecular Catalytic Asymmetric Haloamination Reactions

As with many reactions within the family of halofunctionalization, catalytic halocyclizations piloted catalytic asymmetric haloamination chemistry. The intramolecular nature of the reactions circumvents many problematic features of haliranium ions and enable a less entropically challenged route to nucleophile assisted alkene activation. These methods are precious due to the ubiquitous nature of nitrogen-containing chiral heterocycles in natural products. To avoid halenium ion deactivation via exchange with the nitrogen nucleophile, most groups avoided using basic nitrogen nucleophiles that possess a higher halenium affinity and employed sulfonylimides or nosylsulfonamides, which possess a much lower halenium affinity. It is also possible that with the basic

23

catalysts (cinchona alkaloid or amidine) employed in these reactions, the amine nucleophile **I-75** is deprotonated, thus generating **I-76**, a stronger nucleophile for the reaction.



**I-75**
R = EWG

**I-76**

**I-77**
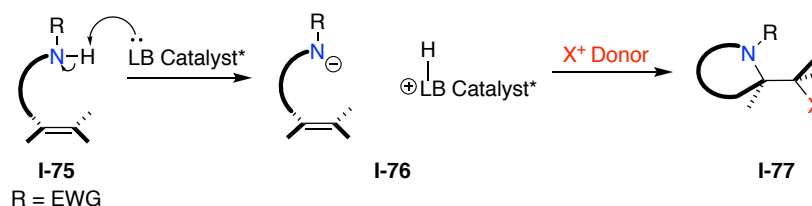
**Figure I-16:** General strategy for the intramolecular catalytic asymmetric haloamidation of alkenes

## I-5-1-1    Halocyclization of Unsaturated Sulfonamides with a Thio-Carbmate Catalyst

In 2011, Yeung and coworkers disclosed the catalytic asymmetric halocyclization of unsaturated sulfonamides with an amino-thiocarbamate catalyst **I-79** yielding pyrrolidine products with high yields and high *ee* (Figure I-17).[29] Selection of the proper amine protecting group was critical to yield, *ee*, and reaction time with 4-Ns in **I-78** providing the optimized result in nearly every category. The authors suggest that the 4-Ns group provided the ideal steric bulk and acidity to enable interaction with the catalyst's quinuclidine moiety. While a broad range of substrates were displayed, only



**I-78**
R = Ar, Alkyl, H

**I-79** (10 mol%)
NBS, CHCl₃, -62 °C

**I-80**
16 examples
61-99% yield
10 -99% ee

**I-79**
R = 2,6-(EtO)₂C₆H₃
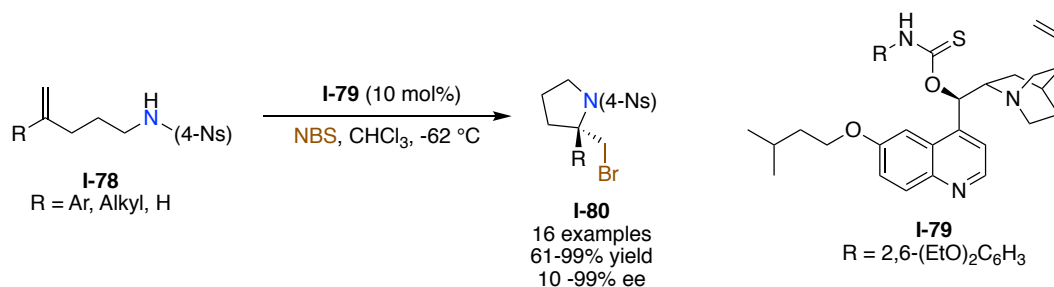
**Figure I-17:** Thiocarbamate catalyzed bromocyclization

24

aryl disubstituted alkenes yielded products with enantiomeric excess greater than 46%.

Additionally, alkenes with high electron density such as 4-MeOC$_4$H$_6$ suffered from

reduced enantioselectivity (19%).

## I-5-1-2    Catalyst Controlled Bromolactamization of Sulfonylimides

In 2015 Yeung and coworkers disclosed the bromolactamization of

sulfonylimides.[30] This reaction presents an additional challenge of nucleophile

chemoselectivity with the imide's oxygen presenting a competitive nucleophile. The

authors suggest that the catalyst **I-84** hydrogen bonds through the imide substrate's

tautomer. The hydrogen bonding confirmation makes it difficult for oxygen to behave as

a nucleophile in the reaction thus yielding **I-82a** in preference to **I-83a** (Figure I-18A). This

method was efficient and provided 22 products with high yield and enantiomeric excess.

Unlike similar work that yielded pyrrolidines, this reaction was more tolerable of electron-

poor and electron-rich substrates. Additionally, 1,2 disubstituted systems cleanly provides

products in high yield and enantioselectivity. Unfortunately, this reaction was limited to indole substrates which hinders its broad applicability and yielded bromination at the 3-position of the indole (Figure I-17b).
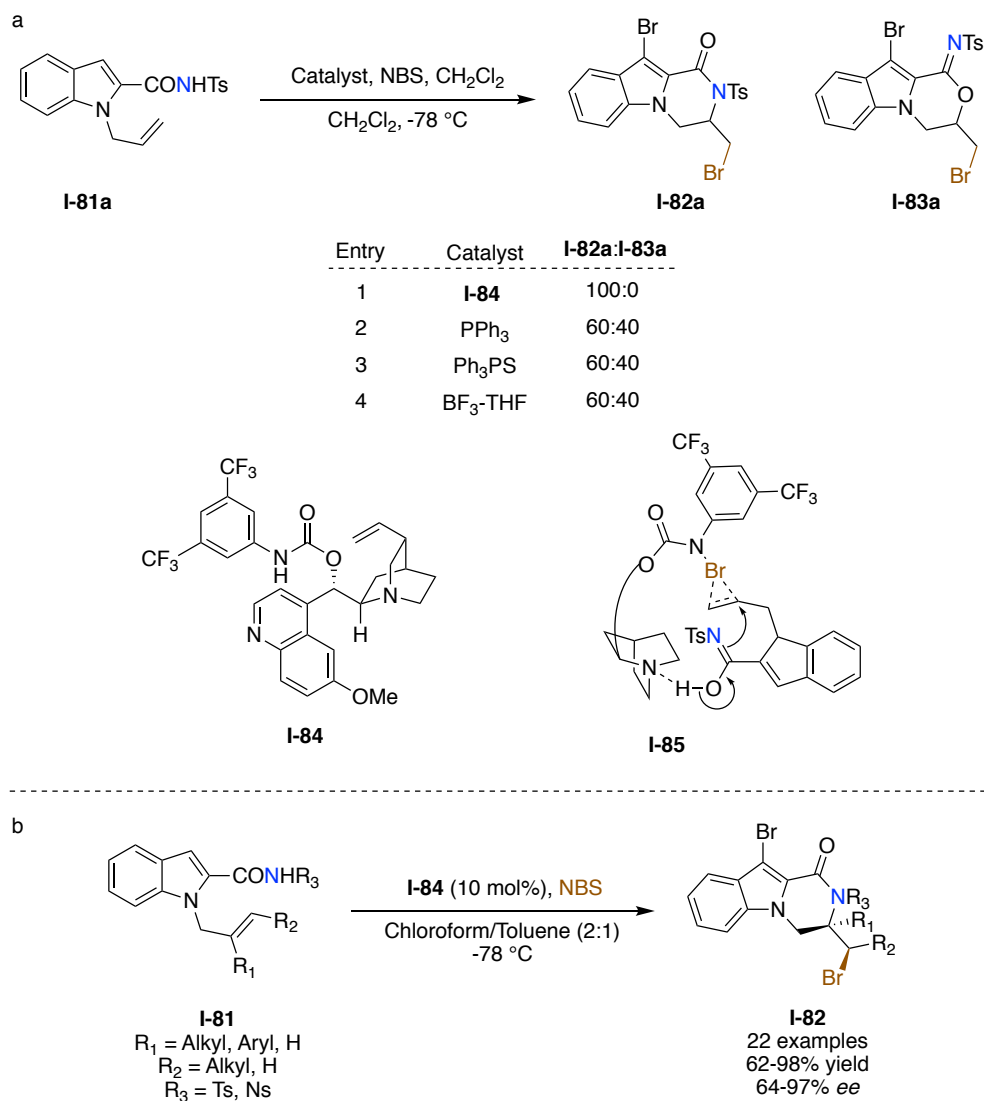


**Figure I-18:** (a) Catalyst control of reaction pathway to preference nitrogen nucleophiles (b) Substrate scope of bromolactamization

## I-5-1-3 Catalytic Asymmetric Intramolecular Iodoamination of Alkenes

In 2018 Johnston and coworkers disclosed the catalytic asymmetric intramolecular iodoamination of alkenes via amine isocyanate capture (Figure I-19).[31] The sulfonyl isocyanate employed forms the reactive sulfonylimine in solution. Like Yeung's work, this reaction can preferentially yield the nitrogen nucleophile in preference to the oxygen nucleophile. This reaction was heavily reliant on aryl alkenes, with most aryl alkenes providing enantiomeric excess near 90% and alkyl systems providing enantiomeric excess less than 50%. Regardless, this method utilizes the substitution of the alkene with subsequent carbocationic stability of haliranium to dictate the product's regiochemistry. The authors are able to leverage this to yield the five-membered cyclic urea **I-87** with 1,1 disubstituted systems and the six-membered cyclic urea **I-89** with the 1,2 disubstituted compounds (Figure I-18A). The utility of the carbon halogen bond is displayed in the further elaboration of the urea product to NK$_1$ inhibitor **I-91** after 4 steps from the haloamine product **I-87a**.
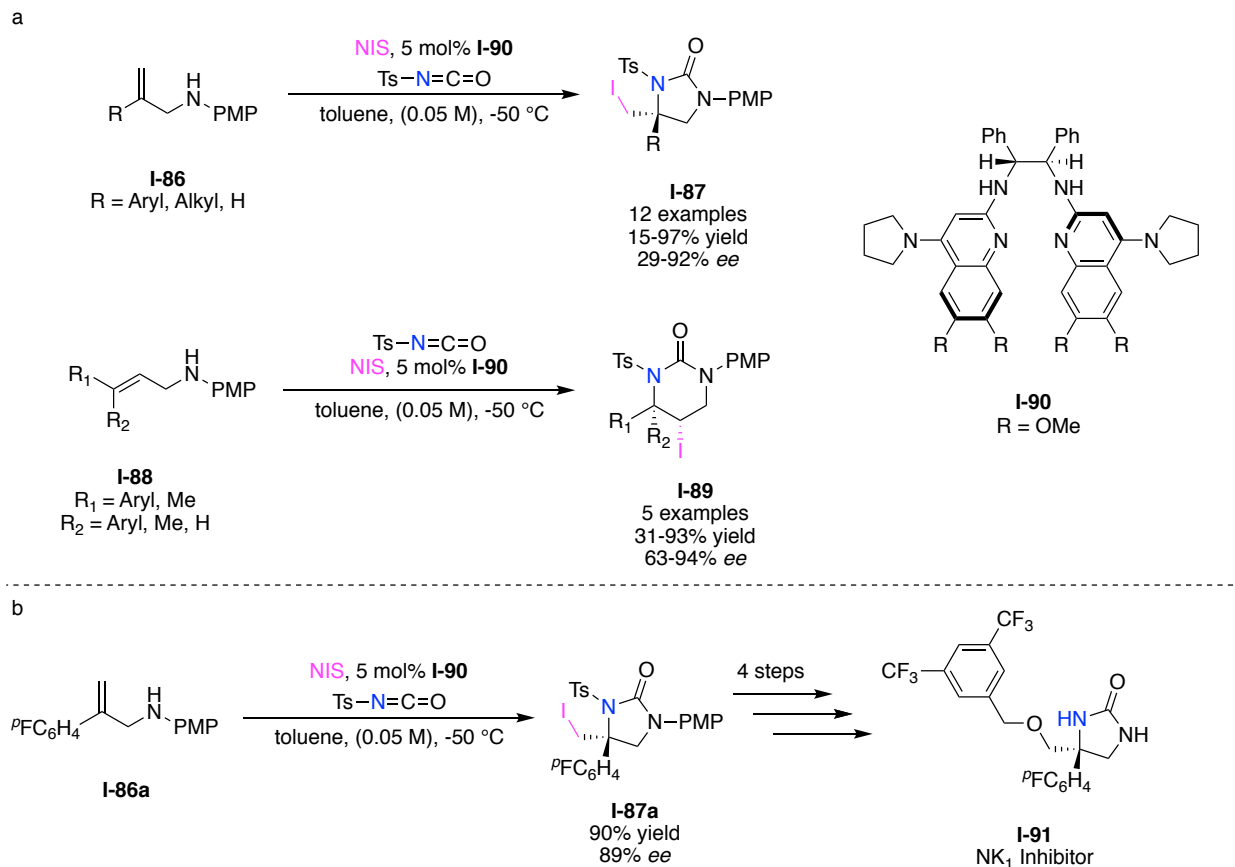
**Figure I-19:** (a) Substrate scope for alkene iodoamination for the synthesis of chiral ureas (b) Product elaboration to NK1 inhibitor

## I-5-2   General Approach of Previous Intermolecular Halenium Induced Haloamination Reactions

As discussed at the beginning of Section **I-5**, most early examples of intermolecular haloamination (both asymmetric and achiral methods) utilized the counter anion of a nitrogen-based halogenating source as a pro-nucleophile in haloamination reactions. This mechanistic pathway proceeds in stepwise mechanism (Figure I-20), often forming a high-energy haliranium (or β-halocarbenium) ion intermediate **I-93** via the halogenation of **I-92** with a nitrogen halenium donor. The nitrogen donor adds back in to the haliranium

28

ion to yield the difunctionalized product **I-94**. A reaction pathway proceeding through haliranium intermediate **I-93** is suspectable to racemization processes as well as competing decomposition reactions. To mitigate side reactions and render a more kinetically suitable pathway, olefins with high halenium affinities are often employed, enabling a more chemical and configurationally stable haliranium ion. This requirement is a significant limitation on the olefin scope as aliphatic substrates are less tolerant to these high-energy intermediates.
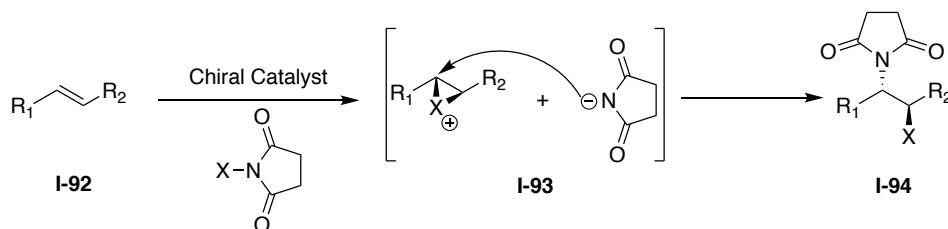


**Figure I-20:** General mechanism for traditional intermolecular catalytic asymmetric haloamidation

## I-5-2-1    Enantioselective $\alpha$-Halogenation of Enecarbamates

In 2012 Masson and co-workers elegantly reported the enantioselective $\alpha$-halogenation of E ene-carbamates with NBS and a BINOL derived chiral phosphoric acid catalyst (Figure I-20a).[32] They propose that the chiral phosphoric acid catalyst acts as a bifunctional catalyst by simultaneously activating the NBS and ene-carbamate **I-95** via hydrogen bonding **I-98**. The subsequent β-halo-iminium ion is trapped by the succinimidate ion to provide the difunctionalized product **I-97a**. The hydrogen bond stabilization of these high-energy intermediates allows for the smooth production of 13 unique vicinal bromo amines. In 2016 this strategy was expanded to include both iodination (Figure I-20b) and chlorination chemistry (Figure I-21c).[33] This methodology's

success originates from the high halenium affinity of the ene-carbamate substrate that can abstract a halenium ion with no nucleophile assistance.
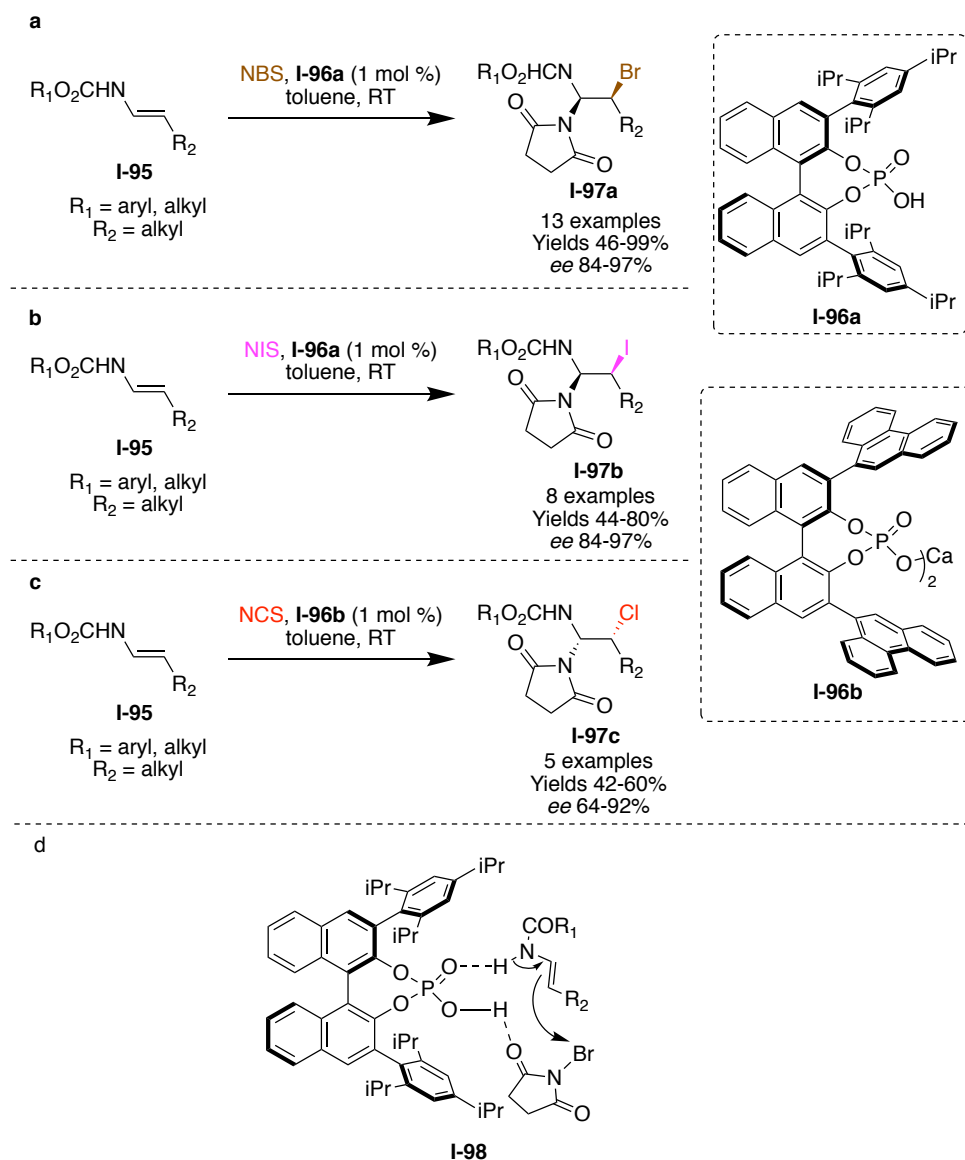


**Figure I-21:** (a) Enantioselective bromoamidation (b) Enantioselective iodoamination (c) Enantioselective chloroamination (d) Proposed mechanism for the enantioselective bromoamidation

## I-5-2-2 Enantioselective Bromoamination of Allylic Alcohols

A similar strategy to Masson's work was reported in 2014 by Zhou (Figure I-22).[34] This method employs a cinchona-derived thiourea catalyst **I-100** as a hydrogen bond donor in the activation of N,N-dibromo-4-nitrobenzene-sulfonamide to assist in the asymmetric transfer of bromenium to the aryl-substituted E alkene **I-99**. Following the bromenium ion transfer, the counter anion attacks the putative bromonium or β-halocarbenium ion. While moderately activated, aryl substituted alkenes do not possess halenium affinities as high as ene-carbamates; however, the use of the highly reactive nosyl-sulfonamide permits the transfer of bromenium to this less reactive species. It should be noted that the alcohols were protected with TBSCl upon reaction completion to yield the protected alcohol **I-101**. The reaction was also limited to trans alkenes, potentially limiting the susceptibility to reduce strain by opening the β-bromocarbenium ion, which would reduce diastereoselectivity.
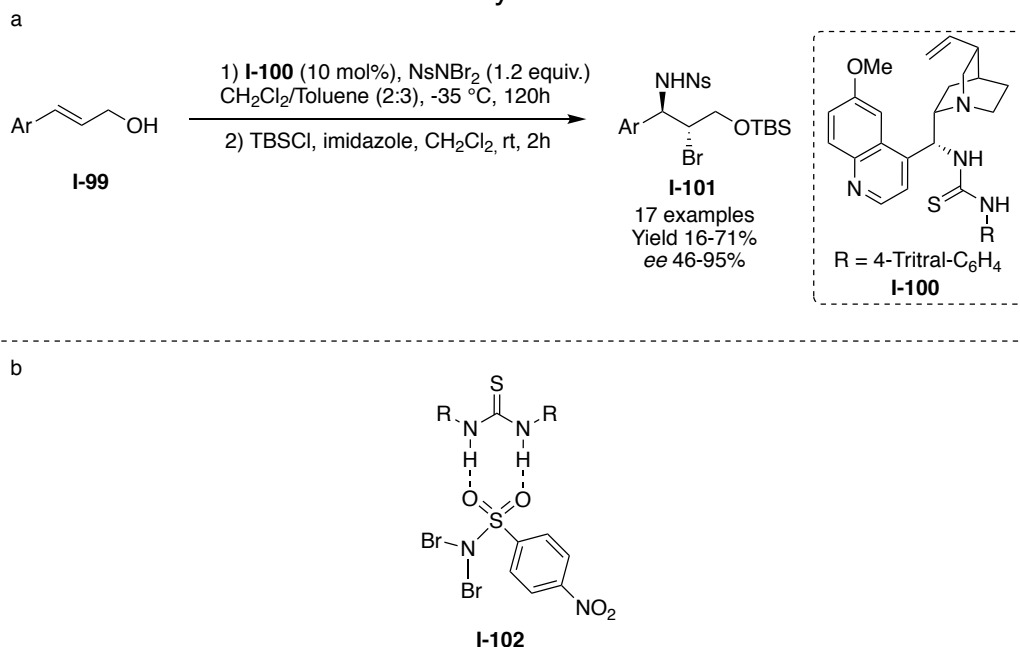


**Figure I-22:** Substrate scope for bromoamidation of allylic-alcohols (b) Proposed activation mode for thiourea catalysts

## I-5-2-3 Haloazidation of Allylic Alcohols

Burns and coworkers' work is slightly different but is derived from the same pro-nucleophile strategy to synthesize haloazides **I-107a** and **I-107B** from allylic alcohol **I-103** (Figure I-23).[35] Like previous work achieved by this group, they rely on reactive species' coordination to a titanium center in a catalytic chiral ligand accelerated approach.[36-39] The work is inspired by Sharpless' regioselective ring opening of epoxides with the in-situ titanium azide complex that releases the azide upon coordination with the epoxy alcohol.[40]
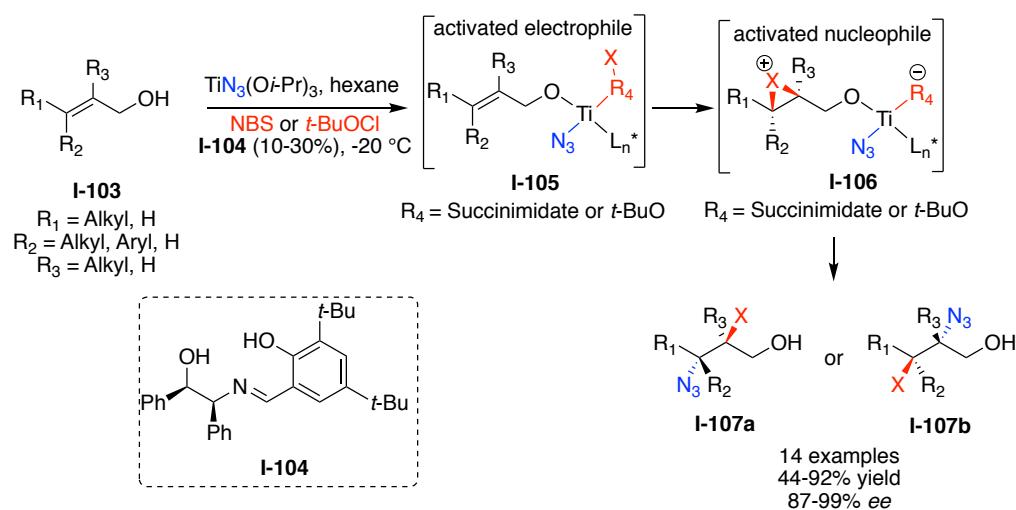


**Figure I-23:** Haloazidation of allylic alcohols

Burns and coworkers' adaptation of this chemistry is reliant on the titanium to play multiple roles in the reaction:

1. The titanium acts as a Lewis acid to activate the halenium source.

2. Upon transfer of the halenium ion, the increased electron density on titanium provided by the counter anion of the halenium ion activates the azide for N-3 (I-108B) transfer to open the haliranium ion.

3. Though formally an intermolecular molecular transformation, the chelation of all three components in **I-106** renders an intramolecular transition state and short lived haliranium ion.

4. The intramolecular nature of haliranium capture obviates many of the racemization and side reaction pathways (Figure I-23). This comes with the ability to reverse regioselectivity via ring closure kinetics/substrate control with Z olefins to yield regioisomer **I-107b** in preference to Markovnikov regioisomer **1-107c** (Figure I-23). While this might be a useful synthetic property of this method, it renders the opposite diastereomer unattainable (Figure I-24).
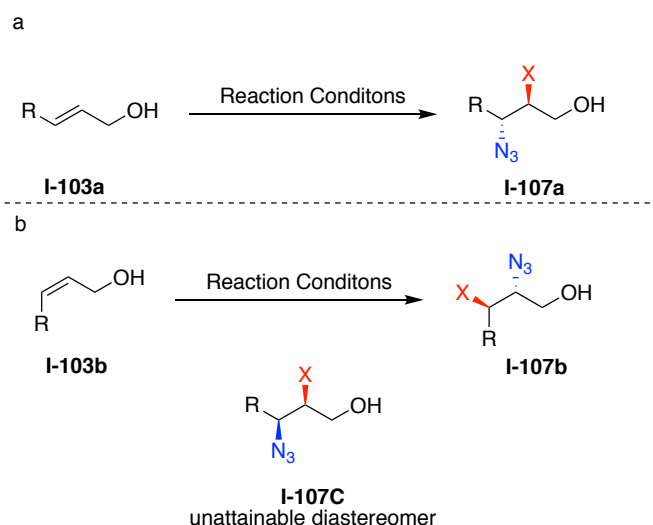


**Figure I-24:** Regiodivergent behavior between Z and E alkenes. (a) Regioselectivity of E olefin. (b) Regioselectivity of Z olefin

Unlike other methods proceeding through a pro-nucleophile mechanism, this work is compatible with unactivated aliphatic alkenes. There are two potential explanations for this tolerance of less reactive alkenes: 1. The titanium center is highly activating for the halenium source, this allows for the halenium transfer to occur without *NAAA* or 2. Though

the nucleophilicity of the titanium coordinated azide is highly attenuated, it can still assist in the transfer of the bromenium via the distal nitrogen. This work is groundbreaking since unactivated alkenes lead to vicinal haloamine products. It also earns high recognition for its use of allylic alcohols; however, the high catalyst loadings and the stoichiometric equivalent of titanium are limitations of this chemistry.

## I-5-2-4    Nucleophile Induced Asymmetric Haloamination of Olefins

While the groups of Masson, Zhou, and Burns employed an olefin with high halenium affinity or a highly reactive halenium source, Feng's strategy was notably different (Figure I-25).[41] Feng's work leverages Michael acceptors **I-108** as highly electrophilic olefins that undergo 1,4 addition with imides or sulfonyl amides. A halenium ion traps the subsequent enolate to provide the haloamine products **I-109a**. Although this transformation was initially proposed to proceed through a haliranium ion pro-nucleophile mechanism, considerations of the high energy nature of haliranium ion on an electron-poor alkene prompted the authors to revise their proposal to a Michael type mechanism (Figure I-25d).[42] This Lewis acid catalyzed pathway relies upon the Lewis acid to lower the pKa of the bound sulfonamide, thus activating it through deprotonation for nucleophilic attack of the alkene while simultaneously activating the Michael acceptor. This stereodefined environment fostered by the chiral ligand provides high yield across a broad range of $\alpha$-β unsaturated carbonyl compounds. This chemistry has been further developed to enable the enantioselective construction of bromoamide (Figure I-25b) and iodoamide (Figure I-25c) products.[42]
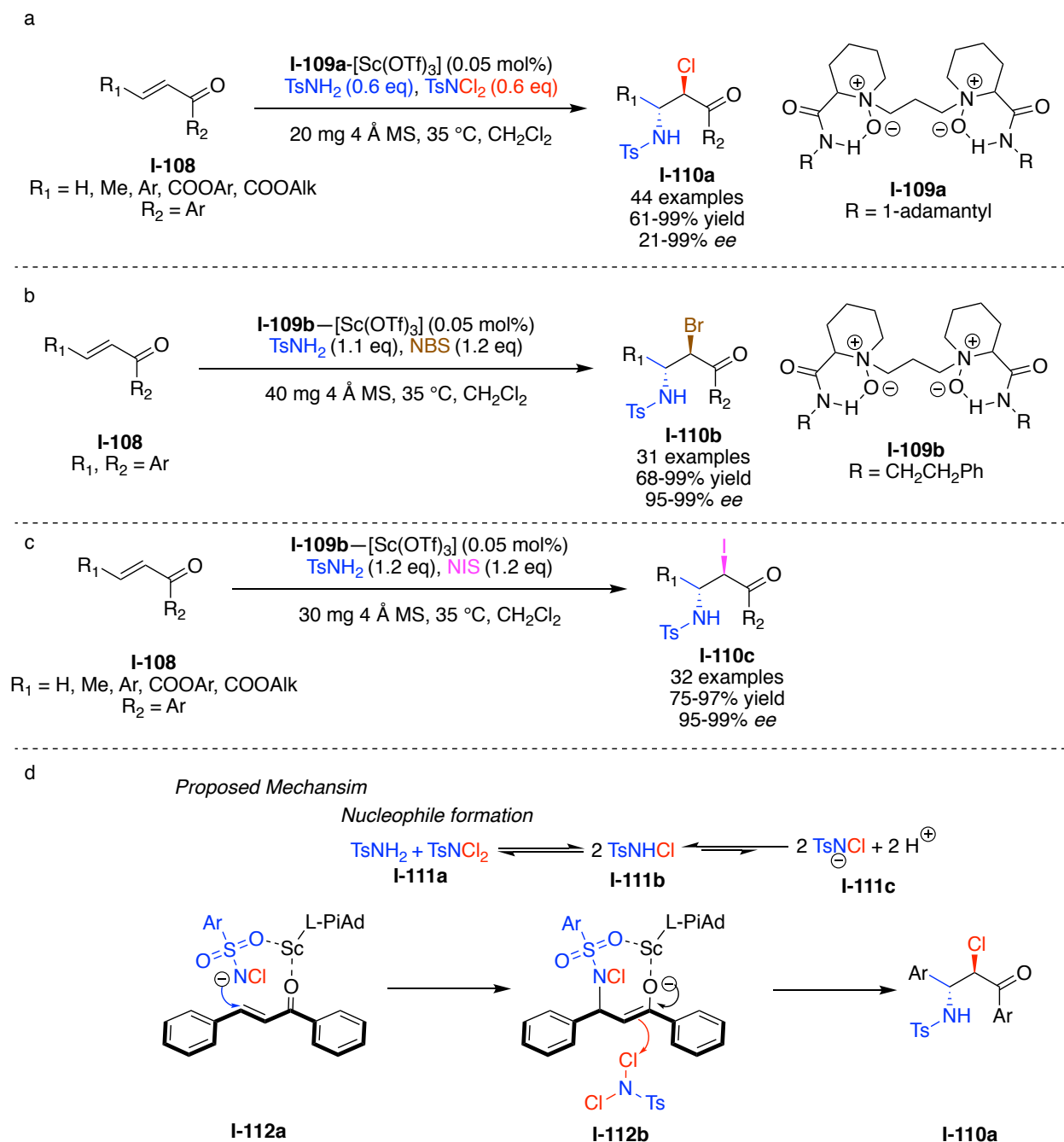
**Figure I-25:** Feng's Lewis acid approach to haloamidation of Michael acceptors. (a) Chloramidation (b) Bromoamidation (c) Idodoamination (d) Mechanistic approach to enable to enable the construction of haloamine products with electron poor alkyl systems

## I-5-3 Design of an Unmasked Nitrogen Nucleophile for Halofunctionalizations

Well aware of the difficulties involved with high halenium affinity nucleophiles (Figure I-26a) and substrate limitations of pro-nucleophile approaches (Figure I-26b), we sought to design a method with a higher tolerance to less reactive alkenes. We were inspired by our intermolecular haloetherification and dihalogenation reactions that were widely successful on a broad range of aliphatic and aromatic substitutions. The extension of this chemistry to aliphatic substrates is partially attributed to the ability for these nucleophiles to participate in a concerted mechanism **I-120** (Figure I-26c) or, as a solvent, quickly capture the haliranium ion before racemization or decomposition pathways can take place. This enables the inclusion of less reactive alkenes and obviates conformational and chemical instabilities involved with the haliranium ion **I-118**. While other intermolecular haloamination processes deserve high recognition, their stepwise pathways to circumvent the halenium affinity of alkenes requires harsh reaction conditions or limited substrate scope. We envisioned employing a nitrogen nucleophile that can assist in the transfer of halenium to the alkene or, if proceeding through a stepwise reaction, immediately capture a haliranium ion. Cognizant of the relatively similar halenium affinities of alkenes and nitrogen atoms, we sought to attenuate the halenium affinity of a nitrogen nucleophile to a lower value than that of the alkene, so that it will not compete for the halenium ion to provide kinetic trap **I-117** (Figure I-26a). We found that acetonitrile, which had actually seen success in racemic alkene haloamination reactions, has a halenium affinity lower than that of alkenes. This reaction is what is known as a

Ritter-type process (Figure I-25d). We became highly interested in the development of
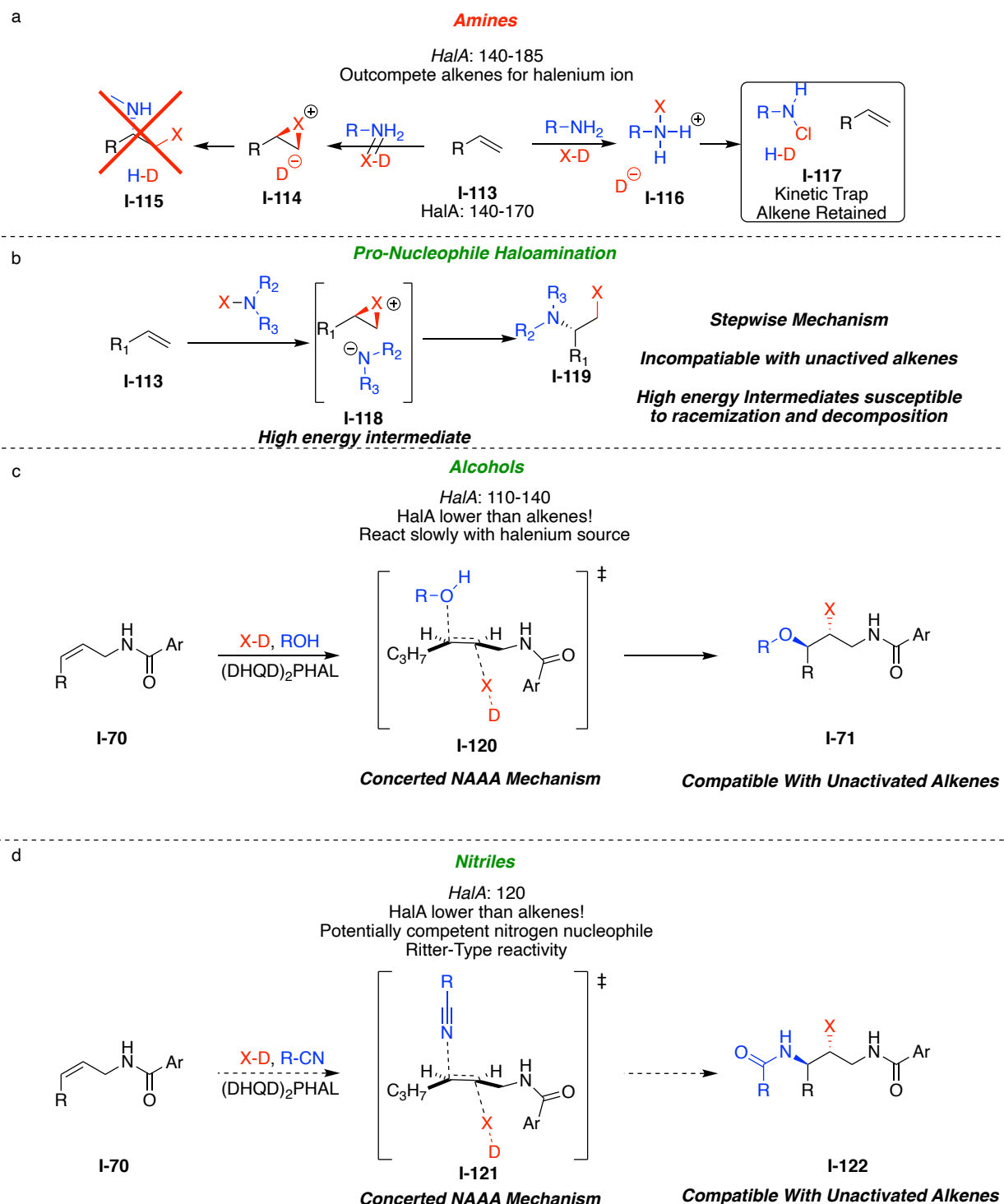


**Figure I-26:** Summary of approaches to intermolecular halofunctionalizations (a) Display of the problematic nature of amines in halofunctionalization reactions. (b) Stepwise pro-nucleophile haloamination (c) Concerted haloetherification reactions. (d) Proposal of a concerted haloamidation via the attenuation of *HalA*

this method when we noticed that there are no known asymmetric Ritter reactions.[43]

## I-5-3-1 Seminal Ritter Reaction

In 1948 Ritter and coworkers disclosed what is known as the Ritter reaction (Figure I-27).[44] This reaction proceeds through the protonation of alkene **I-123** with sulfuric acid. The resulting carbocation **I-124** is trapped with a nitrile to form nitrilium ion **I-125** that is then hydrolyzed to form the corresponding amide product **I-126**. The relative carbocationic stability is responsible for the Markovnikov regioselectivity. Due to the low stability of carbocationic intermediates, the substrate scope is limited to substrates that offer either benzylic or trisubstituted carbocation. This reaction is tolerant to various nitriles, providing practical yields with various aliphatic and aromatic nitriles.
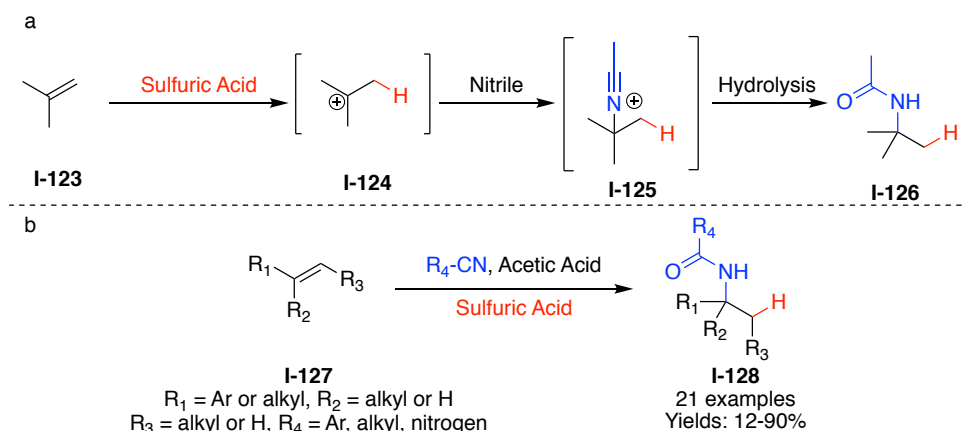


**Figure I-27:** Seminal Ritter reaction (a) Reaction mechanism (b) Reaction scope

## I-5-3-2 Halo-Ritter Reaction from Halohydrins

The first resemblance of a halo-Ritter reaction was reported by Ritter in 1950 and relied on the ability to form the haliranium ion in-situ by subjecting the corresponding halohydrin to sulfuric acid (Figure I-28).[45] Upon solvolysis of the alcohol with sulfuric acid, the β-halocarbenium ion **I-130** or haliranium ion **I-131** forms and then is opened by a

nitrile nucleophile to provide **I-133** following hydrolysis. Reminiscent of the proton induced reactions, the substrate scope was limited to substituents that can effectively stabilize a carbocationic (or haliranium ion) intermediate.
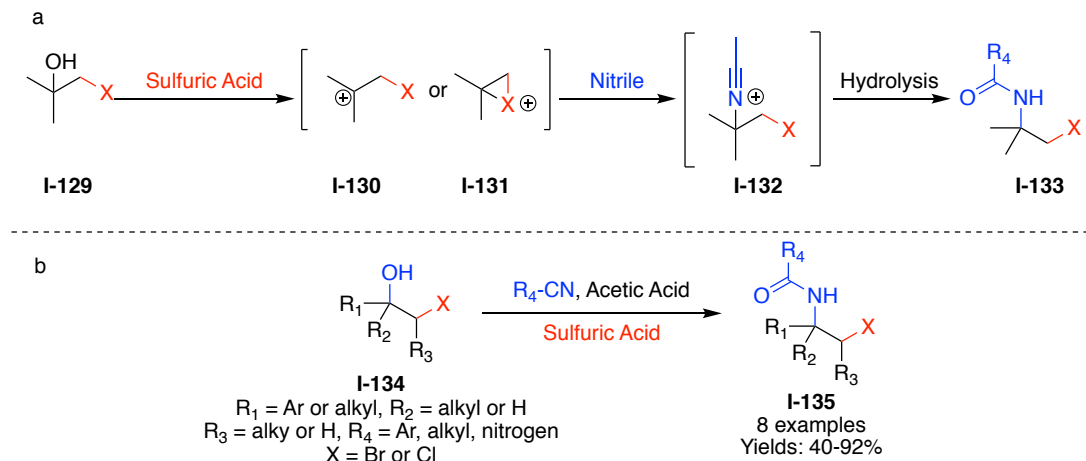


**Figure I-28:** Halo-Ritter reaction (a) Reaction mechanism (b) Reaction scope

## I-5-3-3  Halenium Induced Ritter Reaction with Alkenes

In 1952 Cairns and co-workers disclosed the first halenium induced Ritter reaction (Figure I-29).[46] An advancement from the Ritter report, which relied upon the in-situ formation of a haliranium ion of a pre-functionalized starting material, enabling the direct incorporation of both the halogen and nitrogen from a simple olefin starting material **I-127**. Their report utilized chlorine gas as the electrophile to form β-halocarbenium ion **I-130** or haliranium ion **I-131**. The nitrilium ion **I-132** reacts with a chloride ion to form a Vilsmeier type intermediate **I-136** which they isolated. They reported relatively modest yields maximizing at 58%. It is uncertain if this due to an inefficient reaction or unstable product formation. The authors mention that the dichlorination product is a side product.
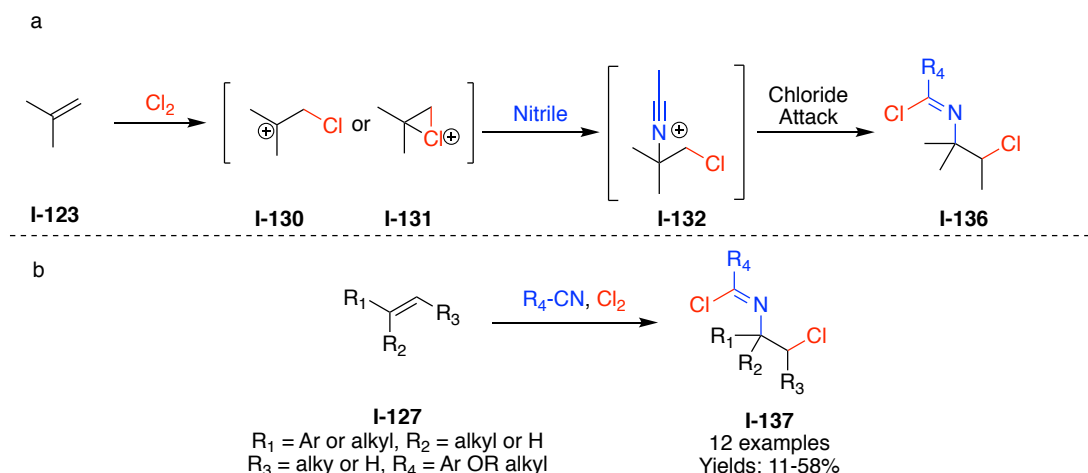
**Figure I-29:** Halenium induced Ritter reaction of alkenes (a) Reaction Mechanism (b) Reaction scope

## I-5-3-4　Lewis acid Catalyzed Bromo-Ritter Reaction and Total Synthesis of Oseltamivir

Corey and coworkers' Lewis acid-catalyzed halo-Ritter reactions offered a distinguished improvement over previous work and displayed the utility of vicinal haloamine products.[47] Utilizing Cairns' strategy, they employed an alkene and a halogenating source as an electrophile in a halenium induced Ritter reaction (Figure I-30a). Their conditions proved to be compatible for to provide bromoamides (**I-139a**), chlooamides(**I-139b**), and iodoamides (**I-139c**), reporting yields in excess of 90% for each reaction. This reaction showed to be broadly applicable, with high yields of aliphatic substrates. The broad applicability is likely due to the Lewis acid activation of the halenium source **I-142**, creating a potent halenium donor that is able to transfer to an unactivated alkene. The widespread success of stereoselective bromoamidation reactions on functionalized starting materials allowed for the incorporation of this chemistry in a more

complex synthesis. This success is further elaborated in the total synthesis of oseltamivir.[48]
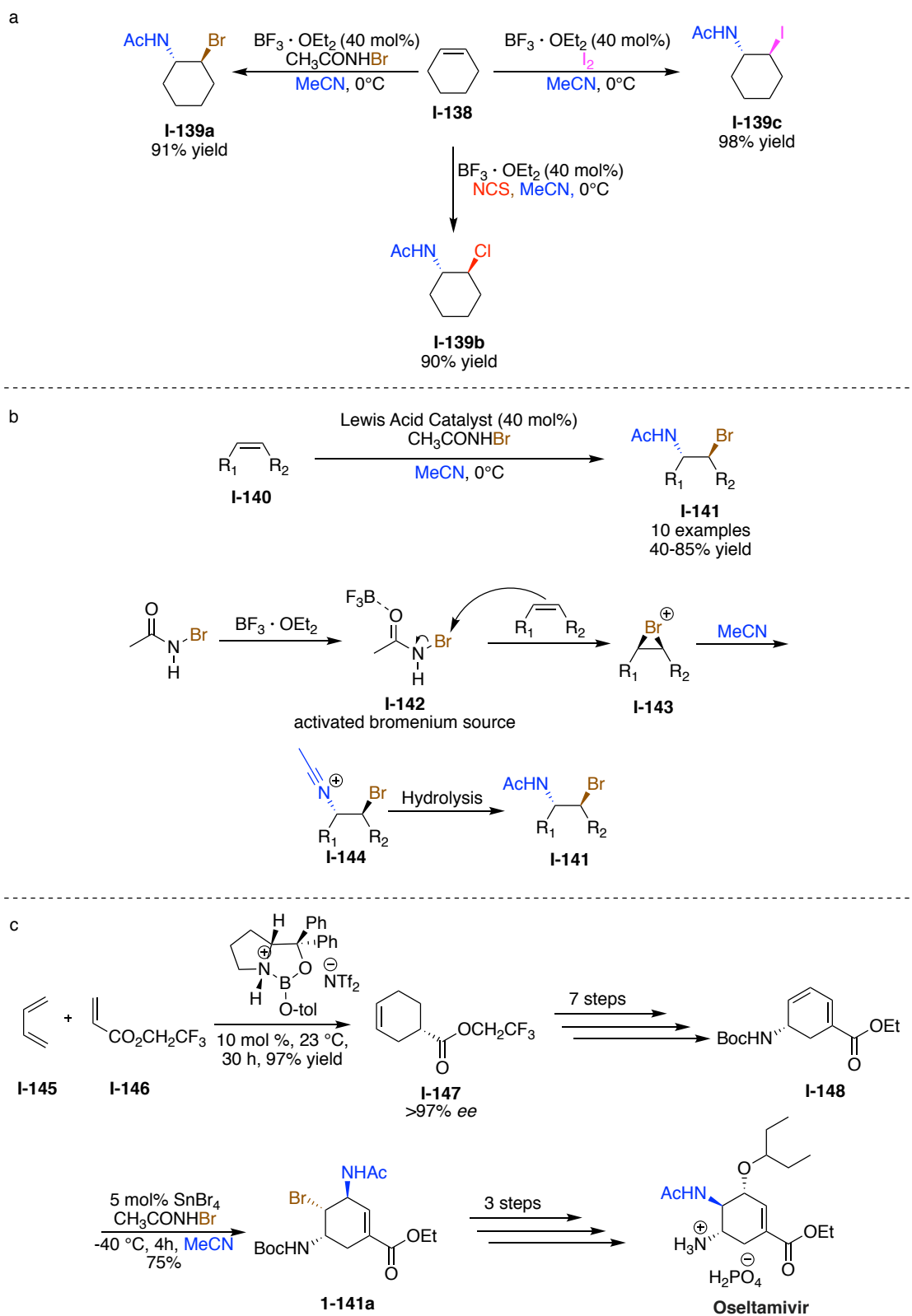
**Figure I-30:** (a) Reaction scope of Ritter-type haloamidations. (b) Proposed reaction mechanism. (c) Synthesis of Oseltamivir with haloamidation as a key step

## I-5-3-5  Lewis Base Catalyzed Chloroamidation of Olefins

In 2013, Yeung and co-workers displayed an alternative catalytic method utilizing a diphenyl selenide Lewis base for the halenium induced halo-ritter reaction of alkenes (Figure I-31).[49] They propose this reaction to proceed through the Lewis base interaction with NCS that transfers the chlorenium ion to the diphenyl selenide to form **I-153** which then transfers the halenium ion to the **1-149**. After transfer of the chlorenium ion to the alkene, the same nitrile interception proposed in above reactions occurs to provide **I-150**. This reaction was most successful with chlorenium sources as analogous bromenium sources provided products with a lower yield.
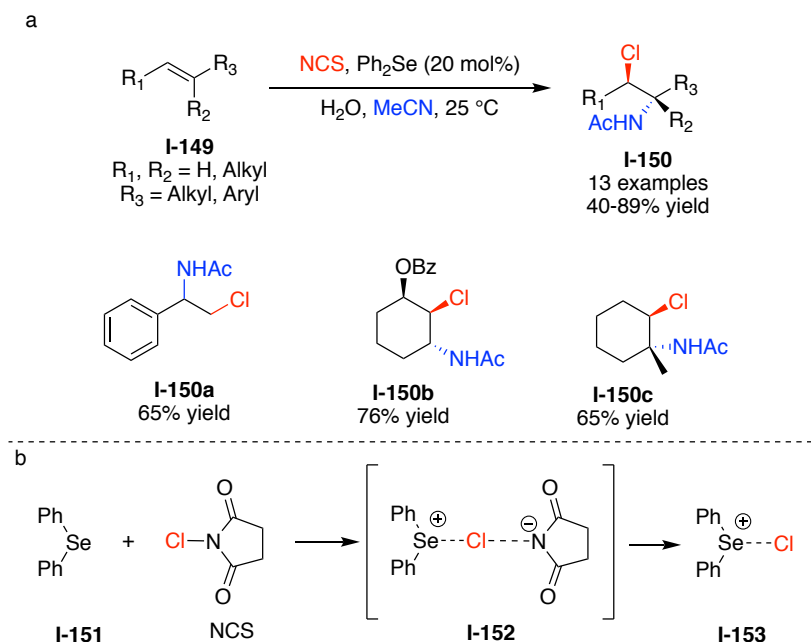


**Figure I-31:** (a) Substrate scope for base catalyzed chloroamidation (b) Proposed mechanism for selenium catalysis

## I-5-3-6 Stoichiometric Chiral Promoter Asymmetric Thio-Ritter Reaction

In 1994 Pasquato and co-workers disclosed a single example of an asymmetric thiiranium Ritter-type reaction (Figure I-32).[50] This reaction relied on a preformed stoichiometric chiral promoter to deliver the thiiranium ion enantioselectively to an olefin. The enantioenriched $C_2$ symmetric intermediate is then subjected to an acetonitrile-water mixture that opens the thiiranium ion to yield the difunctionalized product **I-156** in 90% yield and 86% *ee*.
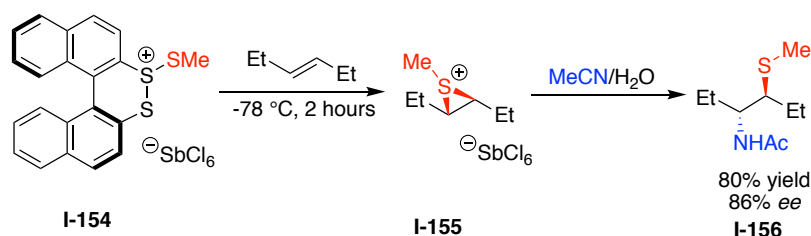


**Figure I-32:** Asymmetric Ritter reaction with stoichiometric chiral promoter

## I-6 Catalytic Asymmetric Ritter-Type Reaction

### I-6-1 Optimization Investigations

Our prior success in employing cinchona alkaloid dimers in the catalytic asymmetric intra- and intermolecular halofunctionalization of allyl amides prompted the following investigation for developing a process for haloamidations. The study was initiated with substrate **I-70a**, which had previously shown excellent results in delivering enantioenriched 1,2-chloroethers.[27] Early exploration of the reaction with acetonitrile, catalytic (DHQD)$_2$PHAL, and 1,3-dichloro-5,5-dimethylhydantoin (DCDMH) revealed the presence of Ritter-type products. Nonetheless, unlike the product of a classical Ritter-

reaction that yields the corresponding amide by trapping of the nitrilium ion intermediate with water,[43, 47, 51] the observed product was the result of the hydantoin anion trap of the nitrilium ion intermediate as indicated by the mass spectrum of the crude product (see **I-122a'**, Table I-3). Mild acid workup hydrolyzed the amidine product **I-122a'** to provide the vicinal chloroamide **I-122a**. Interestingly, without the presence of (DHQD)$_2$PHAL, the

**Table I-3:** Enantioselective chloroamidation optimization
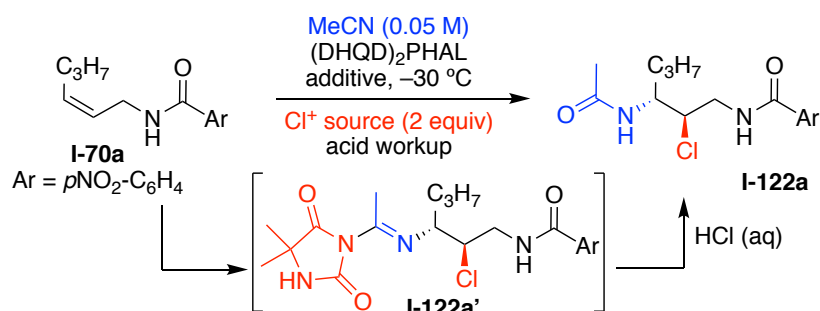


| Entry | Additive (equiv) | Cl$^+$ source | (DHQD)$_2$PHAL (mol%) | Time (h) | Yield (%)[a] | ee (%)[b] |
|-------|-----------------|---------------|----------------------|----------|-----------|---------|
| 1 | none | DCDMH | 10 | 72 | 68 | 96 |
| 2 | HFIP (2) | DCDMH | 10 | 0.5 | 71 | 99 |
| 3 | HFIP (10) | DCDMH | 10 | 0.5 | 78 | 99 |
| 4[c] | HFIP (10) | DCDMH | 10 | 0.5 | 78 | 98 |
| 5[c] | HFIP (10) | NCS | 10 | 96 | 70 | 98 |
| 6 | HFIP (10) | TCCA | 10 | 0.5 | 42 | 98 |
| 7[d] | HFIP (10) | DiCh-T | 10 | 0.5 | 12 | 99 |
| 8 | HFIP (10) | DCDMH | 1 | 0.5 | 76 | 99 |
| 9 | TFE (10) | DCDMH | 1 | 5 | 67 | 96 |
| 10 | PhCO$_2$H (10) | DCDMH | 1 | 2 | 29 | 97 |
| 11[e] | HFIP (10) | DCDMH | 1 | 4 | 53 | 99 |

[a]NMR yield on a 0.05 mmol scale. [b]Enantiomeric excess determined by chiral HPLC. [c]Reaction completed at room temperature. [d]Major product was the incorporation of the p-tolyl sulfonamide from DiCh-T (see **I-173a** for structure). [e]Reaction completed in dichloromethane (0.10 M) with 10 equiv of acetonitrile.

nitrilium ion is trapped by water, as indicated by direct amide formation that yields **I-122a**. The control over product formation suggests that the catalyst is not innocent in the addition of the hydantoin ion to the nitrilium ion. This divergent pathway hints towards an associative complex between (DHQD)$_2$PHAL and DCDMH.[24]

Table I-3 illustrates the optimization of the reaction under various conditions with the *Z* aliphatic substrate **I-70a**. The reaction proceeds to yield a 68% yield of **I-122a** (96% *ee*), however, requiring 72 h to reach completion (entry 1, Table I-3). In our previously reported studies on asymmetric halofunctionalization reactions, had observed an increased performance, both in terms of rate of reaction and yield of products, when a fluorinated alcohol additive was employed.[25-28] Presumably, the acidic nature of the alcohol, and its attenuated nucleophilicity, are good combinations that lead to rate acceleration without nucleophilic participation in the reaction.[52-53] There is also evidence that protonation of cinchona alkaloid dimeric catalysts could lead to altered conformations.[54]

An early screening of solvents showed that the addition of 1,1,1,3,3,3,-hexafluoroisopropanol (HFIP) improved the enantiomeric excess of **I-122a**, while tremendously increasing the rate of the reaction (entries 2-3, Table I-3). DCDMH proved to be the optimal chlorenium source as the less active N-chlorosuccinimide (NCS) (entry 5) was sluggish and gave slightly lower *ee*, while the more active chlorenium trichloroisocyanuric acid (TCCA) (entry 6) gave a lower yield. Use of dichloramine-T returned the product in high *ee*, although in low yields. Interestingly, the mass balance was identified as the *p*-tolyl sulfonylamidine product **I-173a** (addition of the *p*-tolyl sulfonamide to the Ritter intermediate, yielding a stable product, *vide infra*). Lowering the catalyst loading (entry 8) led to a negligible change in reaction proficiency, and thus 1 mol% (DHQD)₂PHAL was chosen as standard for ensuing reactions. Less reactive substrates required increased catalyst loading to achieve optimal proficiency (See I-8-6). A quick screen of acidic additives (entries 9 and 10) proved HFIP's superiority and was thus maintained as part of the standard reaction condition. Decreasing nucleophile equivalents (entry 11) provided slightly lower yield and longer reaction times but retained high enantioselectivity for **I-122a**.

## I-6-2   Optimization of Amide Functional Handle

Next, we examined the nature of the amide on the performance of the reaction (Table I-4). Comparing to the standard substrate **I-70a**, electronic perturbations to the aryl of the amide group did not alter the course or results of the reactions, delivering products **I-122b** to **I-122f** in good yields and high enantioselectivity (entries 1-6, Table-4). The acetamide substrate **I-70g**, though sluggish, provided the chloroamidation product **I-122g** with good enantiocontrol (94% *ee*). Nonetheless, the results were inferior in terms of yield, enantiopurity of product, and time to completion of the reaction in comparison to arylamide substrates **1a-1f**. Interestingly, the *E* aliphatic substrate **1h** was nonreactive without HFIP, but reacted under the standard condition to yield product **2h** in good yield and high enantioselectivity (entry 8).

**Table I-4:** Amide functional handle optimization



| Entry | prd | time (h) | $R_1$ | $R_2$ | $R_3$ | Yield (%)[a] | ee (%)[b] |
|-------|-----|----------|-------|-------|-------|----------|--------|
| 1 | **I-122a** | 0.5 | $p$NO$_2$-C$_6$H$_4$ | C$_3$H$_7$ | H | 90 | 99 |
| 2 | **I-122b** | 2.0 | Ph | C$_3$H$_7$ | H | 81 | 98 |
| 3[c] | **I-122c** | 0.5 | $p$OMe-C$_6$H$_4$ | C$_3$H$_7$ | H | 89 | 99 |
| 4 | **I-122d** | 0.5 | $p$F-C$_6$H$_4$ | C$_3$H$_7$ | H | 85 | 99 |
| 5 | **I-122e** | 0.5 | $p$t-Bu-C$_6$H$_4$ | C$_3$H$_7$ | H | 79 | 99 |
| 6 | **I-122f** | 0.5 | $p$NO$_2$-C$_6$H$_4$ | C$_3$H$_7$ | H | 91 | 99 |
| 7 | **I-122g** | 18 | Me | C$_3$H$_7$ | H | 58 | 94 |
| 8 | **I-122h** | 5 | $p$NO$_2$-C$_6$H$_4$ | H | C$_3$H$_7$ | 81 | 97 |
| 9[c] | **I-122i** | 5 | $p$NO$_2$-C$_6$H$_4$ | H | C$_3$H$_7$ | 59 | 95 |

[a]Isolated yield on a 0.1 mmol scale. [b]Enantiomeric excess determined by chiral HPLC. [c]Absolute stereochemical determination was verified by x-ray crystal analysis. Diastereoselectivity was >20:1 for all examples

## I-6-3  Alternative Functional Handles

The requirement for a secondary amide substrate was briefly examined (Figure I-33) with the analogous imide **I-70j**, ester **I-70k**, and N-methylated tertiary amide **I-70l** (Scheme 1). Substrates **I-70j** and **I-70k** yielded their respective chloroamide products **I-122j** and **I-122k**, respectively, albeit with less enantiocontrol than the aryl amide substrates, while requiring a higher catalyst loading (10 mol%). The anticipated chloroamide product was not observed upon treatment of **I-70l** under slightly modified conditions (10 mol% catalyst instead of 1 mol%, and 0 °C instead of -30 °C), but instead chloroester **I-122l''** was isolated in good yield. As depicted in Scheme 1, **I-122l''** is presumably obtained from the hydrolysis of the postulated intermediate **I-122l'**. Taken together, these results not only indicate the need for a hydrogen bonding element supplied by the 2° amide,
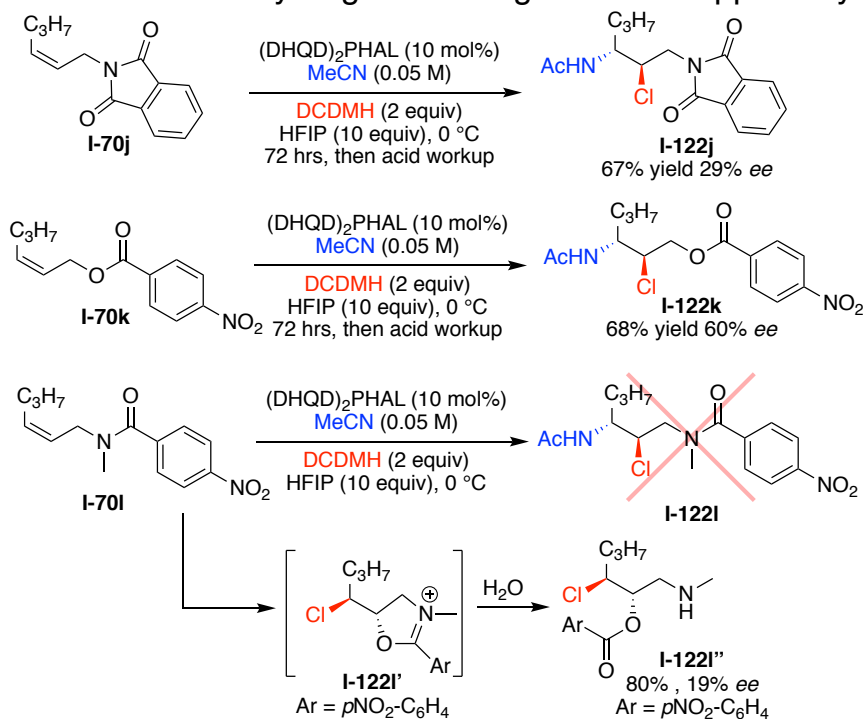


**Figure I-33**: Exploration of alternative functional handles for enantioselective chloroamidation reactions

but also the amide confirmation presumably plays a significant role in the success of these asymmetric catalytic reactions. The modest result from allyl-ester **I-70k**

serves as a potential new substrate to explore with previous chemistry as esters offer facile deprotection to the corresponding alcohol.

## I-6-4 Substrate Scope of the Ritter-Type Asymmetric Chloroamidation Reaction

Figure I-34 illustrates the results of the substrate scope for *E* and *Z* aliphatic allyl-amides. In all cases, the minor diastereomer was not observed. *Z*-olefins reacted smoothly to yield the corresponding chloroamide products in high yields, enantioselectivities (99% *ee* for all examples), and regioselectivities. This was true of the less electronically biased examples **I-70o** and **I-70p**, which often result in lower performance due to inductive changes in polarity, leading to regioisomeric products.[55-56] The extended reaction time required for **I-70p** led to the over-chlorinated product **I-122p'** (resulting from the α-chlorination of the acetamide moiety) in ~2:1 ratio (**I-122p'**:**I-122p**).
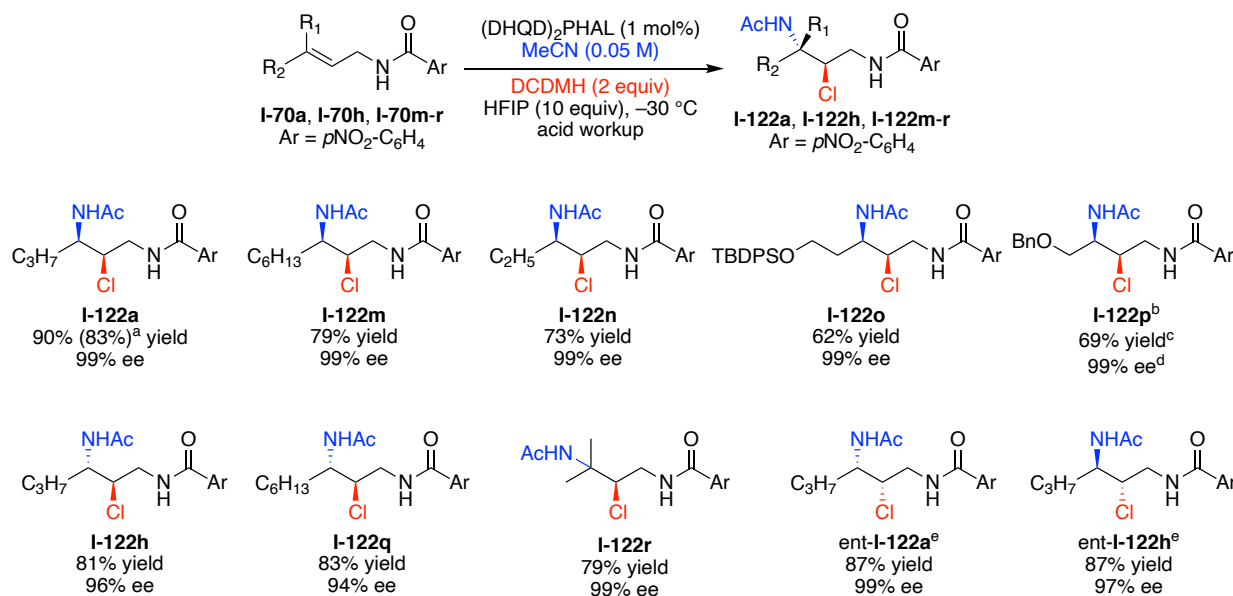


Unless otherwise noted, reactions are isolated yields on 0.1 mmol scale. Enantiomeric Excess determined by chiral HPLC [a]Isolated yield on a 1.0 mmol scale. [b]15 mol% (DHQD)$_2$PHAL was added over the course of the reaction (3 days), maintaining the temperature at 0 °C. [c]Combined yield of the acetamide product and the alpha-chlorinated acetamide product. [d]Both acetamide and alpha-chlorinated acetamide were obtained with 99% ee. [e]Reaction performed with quasi-enantiomeric (DHQ)$_2$PHAL.

**Figure I-34:** Aliphatic substrate scope of allyl amides for chloroamidation

The same success was observed for the corresponding *E*-isomeric substrates, providing the chloroamide products with slightly less enantiocontrol (≥94% *ee*) and excellent yields of products **I-122h** and **I-122q**. The tri-substituted allyl amide **I-70r** was also not problematic, providing the product **2r** in high yield as well as high *ee* (entry 8). The quasi-enantiomeric (DHQ)$_2$PHAL catalyst gave comparable results for the *Z* and *E* isomeric substrates **1a** and **1h**, yielding *ent* **I-122a** and *ent* I-**122h**, in 99% *ee* and 97% *ee*, respectively.

Aryl substituted allyl amide substrates proved more problematic, leading to diastereomeric products, presumably as a result of carbocationic stabilization afforded by the aromatic group (Figure I-35).[27-28] As expected, the more electron rich systems, having the ability to stabilize the benzylic carbocation, resulted in lower selectivity for products **I-122s**, **I-122t**, and **I-122u** while the electron deficient *p*CF$_3$-Ph substituent **I-70v** restored the high diastereomeric selectivity observed with the alkyl systems **I-122v**. Similar to **I-70p**, the extended reaction time required for full conversion of **I-70v** to the product led to a-chlorination of the acetamide functionality as the major product (~5:1 **I-122v'**:**I-122v**). Nonetheless, while the chloroamidation of electron rich aryls led to low *dr*s, each diastereomer wasisolated in high enantiomeric excess, suggesting the olefinic face selectivity is not reduced.

Neither the *E*-substituted alkene **I-70w**, nor the trisubstituted alkene **I-70x** were immune to the observed diminished diastereoselectivity, although in both cases high enantioselectivity of their products were maintained. The reduced yield for product **I-122w** was attributed to competing intramolecular halocyclization, not observed with *Z* alkenes. The quasi-enantiomeric (DHQ)₂PHAL provided *ent*-**I-122s** and *ent*-**I-122w** with similar efficiencies in all categories.



**I-70s-I-70x**
Ar = $p$NO$_2$-C$_6$H$_4$

(DHQD)$_2$PHAL (1 mol%)
MeCN (0.05 M)
DCDMH (2 equiv)
HFIP (10 equiv), −30 °C
acid workup

**I-122s-I-122x**
Ar = $p$NO$_2$-C$_6$H$_4$

**I-122s**
95% yield
65:35 *dr*
99% ee for both diastereomers

**I-122t**
92% yield
66:34 *dr*
98% ee minor 97% ee major

**I-122u**
78% yield
50:50 *dr*
99% ee for both diastereomers

**I-122v**[a]
78% yield[b]
>20:1 *dr*
89% ee[c]

**I-122w**
53% yield
74:26 *dr*
93% ee minor 99% ee major

**I-122x**
57% yield
61:39 *dr*
99% ee minor 97% ee major

*ent*-**I-122s**[d]
84% yield
63:37 *dr*
99% ee for both diastereomers

*ent*-**I-122w**[d]
66% yield
70:30 *dr*
93% ee minor 99% ee major

**I-122y**
55% yield[e]
94% ee

Isolated yields on a 0.1 mmol scale. Diastereomeric ratio determined by NMR. Enantiomeric excess determined by chiral HPLC. [a] 15 mol% (DHQD)$_2$PHAL was added over the course of the reaction, maintaining the temperature at 23 °C. [b] Combined yield of acetamide product and αalpha-chlorinated acetamide product. [c] The alpha-chlorinated acetamide product had enantiomeric excess of 87%. [d] Reaction performed with quasi-enantiomeric (DHQ)$_2$PHAL. [e] No trace of Ritter product

**Figure I-35:** Aromatic substrate scope for allyl-amide chloroamidation

We were surprised to discover that when subjected to haloamidation conditions, the 4-methoxy substituted phenyl ring **I-70y** yielded the 6-endo halocyclization product and no Ritter-product (Figure I-36). The reaction proceeded with decent enantioselectivity and yield. The relative stereochemistry of the major diastereomer was confirmed via x-ray crystallography as formally a syn addition of
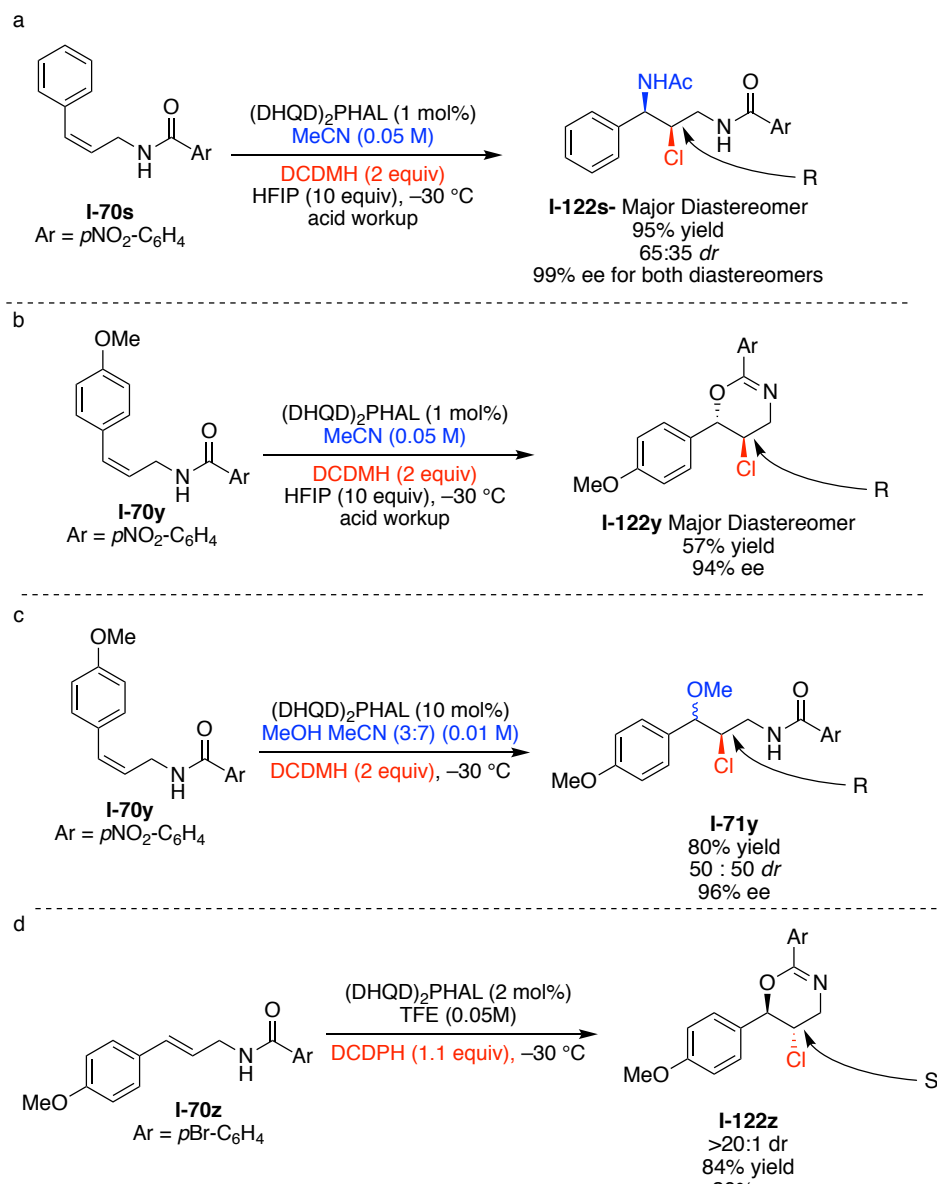


**Figure I-36:** Divergent reactivity in electron rich aromatic systems (a) Halo-Ritter chemistry (b) Attempt of halo Ritter chemistry on highly electron rich system (c) Haloetherification chemistry with highly electron rich systems (d) Stereochemical result of asymmetric chlorocyclization

the chlorenium and oxygen nucleophiles. The absolute stereochemistry matches the chlorenium olefin face selectivity of the Ritter products. This is the opposite face selectivity observed for the (DHQD)$_2$PHAL catalyzed halocyclization of E allyl amides providing **I-122z** (Figure I-36d).[26] It should also be recognized that 4-methoxy phenyl substituted alkenes are known to proceed via a carbocation intermediate.[23] Both Z and E allyl amides providing the same major diastereomer for the 6 endo cyclization suggest that they both proceed via a carbocation and Z substrate's intermediate is susceptible to bond rotation to the less strained intermediate to minimize gauche interactions. These observations suggest that the reaction is proceeding through a mechanism similar to the Ritter-type reaction for chlorenium transfer, yet acetonitrile is not incorporated in the product. Further research in this area is ongoing.

## I-6-5   Preliminary Efforts to Improve Diastereoselectivity in the Asymmetric Chloroamidation Aryl Substituted Ally-Amides

Reminiscent to other intermolecular halofunctionalizations originating in our laboratory, we suffered from deteriorated diastereoselectivity with electron-rich substrates, possessing diastereomeric ratios as poor as 1:1 (Figure I-37).[23] The deterioration of diastereoselectivity was well correlated with the alkene's *HalA*, with **I-70u** possessing a *HalA* of 142.8 kcal/mol that is approaching the *HalA* of DCDMH of 150.0 kcal/mol. We hypothesized that the correlation of diastereoselectivity results from two separate competing mechanisms shown as pathway 1 and pathway 2 below (Figure I-38A). Pathway 1 is a concerted *NAAA* addition and preferences that anti-product through transition state. We rationalize that this is the pathway for electron-poor alkenes that do not possess a high enough *HalA* to abstract the chlorenium ion from the chlorenium donor without a nucleophile's assistance in a concerted mechanism. Conversely, for electron rich alkenes, the

*HalA* is high enough to abstract the chlorenium ion without the nucleophile's assistance and proceeds through a classical stepwise mechanism with a carbocation intermediate. The subsequent carbocation may be attacked from either face, leading to a reduction in diastereoselectivity.

We noticed that our diastereoselectivities for the Ritter-product were lower than those observed for haloetherification reactions.[25] Recognizing that a 3:7 co-solvent methanol acetonitrile mixture is employed in the reaction, we postulated
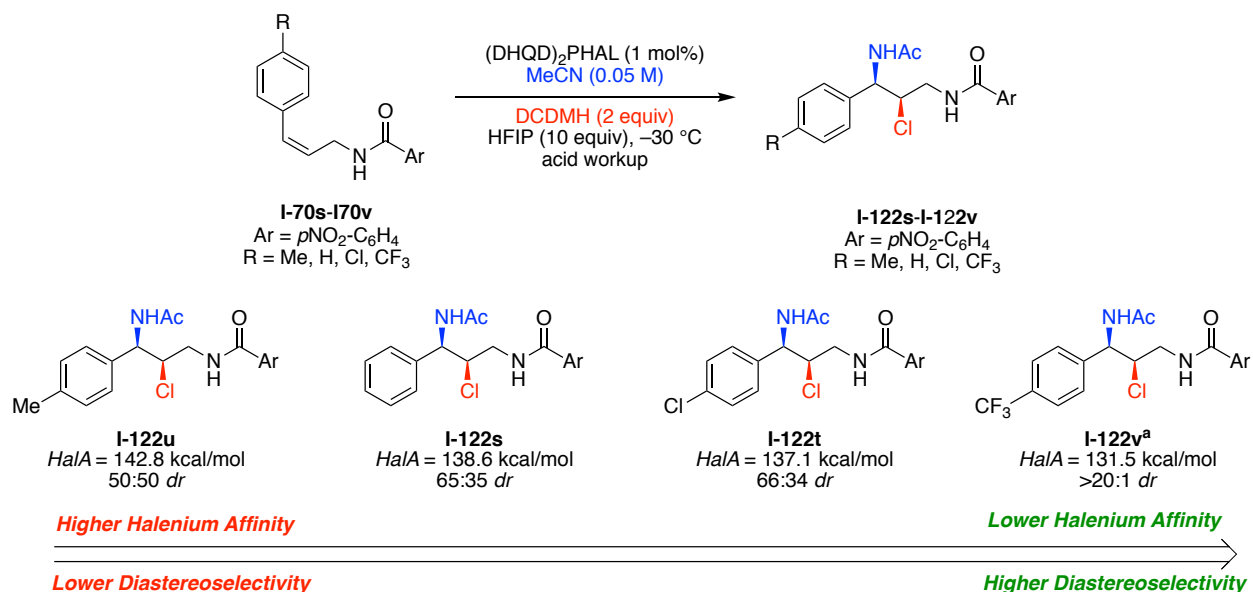


**Figure I-37:** Correlation between alkene *HalA* and diastereoselectivity of halo-Ritter product
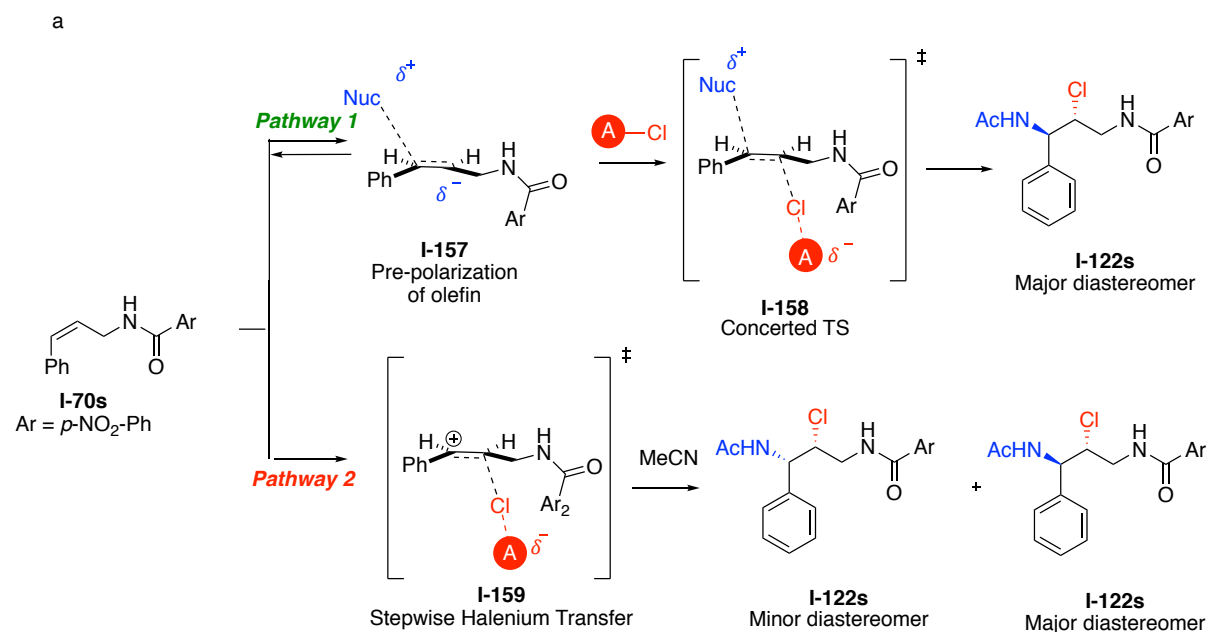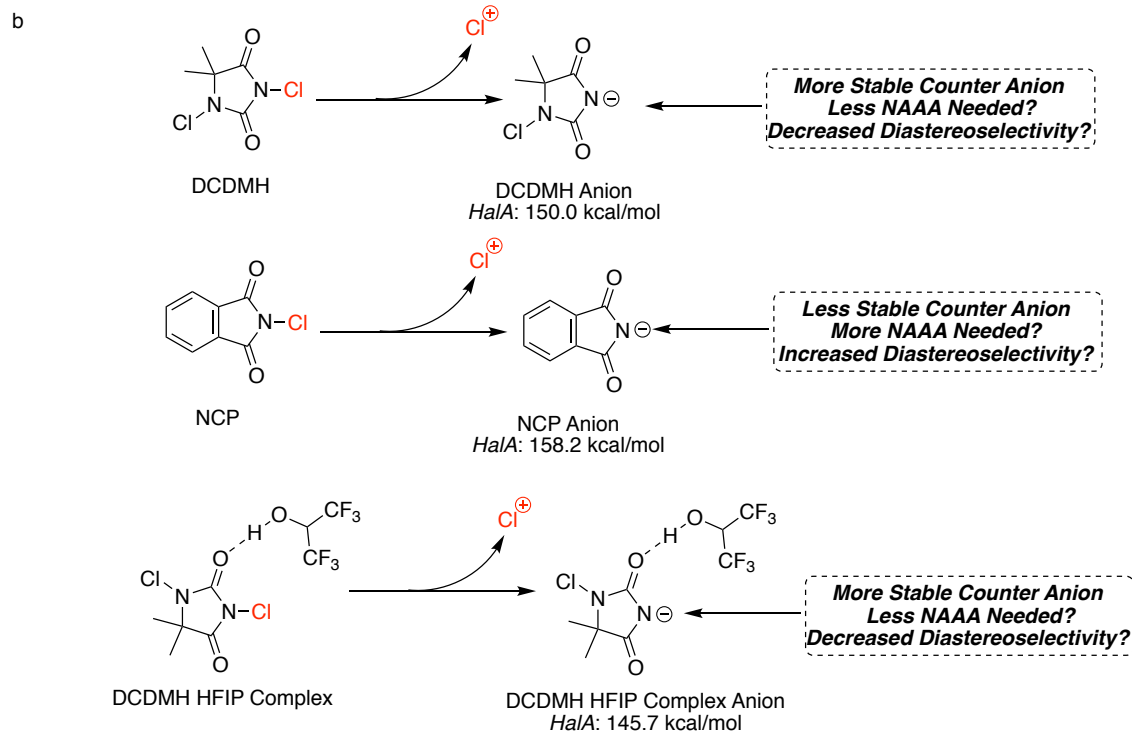
**Figure I-38:** (a) *NAAA* explanation for reduction of diastereoselectivity in halofunctionalizations (b) Potential methods to modulate Halenium affinity of the donor to favor pathway 1

that methanol is a stronger nucleophile, and this stronger nucleophile might, in fact, play in role in improved diastereoselectivity making pathway 1 (Figure I-38a) more likely. As discussed earlier, we hypothesized that the major diastereomer (anti-addition) results from a concerted pathway minor diastereomer might be the result of a carbocationic stepwise pathway that is more likely with a weaker nucleophile such as acetonitrile. We postulated that a less potent chlorenium source would be more likely to proceed through a *NAAA* pathway (Figure I-38b). The summary of our initial efforts is displayed in Table I-5. In an effort to induce a nucleophile assisted concerted mechanism, we employed the less reactive NCP (N-chlorophthalimide) (*HalA* 158.2 kcal/mol) as a chlorenium donor (entry 2-3). To our displeasure, the reaction with the less reactive NCP actually provided a lower diastereoselectivity than the more reactive DCDMH. It should be noted that the sluggish nature of this reaction required slightly elevated temperatures to reach completion. Recognizing that proton donors can stabilize the chlorenium donor's

**Table I-5:** Attempt to improve diastereoselectivity by modulating *HalA* of the chlorenium donor
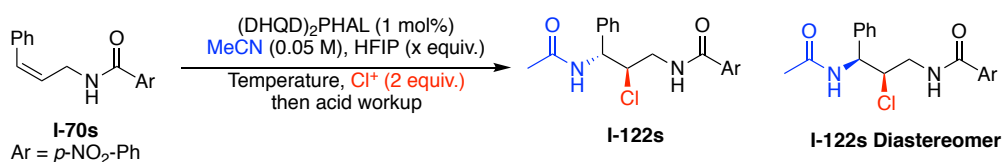


| Entry | Temperature °C | HFIP (equiv.) | Cl+ | d.r[a] |
|---|---|---|---|---|
| 1 | -30 | 10 | DCDMH | 65:35 |
| 2 | 23 | 10 | NCP | 63:37 |
| 3 | -30 | 100 | NCP | 61:39 |
| 4 | -30 | 2 | DCDMH | 66:34 |
| 5 | -30 | 100 | DCDMH | 63:37 |

a. Determined by crude NMR

counteranion, tweaking the proton source's ability to stabilize the chlorenium donor's counteranion can modify the donor's halenium affinity. This effect is seen is with the halenium affinity of DCDMH decreased by 4.3 kcal/mol via hydrogen bonding with HFIP (Figure I-38b). In theory, this hydrogen bonding can temper the propensity to proceed via a stepwise pathway. Additionally, HFIP possesses a

lower pKa than methanol, rendering it superior at activating the chlorenium source than methanol, suggesting that the large excess of HFIP might be responsible for the reduction in diastereoselectivity in chloroamidations relative to chloroetherifications. Modifying equivalents of HFIP proved to be unfruitful (entries 4-5), proving nearly the same diastereoselectivity. While we were displeased with the inability to improve diastereoselectivity via alteration of chlorenium donor halenium affinity, this observation matches the studies performed by Dr. Sarkar on catalytic asymmetric chloroetherifications. He suggested that the halenium ion is transferred to the (DHQD)$_2$PHAL catalyst when protic solvents are present and is then transferred to the alkene. This mechanistic picture provides the same terminal halenium source (quinuclidine) rendering the identity of the initial chlorenium donor a non-participant in transfer of the chlorenium ion to the alkene in transition state **I-160** (Figure I-39).
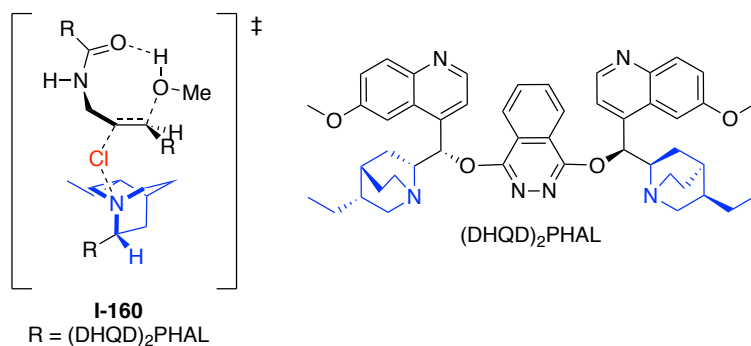


**Figure I-39:** Proposed transition state for enantio-selective chloroetherification of allyl-amides

**NAAA Mechanism**

**Classical Mechanism**

**I-158**
Concerted TS
*Less Polar Transition State*
**Favored in a non-polar solvent?**

**I-159**
Stepwise Rxn
*More Polar Transition State*
**Favored in a Polar Solvent?**
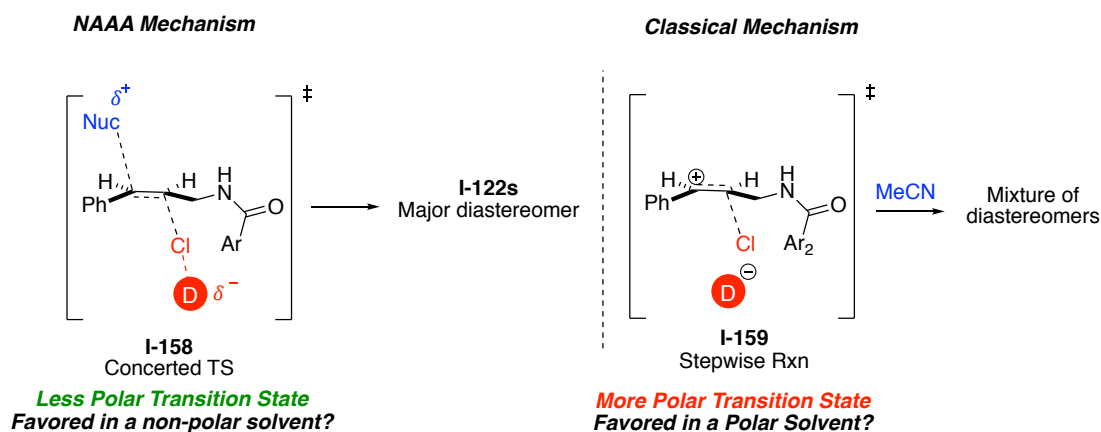
**Figure I-40:** Effort to improve diastereoselectivity by employing a nonpolar cosolvent

We next directed our attention to the possibility that the reaction is proceeding through the same mechanism regardless of chlorenium source. We hypothesized that if the pathway to the minor diastereomer was due to a non-*NAAA* pathway, we could disfavor this highly polarized transition state by employing a non-polar co-solvent (Figure I-40). Non-polar cosolvents dichloromethane and hexane were added in an attempt to improve diastereoselectivity (Table I-6). We observed no notable changes in diastereoselectivity correlated with the polarity or ratio of the cosolvent employed.

**Table I-6:** Solvent polarity and diastereoselectivity
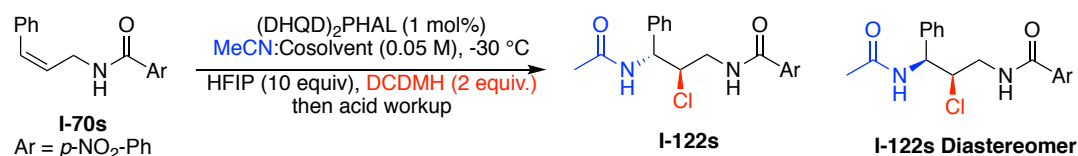


| Entry | Cosolvent | MeCN:Cosolvent | $dr^a$ |
|-------|-----------|----------------|--------|
| 1 | none | NA | 65:35 |
| 2 | DCM | 9:1 | 65:35 |
| 3 | DCM | 7:3 | 63:37 |
| 4 | Hexane[b] | 9:1 | 67:33 |
| 5 | Hexane[b] | 7:3 | 66:34 |

a Diastereomeric ratio determined by crude NMR. b Acetonitrile hexane mixtures are not miscible at low temperature

58

## I-6-6    Varied Nitrile Nucleophiles

The next variable examined was the nitrile nucleophile, yielding different amide products (Figure I-41). Reactions of **I-70a** proceeded smoothly with propionitrile (**I-122aa**), benzonitrile (**I-122ab**), and the bulky pivalonitrile (**I-122ac**). Although the latter two reactions required slightly higher temperatures (0 °C and 23 °C, respectively) to accommodate the higher melting points of their respective nitrile solvents, we did not observe erosion in enantioselectivities. The versatility in choosing different nitrile nucleophiles enables the assembly of more complex amide structures.
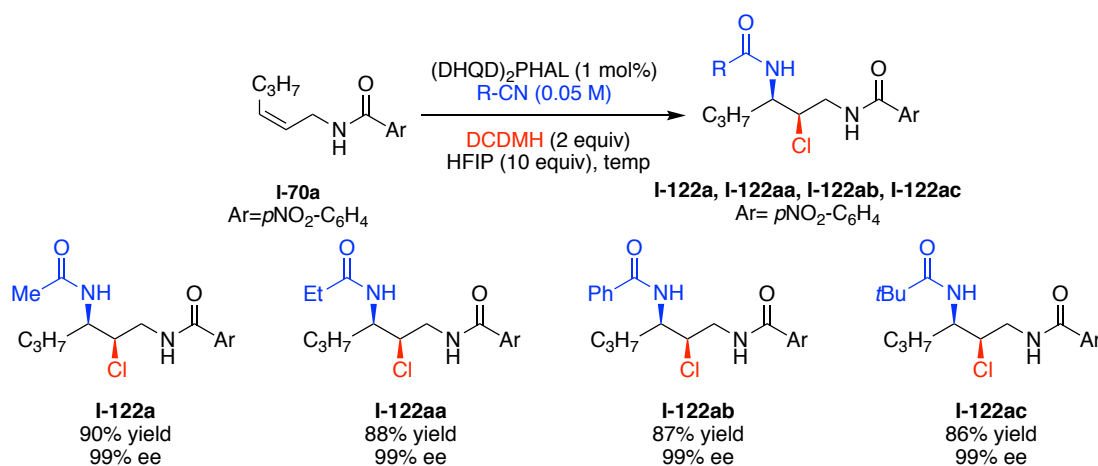


**Figure I-41:** Substrate Scope with varied nitrile nucleophiles

## I-6-7    Catalyst Loading Study for Less Reactive Allyl-Amide I-70v

a



| Entry | R | (DHQD)₂PHAL (mol %) | ee (%) |
|-------|------|------|------|
| 1 | H | 1 | 99 |
| 2 | CF₃ | 1 | 54 |
| 3 | CF₃ | 5 | 90 |
| 4 | CF₃ | 10 | 93 |

b



| Entry | (DHQD)₂PHAL % | catalyst/DCDMH exposure time | Yield (%) | ee |
|-------|------|------|------|------|
| 1 | 1 | None | 76 | 99 |
| 2 | 1 | 48 h | 48 | 1 |
| 3 | 0 | NA | 0 | NA |
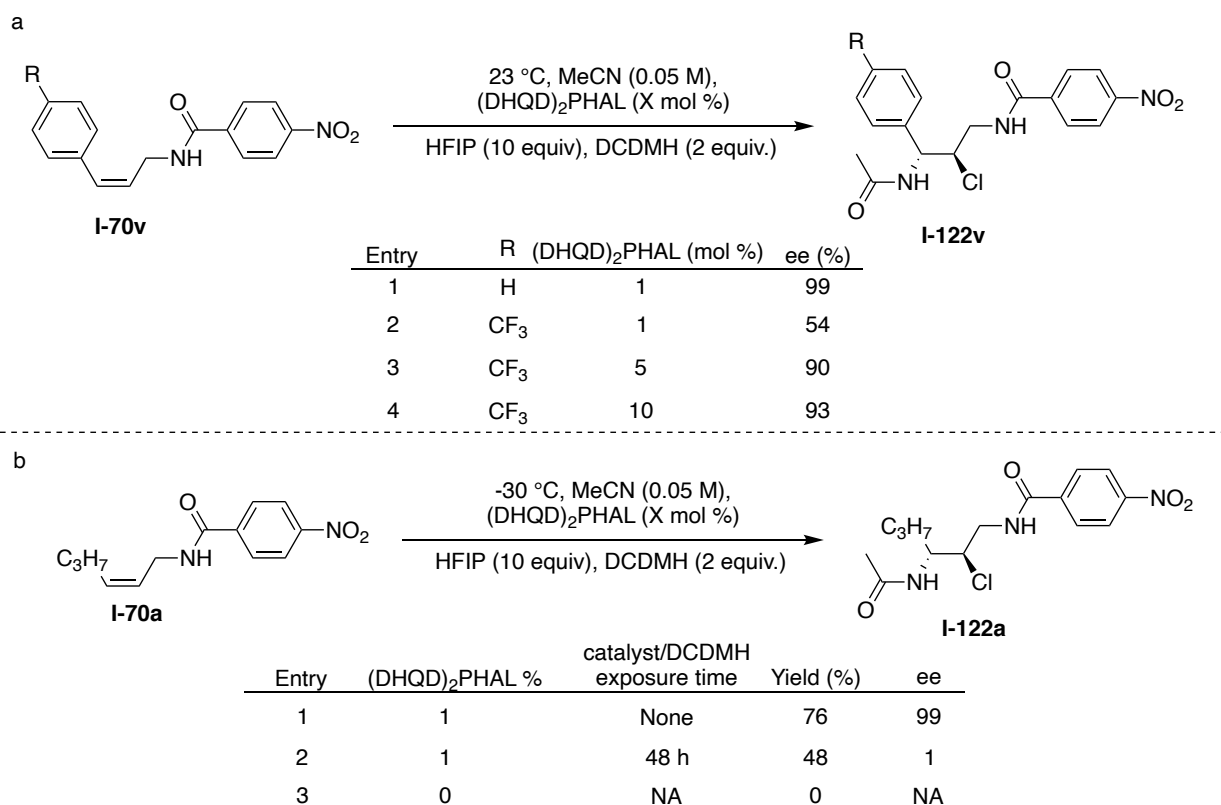
**Figure I-42:** (a) Influence of catalyst loading on **I-70v** relative to **I-70s**. (b) Catalyst incubation study

Optimization studies for **I-70a** showed no decrease in enantioselectivity when the catalyst loading was decreased from 10 mol% to 1 mol%. Many aryl-substituted substrates (**I-70s**, **I-70u**, **I-70w**, **I-70x**) were compatible with these conditions and returned products with enantiomeric excess greater than 90%. When these reaction conditions were extended to the less reactive substrate **II-70v**, the enantiomeric excess decreased to 53% and the rate of the reaction decreased significantly relative to the other aryl substrates (48 h relative to 6 h). When catalyst loading was increased to 5 mol%, modest levels of enantioselectivity were restored. We hypothesized that the decrease in enantiocontrol may be the result of catalyst degradation under reaction conditions. To test this hypothesis, we subjected (DHQD)₂PHAL to reaction conditions for 48 h at room temperature. After 48 h, the reaction mixture was cooled to –30 °C and **I-70a** was added

(note **I-70a** leads to the product **I-122a** in 99% *ee* under optimized conditions). These conditions provided nearly racemic product (entry 2). Nonetheless, the catalyst is still necessary to form the product as no reaction was observed without catalyst (entry 3). We speculate that the catalyst degradation is occurring via chlorination of the quinoline moiety as the C5 position has a halenium affinity of 165.9 kcal/mol (Figure I-43).[22]



(DHQD)$_2$PHAL

*HalA* = 165.9 kcal/mol
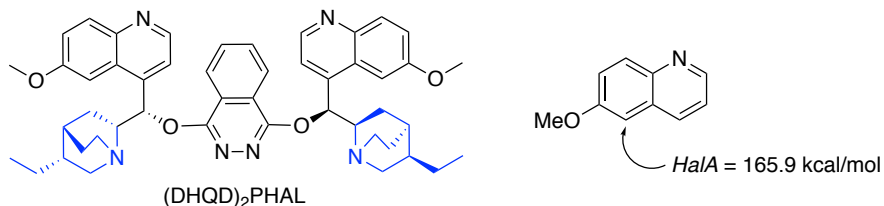
**Figure I-43:** *HalA* of quinoline ring

## I-6-8   Structural Determination of Ritter Trapped Product

Early studies of reaction conditions on **I-70a** revealed that the transformation was not proceeding through a traditional Ritter-type pathway, which would undergo a nitrilium trap by water and provide **I-122a**. Interestingly, mass spectrometry revealed the reaction was undergoing a nitrilium trap by 3-chloro-5,5-dimethylhydantoin, the residue left after chlorenium transfer. The ^{1}H NMR spectrum was complicated, hinting at multiple products, none of which were identified as **I-122a**. This trapped product underwent hydrolysis to provide the amide products previously described. This observation leads to ambiguity of which potential nucleophilic center or centers on the chlorenium donor attacked the

nitrilium cation as it could be the nitrogen atom, or either of the carbonyl oxygen atoms (see structures **I-162a**, **I-163**, and **I-164** in Figure I-43).
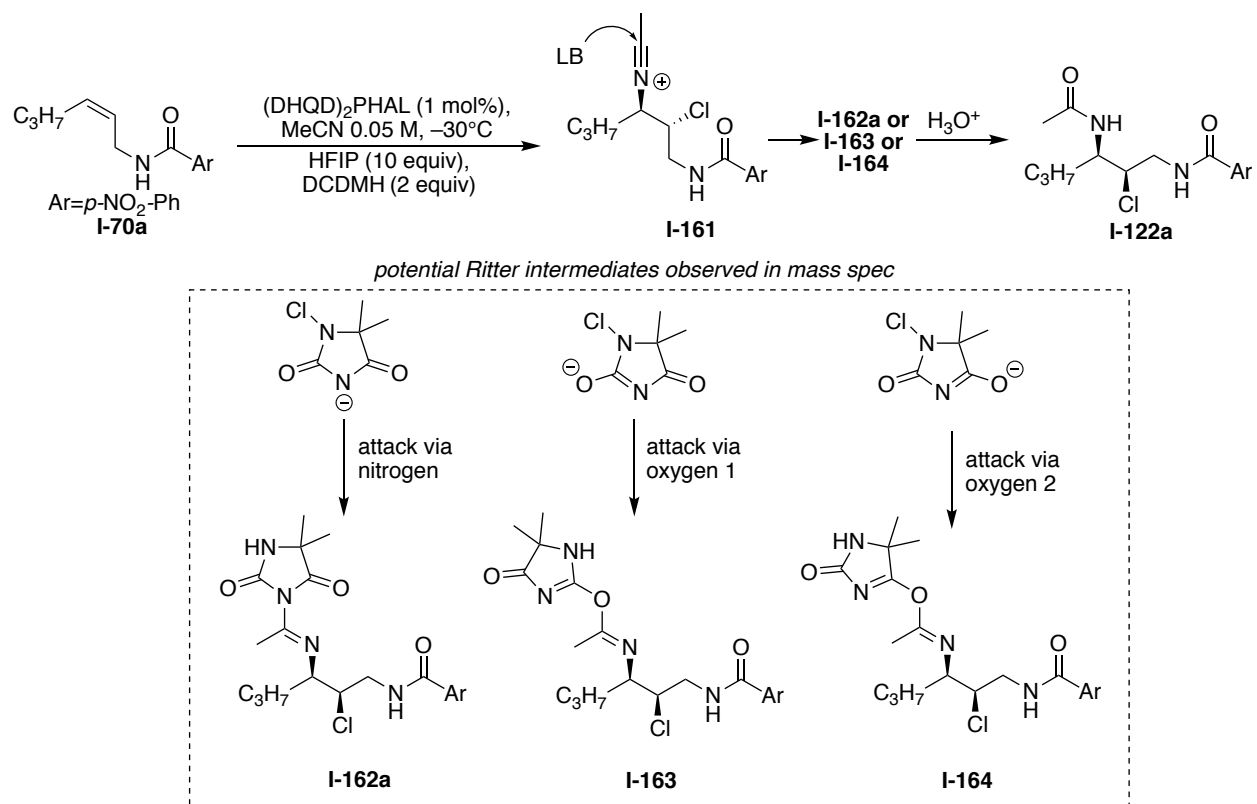


**Figure I-44:** Potential Ritter intermediates

The acid lability of the Ritter intermediate obtained from acetonitrile made analysis of the intermediate challenging. The Ritter intermediate formed when pivalonitrile was employed as a nucleophile was stable under column chromatography (SiO$_2$/EtOAc–Hexanes gradient) and provided two products that could be isolated and analyzed by NMR. These two products were determined to be in equilibrium with each other as 30 min after initial isolation, the formerly pure products began to interconvert back to being the original mixture. This led to the hypothesis that a single product with two roto-isomeric structures such as **I-162a** and **I-162b** were isolated. Interestingly, **I-165**, obtained from the reaction of **I-70a** with pivalonitrile, with NCS as the chlorenium source exhibits only

one rotomeric product, owing to its symmetrical nature (Figure I-45).  This provides further proof that the mixture obtained above is in fact due to rotomeric equilibria, and not the result of having a mix of products as a result of nitrogen and oxygen atoms as nucleophiles.
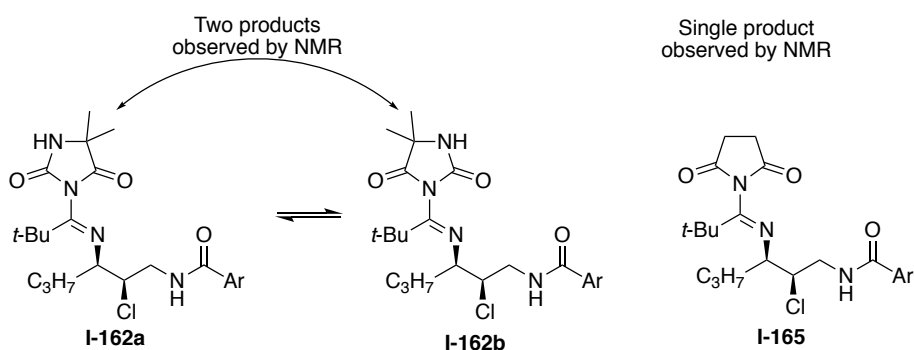


**Figure I-45:** Hypothesis of rotomeric equilibria of a single intermediate
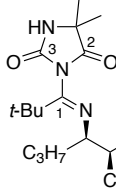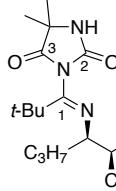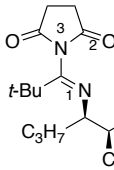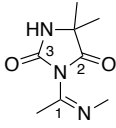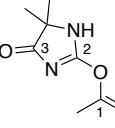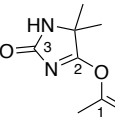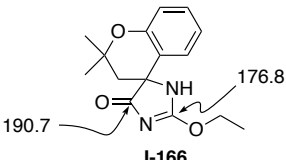
To conclusively determine the structure of the Ritter intermediates, experimentally observed ^{13}C resonances were compared to those obtained for **I-165** and also computationally calculated chemical shifts anticipated for all scenarios.  Comparison of the observed ^{13}C NMR to a computationally generated (EDF2-6-31g*) NMR of simplified substrates (**I-162a** analog, **I-162b** analog, **I-163** analog, and **I-164** analog) were used to predict the structure of the Ritter intermediate. The oxygen atom attack analogs (**I-163** and **I-164**), lead to resonances that do not fit the observed chemical shifts for **I-162 or I-162a**. The validity of the computed chemical shifts was corroborated with examples from the literature for accuracy.  The computed chemical shift for C3 in the **I-163**-analog (190.2 ppm) is much further downfield as compared to other carbonyl carbons in the series investigated.  Fortuitously, a similarly situated carbonyl carbon shown in structure **I-166** has a chemical shift in the same range,[57] thus corroborating the calculations.  The

experimentally observed resonances for **I-165**, along with the calculated chemicals shifts for **I-162** analogs fit well with the observed chemical shifts for **I-162a** and **I-162b**, thus suggesting that not only the nitrogen atom is the nucleophilic participant, but also, the observed mixture is, as described above, a consequence of a rotomeric equilibrium.

## I-6-8-1    Computational details for NMR calculations

All calculations presented in this article were performed using the Spartan'18 (Spartan 18; Wavefunction Inc.: Irvine, CA) software package.  NMR calculations for **I-162a/b**-analog, **I-163**-analog, and **I-164**-analog commenced with finding optimum geometry using a MonteCarlo search function.  The best conformer was then subject to DFT optimization at the B3LYP/6-31G* level.  The geometry optimized structures were then recalculated with EDF2-6-31G* to obtain NMR values.

**Table I-7:** Experimental (**I-162a**, **I-162b**, and **I-165**) and calculated $^{13}$C-NMR values for potential Ritter intermediates



$^{13}$C-resonances (ppm)

|  | I-162a | I-162b | I-165 | I-162a/b analog | I-163 analog | I-164 analog |
|---|---|---|---|---|---|---|
| C1 | 155.4 | 155.3 | 156.5 | 151.7 | 153.3 | 151.7 |
| C2 | 175.3 | 153.5 | 175.1 | 173.5 | 176.3 | 179.0 |
| C3 | 154.9 | 177.0 | 176.6 | 155.6 | 190.2 | 166.0 |

*outlier chemical shifts*

**I-166**
known chemical shifts
see reference 2

## I-6-9   Catalyst Control of Product Formation

**Table I-8:** Catalyst control over product formation
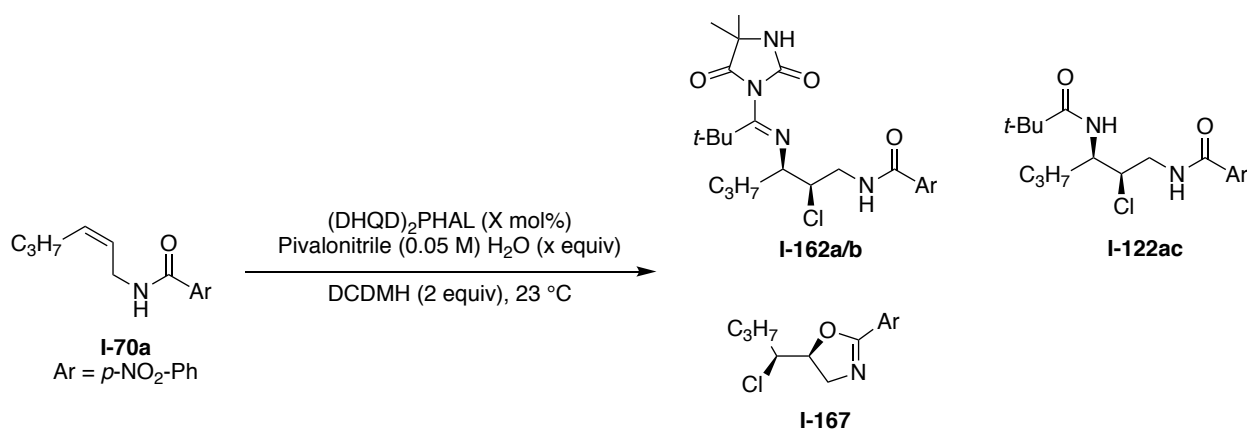


| Entry | Catalyst loading (mol %) | H₂O (equiv) | I-162:I-122ac:I-167 |
|-------|--------------------------|-------------|---------------------|
| 1 | 10 | 0 | 83:6:11 |
| 2 | 0 | 0 | 0:37:63 |

As discussed in **Section I-6-8**, under standard reaction conditions the Lewis base of the chlorenium donor traps the nitrilium ion intermediate (Table I-8 entry 1) to yield **I-122a'** before acid workup. However, when **I-70a** was exposed to pivalonitrile and DCDMH *without* (DHQD)₂PHAL (entry 2), **I-162a/b** was not observed.  In fact, Ritter product **1-122ac**, the result of trapping the nitrilium ion by water, along with the cyclized **I-168**, the product of the non-Ritter intramolecular pathway was isolated. This divergent reaction path hints at an associative complex between the (DHQD)₂PHAL and DCDMH. This associative complex was first observed in seminal halo-lactonization reactions. Subjection of (DHQD)₂PHAL with benzoic acid and dichlorohydantoin (Figure I-46) resulted in diastereotopic splitting of the methylene hydrogens (H$_A$ and H$_B$) of dichlorohydantoin. As an achiral molecule, the diastereotopic splitting indicates that the hydantoin is in the chiral pocket of the catalyst as either complex **I-168** or **I-169**.

Preliminary studies by Dr. Sarkar suggest that the chlorenium ion transfers to the quinuclidine in polar solvents.[24] Interestingly, this catalyst control was not observed with dichloramine-t initiated Ritter reactions which provided the counteranion trapped product with and without the catalyst (Section I-6-10).
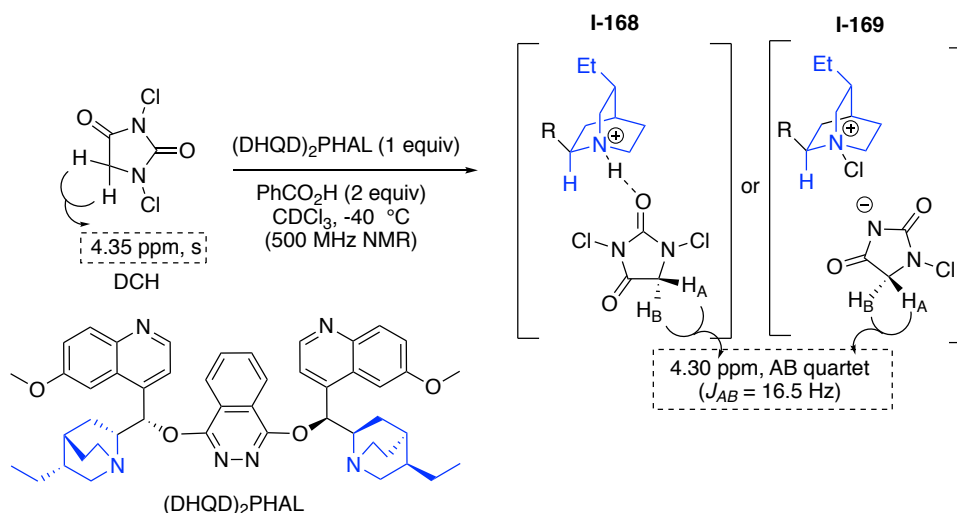


**Figure I-46:** Complexation of DCH with (DHQD)$_2$PHAL

## I-6-10  Redirecting Nitrilium Ion Trap to Provide Precious Diamine Products

The tertiary amidine intermediate **I-122a'** that is directly formed in the DCDMH induced Ritter reaction underwent facile hydrolysis to provide the vicinal chloroamide product **I-122**. We sought to redirect the nitrilium intermediate in our Ritter reactions to directly provide a synthetically useful product. The employment of a 1° amine chlorenium source enables straightforward downstream synthesis of synthetically useful and biologically significant moieties such as enantiopure imidazolines **I-171** and diamines **I-172** (Figure I-47b) through the intramolecular S$_N$2 displacement of the stereodefined chlorine.[58-59] The success of catalytic

enantioselective diamination chemistry is limited (relative to dihydroxylation, epoxidation, aziridination etc.) as diamination products lead to product inhibition
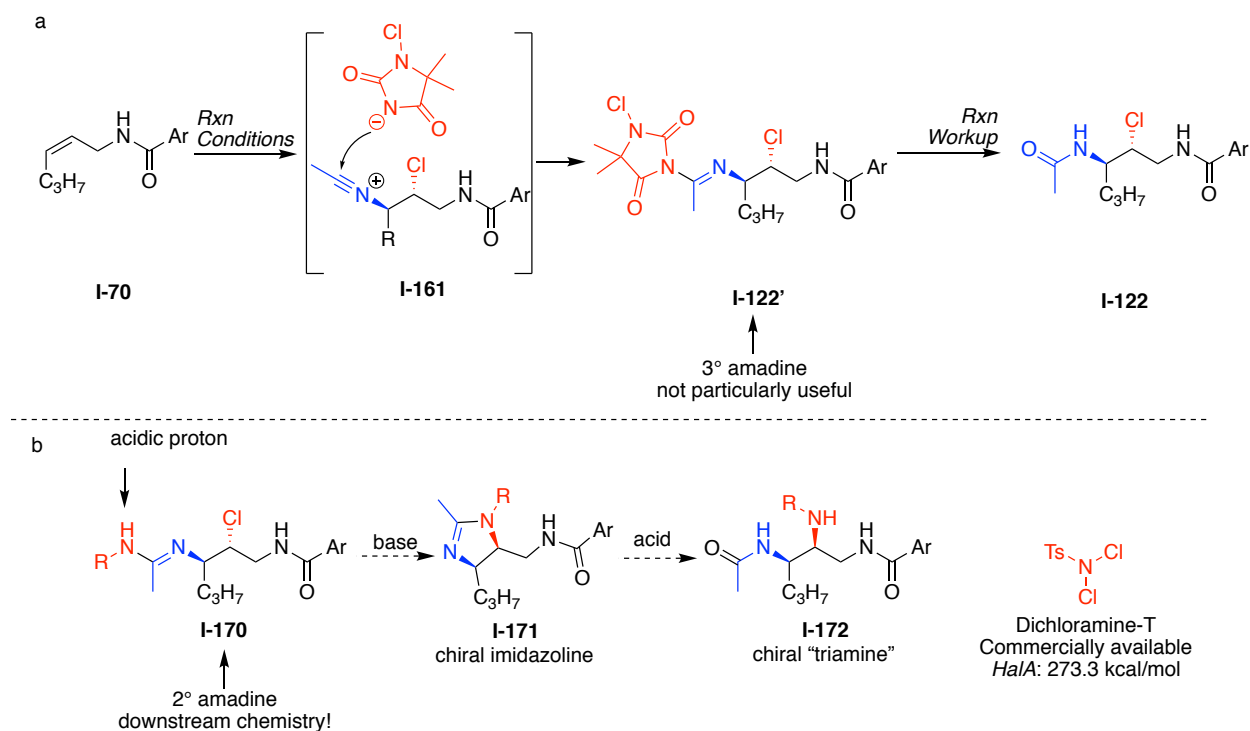


**Figure I-47:** (a) Hydrolysis of tertiary amidine products to provide amides. (b) Redirection of nitrilium intermediate to provide useful products

via chelation with metal catalysts. Recent publications report groundbreaking catalytic asymmetric advancements providing direct synthesis of diamine products from alkenes[60-68] however, the substrate scope is often limited to styrenyl alkenes. An orthogonal approach to these valuable molecules is high interest. We were led to this work when upon the employment of dichloramine-T as a chlorenium source for the chloroamide products (see Table I-3, entry 7). Although reaction conversion was high, analysis of the reaction products led to the identification of the corresponding chlorosulfonylamidine, which results from the capture of the nitrilium ion intermediate with the sulfonylamadine generated upon transfer of the halogen.

# I-6-11 Optimization of Dichloramine-T Chloroamidations

A quick screen led to a slight modification from conditions used in the Ritter-type reactions with DCDMH (Table I-9). Standard conditions used with DCDMH led to a 5.4:1 **173h**:**174h** ratio (entry 1). Not surprisingly, increasing equivalents of HFIP worsened the selectivity (entry 2). As illustrated in entry 3, however, omission of HFIP to eliminate the side product **1-174h** reduces the enantioselectivity of **I-173h**, similar to reactions that employed DCDMH as the chlorenium source. Interestingly, increased equivalents of dichloramine-T greatly enhanced the

**Table I-9:** Optimization of Dichloramine-T Chloroamidations



| Entry | (DHQD)$_2$PHAL (mol %) | DiCh-T (equiv.) | HFIP (equiv.) | Yield **I-173h** (%)[a] | **I-173h:I-174h**[b] | ee (%)[c] **I-173h** |
|-------|------------------------|-----------------|---------------|-------------------------|----------------------|----------------------|
| 1 | 1 | 1.00 | 10 | 43 | 5.4:1 | 94 |
| 2 | 1 | 2.00 | 20 | 39 | 2.6:1 | 94 |
| 3 | 1 | 2.00 | 0 | 45 | NA | 62 |
| 4 | 1 | 3.00 | 10 | 49 | 16:1 | 92 |
| 5 | 1 | 1.25 | 10 | 50 | 2.6:1 | 95 |
| 6 | 5 | 2.00 | 10 | 59 | >20:1 | 96 |

[a]NMR yield on a 0.05 mmol scale [b]Ratios determined by crude NMR. [c]Enantiomeric Excess determined by chiral HPLC

product ratio (16:1, **173h**:**174h**), while maintaining high *ee* (entry 4). Further verification of the latter was the observed diminution of the same ratio (2.6:1) when 1.25 equivalent of dichloramine-T was employed (entry 5). Alternatively, increase in the amount of catalyst (from 1 mol% to 5 mol%), without increasing dichloramine-T (2 equivalents), led to the same high product ratio (entry 6). It is likely that 4h originates from the trap of the nitrilium intermediate, as incubation of **I-173h** in neat HFIP over a prolonged period did not return any **I-174h**.

## I-6-12 Dichloramine-T Mediated Chloroamidination Scope

Figure I-48 lists a short survey of substrates that highlights a similar level of efficiency for the dichloramine-T mediated reaction that yield the



**I-70**
Ar= $p$NO$_2$-C$_6$H$_4$

(DHQD)$_2$PHAL (5 mol%)
MeCN (0.05 M)

Dichloramine-T (2.0 equiv)
HFIP (10 equiv), −30 °C

**I-173**
Ar= $p$NO$_2$-C$_6$H$_4$

**I-173a**
71% yield
>20:1 *dr*
99% *ee*

**I-173h**
65% yield
>20:1 *dr*
95% *ee*

**I-173p**
71% yield
>20:1 *dr*
96% *ee*

**I-173s**
71% yield[a]
>61:39 *dr*
99% *ee* major
97% *ee* minor

Isolated yields yield on a 0.10 mmol scale. *dr* are obtained from NMR of crude reaction mixture. Enantiomeric excess determined by chiral HPLC. (a) NMR yield on 0.05 mmol scale

**Figure I-48:** Dichloramine-T mediated chloroamidination scope

chlorosulfonylamidines as compared to the chloroamides obtained with DCDMH. Z and E aliphatic allyl amides **I-70a** and **I-70h** are converted to their corresponding products 3a and 3h in good yields and high enantiomeric excess (99% and 95%, respectively). The benzyl protected allylic alcohol **I-70p** also returned product **I-173p** with no observable evidence for regio-isomeric products, in high enantiomeric excess (entry 3). As previously detailed, the aryl substituted olefin **I-70s** was more problematic, leading to diastereomeric products, although with high *ee* for each isomer.

## I-6-13 Elaborations of Chlorosulfonylamidines

The utility of the sulfonylamide product **I-173a** was demonstrated via its cyclization to form the imidazoline **I-175a** (Figure I-49). This product was then easily hydrolyzed to the chiral tri-amine **I-176a** upon treatment with dilute HCl,

yielding the orthogonally protected triamine product with two contiguous chiral centers. This could be of synthetic value, as there are few known methods to deliver chiral triamines,[18] in addition, this allows for orthogonal protection. Also illustrated in Figure, is the conversion of **I-70a** to **I-177a**, using dimethylcyanimide as the nucleophile, en route to the cyclic guanidine **I-178a**. The enantioselectivity obtained in the asymmetric transformation is maintained in subsequent reaction for both sequences described below.
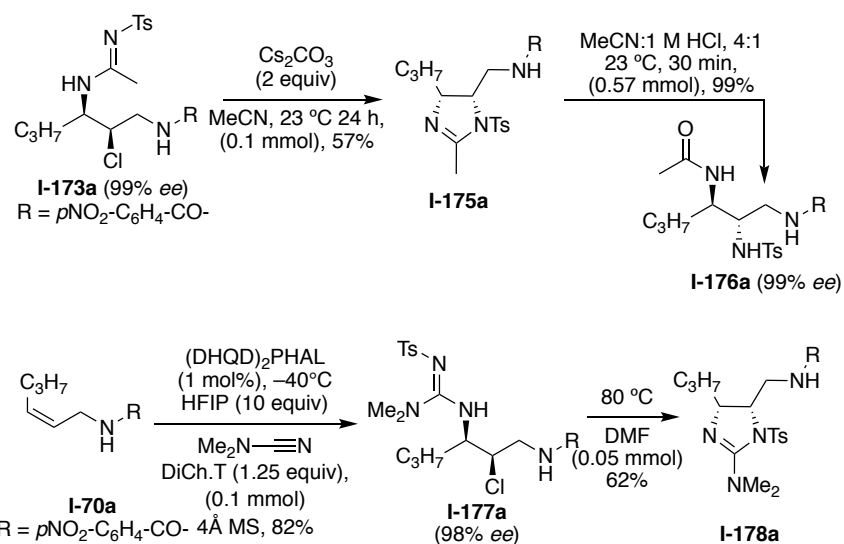


**Figure I-49:** Chloroamidine elaborations to precious enantiopure chiral diamine products

## I-7  Conclusion

The stereodefined carbon nitrogen bond is important in synthesis and biology. Unfortunately, it is largely inaccessible via alkene halofunctionalization. The historic limitations of halenium induced amination reactions are derived from the high halenium affinity of the nitrogen atom which out competes the alkene for the halenium ion. We employed the *HalA* scale to identify acetonitrile as a potential nucleophile in this chemistry due to its attenuated halenium affinity which falls below the range of alkenes. We

envisioned this reaction proceeding through a Ritter-type pathway, enabling a nucleophile assisted pathway that can tolerate electron poor unactivated alkenes. While other haloamination reactions exist, many of them proceed through a stepwise "pronucleophile" pathway that necessitates alkenes with high halenium affinity. Furthermore, we were able to display the versatility of the nitrilium ion by intercepting it with alternative chlorenium donors which led to the synthesis of precious diamine products with high enantioselectivity. We hope that this example will enable scientists to design difunctionalization reactions with a comprehension of the affinity an electrophile might have for a nucleophile in a three-component reaction. Additionally, this is the first example of a Ritter-type reaction in the literature, thus expanding the toolbox to forge stereodefined carbon nitrogen bonds.

## I-8  Experimental Section

### I-8-1  Materials and General Instrumentations

Commercially available reagents were purchased from Sigma-Aldrich or Alfa-Aesar and used as received. $CH_2Cl_2$ and acetonitrile were freshly distilled over $CaH_2$ prior to use. THF was distilled over sodium-benzophenone ketyl. All other solvents were used as purchased. DCDMH was purified by recrystallization in chloroform. Dichloramine-T was purchased from TCI and used without further purification. Enantiomeric excess for all products was determined by HPLC analysis using DAICEL Chiralcel® OJ-H and OD-H or Chiralpak® IA, AD-H, and AS-H columns. Optical rotations of all products were measured in chloroform. All substrates prior to section I-6 were synthesized in the cited work. Allyl amides **I-70a**, **I-70f**, **I-70h**, **I-70i**, **I-70m-p**, **I-70r**, **I-70s**, **I-70u**, **I-70v** were

71

synthesized as reported previously and analytical data matched reported values.[27] Substrates **I-70b-e**, **I-70g**, **I-70k**, **I-70l**, **I-70q**, **I-70t**, **I-70u**, **I-70x** were synthesized by the same procedure described for substrates above, and provided overall yields ranging from 40-60%. Analytical data for the new substrates can be found below in Section I-9.

## I-8-2 General procedure for the catalytic asymmetric chloroamidation of unsaturated amides with DCDMH to yield vicinal chloroamides
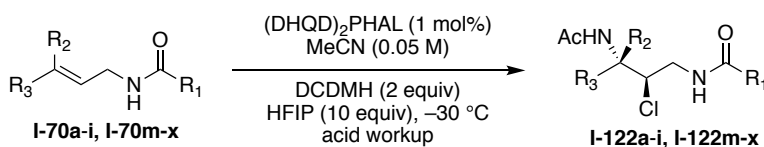


**Figure I-50:** General procedure for the catalytic asymmetric chloroamidation of unsaturated amides with DCDMH to yield vicinal chloroamides

The substrate (**I-70a-i**, **I-70m-x)** (0.1 mmol, 1.0 equiv) and (DHQD)$_2$PHAL (0.8 mg, 1 mol%) were suspended in acetonitrile (2 mL) in a test tube with a magnetic stir bar and capped with a rubber septa. HFIP (105 $\mu$L, 1.0 mmol, 10 equiv) was added via syringe. The resulting suspension was cooled to –30 °C in an immersion cooler. After stirring for 10 min, DCDMH (39.4 mg, 0.2 mmol, 2 equiv) was added. The reaction was monitored by TLC and upon competition was quenched by the addition of saturated Na$_2$S$_2$O$_3$ (2 mL). The reaction was concentrated to remove acetonitrile and the resultant aqueous layer was extracted with DCM (3 x 5 mL). The combined organics were concentrated. To the concentrated vial with a stir bar, acetonitrile (1 mL) and a solution of HCl (1 M, 0.2 mL) were added and stirred for 5 min. Water (3 mL) was added and the solution was concentrated in vacuo and extracted with DCM (3 x 5 mL). The combined organic layers

were dried with anhydrous $Na_2SO_4$ and concentrated. Column chromatography (SiO$_2$/EtOAc–Hexanes gradient) provided the desired product (**2a-i**, **2m-x**).

## I-8-3   Procedure for the catalytic asymmetric chloroamidation of 1a with DCDMH and 10 equivalents of acetonitrile to yield vicinal chloroamides
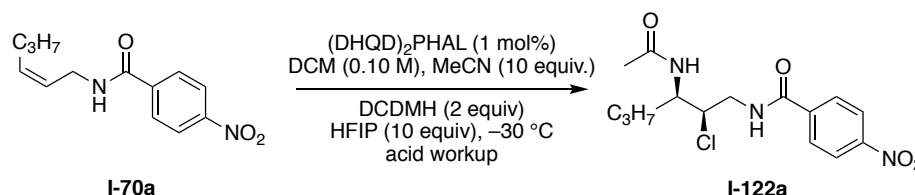


**Figure I-51:** Procedure for the catalytic asymmetric chloroamidation of **1a** with DCDMH and 10 equivalents of acetonitrile to yield vicinal chloroamides

The substrate **I-70a** (12.4. mg, 0.05 mmol, 1.0 equiv) and (DHQD)$_2$PHAL (0.4 mg, 1 mol%) were suspended in dichloromethane (0.5 mL) in a test tube with a magnetic stir bar and capped with a rubber septa. HFIP (50 $\mu$L, 0.50 mmol, 10 equiv) and acetonitrile (26 $\mu$L, 0.50 mmol, 10 equiv) were added via syringe. The resulting suspension was cooled to –30 °C in an immersion cooler. After stirring for 10 min, DCDMH (19.7 mg, 0.10, mmol, 2 equiv) was added. The reaction was monitored by TLC and upon competition was quenched by the addition of saturated $Na_2S_2O_3$ (2 mL). The resultant aqueous layer was extracted with DCM (3 x 5 mL). The combined organics were concentrated. To the concentrated vial with a stir bar, acetonitrile (1 mL) and a solution of HCl (1 M, 0.2 mL) were added and stirred for 15 min. Water (3 mL) was added and the solution was concentrated in vacuo and extracted with DCM (3 x 5 mL). The combined organic layers were dried with anhydrous $Na_2SO_4$ and concentrated. Column chromatography

(SiO$_2$/EtOAc–Hexanes gradient) provided the desired product **I-122a** (53% yield with triphenylmethane NMR standard, 99% *ee*).

## I-8-4   Procedure for the chloroamidation of allyl-phthalimide 1j and allyl-ester 1k substrates
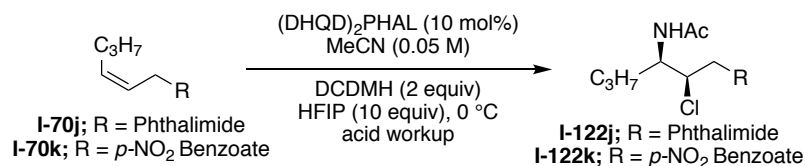


**Figure I-52:** Procedure for the chloroamidation of allyl-phthalimide **1j** and allyl-ester **1k** substrates

The substrate (**I-70j, I-70k**) (0.1 mmol, 1.0 equiv) and (DHQD)$_2$PHAL (7.8 mg, 10 mol%) were suspended in acetonitrile (2 mL) HFIP (105 $\mu$L, 1.0 mmol, 10 equiv) was added via a syringe. The resulting suspension was cooled to 0 °C in an immersion cooler. After stirring for 10 min, DCDMH (39.4 mg, 0.2 mmol, 2 equiv) was added. Upon completion, the reaction was quenched by the addition of saturated Na$_2$S$_2$O$_3$ (2 mL). The reaction was concentrated to remove the acetonitrile and the resultant aqueous layer was extracted with DCM (3 x 5 mL). The combined organics were concentrated. To the concentrated product in the vial with a stir bar, acetonitrile (1 mL) and a solution of HCl (1 M, 0.2 mL) were added and stirred for 15 min. Water (3 mL) was added and the solution was concentrated and extracted with DCM (3 x 4 mL). The combined organic layers were dried with anhydrous Na$_2$SO$_4$ and concentrated. Column chromatography (SiO$_2$/EtOAc–Hexanes gradient) provided the desired product (**I-122j**, **I-122k**).

## I-8-5 Procedure for the 1 mmol scale catalytic asymmetric chloroamidation of unsaturated amides with DCDMH to yield vicinal chloroamides
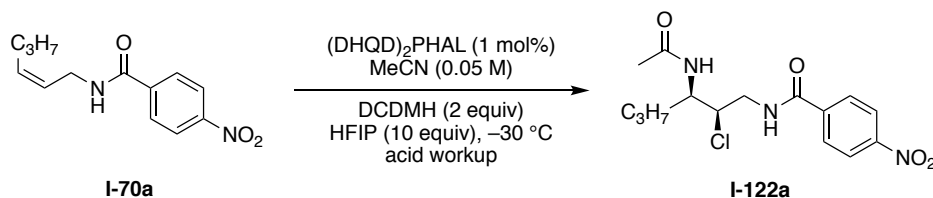


**Figure I-53:** Procedure for the 1 mmol scale catalytic asymmetric chloroamidation of unsaturated amides with DCDMH to yield vicinal chloroamides

The substrate **I-70a** (248.0 mg, 1.0 mmol, 1.0 equiv) and (DHQD)$_2$PHAL (7.8 mg, 1 mol%) were suspended in acetonitrile (20 mL) in a test tube with a magnetic stir bar and capped with a rubber septa. HFIP (1.05 mL, 10.0 mmol, 10 equiv) was added via syringe. The resulting suspension was cooled to –30 °C in an immersion cooler. After stirring for 10 min, DCDMH (394.0 mg, 2 mmol, 2 equiv) was added. The reaction was monitored by TLC and upon competition was quenched by the addition of saturated Na$_2$S$_2$O$_3$ (10 mL). The reaction was concentrated to remove acetonitrile and the resultant aqueous layer was extracted with DCM (3 x 10 mL). The combined organics were concentrated. To the concentrated vial with a stir bar, acetonitrile (5 mL) and a solution of HCl (1 M, 1 mL) were added and stirred for 15 min. Water (3 mL) was added and the solution was concentrated in vacuo and extracted with DCM (3 x 5 mL). The combined organic layers were dried with anhydrous Na$_2$SO$_4$ and concentrated. Column chromatography (SiO$_2$/EtOAc–Hexanes gradient) provided the desired product **I-122a** (282.0 mg, 83% yield, 99% *ee*).

## I-8-6  General procedure for the chloroamidation of allyl-amides with different nitrile solvents
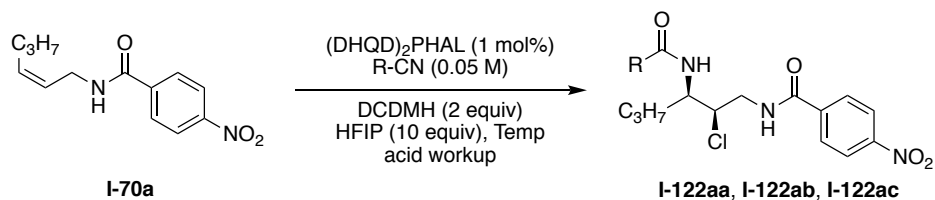


**Figure I-54:** General procedure for the chloroamidation of allyl-amides with different nitrile solvents

The substrate **I-70a** (24.8 mg, 0.1 mmol, 1.0 equiv) and (DHQD)$_2$PHAL (0.8 mg, 1 mol%) were suspended in a nitrile solvent (2 mL) in a test tube with a magnetic stir bar and capped with a rubber septa. HFIP (105 $\mu$L, 1.0 mmol, 10 equiv) was added via syringe. The reaction mixtures were then cooled to a temperature to accommodate the freezing point of the solvent (I-12**2aa**: –30 °C, **I-122ab**: 0 °C, **I-122ac**: 23 °C). After stirring for 10 min, DCDMH (39.4 mg, 0.2 mmol, 2 equiv) was added. The reaction was monitored by TLC and upon competition was quenched by the addition of saturated Na$_2$S$_2$O$_3$ (2 mL). The resultant aqueous layer was extracted with DCM (3 x 5 mL). The combined organics were concentrated. To the concentrated vial with a stir bar, acetonitrile (1 mL) and a solution of HCl (1 M, 0.2 mL) were added and stirred for 15 min. Water (3 mL) was added and the solution was concentrated in vacuo and extracted with DCM (3 x 5 mL). The combined organic layers were dried with anhydrous Na$_2$SO$_4$ and concentrated. Column chromatography (SiO$_2$/EtOAc–Hexanes gradient) provided the desired product (**I-122aa**, **I-122ab**, **I-122ac**).

## I-8-7 General procedure for the catalytic asymmetric chloroamidination of unsaturated amides with dichloramine-T as the chlorinating reagent to yield vicinal chlorosulfonylamidines
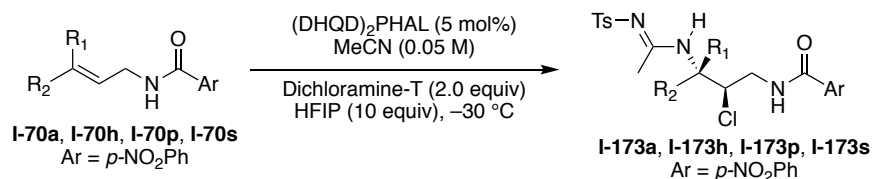


**Figure I-55:** General procedure for the catalytic asymmetric chloroamidination of unsaturated amides with dichloramine-T as the chlorinating reagent to yield vicinal chlorosulfonylamidines

The substrate (**I-70a**, **I-70h**, **I-70p**, **I-70s**) (0.1 mmol, 1.0 equiv) and (DHQD)$_2$PHAL (3.9 mg, 5 mol%) were suspended in acetonitrile (2 mL) in a test tube with a magnetic stir bar and capped with a rubber septa. HFIP (105 $\mu$L, 1.0 mmol, 10 equiv) was added via syringe. The resulting suspension was cooled to –30 °C in an immersion cooler. After stirring for 10 min dichloramine-T (48.0 mg, 0.2 mmol, 2 equiv) was added. The reaction was monitored by TLC and upon completion was quenched by the addition of saturated Na$_2$S$_2$O$_3$ (2 mL). The reaction was concentrated to remove acetonitrile and the resultant aqueous layer was extracted with DCM (3 x 5 mL). The combined organic layers were dried with anhydrous Na$_2$SO$_4$ and concentrated. Column chromatography (SiO$_2$/EtOAc–Hexanes gradient) provided the desired product (**I-173a**, **I-173h**, **I-173p**, **I-173s**).

## I-8-8 Procedure for the synthesis of enantiomeric mixtures of chloroamide compounds for HPLC separations
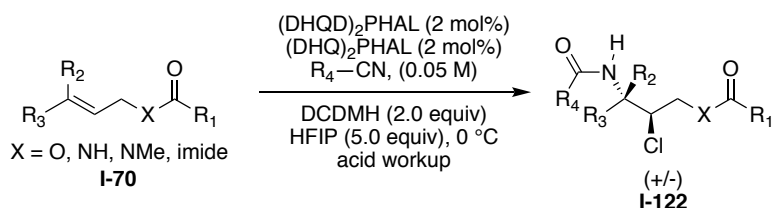


**Figure I-56:** Procedure for the synthesis of enantiomeric mixtures of chloroamide compounds for HPLC separations

The enantiomeric mixtures used for HPLC analysis in determining enantiopurity were synthesized as follows by using the quasi-enantiomeric cinchona alkaloid dimers.

The substrate (**1a-1x**, 0.05 mmol, 1.0 equiv), (DHQD)$_2$PHAL (0.8 mg, 2 mol%), and (DHQ)$_2$PHAL (0.8 mg, 2 mol%) were placed in a test tube with a magnetic stir bar and dissolved in the nitrile solvent of choice (1 mL), capped with a rubber septa. HFIP (25 $\mu$L, 0.25 mmol, 5 equiv) was added via a syringe. The resulting suspension was cooled to 0 ºC in an immersion cooler. After stirring for 10 min, DCDMH (19.7 mg, 0.1 mmol, 2 equiv) was added. The reaction was monitored by TLC and upon competition was quenched by the addition of saturated Na$_2$S$_2$O$_3$ (2 mL). The reaction was concentrated to remove acetonitrile and the resultant aqueous layer was extracted with DCM (3 x 5 mL). The combined organics were concentrated under reduced pressure. To the concentrated vial with a stir bar, acetonitrile (1 mL) and a solution of HCl (1 M, 0.2 mL) were added and stirred for 5 min. Water (3 mL) was added and the solution was concentrated in vacuo and extracted with DCM (3 x 5 mL). The combined organic layers were dried with anhydrous Na$_2$SO$_4$ and concentrated. Column chromatography (SiO$_2$/EtOAc–Hexanes

gradient) provided the desired products as mixture of enantiomers (**I-122a-x, I-122aa, I-122ab, I-122ac**).

## I-8-9 Procedure for the synthesis of enantiomeric mixtures of chloroamidine compounds for HPLC separations
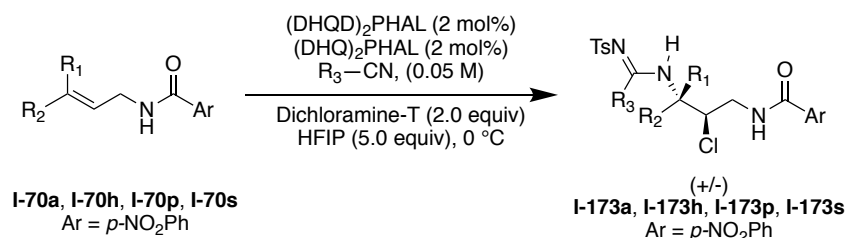


**Figure I-57:** Procedure for the synthesis of enantiomeric mixtures of chloroamidine compounds for HPLC separations

The enantiomeric mixtures used for HPLC analysis in determining enantiopurity were synthesized as follows by using the quasi-enantiomeric cinchona alkaloid dimers.

The substrate (**I-70a, I-70h, I-70p, I70s,** (0.05 mmol, 1.0 equiv), (DHQD)$_2$PHAL (0.8 mg, 2 mol%), and (DHQ)$_2$PHAL (0.8 mg, 2 mol%) were placed in a test tube with a magnetic stir bar and dissolved in the nitrile solvent of choice (1 mL), capped with a rubber septa. HFIP (25 $\mu$L, 0.25 mmol, 5 equiv) was added via syringe. The resulting suspension was cooled to 0 °C in an immersion cooler. After stirring for 10 min, Dichloramine-T (24.0 mg, 0.1 mmol, 2 equiv) was added. The reaction was monitored by TLC and upon competition was quenched by the addition of saturated Na$_2$S$_2$O$_3$ (2 mL). The reaction was concentrated to remove acetonitrile and the resultant aqueous layer was extracted with DCM (3 x 5 mL). The combined organic layers were dried with anhydrous Na$_2$SO$_4$ and concentrated. Column chromatography (SiO$_2$/EtOAc–Hexanes gradient) provided the desired products as mixture of enantiomers (**I-173a, I-173h, I-173p, I-173s, I-177a**).

79

## I-8-10 Procedure for the Determination of the Absolute and Relative Stereochemistry of Vicinal Chlorosulfonylamidine Products

The absolute and relative stereochemistry of chloroamide products **2c** and **2i** were determined by single crystal X-ray diffraction. The stereochemistry of other chloroamide products were inferred. We were unable to obtain crystals for vicinal chlorosulfonylamidine products and resorted to chemical transformations. We observed that the Ritter intermediate **I-122a'** obtained from the hydantoin mediated reaction could be converted to the sulfonylamidine product **I-173a** with the addition of para-toluene sulfonamide (10 equiv) in a stereoretentive reaction. The HPLC trace for **I-173a** obtained by the procedure described in **Section I-8-7** and the HPLC trace of presumed **I-173a**, obtained via the derivatization of **I-122a'** matched, and thus confirmed the absolute stereochemistry of **I-173a** as illustrated. The relative and absolute stereochemistries of **I-173h**, **I-173p**, **I-173s**, **I-174h**, **I-175a**, **I-176a**, **I-177a**, and **I-178a** were inferred as a result of this observation.
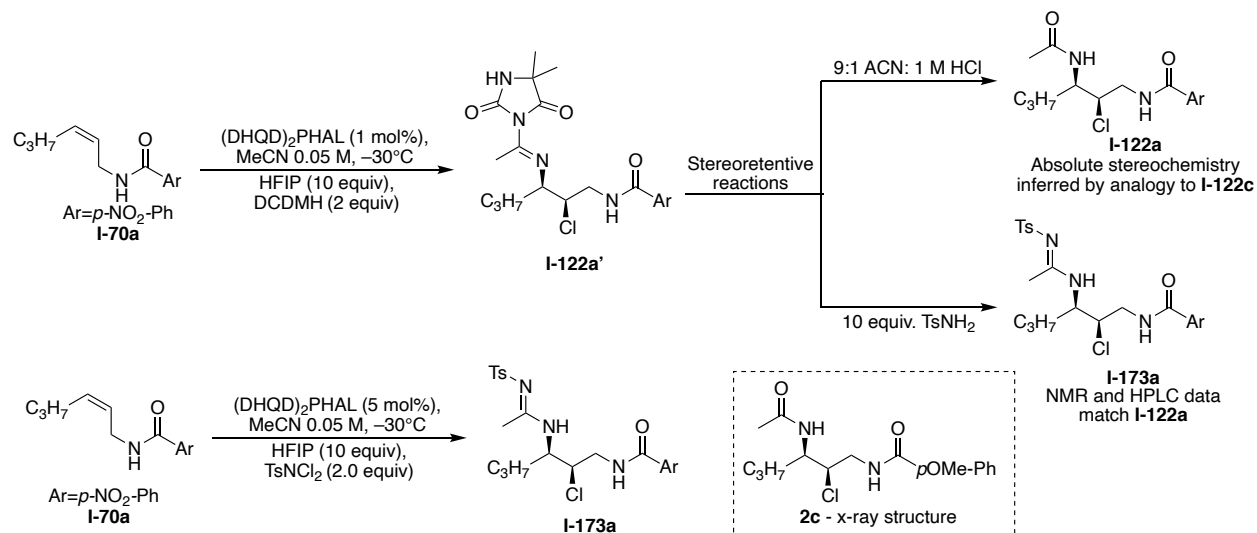
**Figure I-58:** Chemical transformations to determine the absolute stereochemistry of chlorosulfonylamidines
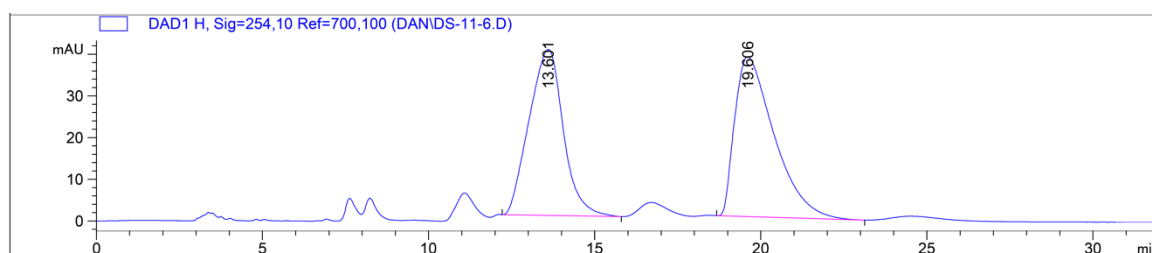


**Figure I-59:** HPLC trace of **I-173a** and ent- **I-173a**
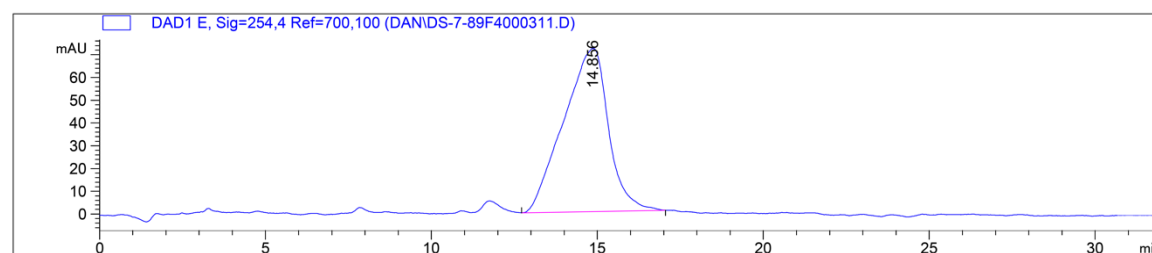


**Figure I-60:** HPLC trace of I-173a following procedure for the chlorosulfonylamidation of allyl amides
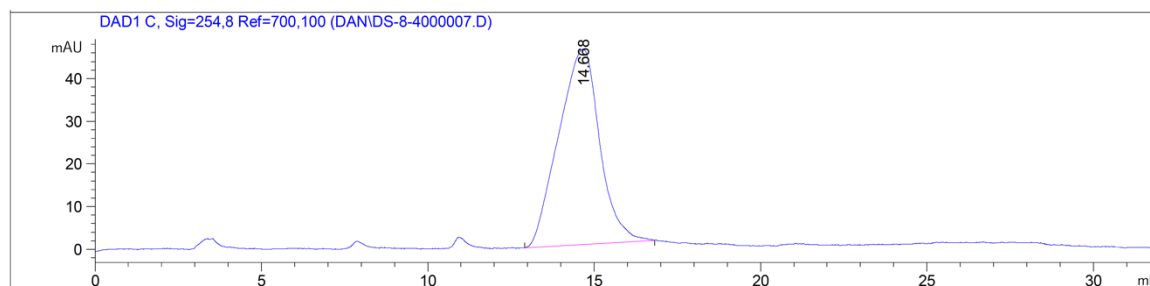
**Figure I-61:** HPLC trace of I-173a obtained from derivatization of I-122a'

## I-9   Analytical Data

### I-9-1   Analytical Data for Chloroamide Products
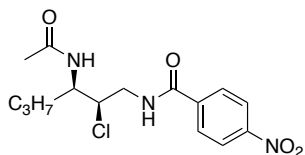


**I-122a**, *N*-((2*R*,3*R*)-3-acetamido-2-chlorohexyl)-4-nitrobenzamide

Compound **I-122a** (30.7 mg, 90% yield, 99% *ee*) was synthesized following the procedure

detailed in Section I-8-2 using **I-70a** (24.8 mg, 0.10 mmol) as starting material.

**R$_f$:** 0.14 (60% EtOAC/Hex)

**$^1$H NMR (500 MHz, CDCl$_3$)** δ 8.35 – 8.27 (m, 3H), 8.08 (d, *J* = 8.6 Hz, 2H), 5.72 (d, *J* =

9.3 Hz, 1H), 4.38 – 4.25 (m, 2H), 4.13 (ddd, *J* = 11.0, 5.2, 1.7 Hz, 1H), 2.93 (ddd, *J* = 13.7,

11.0, 4.3 Hz, 1H), 2.15 (s, 3H), 1.67 (dtd, *J* = 13.8, 8.6, 6.7 Hz, 1H), 1.61 – 1.52 (m, 1H),

1.41 – 1.32 (m, 2H), 0.90 (t, *J* = 7.3 Hz, 3H).

**$^{13}$C NMR (126 MHz, CDCl$_3$)** δ 172.2, 164.8, 149.7, 139.2, 128.4, 123.9, 61.2, 49.4, 42.6,

34.7, 23.3, 19.3, 13.7.

**Resolution of enantiomers:** DAICEL Chiralpak®, AD-H 10% IPA/Hexane 1ml/min, 254

nm, RT 1 (major)=10.6 min, RT 2 (minor) =12.6 min.

**HRMS analysis (ESI):** calculated for [M+H]$^+$: C$_{15}$H$_{21}$ClN$_3$O4: 342.1221; Found: 342.1223

**Optical activity:** [α]$_D^{20}$ = -35.2 (c = 0.4, CHCl$_3$, 99% *ee*)



**I-122b**, *N*-((2*R*,3*R*)-3-acetamido-2-chlorohexyl)benzamide

Compound **I-122b** (24.1 mg, 81% yield, 98% *ee*) was synthesized following the procedure

detailed in Section I-8-2 using **I-70b** (20.3 mg, 0.10 mmol) as starting material.

**R$_f$:** 0.16 (50% EtOAC/Hex)

**$^1$H NMR (500 MHz, CDCl$_3$)** δ 8.00 (dd, *J* = 8.7, 4.5 Hz, 1H),7.92 (d, *J* = 7.0 Hz, 2H), 7.51

(t, *J* = 7.3 Hz, 1H), 7.46 (t, *J* = 7.4 Hz, 2H), 5.69 (d, *J* = 9.4 Hz, 1H), 4.43 – 4.22 (m, 2H),

4.15 (ddd, *J* = 10.8, 5.1, 1.7 Hz, 1H), 2.93 (ddd, *J* = 13.6, 10.8, 4.5 Hz, 1H), 2.14 (s, 3H),

1.69 – 1.60 (m, 1H), 1.54 (dtd, *J* = 13.6, 7.9, 5.5 Hz, 1H), 1.36 (dq, *J* = 15.0, 7.6 Hz, 2H),

0.90 (t, *J* = 7.4 Hz, 3H).

**$^{13}$C NMR (126 MHz, CDCl$_3$) δ** 171.8, 167.0, 133.7, 131.7, 128.6, 127.1, 61.7, 49.2, 42.5,

34.8, 23.2, 19.2, 13.7.

**Resolution of enantiomers:** DAICEL Chiralpak®, AD-H 10% IPA/Hexane 1ml/min, 254

nm, RT 1 (major)=8.8 min, RT 2 (minor) =10.2 min.

**HRMS analysis (ESI): calculated for [M+H]$^+$:** C$_{15}$H$_{22}$ClN$_2$O$_2$: 297.1370; Found:

297.1369

**Optical Activity:** [α]$_D^{20}$ = -31.2 (c = 0.40, CHCl$_3$, 98% *ee*)
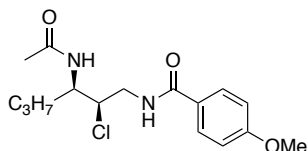
**I-122c**, *N*-((2*R*,3*R*)-3-acetamido-2-chlorohexyl)-4-methoxybenzamide

Compound **I-122c** (29.0 mg, 89% yield, 99% *ee*) was synthesized following the procedure

detailed in Section I-8-2 using **I-70c** (22.3 mg, 0.10 mmol) as starting material.

**R$_f$:** 0.12 (50% EtOAC/Hex)

**$^1$H NMR (500 MHz, CDCl$_3$)** δ 7.93 – 7.81 (m, 3H), 6.95 (d, *J* = 8.9 Hz, 2H), 5.58 (d, *J* =

9.5 Hz, 1H), 4.38 – 4.24 (m, 2H), 4.14 (ddd, *J* = 10.8, 5.2, 1.7 Hz, 1H), 3.85 (s, 3H), 2.90

(ddd, *J* = 13.7, 10.8, 4.5 Hz, 1H), 2.14 (s, 3H), 1.68 – 1.60 (m, 1H), 1.54 (dtd, *J* = 13.7,

7.9, 5.5 Hz, 1H), 1.37 (ddd, *J* = 15.0, 8.0, 6.4 Hz, 2H), 0.90 (t, *J* = 7.4 Hz, 3H).

**$^{13}$C NMR (126 MHz, CDCl$_3$)** δ 171.8, 166.6, 162.3, 129.0, 126.0, 113.8, 61.8, 55.4, 49.2,

42.4, 34.8, 23.3, 19.3, 13.7.

**Resolution of enantiomers:** DAICEL Chiralpak®, IA 10% IPA/Hexane 1ml/min, 254 nm,

RT 1 (major)=13.9 min, RT 2 (minor) =17.8 min.

**HRMS analysis (ESI):** calculated for [M+H]$^+$: C$_{16}$H$_{24}$ClN$_2$O$_3$: 327.1476; Found: 327.1475

**Optical activity:** [α]$_D^{20}$ = -19.8 (c = 0.10, CHCl$_3$, 99% *ee*)
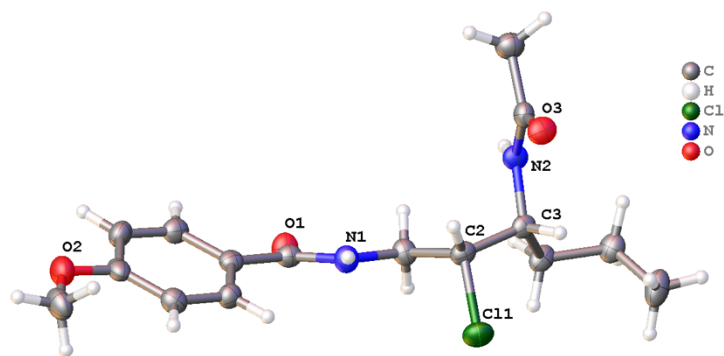


Single colorless needle-shaped crystals of **I-122c** were obtained from a mixture of

methanol and hexanes by slow evaporation in a silicone coated NMR tube.
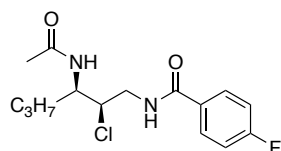
**I-122d**, *N*-((2*R*,3*R*)-3-acetamido-2-chlorohexyl)-4-fluorobenzamide

Compound **I-122d** (26.7 mg, 85% yield, 99% *ee*) was synthesized following the procedure

detailed in Section I-8-2 using **I-70d** (22.1 mg, 0.10 mmol) as starting material.

**R$_f$:** 0.25 (50% EtOAC/Hex)

**¹H NMR (500 MHz, CDCl₃)** δ 8.01 (dd, *J* = 8.6, 4.4 Hz, 1H), 7.93 (dd, *J* = 8.8, 5.3 Hz, 2H),

7.13 (t, *J* = 8.6 Hz, 2H), 5.69 (d, *J* = 9.4 Hz, 1H), 4.35 – 4.25 (m, 2H), 4.13 (ddd, *J* = 10.9,

5.1, 1.7 Hz, 1H), 2.90 (ddd, *J* = 13.6, 10.9, 4.4 Hz, 1H), 2.14 (s, 3H), 1.70 – 1.59 (m, 1H),

1.60 – 1.49 (m, 1H), 1.41 – 1.30 (m, 2H), 0.90 (t, *J* = 7.4 Hz, 3H).

**¹³C NMR (126 MHz, CDCl₃)** δ 171.9, 165.9, 164.9 (d, *J* = 251.8 Hz).

129.9 (d, *J* = 3.0 Hz), 129.5 (d, *J* = 9.0 Hz), 115.7 (d, *J* = 21.9 Hz), 61.5, 49.2, 42.5, 34.8,

23.3, 19.3, 13.7.

**¹⁹F NMR (470 MHz, CDCl₃)** δ -108.06.

**Resolution of enantiomers:** DAICEL Chiralpak®, IA 5% IPA/Hexane 1ml/min, 254 nm,

RT 1 (major)=20.9 min, RT 2 (minor) =22.1 min.

**HRMS analysis (ESI):** calculated for [M+H]⁺: C₁₅H₂₁ClN₂O₂: 315.1276; Found: 315.1274

**Optical Activity:** [α]$_D^{20}$ = -23.9 (c = 0.10, CHCl₃, 99% *ee*)
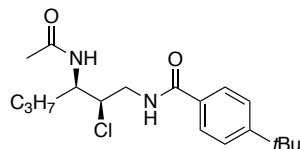


**I-122e**, *N*-((2*R*,3*R*)-3-acetamido-2-chlorohexyl)-4-(*tert*-butyl)benzamide

Compound **I-122e** (27.8 mg, 79% yield, 99% *ee*) was synthesized following the procedure detailed in Section I-8-2 using **I-70e** (25.9 mg, 0.10 mmol) as starting material.

**R$_f$:** 0.21 (70% EtOAC/Hex)

**¹H NMR (500 MHz, CDCl₃)** δ 7.92 (s, 1H), 7.84 (d, *J* = 8.6 Hz, 2H), 7.47 (d, *J* = 8.6 Hz, 2H), 5.59 (s, 1H), 4.37 − 4.24 (m, 2H), 4.19 − 4.05 (m, 1H), 2.91 (ddd, *J* = 13.6, 10.8, 4.5 Hz, 1H), 2.13 (s, 3H), 1.68 − 1.58 (m, 1H), 1.53 (dtd, *J* = 13.6, 7.9, 5.5 Hz, 1H), 1.38-1.32 (m, 2H), 1.32 (s, 9H), 0.89 (t, *J* = 7.3 Hz, 3H).

**¹³C NMR (126 MHz, CDCl3)** δ 171.7, 166.9, 155.1, 130.9, 127.0, 125.6, 61.8, 49.2, 42.4, 34.9, 34.9, 31.2, 23.3, 19.3, 13.7.

**Resolution of enantiomers:** DAICEL Chiralpak®, IA 10% IPA/Hexane 1ml/min, 254 nm, RT 1 (major)=8.2 min, RT 2 (minor) =11.7 min.

**HRMS analysis (ESI):** calculated for [M+H]⁺: $C_{19}H_{30}ClN_2O_2$: 353.1996; Found: 353.1989

**Optical activity:** $[\alpha]_D^{20}$ = -27.1 (c = 0.10, CHCl₃, 99% *ee*)
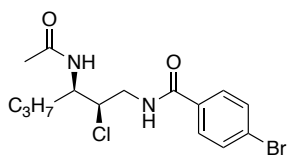


**I-122f**, *N*-((2*R*,3*R*)-3-acetamido-2-chlorohexyl)-4-bromobenzamide

**R$_f$:** 0.21 (50% EtOAC/Hex)

Compound **I-122f** (34.2 mg, 91% yield, 99% *ee*) was synthesized following the procedure detailed in Section I-8-2 using **I-70f** (28.2 mg, 0.10 mmol) as starting material.

**¹H NMR (500 MHz, CDCl₃)** δ 8.04 (dd, *J* = 8.6, 4.7 Hz, 1H), 7.78 (d, *J* = 8.5 Hz, 2H), 7.59 (d, *J* = 8.5 Hz, 2H), 5.65 (d, *J* = 9.4 Hz, 1H), 4.29 (ddd, *J* = 13.7, 8.8, 5.2 Hz, 2H), 4.12 (ddd, *J* = 10.9, 5.1, 1.7 Hz, 1H), 2.90 (ddd, *J* = 13.5, 10.9, 4.4 Hz, 1H), 2.14 (s, 3H), 1.70

– 1.59 (m, 1H), 1.54 (dtd, $J$ = 13.6, 7.8, 5.5 Hz, 1H), 1.36 (h, $J$ = 7.5 Hz, 2H), 0.90 (t, $J$ = 7.3 Hz, 3H).

**13C NMR (126 MHz, CDCl3)** δ 171.9, 166.0, 132.5, 131.9, 128.8, 126.5, 61.5, 49.2, 42.5, 34.8, 23.3, 19.3, 13.7.

**Resolution of enantiomers:** DAICEL Chiralpak®, AD-H 15% IPA/Hexane 1ml/min, 254 nm, RT 1 (major)=6.1 min, RT 2 (minor) =7.6 min.

**HRMS analysis (ESI):** calculated for [M+H]$^+$: $C_{15}H_{21}BrClN_2O_2$: 375.0475; Found: 375.0473

**Optical activity:** $[\alpha]_D^{20}$ = -13.2 (c = 0.40, CHCl3, 99% *ee*)
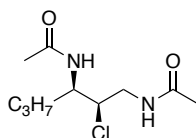


**I-122g**, *N,N'*-((2*R*,3*R*)-2-chlorohexane-1,3-diyl)diacetamide

Compound **I-122g** (13.6 mg, 58% yield, 94% *ee*) was synthesized following the procedure detailed in Section I-8-2 using **I-70g** (14.1 mg, 0.10 mmol) as starting material.

**1H NMR (500 MHz, CDCl3)** δ 6.93 (s, 1H), 5.57 (d, $J$ = 9.5 Hz, 1H), 4.25 (tdd, $J$ = 9.2, 5.6, 1.5 Hz, 1H), 4.07 – 3.90 (m, 2H), 2.85 – 2.68 (m, 1H), 2.07 (s, 3H), 2.00 (s, 3H), 1.67 – 1.57 (m, 1H), 1.58 – 1.48 (m, 1H), 1.36 (h, $J$ = 7.4 Hz, 2H), 0.92 (t, $J$ = 7.3 Hz, 3H).

**13C NMR (126 MHz, CDCl3)** δ 171.4, 170.4, 61.9, 49.0, 42.39, 35.9, 23.3, 23.2, 19.2, 13.7.

**Resolution of enantiomers:** DAICEL Chiralcel®, OD-H 8% IPA/Hexane 1 ml/min, 214 nm, RT 1 (minor)=10.5 min, RT 2 (major) =11.6 min.

**HRMS analysis (ESI):** calculated for [M+H]$^+$: $C_{10}H_{20}ClN_2O_2$: 235.1213; Found: 235.1208

**Optical activity:** $[\alpha]_D^{20}$ = -22.3 (c = 0.10, CHCl3, 94% *ee*)

**I-122h**, *N*-((2*R*,3*S*)-3-acetamido-2-chlorohexyl)-4-nitrobenzamide

Compound **I-122h** (27.7 mg, 81% yield, 97% *ee*) was synthesized following the procedure

detailed in Section I-8-2 using **I-70h** (24.8 mg, 0.10 mmol) as starting material.

**R$_f$:** 0.16 (50% EtOAC/Hex)

**$^1$H NMR (500 MHz, C$_2$D$_6$SO)** δ 9.05 (t, *J* = 5.7 Hz, 1H), 8.33 (d, *J* = 8.8 Hz, 2H), 8.06 (d,

*J* = 8.8 Hz, 2H), 7.98 (d, *J* = 8.4 Hz, 1H), 4.23 (dt, *J* = 8.3, 4.9 Hz, 1H), 4.08 – 3.99 (m,

1H), 3.70 (dt, *J* = 14.0, 5.2 Hz, 1H), 3.48 (ddd, *J* = 14.3, 8.4, 6.1 Hz, 1H), 1.85 (s, 3H),

1.61 (dddd, *J* = 12.9, 9.6, 6.7, 2.9 Hz, 1H), 1.51 – 1.41 (m, 1H), 1.41 – 1.32 (m, 1H), 1.29

– 1.13 (m, 1H), 0.86 (t, *J* = 7.3 Hz, 3H).

**$^{13}$C NMR (126 MHz, C$_2$D$_6$SO)** δ 169.5, 164.8, 149.1, 149.8, 128.7, 123.7, 64.8, 50.6, 43.2,

30.8, 22.5, 18.8, 13.7.

**Resolution of enantiomers:** DAICEL Chiralpak®, AD-H 10% IPA/Hexane 1ml/min, 254

nm, RT 1 (minor)=10.8 min, RT 2 (major) =12.0 min. (97% *ee*)

**HRMS analysis (ESI):** calculated for [M+H]+: C$_{15}$H$_{21}$ClN$_3$O$_4$: 342.1221; Found: 342.1220.

**Optical activity:** [α]$_D^{20}$ = +63.3 (c = 0.4, CHCl$_3$, 97% *ee*)
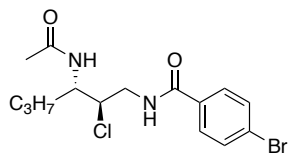


**I-122i**, *N*-((2*R*,3*S*)-3-acetamido-2-chlorohexyl)-4-bromobenzamide

Compound **I-122i** (22.1 mg, 59% yield, 95% *ee*) was synthesized following the procedure detailed in Section I-8-2 using **I-70i** (28.2 mg, 0.10 mmol) as starting material.

**R$_f$:** 0.23 (70% EtOAC/Hex)

**$^1$H NMR (500 MHz, DMSO-$d_6$)** δ 8.80 (t, *J* = 5.7 Hz, 1H), 7.97 (d, *J* = 8.4 Hz, 1H), 7.78 (d, *J* = 8.7 Hz, 2H), 7.70 (d, *J* = 8.5 Hz, 2H), 4.22 (dt, *J* = 8.1, 5.0 Hz, 1H), 4.06 – 3.97 (m, 1H), 3.68 (dt, *J* = 14.0, 5.3 Hz, 1H), 3.44 (ddd, *J* = 14.2, 8.2, 6.1 Hz, 1H), 1.85 (s, 3H), 1.62 (dddd, *J* = 12.8, 9.5, 6.6, 2.9 Hz, 1H), 1.51 – 1.42 (m, 1H), 1.36 (dd, *J* = 6.5, 3.1 Hz, 1H), 1.28 – 1.18 (m, 1H), 0.7 (t, *J* = 7.3 Hz, 3H).

**$^{13}$C NMR (126 MHz, DMSO-$d_6$)** δ 169.5, 165.5, 133.3, 131.4, 129.3, 125.1, 64.9, 50.5, 43.0, 30.8, 22.5, 18.8, 13.7.

**Resolution of enantiomers:** DAICEL Chiralpak®, ad-h 10% IPA/Hexane 1ml/min, 254 nm, RT 1 (major)=8.1 min, RT 2 (minor) =10.2 min.

**HRMS analysis (ESI):** calculated for [M+H]$^+$: $C_{15}H_{21}BrClN_2O_2$: 375.0475; Found: 375.0477

**Optical activity:** [α]$_D^{20}$ = +32.8 (c = 0.1, CHCl$_3$, 96% *ee*)
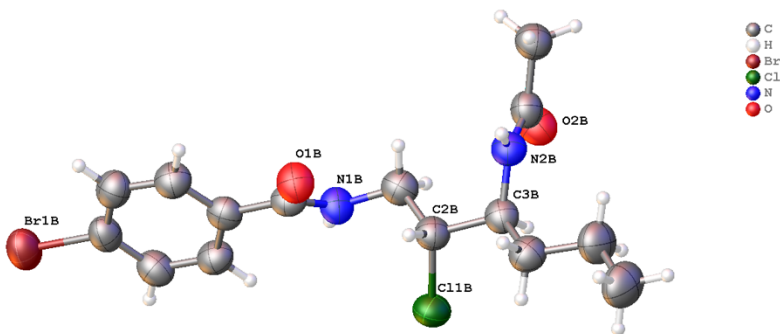


Single colorless needle-shaped crystals of **I-122i** were recrystallized from a mixture of dichloromethane and hexanes by slow evaporation in a silicone coated NMR tube.
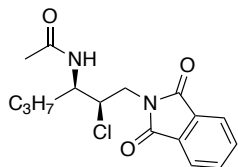
**I-122j**, *N*-((2*R*,3*R*)-2-chloro-1-(1,3-dioxoisoindolin-2-yl)hexan-3-yl)acetamide

Compound **I-122j** (19.1 mg, 67% yield, 29% *ee*) was synthesized following the procedure

detailed in Section I-8-4 using **I-70j** (22.9 mg, 0.10 mmol) as starting material.

**R$_f$:** 0.21 (50% EtOAC/Hex)

**$^1$H NMR (500 MHz, CDCl$_3$)** δ 7.87 (dd, *J* = 5.4, 3.1 Hz, 2H), 7.74 (dd, *J* = 5.5, 3.0 Hz, 2H),

5.61 (d, *J* = 9.7 Hz, 1H), 4.58 (ddd, *J* = 10.2, 4.2, 1.8 Hz, 1H), 4.43 (dddd, *J* = 10.1, 8.2,

5.9, 1.8 Hz, 1H), 4.02 (dd, *J* = 14.5, 10.2 Hz, 1H), 3.91 (dd, *J* = 14.5, 4.2 Hz, 1H), 2.10 (s,

3H), 1.67 − 1.53 (m, 2H), 1.44 − 1.33 (m, 2H), 0.94 (t, *J* = 7.3 Hz, 3H).

**$^{13}$C NMR (126 MHz, CDCl$_3$)** δ 170.1, 168.0, 134.2, 131.8, 123.5, 63.0, 49.7, 42.5, 35.8,

23.4, 19.0, 13.8.

**Resolution of enantiomers:** DAICEL Chiralpak®, AD-H 10% IPA/Hexane 1 ml/min, 230

nm, RT 1 (minor)=13.0 min, RT 2 (major) = 15.8 min.

**HRMS analysis (ESI):** calculated for [M+H]$^+$: C$_{16}$H$_{20}$ClN$_2$O$_3$: 323.1162; Found: 323.1162

**Optical activity:** [α]$_D^{20}$ = +2.1 (c = 0.10, CHCl$_3$, 29% *ee*)
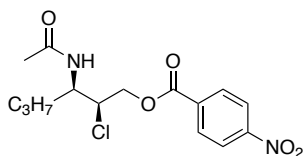


**I-122k**, (2*S*,3*R*)-3-acetamido-2-chlorohexyl 4-nitrobenzoate

Compound **I-122k** (23.3 mg, 68% yield, 60% *ee*) was synthesized following the procedure

detailed in Section I-8-4 using **I-70k** (24.9 mg, 0.10 mmol) as starting material.

**R_f:** 0.23 (50% EtOAC/Hex)

**¹H NMR (500 MHz, CDCl₃)** δ 8.31 (d, $J$ = 8.9 Hz, 2H), 8.25 (d, $J$ = 9.0 Hz, 2H), 5.50 (d, $J$ = 9.7 Hz, 1H), 4.57 – 4.43 (m, 3H), 4.35 (ddd, $J$ = 7.6, 6.5, 1.8 Hz, 1H), 2.05 (s, 3H), 1.71 – 1.52 (m, 2H), 1.44 – 1.35 (m, 2H), 0.95 (t, $J$ = 7.3 Hz, 3H).

**¹³C NMR (126 MHz, CDCl₃)** δ 169.9, 164.1, 150.7, 135.0, 131.0, 123.7, 66.1, 62.0, 48.7, 35.3, 23.3, 19.1, 13.8.

**Resolution of enantiomers:** DAICEL Chiralcel®, OD-H 15% IPA/Hexane 1 ml/min, 254 nm, RT 1 (major)=11.6 min, RT 2 (minor) =15.9 min.

**HRMS analysis (ESI):** calculated for [M+H]⁺: $C_{15}H_{20}ClN_2O_5$: 343.1061; Found: 343.1058

**Optical activity:** $[\alpha]_D^{20}$ = +3.0 (c = 0.1, CHCl₃, 60% *ee*)
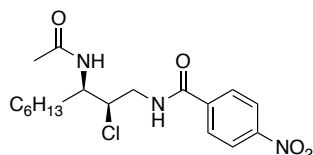


**I-122m**, *N*-((2*R*,3*R*)-3-acetamido-2-chlorononyl)-4-nitrobenzamide

**R_f:** 0.22 (50% EtOAC/Hex).

Compound **I-122m** (30.3 mg, 79% yield, 99% *ee*) was synthesized following the procedure detailed in Section I-8-2 using **I-70m** (29.0 mg, 0.10 mmol) as starting material.

**¹H NMR (500 MHz, CDCl₃)** δ 8.33 – 8.23 (m, 3H), 8.08 (d, $J$ = 8.8 Hz, 2H), 5.58 (d, $J$ = 9.4 Hz, 1H), 4.34 (ddd, $J$ = 13.8, 8.8, 5.2 Hz, 1H), 4.26 (tdd, $J$ = 8.7, 5.7, 1.7 Hz, 1H), 4.13 (ddd, $J$ = 11.1, 5.2, 1.7 Hz, 1H), 2.92 (ddd, $J$ = 13.7, 11.0, 4.3 Hz, 1H), 2.15 (s, 3H), 1.71 – 1.54 (m, 2H), 1.36 – 1.16 (m, 8H), 0.84 (t, $J$ = 7.4 Hz, 3H).

**¹³C NMR (126 MHz, CDCl₃)** δ 172.0, 164.8, 149.7, 139.2, 128.4, 123.9, 61.1, 49.7, 42.5, 32.8, 31.5, 28.9, 26.0, 23.3, 22.5, 14.0.

**Resolution of enantiomers:** DAICEL Chiralpak®, AD-H 4% IPA/Hexane 1 ml/min, 254 nm, RT 1 (major)=28.1 min, RT 2 (major) =31.0 min.

**HRMS analysis (ESI):** calculated for $[M+H]^+$: $C_{18}H_{27}ClN_3O_4$: 384.1690; Found: 384.1688

**Optical activity:** $[\alpha]_D^{20}$ = -35.3 (c = 0.20, CHCl$_3$, 99% *ee*)
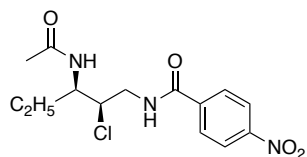


**I-122n**, *N*-((2*R*,3*R*)-3-acetamido-2-chloropentyl)-4-nitrobenzamide

Compound **I-122n** (23.3 mg, 73% yield, 99% *ee*) was synthesized following the procedure detailed in Section I-8-2 using **I-70n** (23.4 mg, 0.10 mmol) as starting material.

**R$_f$:** 0.16 (50% EtOAC/Hex)

**¹H NMR (500 MHz, CDCl$_3$)** δ 8.35 – 8.27 (m, 3H), 8.10 (d, *J* = 9.0 Hz, 2H), 5.62 (d, *J* = 9.3 Hz, 1H), 4.35 (ddd, *J* = 13.8, 8.8, 5.1 Hz, 1H), 4.23 – 4.09 (m, 2H), 2.94 (ddd, *J* = 13.6, 11.0, 4.3 Hz, 1H), 2.17 (s, 3H), 1.78 – 1.58 (m, 2H), 0.96 (t, *J* = 7.4 Hz, 3H).

**¹³C NMR (126 MHz, CDCl$_3$)** δ 172.2, 164.8, 149.7, 139.2, 128.4, 123.9, 60.8, 51.3, 42.5, 25.9, 23.3, 10.6.

**Resolution of enantiomers:** DAICEL Chiralpak®, AD-H 15% IPA/Hexane 1 ml/min, 214 nm, RT 1 (major)=7.8 min, RT 2 (minor) =9.4 min.

**HRMS analysis (ESI):** calculated for $[M+H]^+$: $C_{14}H_{19}ClN_3O_4$: 328.1064; Found: 328.1061

**Optical activity:** $[\alpha]_D^{20}$ = -40.5 (c = 0.2, CHCl$_3$, 99% *ee*)
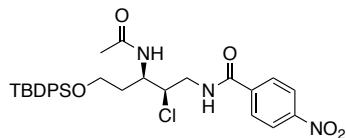
**I-122o**, *N*-((2*R*,3*R*)-3-acetamido-5-((*tert*-butyldiphenylsilyl)oxy)-2-chloropentyl)-4-nitrobenzamide

Compound **I-122o** (36.1 mg, 62% yield, 99% *ee*) was synthesized following the procedure detailed in Section I-8-2 using **I-70o** (48.8 mg, 0.10 mmol) as starting material.
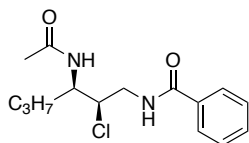
**R$_f$:** 0.36 (50% EtOAC/Hex)

**$^1$H NMR (500 MHz, CDCl$_3$)** δ 8.49 (dd, *J* = 8.9, 4.2 Hz, 1H), 8.25 (d, *J* = 8.9 Hz, 2H), 8.09 (d, *J* = 8.8 Hz, 2H), 7.51-7.55 (m, *J* = 9.7, 6.7, 1.5 Hz, 4H), 7.45 – 7.39 (m, 2H), 7.39-7.34 (m, 4H), 5.61 (d, *J* = 9.3 Hz, 1H), 4.77 (dtd, *J* = 8.9, 6.9, 1.7 Hz, 1H), 4.40 (ddd, *J* = 13.9, 8.9, 5.1 Hz, 1H), 4.17 (ddd, *J* = 11.2, 5.1, 1.7 Hz, 1H), 3.76 – 3.58 (m, 2H), 2.93 (ddd, *J* = 13.7, 11.2, 4.2 Hz, 1H), 2.11 (s, 3H), 1.84 (q, *J* = 6.4 Hz, 2H), 0.89 (s, 9H).

**$^{13}$C NMR (126 MHz, CDCl$_3$)** δ 172.2, 164.7, 149.7, 139.1, 135.5, 135.4, 133.0, 133.0, 129.8, 129.8, 128.4, 127.8, 127.8, 123.8, 61.5, 59.5, 46.4, 42.4, 35.6, 26.7, 23.3, 19.0.

**Resolution of enantiomers:** DAICEL Chiralcel®, OD-H 7% IPA/Hexane 1ml/min, 254 nm, RT 1 (minor)=21.5 min, RT 2 (major) =26.4 min.

**HRMS analysis (ESI):** calculated for [M+H]$^+$: C$_{30}$H$_{37}$ClN$_3$O$_5$Si: 582.2191; Found: 582.2188

**Optical activity:** [α]$_D^{20}$ = -173.2 (c = 0.05, CHCl$_3$, 99% *ee*)
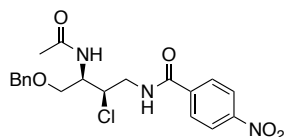


**I-122p**, *N*-((2*R*,3*R*)-3-acetamido-4-(benzyloxy)-2-chlorobutyl)-4-nitrobenzamide

The substrate **I-70p** (32.6 mg, 0.1 mmol, 1.0 equiv) and (DHQD)$_2$PHAL (1.6 mg, 2 mol%) were suspended in acetonitrile (1 mL) in a test tube with a magnetic stir bar and capped

with a rubber septa. HFIP (105 $\mu$L, 1.0 mmol, 10 equiv) was added via a syringe. The resulting suspension was stirred at 23 °C. After stirring for 10 min DCDMH (39.4 mg, 0.2 mmol, 2 equiv) was added. The reaction was monitored by TLC and (DHQD)$_2$PHAL (1.6 mg, 2 mol%) was added every 12 h until the reaction reached completion. Upon completion, the reaction was quenched by the addition of saturated $Na_2S_2O_3$ (2 mL). The reaction was concentrated to remove the acetonitrile and the resultant aqueous layer was extracted with DCM (3 x 4 mL). The combined organics were concentrated. To the concentrated product in the vial with a stir bar, acetonitrile (1 mL) and a solution of HCl (1 M, 0.2 mL) were added and stirred for 15 min. Water (3 mL) was added and the solution was concentrated and extracted with DCM (3 x 4 mL). The combined organic layers were dried with anhydrous $Na_2SO_4$ and concentrated. Column chromatography (SiO$_2$/EtOAc– Hexanes gradient) provided the desired product **I-122p** in a 23 % yield (9.7 mg, 99% *ee*)

**R$_f$:** 0.10 (50% EtOAC/Hex)

**$^1$H NMR (500 MHz, CDCl$_3$)** δ 8.31 (d, *J* = 8.8 Hz, 2H), 8.19 – 8.12 (m, 1H), 8.08 (d, *J* = 8.9 Hz, 2H), 7.38 – 7.27 (m, 5H), 5.73 (d, *J* = 9.2 Hz, 1H), 4.62 – 4.44 (m, 3H), 4.38 – 4.25 (m, 2H), 3.59 (d, *J* = 6.8 Hz, 2H), 3.00 (ddd, *J* = 15.2, 12.1, 4.5 Hz, 1H), 2.14 (s, 3H).

**$^{13}$C NMR (126 MHz, CDCl$_3$)** δ 172.3, 164.8, 149.7, 139.2, 137.2, 128.6, 128.4, 128.1, 127.9, 123.8, 73.5, 69.3, 58.5, 49.4, 42.2, 23.3.

**Resolution of enantiomers:** DAICEL Chiralcel®, OD-H 10% IPA/Hexane 1 ml/min, 254 nm, RT 1 (major)=42.7 min, RT 2 (minor) =66.8 min.

**HRMS analysis (ESI):** calculated for [M+H]$^+$: $C_{20}H_{23}ClN_3O_5$: 420.1326; Found: 420.1328

**Optical activity:** $[\alpha]_D^{20}$ = -21.5 (c = 0.1, CHCl$_3$, 99% *ee*)
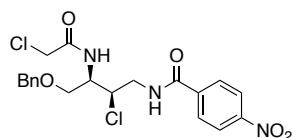
**I-122p'**, *N*-((2*R*,3*R*)-4-(benzyloxy)-2-chloro-3-(2-chloroacetamido)butyl)-4-nitrobenzamide

The substrate **I-70p** (32.6 mg, 0.1 mmol, 1.0 equiv) and (DHQD)₂PHAL (1.6 mg, 2 mol%) were suspended in acetonitrile (1 mL) in a test tube with a magnetic stir bar and capped with a rubber septa. HFIP (105 $\mu$L, 1.0 mmol, 10 equiv) was added via a syringe. The resulting suspension was stirred at 23 °C. After stirring for 10 min DCDMH (39.4 mg, 0.2 mmol, 2 equiv) was added. The reaction was monitored by TLC and (DHQD)₂PHAL (1.6 mg 2 mol%) was added every 12 h until the reaction reached completion. Upon completion, the reaction was quenched by the addition of saturated Na₂S₂O₃ (2 mL). The reaction was concentrated to remove the acetonitrile and the resultant aqueous layer was extracted with DCM (3 x 4 mL). The combined organics were concentrated. To the concentrated product in the vial with a stir bar, acetonitrile (1 mL) and a solution of HCl (1 M, 0.2 mL) were added and stirred for 15 min. Water (3 mL) was added and the solution was concentrated and extracted with DCM (3 x 4 mL). The combined organic layers were dried with anhydrous Na₂SO₄ and concentrated. Column chromatography (SiO₂/EtOAc–Hexanes gradient) provided product **I-122p'** in a 20.8 mg yield (46% yield, 99% *ee*).

**R$_f$:** 0.35 (50% EtOAC/Hex)

**¹H NMR (500 MHz, CDCl₃)** δ 8.31 (d, *J* = 8.9 Hz, 2H), 8.04 (d, *J* = 8.8 Hz, 2H), 7.77 (dd, *J* = 8.1, 4.6 Hz, 1H), 7.38 − 7.29 (m, 5H), 6.78 (d, *J* = 9.3 Hz, 1H), 4.61 − 4.51 (m, 3H),

4.40 (ddd, $J$ = 10.2, 5.6, 2.0 Hz, 1H), 4.26 (ddd, $J$ = 13.9, 8.2, 5.7 Hz, 1H), 4.17 (d, $J$ = 1.9 Hz, 2H), 3.65 (d, $J$ = 6.7 Hz, 2H), 3.09 (ddd, $J$ = 13.9, 10.2, 4.8 Hz, 1H).

**$^{13}$C NMR (126 MHz, CDCl$_3$)** δ 168.0, 164.9, 149.8, 139.1, 137.1, 128.6, 128.4, 128.1, 127.8, 123.9, 73.6, 69.0, 58.2, 50.0, 42.4, 42.4.

**Resolution of enantiomers:** DAICEL Chiralpak®, IA 20% IPA/Hexane 1ml/min, 254 nm, RT 1 (major)=11.8 min, RT 2 (minor) =15.9 min.

**HRMS analysis (ESI):** calculated for [M+H]$^+$: C$_{20}$H$_{22}$Cl$_2$N$_3$O$_5$: 454.0937; Found: 454.0938

**Optical activity:** $[\alpha]_D^{20}$ = +15.1 (c = 0.1, CHCl$_3$, 99% *ee*)
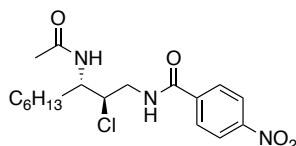


**I-122q**, *N*-((2*R*,3*S*)-3-acetamido-2-chlorononyl)-4-nitrobenzamide

**R$_f$:** 0.28 (70% EtOAC/Hex)

Compound **I-122q** (31.7 mg, 83% yield, 94% *ee*) was synthesized following the procedure detailed in Section I-8-2 using **I-70q** (29.0 mg, 0.10 mmol) as starting material.

**$^1$H NMR (500 MHz, C$_2$D$_6$SO)** δ 9.04 (t, $J$ = 5.7 Hz, 1H), 8.33 (d, $J$ = 8.9 Hz, 2H), 8.05 (d, $J$ = 8.8 Hz, 2H), 7.99 (d, $J$ = 8.4 Hz, 1H), 4.22 (dt, $J$ = 8.3, 4.9 Hz, 1H), 4.10 – 3.89 (m, 1H), 3.69 (dt, $J$ = 14.1, 5.2 Hz, 1H), 3.48 (ddd, $J$ = 14.3, 8.4, 6.1 Hz, 1H), 1.85 (s, 3H), 1.60-1.68 (m, 1H), 1.53 – 1.40 (m, 1H), 1.37 – 1.15 (m, 8H), 0.84 (t, $J$ = 7.4 Hz, 3H).

**$^{13}$C NMR (126 MHz, C$_2$D$_6$SO)** δ 170.0, 165.3, 149.6, 140.2, 129.2, 124.1, 65.2, 51.3, 43.5, 31.6, 29.2, 28.9, 25.9, 22.9, 22.5, 14.4.

**Resolution of enantiomers:** DAICEL Chiralcel®, OD-H 5% IPA/Hexane 1 ml/min, 254 nm, RT 1 (major)=17.1 min, RT 2 (minor) =23.0 min.

**HRMS analysis (ESI):** calculated for [M+H]$^+$: C$_{18}$H$_{27}$ClN$_3$O$_4$: 384.1690; Found: 384.1689

**Optical activity:** [α]$_D^{20}$ = +72.1 (c = 0.20, CHCl$_3$, 95% *ee*)



**I-122r**, (*R*)-*N*-(3-acetamido-2-chloro-3-methylbutyl)-4-nitrobenzamide

Compound **I-122r** (25.9 mg, 79% yield, 99% *ee*) was synthesized following the procedure

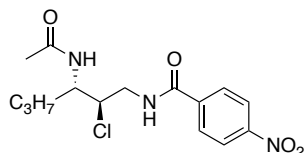detailed in Section I-8-2 using **I-70r** (23.4 mg, 0.10 mmol) as starting material.

**R$_f$:** 0.13 (70% EtOAC/Hex)

**$^1$H NMR (500 MHz, CDCl$_3$)** δ 8.31 (d, *J* = 8.8 Hz, 2H), 7.96 (d, *J* = 8.8 Hz, 2H), 6.79 (s,

1H), 5.54 (s, 1H), 4.90 (dd, *J* = 9.5, 3.2 Hz, 1H), 4.21 − 4.10 (m, 1H), 3.57 − 3.47 (m, 1H),

1.98 (s, 3H), 1.54 (s, 3H), 1.50 (s, 3H)

**$^{13}$C NMR (126 MHz, CDCl$_3$)** δ 170.3, 165.5, 149.7, 139.6, 128.2, 123.9, 66.6, 56.6, 42.9,

24.5, 24.4, 24.0.

**Resolution of enantiomers:** DAICEL Chiralpak®, AD-H 10% IPA/Hexane 1 ml/min, 254

nm, RT 1 (major)=17.5 min, RT 2 (minor) =22.6 min.

**HRMS analysis (ESI):** calculated for [M+H]$^+$: C$_{14}$H$_{19}$ClN$_3$O$_4$: 328.1064; Found: 328.1064

**Optical activity**: [α]$_D^{20}$ = +62.4 (c = 0.10, CHCl$_3$, 99 % *ee*)
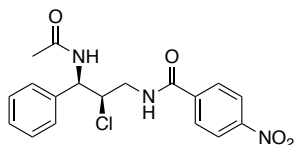


**I-122s**, *N*-((2*R*,3*R*)-3-acetamido-2-chloro-3-phenylpropyl)-4-nitrobenzamide

Compound **I-122s** (35.6 mg, 95% yield, 65:35 *dr*, 99% *ee*) was synthesized following the

procedure detailed in Section I-8-2 using **I-70s** (28.2 mg, 0.10 mmol) as starting material.

**R$_f$:** 0.11 (50% EtOAC/Hex)

**¹H NMR (500 MHz, CDCl₃)** δ 8.32 (d, $J$ = 8.7 Hz, 2H), 8.11 (m, 3H), 7.42 – 7.36 (m, 2H), 7.36 – 7.29 (m, 3H), 6.29 (d, $J$ = 9.7 Hz, 1H), 5.63 (dd, $J$ = 9.6, 1.8 Hz, 1H), 4.56 (ddd, $J$ = 10.5, 5.4, 1.8 Hz, 1H), 4.39 (ddd, $J$ = 13.8, 8.3, 5.4 Hz, 1H), 3.14 (ddd, $J$ = 13.8, 10.5, 4.7 Hz, 1H), 2.25 (s, 3H).

**¹³C NMR (126 MHz, CDCl₃)** δ 171.8, 165.0, 149.8, 139.1, 137.1, 128.8, 128.4, 128.3, 126.6, 123.9, 61.2, 52.2, 43.0, 23.4.

**Resolution of enantiomers:** DAICEL Chiralcel®, OD-H 20% IPA/Hexane 1 ml/min, 254 nm, RT 1 (major)=12.1 min, RT 2 (minor) = 16.9 min.

**HRMS analysis (ESI):** calculated for [M+H]⁺: C₁₈H₁₉ClN₃O₄: 376.1064; Found: 376.1057.

**Optical activity:** [α]$_D^{20}$ = -33.5 (c = 0.2, CHCl₃, 99% *ee*)
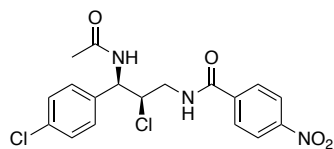


**I-122t**, *N*-((2*R*,3*R*)-3-acetamido-2-chloro-3-(4-chlorophenyl)propyl)-4-nitrobenzamide

Compound **I-122t** (37.6 mg, 92% yield, 64:36 *dr*, 97% *ee*) was synthesized following the procedure detailed in Section I-8-2 using **I-70t** (31.6 mg, 0.10 mmol) as starting material.

**R$_f$:** 0.08 (50% EtOAC/Hex)

**¹H NMR (500 MHz, CDCl₃)** δ 8.32 (d, $J$ = 8.8 Hz, 2H), 8.09 (d, $J$ = 8.8 Hz, 2H), 8.01 (dd, $J$ = 8.0, 4.7 Hz, 1H), 7.39 – 7.32 (m, 2H), 7.29 – 7.23 (m, 2H), 6.29 (d, $J$ = 9.7 Hz, 1H), 5.61 (dd, $J$ = 9.8, 1.9 Hz, 1H), 4.52 (ddd, $J$ = 10.3, 5.5, 1.9 Hz, 1H), 4.35 (ddd, $J$ = 13.8, 8.1, 5.4 Hz, 1H), 3.14 (ddd, $J$ = 13.9, 10.3, 4.8 Hz, 1H), 2.25 (s, 3H).

**$^{13}$C NMR (126 MHz, CDCl$_3$)** δ 171.7, 165.1, 149.8, 138.9, 135.6, 134.2, 129.0, 128.4, 128.1, 123.9, 61.0, 51.7, 43.0, 23.4.

**Resolution of enantiomers:** DAICEL Chiralpak®, IA 20% IPA/Hexane 1 ml/min, 254 nm, RT 1 (minor)=10.8 min, RT 2 (major) =17.6 min.

**HRMS analysis (ESI):** calculated for [M+H]$^+$: C$_{18}$H$_{18}$Cl$_2$N$_3$O$_4$: 410.0674; Found: 410.0668.

**Optical activity:** [α]$_D^{20}$ = -28.2 (c = 0.2, CHCl$_3$, 97% *ee*)
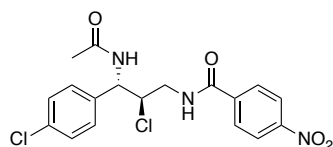


**I-122t-Diastereomer**, *N*-((2*R*,3*S*)-3-acetamido-2-chloro-3-(4-chlorophenyl)propyl)-4-nitrobenzamide

**R$_f$:** 0.15 (70% EtOAC/Hex)

**$^1$H NMR (500 MHz, CDCl$_3$)** δ 8.31 (d, *J* = 8.7 Hz, 2H), 8.01 (d, *J* = 8.7 Hz, 2H), 7.55 (dd, *J* = 8.3, 3.9 Hz, 1H), 7.36 (d, *J* = 8.6 Hz, 2H), 7.30 (d, *J* = 8.5 Hz, 2H), 6.26 (d, *J* = 8.7 Hz, 1H), 5.23 (t, *J* = 8.5 Hz, 1H), 4.46 – 4.37 (m, 2H), 3.34 (ddd, *J* = 15.4, 5.9, 3.8 Hz, 1H), 2.07 (s, 3H).

**$^{13}$C NMR (126 MHz, CDCl$_3$)** δ 170.6, 165.6, 149.7, 139.4, 136.1, 134.7, 129.3, 128.9, 128.3, 123.9, 62.0, 55.6, 42.7, 23.4.

**Resolution of enantiomers:** DAICEL Chiralcel®, OJ-H 8% IPA/Hexane 1 ml/min, 254 nm, RT 1 (major)=22.2 min, RT 2 (minor) =31.9 min.

**HRMS analysis (ESI):** calculated for [M+H]$^+$: C$_{18}$H$_{18}$Cl$_2$N$_3$O$_4$: 410.0674; Found: 410.0666.

**Optical activity:** [α]$_D^{20}$ = +90.8 (c = 0.2, CHCl$_3$, 98% *ee*)
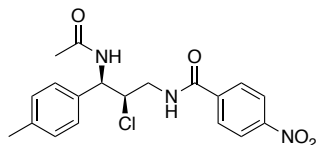
**I-122u**, *N*-((2*R*,3*R*)-3-acetamido-2-chloro-3-(*p*-tolyl)propyl)-4-nitrobenzamide

Compound **I-122u** (30.3 mg, 78% yield, 50:50 *dr*, 99% *ee*) was synthesized following the procedure detailed in Section I-8-2 using **I-70u** (29.6 mg, 0.10 mmol) as starting material.

**R$_f$:** 0.08 (50% EtOAC/Hex)

**$^1$H NMR (500 MHz, CDCl$_3$)** δ 8.31 (d, *J* = 8.8 Hz, 2H), 8.13 (dd, *J* = 8.3, 4.8 Hz, 1H), 8.09 (d, *J* = 8.8 Hz, 2H), 7.19 (s, 4H), 6.27 (d, *J* = 9.7 Hz, 1H), 5.57 (d, *J* = 9.7 Hz, 1H), 4.52 (ddd, *J* = 10.5, 5.4, 1.9 Hz, 1H), 4.37 (ddd, *J* = 13.8, 8.3, 5.4 Hz, 1H), 3.11 (ddd, *J* = 13.8, 10.5, 4.7 Hz, 1H), 2.34 (s, 3H), 2.23 (s, 3H).

**$^{13}$C NMR (126 MHz, CDCl$_3$)** δ 171.7, 165.0, 149.8, 139.1, 138.1, 134.0, 129.5, 128.4, 126.5, 123.9, 61.3, 52.0, 43.0, 23.4, 21.0.

**Resolution of enantiomers:** DAICEL Chiralpak®, IA 15% IPA/Hexane 1 ml/min, 254 nm, RT 1 (minor)=17.6 min, RT 2 (major) = 23.6 min.

**HRMS analysis (ESI):** calculated for [M+H]$^+$: C$_{19}$H$_{21}$ClN$_3$O$_4$: 390.1221; Found: 390.1214.

**Optical activity:** [α]$_D^{20}$ = +157.3 (c = 0.1, CHCl$_3$, 99% *ee*)
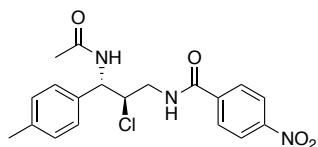


**I-122u-Diastereomer**,          *N*-((2*R*,3*R*)-3-acetamido-2-chloro-3-(*p*-tolyl)propyl)-4-nitrobenzamide

**R$_f$:** 0.22 (70% EtOAC/Hex)

**¹H NMR (500 MHz, CDCl₃)** δ 8.32 (d, *J* = 8.8 Hz, 2H), 8.05 (d, *J* = 8.8 Hz, 2H), 7.65 (d, *J* = 8.1 Hz, 1H), 7.27 – 7.17 (m, 4H), 6.00 (d, *J* = 8.4 Hz, 1H), 5.19 (t, *J* = 8.7 Hz, 1H), 4.50 (ddd, *J* = 14.5, 8.9, 3.5 Hz, 1H), 4.43 (ddd, *J* = 8.5, 4.7, 3.5 Hz, 1H), 3.37 (ddd, *J* = 14.6, 4.7, 3.7 Hz, 1H), 2.37 (s, 3H), 2.07 (s, 3H).

**¹³C NMR (126 MHz, CDCl₃)** δ 170.7, 165.5, 149.7, 139.6, 138.8, 134.6, 129.8, 128.4, 127.3, 123.8, 62.2, 56.1, 42.5, 23.4, 21.2.

**Resolution of enantiomers:** DAICEL Chiralcel®, OJ-H 5% IPA/Hexane 1 ml/min, 254 nm, RT 1 (major)=39.7 min, RT 2 (minor) =49.4 min.

**HRMS analysis (ESI):** calculated for [M+H]⁺: $C_{19}H_{21}ClN_3O_4$: 390.1221; Found: 390.1212.

**Optical activity:** +80.1 (90% *ee*) (c = 0.1, CHCl₃, 99% *ee*)
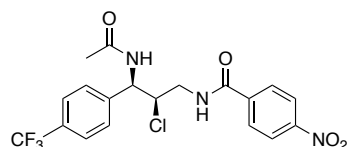


**I-122v**, *N*-((2*R*,3*R*)-3-acetamido-2-chloro-3-(4-(trifluoromethyl)phenyl)propyl)-4-nitrobenzamide

The substrate **I-70v** (0.1 mmol, 1.0 equiv) and (DHQD)₂PHAL (1.6 mg, 2 mol%) were suspended in acetonitrile (1 mL) in a test tube with a magnetic stir bar and capped with a rubber septa. HFIP (105 µL, 1.0 mmol, 10 equiv) was added via a syringe. The resulting suspension was stirred at 23 °C. After stirring for 10 min DCDMH (39.4 mg, 0.2 mmol, 2 equiv) was added. The reaction was monitored by TLC and (DHQD)₂PHAL (1.6 mg 2 mol%) was added every 12 h until the reaction reached completion. Upon completion, the reaction was quenched by the addition of saturated Na₂S₂O₃ (2 mL). The reaction was concentrated to remove the acetonitrile and the resultant aqueous layer was extracted

with DCM (3 x 4 mL). The combined organics were concentrated. To the concentrated product in the vial with a stir bar, acetonitrile (1 mL) and a solution of HCl (1 M, 0.2 mL) were added and stirred for 15 min. Water (3 mL) was added and the solution was concentrated and extracted with DCM (3 x 4 mL). The combined organic layers were dried with anhydrous $Na_2SO_4$ and concentrated. Column chromatography ($SiO_2$/EtOAc–Hexanes gradient) provided the desired product **I-122v** (5.1 mg, 12% yield, 89% *ee*).

**$R_f$:** 0.28 (50% EtOAC/Hex)

**$^1$H NMR (500 MHz, CDCl$_3$)** δ 8.34 (d, *J* = 8.9 Hz, 2H), 8.11 (d, *J* = 8.8 Hz, 2H), 7.95 (t, *J* = 6.8 Hz, 1H), 7.66 (d, *J* = 8.2 Hz, 2H), 7.46 (d, *J* = 8.1 Hz, 2H), 6.27 (d, *J* = 9.9 Hz, 1H), 5.71 (d, *J* = 9.8 Hz, 1H), 4.58 (ddd, *J* = 10.3, 5.5, 1.8 Hz, 1H), 4.39 (ddd, *J* = 13.8, 8.2, 5.5 Hz, 1H), 3.17 (ddd, *J* = 13.7, 10.3, 4.8 Hz, 1H), 2.28 (s, 3H).

**$^{13}$C NMR (126 MHz, CDCl$_3$)** δ 171.7, 165.1, 149.9, 140.6, 138.5, 130.8 (q, $J_{CF}$ = 31.25 Hz), 128.4, 127.1, 125.7 (q, $J_{CF}$ = 3.75 Hz), 123.8 (q, $J_{CF}$ = 145.00 Hz), 124.0, 60.9, 51.9, 43.1, 23.5.

**$^{19}$F NMR (470 MHz, CDCl$_3$)** δ -62.72.

**Resolution of enantiomers:** DAICEL Chiralcel®, IA 20% IPA/Hexane 1 ml/min, 254 nm, RT 1 (minor)=8.4 min, RT 2 (major) =15.1 min.

**HRMS analysis (ESI):** calculated for [M+H]$^+$: $C_{19}H_{18}ClF_3N_3O_4$: 444.0938; Found: 444.0932.

**Optical activity:** $[α]_D^{20}$ = -18.2 (c = 0.1, CHCl$_3$, 89% *ee*)
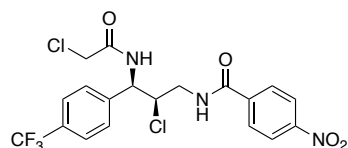
**I-122v'**,  *N*-((2*R*,3*R*)-2-chloro-3-(2-chloroacetamido)-3-(4-(trifluoromethyl)phenyl)propyl)-4-nitrobenzamide

The substrate **I-70v** (0.1 mmol, 1.0 equiv) and (DHQD)$_2$PHAL (1.6 mg, 2 mol%) were suspended in acetonitrile (1 mL) in a test tube with a magnetic stir bar and capped with a rubber septa. HFIP (105 $\mu$L, 1.0 mmol, 10 equiv) was added via a syringe. The resulting suspension was stirred at 23 °C. After stirring for 10 min DCDMH (39.4 mg, 0.2 mmol, 2 equiv) was added. The reaction was monitored by TLC and (DHQD)$_2$PHAL (1.6 mg 2 mol%) was added every 12 h until the reaction reached completion.  Upon completion, the reaction was quenched by the addition of saturated Na$_2$S$_2$O$_3$ (2 mL). The reaction was concentrated to remove the acetonitrile and the resultant aqueous layer was extracted with DCM (3 x 4 mL). The combined organics were concentrated. To the concentrated product in the vial with a stir bar, acetonitrile (1 mL) and a solution of HCl (1 M, 0.2 mL) were added and stirred for 15 min. Water (3 mL) was added and the solution was concentrated and extracted with DCM (3 x 4 mL). The combined organic layers were dried with anhydrous Na$_2$SO$_4$ and concentrated. Column chromatography (SiO$_2$/EtOAc–Hexanes gradient) provided the desired product **I-122v'** (30.5 mg, 64% yield, 87% *ee*).

**R$_f$:** 0.54 (50% EtOAC/Hex)

**$^1$H NMR (500 MHz, CDCl$_3$)** δ 8.32 (d, *J* = 8.7 Hz, 2H), 8.06 (d, *J* = 8.7 Hz, 2H), 7.67 (d, *J* = 8.2 Hz, 2H), 7.65 – 7.58 (m, 1H), 7.46 (d, *J* = 8.4 Hz, 3H), 5.67 (d, *J* = 9.7 Hz, 1H), 4.62

(ddd, $J$ = 8.8, 6.1, 2.1 Hz, 1H), 4.27 (d, $J$ = 5.0 Hz, 2H), 4.26 – 4.19 (m, 1H), 3.34 (ddd, $J$ = 14.3, 9.3, 5.3 Hz, 1H).

**¹³C NMR (126 MHz, CDCl₃)** δ 167.4, 165.2, 149.9, 140.6, 138.8, 130.8 (q, $J_{CF}$ = 31.25 Hz), 128.4, 127.0, 126.0 (q, $J_{CF}$ = 3.75 Hz), 124.3 (q, $J_{CF}$ = 145.00 Hz), 124.0, 61.2, 52.7, 43.4, 42.6.

**¹⁹F NMR (470 MHz, CDCl₃)** δ -62.8.

**Resolution of enantiomers:** DAICEL Chiralcel®, OD-H 15% IPA/Hexane 1 ml/min, 254 nm, RT 1 (major)=22.2 min, RT 2 (minor) =29.9 min.

**HRMS analysis (ESI):** calculated for [M+H]⁺: $C_{19}H_{17}Cl_2F_3N_3O_4$: 478.0548; Found: 478.0558.

**Optical activity:** $[\alpha]_D^{20}$ = -14.3 (c = 0.1, CHCl₃, 87% *ee*)
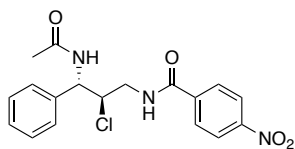


**I-122w**, *N*-((2*R*,3*S*)-3-acetamido-2-chloro-3-phenylpropyl)-4-nitrobenzamide

Compound **I-122w** (19.8 mg, 53% yield, 74:26 *dr*, 99% *ee*) was synthesized following the procedure detailed in Section I-8-2 using **I-70w** (28.2 mg, 0.10 mmol) as starting material.

$R_f$: 0.19 (70% EtOAC/Hex)

**¹H NMR (500 MHz, CDCl₃)** δ 8.31 (d, $J$ = 8.8 Hz, 2H), 8.04 (d, $J$ = 8.8 Hz, 2H), 7.68 (dd, $J$ = 8.7, 3.7 Hz, 1H), 7.44 – 7.31 (m, 5H), 6.16 (d, $J$ = 8.5 Hz, 1H), 5.23 (t, $J$ = 8.6 Hz, 1H), 4.54 – 4.39 (m, 2H), 3.47 – 3.30 (m, 1H), 2.08 (s, 3H).

**¹³C NMR (126 MHz, CDCl₃)** δ 170.7, 165.5, 149.7, 139.6, 137.6, 129.2, 128.9, 128.4, 127.5, 123.8, 62.1, 56.3, 42.5, 23.4.

**Resolution of enantiomers:** DAICEL Chiralcel®, OJ-H 10% IPA/Hexane 1 ml/min, 254 nm, RT 1 (major)=18.7 min, RT 2 (minor) =23.5 min.

**HRMS analysis (ESI):** calculated for [M+H]$^+$: C$_{18}$H$_{19}$ClN$_3$O$_4$: 376.1064; Found: 376.1057.

**Optical activity:** $[\alpha]_D^{20}$ = +86.8 (c = 0.1, CHCl$_3$, 99% *ee*)
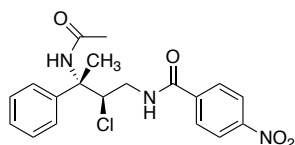


**I-122x**, *N*-((2*R*,3*S*)-3-acetamido-2-chloro-3-phenylbutyl)-4-nitrobenzamide

**R$_f$:** 0.23 (70% EtOAC/Hex)

Compound **I-122x** (22.2 mg, 57% yield, 61:39 *dr*, 97% *ee*) was synthesized following the procedure detailed in Section I-8-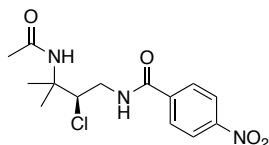2 using **I-70x** (29.6 mg, 0.10 mmol) as starting material. Following column chromatography (SiO$_2$/EtOAc–Hexanes gradient), though inseparable by column chromatography, the diastereomers were able to be separated by HPLC (IA, 10% IPA/Hexanes).

**$^1$H NMR (500 MHz, CDCl$_3$)** δ 8.21 (d, *J* = 8.8 Hz, 2H), 7.68 (d, *J* = 8.8 Hz, 2H), 7.43 (d, *J* = 7.3 Hz, 2H), 7.31 (t, *J* = 7.8 Hz, 2H), 7.24 – 7.18 (m, 1H), 6.71 (t, *J* = 5.8 Hz, 1H), 6.13 (s, 1H), 4.90 (dd, *J* = 8.0, 5.2 Hz, 1H), 3.85 (ddd, *J* = 14.5, 6.3, 5.2 Hz, 1H), 3.49 (ddd, *J* = 14.2, 8.0, 6.0 Hz, 1H), 2.14 (s, 3H), 1.93 (s, 3H).

**$^{13}$C NMR (126 MHz, CDCl$_3$)** δ 170.1, 165.2, 149.6 (HMBC correlation), 140.5, 139.2, 128.6, 128.1, 127.7, 125.9, 123.7, 67.4, 61.6, 43.5, 29.7, 24.5.

**Resolution of enantiomers:** DAICEL Chiralcel®, IA 10% IPA/Hexane 1 ml/min, 254 nm, RT 1 (major)=15.8 min, RT 2 (minor) =18.0 min.

**HRMS analysis (ESI):** calculated for [M+H]$^+$: C$_{19}$H$_{21}$ClN$_3$O$_4$: 390.1221; Found: 390.1215.

**Optical activity:** [α]$_D^{20}$ = -19.2 (c = 0.1, CHCl$_3$, 97% *ee*)
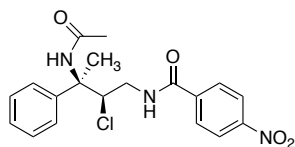


**I-122x-Diastereomer-,** *N*-((2*R*,3*R*)-3-acetamido-2-chloro-3-phenylbutyl)-4-nitrobenzamide

**R$_f$:** 0.23 (70% EtOAC/Hex)

**¹H NMR (500 MHz, CDCl₃)** δ 8.27 (d, *J* = 8.8 Hz, 2H), 7.82 (d, *J* = 8.8 Hz, 2H), 7.50 – 7.45 (m, 2H), 7.39 (dd, *J* = 8.6, 7.0 Hz, 2H), 7.34 – 7.29 (m, 1H), 6.32 (t, *J* = 5.4 Hz, 1H), 6.24 (s, 1H), 4.73 (dd, *J* = 9.2, 3.5 Hz, 1H), 3.92 (ddd, *J* = 14.4, 6.6, 3.5 Hz, 1H), 3.39 (ddd, *J* = 14.5, 9.3, 5.3 Hz, 1H), 2.04 (s, 3H), 1.97 (s, 3H).

**¹³C NMR (126 MHz, CDCl₃)** δ 169.4, 165.4, 149.8, 141.2, 139.2, 128.8, 128.2, 128.1, 126.0, 123.9, 68.7, 61.4, 42.7, 24.4, 20.3.

**Resolution of enantiomers:** DAICEL Chiralcel®, IA 10% IPA/Hexane 1 ml/min, 254 nm, RT 1 (major)=22.1 min, RT 2 (minor) =28.1 min.

**HRMS analysis (ESI):** calculated for [M+H]⁺: C$_{19}$H$_{21}$ClN$_3$O$_4$: 390.1221; Found: 390.1187.

**Optical activity:** [α]$_D^{20}$ = -35.6 (c = 0.05, CHCl$_3$, 97% *ee*)
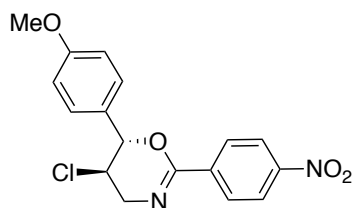


**I-122y** (5R,6S)-5-chloro-6-(4-methoxyphenyl)-2-(4-nitrophenyl)-5,6-dihydro-4H-1,3-oxazine

**¹H NMR (500 MHz, CDCl₃)** δ 8.23 (d, J = 8.9 Hz, 2H), 8.13 (d, J = 8.9 Hz, 2H), 7.31 (d, J = 8.7 Hz, 2H), 6.97 (d, J = 8.7 Hz, 2H), 5.21 (d, J = 7.8 Hz, 1H), 4.22 (td, J = 7.9, 4.8 Hz, 1H), 4.05 (dd, J = 17.4, 4.8 Hz, 1H), 3.87 − 3.78 (m, 4H).

**¹³C NMR (126 MHz, CDCl₃)** δ 160.3, 153.6, 149.3, 138.4, 128.6, 128.4, 128.1, 123.4, 114.2, 80.8, 55.4, 53.6, 50.3.

 **Resolution of enantiomers:** DAICEL Chiralpak®, AD-H 10% IPA/Hexane 1 ml/min, 254 nm, RT 1 (minor)=17.6  min, RT 2 (major) =20.8 min.
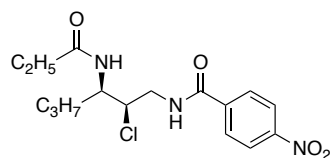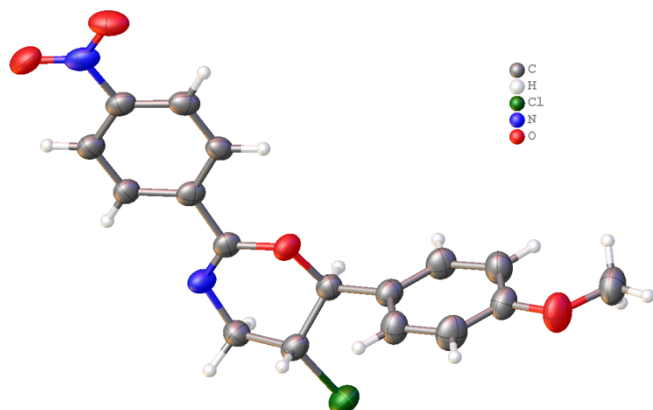




**I-122aa**, *N*-((2*R*,3*R*)-2-chloro-3-propionamidohexyl)-4-nitrobenzamide

Compound **I-122aa** (31.2 mg, 88% yield, 99% *ee*) was synthesized following the procedure detailed in Section I-8-6 using **I-70a** (24.8 mg, 0.10 mmol) as starting material.

**Rf:** 0.29 (50% EtOAC/Hex)

**¹H NMR (500 MHz, CDCl₃)** δ 8.36 – 8.25 (m, 3H), 8.09 (d, $J$ = 9.0 Hz, 2H), 5.56 (d, $J$ = 9.3 Hz, 1H), 4.40 – 4.22 (m, 2H), 4.13 (ddd, $J$ = 11.0, 5.2, 1.7 Hz, 1H), 2.89 (ddd, $J$ = 13.6, 11.0, 4.3 Hz, 1H), 2.36 (q, $J$ = 7.6 Hz, 2H), 1.71 – 1.61 (m, 1H), 1.61 – 1.51 (m, 1H), 1.41 – 1.32 (m, 2H), 1.24 (t, $J$ = 7.6 Hz, 3H), 0.90 (t, $J$ = 7.4 Hz, 3H).

**¹³C NMR (126 MHz, CDCl₃)** δ 176.0, 164.8, 149.7, 139.2, 128.4, 123.9, 61.2, 49.0, 42.5, 34.8, 29.9, 19.3, 13.7, 10.2.

**HRMS analysis (ESI):** calculated for [M+H]⁺: $C_{16}H_{23}ClN_3O_4$: 356.1377; Found: 356.1378.

**Resolution of enantiomers:** DAICEL Chiralpak®, AS-H 10% IPA/Hexane 1 ml/min, 254 nm, RT 1 (minor)=13.5 min, RT 2 (major) = 28.7 min.

**Optical Activity:** $[α]_D^{20}$ = -40.8 (c = 0.40, CHCl₃, 99% *ee*)
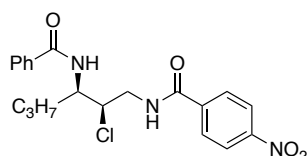


**I-122ab**, *N*-((2*R*,3*R*)-3-benzamido-2-chlorohexyl)-4-nitrobenzamide

Compound **I-122ab** (35.0 mg, 86% yield, 98% *ee*) was synthesized following the procedure detailed in Section I-8-6 using **I-70a** (24.8 mg, 0.10 mmol) as starting material.

**R_f:** 0.65 (50% EtOAC/Hex)

**¹H NMR (500 MHz, CDCl₃)** δ 8.44 – 8.36 (m, 1H), 8.33 (d, $J$ = 8.9 Hz, 2H), 8.15 (d, $J$ = 8.9 Hz, 2H), 7.86 – 7.81 (m, 2H), 7.62 – 7.57 (m, 1H), 7.55 – 7.48 (m, 2H), 6.23 (d, $J$ = 9.4 Hz, 1H), 4.53 (tdd, $J$ = 9.2, 5.4, 1.7 Hz, 1H), 4.35 (ddd, $J$ = 13.8, 8.7, 5.2 Hz, 1H), 4.24 (ddd, $J$ = 10.9, 5.2, 1.7 Hz, 1H), 3.00 (ddd, $J$ = 13.7, 10.9, 4.4 Hz, 1H), 1.81 (dtd, $J$ = 14.0, 8.5, 6.6 Hz, 1H), 1.74 – 1.63 (m, 1H), 1.49 – 1.39 (m, 2H), 0.93 (t, $J$ = 7.3 Hz, 3H).

**¹³C NMR (126 MHz, CDCl₃)** δ 169.3, 164.9, 149.7, 139.2, 133.2, 132.4, 129.0, 128.4, 128.0, 123.9, 61.5, 50.0, 42.7, 34.9, 19.4, 13.7.

**Resolution of enantiomers:** DAICEL Chiralcel®, OD-H 15% IPA/Hexane 1 ml/min, 254 nm, RT 1 (minor)=15.4 min, RT 2 (major) =30.0 min.

**HRMS analysis (ESI):** calculated for [M+H]⁺: $C_{20}H_{23}ClN_3O_4$: 404.1377; Found: 404.1383.

**Optical activity:** $[\alpha]_D^{20}$ = -119.2 (c = 0.39, CHCl₃), 98% *ee*)
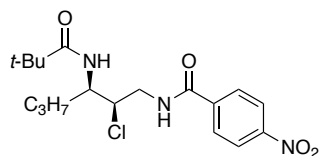


**I-122ac**, *N*-((2*R*,3*R*)-2-chloro-3-pivalamidohexyl)-4-nitrobenzamide

Compound **I-122ac** (33.0 mg, 86% yield, 99% *ee*) was synthesized following the procedure detailed in Section I-8-6 (heated to 80 °C during hydrolysis) using **I-70a** (24.8 mg, 0.10 mmol) as starting material.

**R_f:** 0.65 (30% EtOAC/Hex)

**¹H NMR (500 MHz, CDCl₃)** δ 8.39 − 8.27 (m, 3H), 8.11 (d, *J* = 9.0 Hz, 2H), 5.72 (d, *J* = 9.3 Hz, 1H), 4.38 − 4.25 (m, 2H), 4.14 (ddd, *J* = 11.0, 5.1, 1.7 Hz, 1H), 2.81 (ddd, *J* = 13.6, 11.0, 4.3 Hz, 1H), 1.75 − 1.65 (m, 1H), 1.61 − 1.52 (m, 1H), 1.37 (dt, *J* = 15.0, 7.5 Hz, 2H), 1.29 (s, 9H), 0.91 (t, *J* = 7.3 Hz, 3H).

**¹³C NMR (126 MHz, CDCl₃)** δ 180.7, 164.8, 149.7, 139.3, 128.4, 123.9, 61.5, 48.7, 42.6, 39.2, 34.8, 27.7, 19.3, 13.7.

**Resolution of enantiomers:** DAICEL Chiralpak®, IA 7% IPA/Hexane 1 ml/min, 254 nm, RT 1 (minor)=8.9 min, RT 2 (major) = 10.6 min.

**HRMS analysis (ESI):** calculated for [M+H]⁺: $C_{18}H_{27}ClN_3O_4$: 384.1690; Found: 384.1683.

**Optical activity:** $[\alpha]_D^{20}$ = -38.9 (c = 0.2, CHCl$_3$) (99% *ee*)

## I-9-2  Analytical data for vicinal chloroamidine products
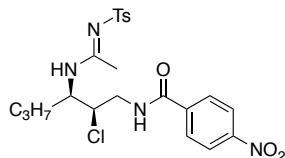


**I-173a**, *N*-((2*R*,3*R*)-2-chloro-3-*N'*-tosylacetimidamido)hexyl)-4-nitrobenzamide

Compound **I-173a** (35.1 mg, 71% yield, 99% *ee*) was synthesized following the procedure

detailed in Section I-8-7 using **I-70a** (24.8 mg, 0.10 mmol) as starting material.

**R$_f$:** 0.26 (50% EtOAC/Hex)

**¹H NMR (500 MHz, CDCl₃)** δ ¹H NMR (500 MHz, CDCl3) δ 8.28 (d, *J* = 8.8 Hz, 2H), 8.21

(d, *J* = 8.8 Hz, 2H), 8.00 (t J=6.2 Hz, 1H), 7.71 (d, *J* = 8.2 Hz, 2H), 7.25 (d, *J* = 8.2 Hz,

2H), 5.63 (d, *J* = 9.1 Hz, 1H), 4.54 (td, *J*= 9.1, 5.5 Hz, 1H), 4.28 – 4.20 (m, 2H), 3.06 (ddd,

*J* = 14.5, 12.2, 5.1 Hz, 1H).2.41 (s, 3H), 2.41 (s, 3H), 1.69 (dtd, *J* = 15.2, 9.0, 7.1 Hz, 1H),

1.60 – 1.52 (m, 1H), 1.31 (q, *J* = 7.5 Hz, 2H), 0.86 (t, *J* = 7.3 Hz, 3H).

**¹³C NMR (126 MHz, CDCl₃)** δ 168.0, 165.6, 149.8, 143.3, 139.1, 138.5, 129.7, 128.9,

126.4, 123.7, 60.8, 51.2, 43.3, 34.6, 21.5, 20.9, 19.1, 13.5.

**Resolution of enantiomers:** DAICEL Chiralpak®, IA 15% IPA/Hexane 1 ml/min, 254 nm,

RT 1 (major)=13.6 min, RT 2 (minor) =19.6 min.

**HRMS analysis (ESI):** calculated for [M+H]⁺: C$_{22}$H$_{28}$ClN$_4$O$_5$S: 495.1469; Found:

495.1473.

**Optical activity:** $[\alpha]_D^{20}$ = +39.7 (c = 0.2, CHCl$_3$) (99% *ee*)
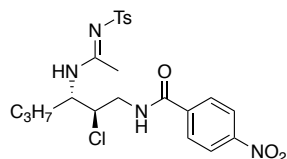
**I-173h**, *N*-((2*R*,3*S*)-2-chloro-3-*N*'-tosylacetimidamido)hexyl)-4-nitrobenzamide

**R$_f$:** 0.10 (50% EtOAC/Hex)

Compound **I-173h** (32.1 mg, 65% yield, 95% *ee*) was synthesized following the procedure detailed in Section I-8-7 using **I-70h** (24.8 mg, 0.10 mmol) as starting material.

**$^1$H NMR (500 MHz, CDCl$_3$)** δ 8.25 (d, *J* = 8.8 Hz, 2H), 8.01 (d, *J* = 8.8 Hz, 2H), 7.71 (d, *J* = 8.3 Hz, 2H), 7.23 (d, *J* = 8.0 Hz, 2H), 7.13 (dd, *J* = 7.0, 4.8 Hz, 1H), 5.99 (d, *J* = 8.7 Hz, 1H), 4.37 (tt, *J* = 10.3, 8.4, 3.1 Hz, 1H), 4.24 (q, *J* = 5.7 Hz, 1H), 4.14 (ddd, *J* = 13.7, 7.8, 5.6 Hz, 1H), 3.49 (ddd, *J* = 14.3, 6.1, 4.5 Hz, 1H), 2.39 (s, *J* = 1.8 Hz, 6H), 1.81 (dddd, *J* = 13.6, 9.8, 6.8, 2.9 Hz, 1H), 1.56 (dtd, *J* = 14.6, 10.1, 4.6 Hz, 1H), 1.45 – 1.32 (m, 1H), 1.32-1.22 (m, 1H), 0.89 (t, *J* = 7.3 Hz, 3H).

**$^{13}$C NMR (126 MHz, CDCl$_3$)** δ 166.9, 166.1, 149.7, 142.9, 139.7, 139.3, 129.5, 128.5, 126.3, 123.8, 62.5, 53.3, 42.9, 31.8, 21.5, 21.2, 19.0, 13.7.

**Resolution of enantiomers:** DAICEL Chiralpak®, IA 15% IPA/Hexane 1 ml/min, 254 nm, RT 1 (minor)=11.4 min, RT 2 (major) =17.3 min.

**HRMS analysis (ESI):** calculated for [M+H]$^+$: C$_{22}$H$_{28}$ClN$_4$O$_5$S: 495.1469; Found: 495.1470.

**Optical activity:** [α]$_D^{20}$ = -15.8 (c = 0.1, CHCl$_3$, 95% *ee*)
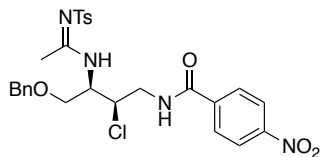
**I-173p**,                N-((2R,3R)-4-(benzyloxy)-2-chloro-3-(N'-tosylacetimidamido)butyl)-4-

nitrobenzamide

The substrate **I-70p** (0.1 mmol, 1.0 equiv) and (DHQD)$_2$PHAL (3.9 mg, 5 mol%) were

suspended in acetonitrile (2 mL) in a test tube with a magnetic stir bar and capped with a

rubber septa. HFIP (105 $\mu$L, 1.0 mmol, 10 equiv) was added via syringe. The resulting

suspension was cooled to 0 °C in an immersion cooler. After stirring for 10 min

Dichloramine-T (48.0 mg, 0.2 mmol, 2 equiv) was added. The reaction was monitored by

TLC and upon completion was quenched by the addition of saturated $Na_2S_2O_3$ (2 mL).

The reaction was concentrated to remove acetonitrile and the resultant aqueous layer

was extracted with DCM (3 x 5 mL). The combined organic layers were dried with

anhydrous $Na_2SO_4$ and concentrated. Column chromatography (SiO$_2$/EtOAc–Hexanes

gradient) provided the desired product **I-173p** in a 65% yield (34.3 mg, 96% *ee*).

**R$_f$:** 0.10 (50% EtOAC/Hex)

**$^1$H NMR (500 MHz, CDCl$_3$)** δ 8.27 (d, *J* = 8.8 Hz, 2H), 8.20 (d, *J* = 8.8 Hz, 2H), 7.93 (dd,

*J* = 7.6, 5.1 Hz, 1H), 7.71 (d, *J* = 8.3 Hz, 2H), 7.32 – 7.28 (m, 3H), 7.26 – 7.20 (m, 4H),

5.79 (d, *J* = 8.8 Hz, 1H), 4.78 (dtd, *J* = 8.6, 6.7, 1.5 Hz, 1H), 4.51 – 4.42 (m, 2H), 4.37

(ddd, *J* = 11.0, 4.7, 1.5 Hz, 1H), 4.22 (ddd, *J* = 13.6, 7.5, 4.8 Hz, 1H), 3.60 (qd, *J* = 10.0,

6.6 Hz, 2H), 3.13 (ddd, *J* = 13.7, 10.9, 5.1 Hz, 1H), 2.40 (s, 3H), 2.39 (s, 3H).

**$^{13}$C NMR (126 MHz, CDCl$_3$)** δ 168.3, 165.6, 149.8, 143.3, 138.9, 138.6, 136.9, 129.7,

128.9, 128.6, 128.2, 127.8, 126.5, 123.7, 73.4, 69.3, 58.1, 51.2, 43.1, 21.5, 20.9.

**Resolution of enantiomers:** DAICEL Chiralcel®, OD-H 17.5% IPA/Hexane 1 ml/min,

254 nm, RT 1 (major)=27.1 min, RT 2 (minor) =42.8 min.

**HRMS analysis (ESI):** calculated for [M+H]$^+$: C$_{27}$H$_{30}$ClN$_4$O$_6$S: 573.1575; Found: 573.1577.

**Optical activity:** [α]$_D^{20}$ = +29.5 (c = 0.1, CHCl$_3$, 95% *ee*)
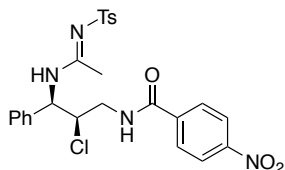


**I-173s**,            *N*-((2*R*,3*S*)-2-chloro-3-phenyl-3-((*N'*-tosylacetimidamido)propyl)-4-nitrobenzamide

**R$_f$:** 0.20 (50% EtOAC/Hex)

Compound **I-173s** (17.2 mg, 54% yield, 99% *ee*) was synthesized following the procedure detailed in Section I-8-7 using **I-70s** (14.1 mg, 0.05 mmol) as starting material.

**$^1$H NMR (500 MHz, CDCl$_3$)** δ 8.28 (d, *J* = 8.9 Hz, 2H), 8.20 (d, *J* = 8.9 Hz, 2H), 8.00 – 7.88 (m, 1H), 7.72 (d, *J* = 8.3 Hz, 2H), 7.43 – 7.31 (m, 3H), 7.31 – 7.22 (m, 4H), 6.13 (d, *J* = 9.3 Hz, 1H), 5.82 (d, *J* = 9.0 Hz, 1H), 4.68 (ddd, *J* = 10.8, 4.9, 1.5 Hz, 1H), 4.28 (ddd, *J* = 13.7, 7.1, 4.9 Hz, 1H), 3.25 (ddd, *J* = 13.8, 10.7, 5.3 Hz, 1H), 2.51 (s, 3H), 2.40 (s, 3H).

**$^{13}$C NMR (126 MHz, CDCl$_3$)** δ 167.4, 165.8, 149.8, 143.4, 138.9, 138.5, 136.2, 129.7, 129.0, 128.9, 128.7, 126.7, 126.5, 123.8, 60.6, 53.9, 43.8, 21.5, 21.3.

**Resolution of enantiomers:** DAICEL Chiralpak®, IA 20% IPA/Hexane 1 ml/min, 254 nm, RT 1 (major)=32.0 min, RT 2 (minor) =41.3 min.

**HRMS analysis (ESI):** calculated for [M+H]$^+$: C$_{25}$H$_{26}$ClN$_4$O$_5$S: 529.1312; Found: 592.1312.

**Optical activity:** [α]$_D^{20}$ = +120.2 (c = 0.1, CHCl$_3$, 99% *ee*)
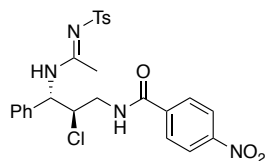
**I-173s-Diastereomer**, *N*-((2*R*,3*R*)-2-chloro-3-phenyl-3-(*N'*-tosylacetimidamido)propyl)-4-nitrobenzamide

**R$_f$:** 0.12 (50% EtOAC/Hex)

**$^1$H NMR (500 MHz, CD$_3$CN)** δ 8.27 (d, *J* = 8.9 Hz, 2H), 7.97 (d, *J* = 8.9 Hz, 2H), 7.59 (d, *J* = 8.2 Hz, 2H), 7.56 – 7.47 (m, 2H), 7.46 – 7.34 (m, 5H), 7.26 (d, *J* = 8.0 Hz, 2H), 5.44 (dd, *J* = 8.4, 6.5 Hz, 1H), 4.70 (td, *J* = 6.8, 4.6 Hz, 1H), 3.91 (dt, *J* = 14.4, 5.4 Hz, 1H), 3.51 (dt, *J* = 14.3, 6.4 Hz, 1H), 2.38 (s, 3H), 2.37 (s, 3H).

**$^{13}$C NMR (126 MHz, CDCl$_3$)** δ 166.0, 165.8, 149.8, 142.7, 139.6, 139.0, 136.2, 129.4, 129.0, 128.9, 128.4, 127.7, 126.4, 123.8, 61.6, 57.8, 43.2, 21.5, 21.3.

**Resolution of enantiomers:** DAICEL Chiralpak®, IA 22% IPA/Hexane 1 ml/min, 254 nm, RT 1 (minor)=11.9 min, RT 2 (minor) =35.3 min

**HRMS analysis (ESI):** calculated for [M+H]$^+$: C$_{25}$H$_{26}$ClN$_4$O$_5$S: 529.1312; Found: 592.1312.

**Optical activity:** [α]$_D^{20}$ = +54.2 (c = 0.1, CHCl$_3$, 97% *ee*)

## I-9-3 Analytical data for derivatives
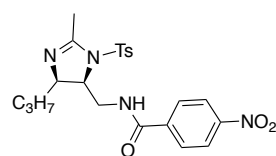


**I-175a**, *N*-(((4*R*,5*S*)-2-(methyl)-4-propyl-1-tosyl-4,5-dihydro-1*H*-imidazol-5-yl)methyl)-4-nitrobenzamide

To a solution of **I-73a** (49.4 mg, 0.1 mmol, 1 equiv) in acetonitrile (1 mL) at room temperature, $Cs_2CO_3$ was added and allowed to stir for 48 h. The reaction was quenched with the addition of water (3 mL) and extracted with DCM (3 x 4 mL). The combined organic layers were dried with anhydrous $Na_2SO_4$ and concentrated in vacuo. Column chromatography (SiO$_2$/EtOAc–Hexanes gradient) gave the desired product I-**175a** in a 57% yield (26.2 mg).

**R$_f$:** 0.55 (60% EtOAC/Hex)

**$^1$H NMR (500 MHz, CDCl$_3$)** δ 8.31 (d, $J$ = 8.9 Hz, 2H), 8.09 (d, $J$ = 8.8 Hz, 2H), 7.70 (d, $J$ = 8.4 Hz, 2H), 7.55 – 7.47 (m, 1H), 7.39 – 7.32 (m, 2H), 4.18 (ddd, $J$ = 11.2, 8.3, 2.7 Hz, 1H), 3.81 (ddd, $J$ = 13.9, 6.4, 2.7 Hz, 1H), 3.46 – 3.35 (m, 1H), 3.27 (ddd, $J$ = 14.2, 11.3, 3.0 Hz, 1H), 2.45 (s, 3H), 2.37 (d, $J$ = 2.2 Hz, 3H), 1.62 – 1.46 (m, 2H), 1.38 – 1.28 (m, 2H), 0.90 (t, $J$ = 7.0 Hz, 3H).

**$^{13}$C NMR (126 MHz, CDCl$_3$)** δ 165.7, 155.7, 149.7, 145.4, 139.6, 135.6, 130.5, 128.4, 126.7, 123.9, 67.6, 62.4, 39.8, 31.3, 21.7, 20.9, 17.9, 14.0.

**HRMS analysis (ESI):** calculated for [M+H]$^+$: $C_{22}H_{27}N_4O_5S$: 459.1702; Found: 459.1700.

**Optical activity:** $[\alpha]_D^{20}$ = +183.2 (c = 0.5, CHCl$_3$, 99% *ee*)
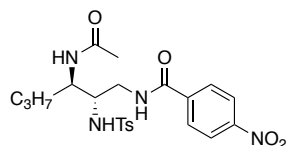


**I-176a**, *N*-((2*S*,3*R*)-3-acetamido-2-((4-methylphenyl)sulfonamido)hexyl)-4-nitrobenzamide

**R$_f$:** 0.25 (60% EtOAC/Hex)

Imidazoline **I-175a** (26.2 mg, 0.57 mmol), acetonitrile (1 mL) and a solution of HCl (1 M, 0.2 mL) were added to a vial and stirred for 15 min. Water (3 mL) was added and the solution was concentrated in vacuo and extracted with DCM (3 x 4 mL). The combined organic layers were dried with anhydrous $Na_2SO_4$ and concentrated. Column chromatography ($SiO_2$/EtOAc–Hexanes gradient) provided the desired product **I-176a** in a 99% yield (27.1 mg, 99% *ee*).

**$^1$H NMR (500 MHz, CDCl$_3$)** δ 8.31 (d, *J* = 8.8 Hz, 2H), 8.05 (d, *J* = 8.8 Hz, 2H), 7.86 (d, *J* = 8.3 Hz, 2H), 7.77 (s, 1H), 7.34 (d, *J* = 8.5 Hz, 2H), 6.66 (d, *J* = 6.6 Hz, 1H), 5.66 (d, *J* = 7.8 Hz, 1H), 3.69 (dq, *J* = 8.7, 4.4 Hz, 1H), 3.60 (dd, *J* = 10.7, 6.6 Hz, 1H), 3.35 – 3.17 (m, 2H), 2.43 (s, 3H), 2.00 (s, 3H), 1.63-1.57 (m, 1H), 1.44 – 1.33 (m, 1H), 1.23 – 1.13 (m, 2H), 0.77 (t, *J* = 7.3 Hz, 3H).

**$^{13}$C NMR (126 MHz, CDCl$_3$)** δ 172.6, 166.3, 149.8, 143.9, 139.0, 136.8, 129.9, 128.4, 127.3, 123.9, 57.6, 52.3, 40.5, 33.6, 23.1, 21.6, 19.3, 13.4.

**Resolution of enantiomers:** DAICEL Chiralpak®, AD-H 15% IPA/Hexane 1 ml/min, 254 nm, RT 1 (minor)=15.2 min, RT 2 (major) =22.8 min

**HRMS analysis (ESI):** calculated for [M+H]$^+$: $C_{22}H_{29}ClN_4O_5S$: 477.1808; Found: 477.1804.

**Optical activity:** [α]$_D^{20}$ = +65.2 (c = 0.2, CHCl$_3$, 99% *ee*)
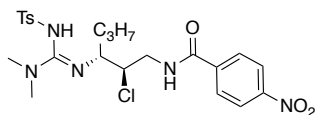
**I-177a**, *N*-((2*R*,3*R*)-2-chloro-3-(((*Z*)-(dimethylamino)((4-methylphenyl)sulfonamido)methylene)amino)hexyl)-4-nitrobenzamide

The substrate **I-70a** (24.8 mg, 0.1 mmol, 1.0 equiv), (DHQD)₂PHAL (0.8 mg, 1 mol%), and MS4Å (20 mg) were suspended in dimethylcyanamide (1 mL) in a test tube with a magnetic stir bar and capped with a rubber septa. HFIP (105 *μ*L, 1.0 mmol, 10 equiv) was added via syringe. The resulting suspension was cooled to 0 °C in an immersion cooler. After stirring for 10 min dichloramine-T (48.0 mg, 0.2 mmol, 2 equiv) was added. The reaction was monitored by TLC and upon completion was quenched by the addition of saturated Na₂S₂O₃ (2 mL). The reaction was concentrated to remove acetonitrile and the resultant aqueous layer was extracted with DCM (3 x 5 mL). The combined organic layers were dried with anhydrous Na₂SO₄ and concentrated. Column chromatography (SiO₂/EtOAc–Hexanes gradient) provided the desired product **I-177a** in an 82% yield (42.9 mg, 98% *ee*).

**R$_f$:** 0.35 (70% EtOAC/Hex)

**¹H NMR (500 MHz, CDCl₃)** δ 8.66 – 8.54 (m, 1H), 8.25 (d, *J* = 8.9 Hz, 2H), 8.17 (d, *J* = 8.9 Hz, 2H), 7.72 (d, *J* = 8.3 Hz, 2H), 7.20 (d, *J* = 8.3 Hz, 2H), 5.09 (d, *J* = 9.9 Hz, 1H), 4.67 – 4.54 (m, 1H), 4.33 – 4.18 (m, 2H), 3.30 (ddd, *J* = 13.3, 10.1, 4.9 Hz, 1H), 3.05 (s, 6H), 2.37 (s, 3H), 1.67 – 1.53 (m, 2H), 1.42 – 1.29 (m, 1H), 1.28 – 1.17 (m, 1H), 0.88 (t, *J* = 7.4 Hz, 3H).

**¹³C NMR (126 MHz, CDCl3)** δ 165.8, 156.7, 149.6, 142.1, 141.8, 139.1, 129.3, 128.9, 125.4, 123.6, 61.5, 53.7, 42.7, 39.3, 36.3, 21.4, 19.1, 13.7.

**Resolution of enantiomers:** DAICEL Chiralpak®, IA 16% IPA/Hexane 1ml/min, 254 nm, RT 1 (major)=43.8 min, RT 2 (minor) =51.9 min.

**HRMS analysis (ESI):** calculated for [M+H]$^+$: $C_{23}H_{31}N_5O_5S$: 524.1735; Found: 524.1732.

**Optical activity:** $[\alpha]_D^{20}$ = -31.9 (c = 0.50, CHCl$_3$) (98% *ee*)
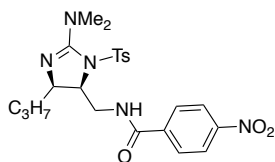


**I-178a**,    *N*-((((4*R*,5*S*)-2-(dimethylamino)-4-propyl-1-tosyl-4,5-dihydro-1*H*-imidazol-5-yl)methyl)-4-nitrobenzamide

**I-177a** (26.2 mg, 0.05 mmol) was added to a 10 mL test tube with a magnetic stir bar. DMF (0.5 mL) was added via syringe. The reaction was heated to 80 °C and monitored by TLC. After the reaction reached competition reaction, it was cooled, quenched with water (5 mL) and extracted with dichloromethane (3x 5 mL). The combined organic layers were dried with anhydrous Na$_2$SO$_4$ and concentrated in vacuo. Column chromatography (SiO$_2$/EtOAc–Hexanes gradient) provided the desired product **I-178a** in a 62% yield (15.1 mg).

**R$_f$:** 0.30 (100% EtOAC)

**$^1$H NMR (500 MHz, CDCl$_3$)** δ 8.32 (d, *J* = 8.5 Hz, 2H), 8.10 (d, *J* = 8.4 Hz, 2H), 7.73 (d, *J* = 8.0 Hz, 2H), 7.48 (t, *J* = 4.5 Hz, 1H), 7.37 (d, *J* = 8.0 Hz, 2H), 3.87 (dt, *J* = 11.1, 2.9 Hz, 1H), 3.59 (ddd, *J* = 13.9, 5.8, 3.3 Hz, 1H), 3.38 (ddd, *J* = 14.2, 11.0, 3.5 Hz, 1H), 3.25 (ddd, *J* = 8.8, 6.1, 2.2 Hz, 1H), 2.92 (s, 6H), 2.46 (s, 3H), 1.20 − 0.93 (m, 2H), 0.63 (t, *J* = 7.3 Hz, 3H), 0.57 (ddd, *J* = 16.5, 9.0, 5.3 Hz, 1H), -0.16 (dtd, *J* = 14.0, 9.6, 5.1 Hz, 1H).

**¹³C NMR (126 MHz, CDCl₃)** δ 165.6, 156.0, 149.6, 145.5, 139.6, 133.3, 130.0, 128.4, 127.9, 123.9, 66.6, 64.5, 44.7, 41.6, 38.0, 21.6, 18.9, 13.7.

**HRMS analysis (ESI):** calculated for [M+H]⁺: $C_{23}H_{30}N_5O_5S$: 488.1968; Found: 488.1978.

**Optical activity:** $[\alpha]_D^{20}$ = +40.2 (c = 0.25, CHCl₃)

## I-9-4  Analytical data for miscellaneous products/byproducts
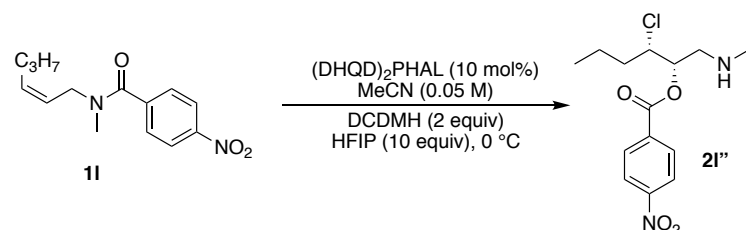


**I-122I"**, *N*-((2*R*,3*R*)-3-chloro-2-hydroxyhexyl)-*N*-methyl-4-nitrobenzamide

**I-70I** (0.1 mmol, 1.0 equiv) and (DHQD)₂PHAL (7.8 mg, 10 mol%) were suspended in acetonitrile (2 mL) in a test tube with a magnetic stir bar and capped with a rubber septa. HFIP (105 *μ*L, 1.0 mmol, 10 equiv) was added via a syringe. The resulting suspension was cooled to 0 °C in an immersion cooler. After stirring for 10 min, DCDMH (39.4 mg, 0.2 mmol, 2 equiv) was added. Upon completion, the reaction was quenched by the addition of saturated Na₂S₂O₃ (2 mL). The reaction was concentrated to remove the acetonitrile and the resultant aqueous layer was extracted with DCM (3 x 5 mL). The combined organics were concentrated. The combined organic layers were dried with anhydrous Na₂SO₄ and concentrated. Column chromatography (SiO₂/EtOAc–Hexanes gradient) provided **I-122I"** (25.1 mg, 80% yield, 19% *ee*).

R_f 0.68 (20% EtOAC/Hex)

**¹H NMR (500 MHz, CDCl₃)** δ 8.32 (d, *J* = 9.0 Hz, 2H), 8.27 (d, *J* = 9.0 Hz, 2H), 5.68 (td, *J* = 6.2, 2.2 Hz, 1H), 4.30 (ddd, *J* = 8.2, 5.8, 2.2 Hz, 1H), 3.31 (dd, *J* = 6.1, 1.7 Hz, 2H),

3.01 (s, 3H), 1.84 – 1.69 (m, 2H), 1.69 – 1.55 (m, 2H), 1.56 – 1.42 (m, 1H), 0.94 (t, $J$ = 7.3 Hz, 3H).

**$^{13}$C NMR (126 MHz, CDCl$_3$)** δ 163.8, 150.8, 134.9, 131.1, 123.7, 73.5, 66.2, 61.6, 53.7, 37.0, 19.8, 13.4.

**Resolution of enantiomers:** DAICEL Chiralpak®, AD-H 5% IPA/Hexane 1 ml/min, 254 nm, RT 1 (minor)=6.6 min, RT 2 (major) =7.9 min.

**HRMS analysis (ESI):** calculated for [M+H]$^+$: C$_{14}$H$_{20}$ClN$_2$O$_4$: 315.1111; Found: 315.1108
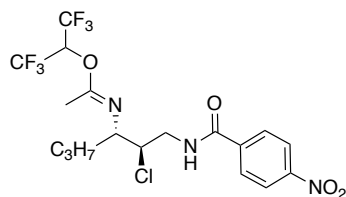


**I-174h**, 1,1,1,3,3,3-hexafluoropropan-2-yl-$N$-((2$R$,3$S$)-2-chloro-1-(4-nitrobenzamido)hexan-3-yl)acetimidate

**R$_f$:** 0.39 (25% EtOAC/Hex)

**$^1$H NMR (500 MHz, CDCl$_3$)** δ 8.32 (d, $J$ = 8.8 Hz, 2H), 7.96 (d, $J$ = 8.8 Hz, 2H), 6.54 (s, 1H), 6.34 (hept, $J$ = 6.5 Hz, 1H), 4.32 – 4.21 (m, 2H), 3.69 (dt, $J$ = 9.2, 4.0 Hz, 1H), 3.34 (ddd, $J$ = 13.8, 9.6, 4.0 Hz, 1H), 2.08 (s, 3H), 1.75 (tdd, $J$ = 10.1, 6.2, 3.0 Hz, 1H), 1.64 (ddt, $J$ = 18.7, 9.6, 5.0 Hz, 1H), 1.34 – 1.17 (m, 2H), 0.94 (t, $J$ = 7.3 Hz, 3H).

**$^{13}$C NMR (126 MHz, CDCl$_3$)** δ 165.5, 158.7, 149.8, 139.6, 128.2, 124.0, 65.5, 62.5, 42.3, 35.9, 19.4, 14.7, 13.9 (note the trifluoromethyl carbons and the methine of the HFIP addition are not listed since they could not be assigned with confidence, presumably due to their splitting, which led to small intensity in the NMR spectrum.

**$^{19}$F NMR (470 MHz, CDCl$_3$)** δ -73.01 – -73.10 (m), -73.29 – -73.44 (m).

**HRMS analysis (ESI):** calculated for $[M+H]^+$: $C_{18}H_{21}ClF_6N_3O_4$: 492.1125, found: 492.1110

**Optical activity:** $[\alpha]_D^{20}$ = 27.9 (c = 0.20, CHCl₃)
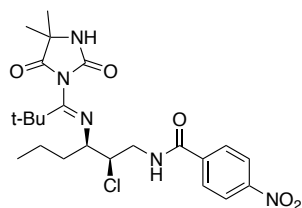


**I-162a/b**, *N*-((2*R*,3*R*)-2-chloro-3-((( 1-(4,4-dimethyl-2,5-dioxoimidazolidin-1-yl)-2,2-dimethylpropylidene)amino)hexyl)-4-nitrobenzamide

*Less polar rotamer*

**Rf:** 0.25 (30% EtOAC/Hex)

**¹H NMR (500 MHz, CDCl₃)** δ 8.25 (d, *J* = 8.8 Hz, 2H), 8.09 (d, *J* = 8.8 Hz, 2H), 7.77 (t, 1H, *J* = 7.5 Hz), 6.23 (s, 1H), 4.20 (ddd, *J* = 9.8, 4.8, 1.9 Hz, 1H), 4.15 − 4.04 (m, 1H), 3.45 (ddd, *J* = 9.2, 5.1, 1.9 Hz, 1H), 3.35 (ddd, *J* = 13.4, 9.9, 5.1 Hz, 1H), 1.89 (dtd, *J* = 13.2, 9.3, 4.4 Hz, 1H), 1.56 (s, 3H), 1.48 (s, 3H), 1.27 (s, 9H), 1.32-1.11 (m, 3H), 0.85 (t, *J* = 7.2 Hz, 3H).

**¹³C NMR (126 MHz, CDCl₃)** δ 175.5, 165.5, 155.4, 154.9, 149.3, 139.6, 128.8, 123.6, 60.1, 60.0, 59.4, 43.4, 41.3, 34.3, 28.4, 25.4, 25.3, 18.8, 14.0.

**I-162a/b**, *More polar rotamer*

**Rf:** 0.25 (30% EtOAC/Hex)

**¹H NMR (500 MHz, CDCl₃)** δ 8.29 (d, *J* = 8.9 Hz, 2H), 8.05 (d, *J* = 8.8 Hz, 2H), 7.29 (t, *J* = 6.3 Hz, 1H), 5.79 (s, 1H), 4.22 (ddd, *J* = 8.9, 5.7, 2.2 Hz, 1H), 3.98 (ddd, *J* = 13.7, 6.8,

5.7 Hz, 1H), 3.48 (td, *J* = 8.7, 4.5 Hz, 1H), 3.35 (td, *J* = 5.6, 2.7 Hz, 1H), 1.96 − 1.85 (m, 1H), 1.68 (s, 3H), 1.52 (s, 3H), 1.41 − 1.28 (m, 3H), 1.25 (s, 9H), 0.85 (t, *J* = 7.2, 3H).

**¹³C NMR (126 MHz, CDCl₃)** δ 177.0, 165.6, 155.3, 153.5, 149.6, 139.5, 128.6, 123.6, 60.6, 59.7, 59.7, 43.5, 41.2, 33.5, 28.4, 25.6, 25.2, 18.7, 13.8.

**HRMS analysis (ESI): calculated for [M+H]⁺:** $C_{23}H_{33}ClN_5O_5$: 494.2170; Found: 494.2149

**Optical activity:** $[\alpha]_D^{20}$ = +40.2 (c = 0.25, CHCl₃)
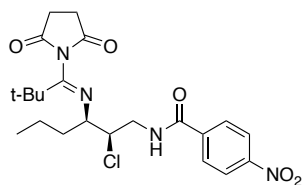


**I-165**, *N*-((2*R*,3*R*)-2-chloro-3-(((1-(2,5-dioxopyrrolidin-1-yl)-2,2-dimethylpropylidene)amino)hexyl)-4-nitrobenzamide

**R_f:** 0.20 (30% EtOAC/Hex)

**¹H NMR (500 MHz, CDCl₃)** δ 8.29 (d, *J* = 8.8 Hz, 2H), 8.02 (d, *J* = 8.8 Hz, 2H), 7.16 − 7.09 (m, 1H), 4.19 (ddd, *J* = 8.2, 6.4, 2.2 Hz, 1H), 3.85 (dt, *J* = 13.9, 6.4 Hz, 1H), 3.57 (ddd, *J* = 13.8, 8.0, 5.7 Hz, 1H), 3.24 (ddd, *J* = 8.0, 5.4, 2.3 Hz, 1H), 2.97 − 2.62 (m, 4H), 1.94 − 1.81 (m, 1H), 1.33 − 1.23 (m, 3H), 1.21 (s, 9H), 0.84 (t, *J* = 7.1 Hz, 3H).

**¹³C NMR (126 MHz, CDCl₃)** δ 176.6, 175.1, 165.4, 156.5, 149.6, 139.5, 128.5, 123.7, 61.3, 60.3, 43.6, 40.8, 33.6, 28.7, 28.7, 28.4, 18.7, 13.9.

**HRMS analysis (ESI):** calculated for [M+H]⁺: $C_{22}H_{30}ClN_4O_5$: 465.1905; Found; 465.1907

**Optical activity:** $[\alpha]_D^{20}$ = +63.8 (c = 0.35, CHCl₃)

## I-9-5　Analytical Data for Starting Materials
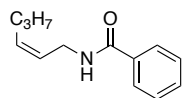


**I-70b,** (*Z*)-*N*-(hex-2-en-1-yl)benzamide

**R$_f$:** 0.26 (20% EtOAC/Hex)

**$^1$H NMR (500 MHz, CDCl$_3$)** δ 7.81-7.76 (m, 2H), 7.53 – 7.47 (m, 1H), 7.46-7.41 (m, 2H), 6.06 (s, 1H), 5.64 (dtt, *J* = 10.3, 7.4, 1.4 Hz, 1H), 5.53 (dtt, *J* = 10.7, 7.0, 1.5 Hz, 1H), 4.11 (t, *J* = 6.1 Hz, 2H), 2.13 (q, *J* = 7.4 Hz, 2H), 1.43 (dt, *J* = 14.8, 7.4 Hz, 2H), 0.94 (t, *J* = 7.3 Hz, 3H).

**$^{13}$C NMR (126 MHz, CDCl$_3$)** δ 167.5, 134.7, 134.3, 131.5, 128.7, 127.0, 125.3, 37.3, 29.6, 22.8, 13.9.

**HRMS analysis (ESI):** calculated for [M+H]$^+$: C13H18NO: 204.1388; Found: 204.1386
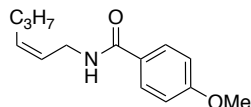


**I-70c**, (*Z*)-*N*-(hex-2-en-1-yl)-4-methoxybenzamide

**R$_f$:** 0.38 (20% EtOAC/Hex)

**$^1$H NMR (500 MHz, CDCl$_3$)** δ 7.74 (d, *J* = 8.9 Hz, 2H), 6.93 (d, *J* = 8.9 Hz, 2H), 5.94 (s, 1H), 5.63 (dtt, *J* = 10.4, 7.3, 1.4 Hz, 1H), 5.56 – 5.46 (m, 1H), 4.10 (, *J* = 6.1 Hz, 2H), 3.86 (s, 3H), 2.13 (q, *J* = 6.7 Hz, 2H), 1.43 (h, *J* = 7.4 Hz, 2H), 0.94 (t, *J* = 7.4 Hz, 3H).

**$^{13}$C NMR (126 MHz, CDCl$_3$)** δ 166.9, 162.1, 134.0, 128.6, 126.9, 125.2, 113.7, 55.4, 37.1, 29.4, 22.7, 13.7.

**HRMS analysis (ESI):** calculated for [M+H]$^+$: C14H20NO2: 234.1494; Found: 234.1490
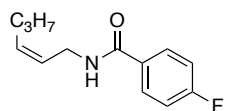
**I-70d**, (*Z*)-4-fluoro-*N*-(hex-2-en-1-yl)benzamide

**R$_f$:** 0.15 (10% EtOAC/Hex)

**$^1$H NMR (500 MHz, CDCl$_3$)** δ 7.78 (dd, *J* = 8.6, 5.3 Hz, 2H), 7.09 (t, *J* = 8.6 Hz, 2H), 6.11 (s, 1H), 5.67 – 5.56 (m, 1H), 5.56 – 5.46 (m, 1H), 4.08 (t, *J* = 6.1 Hz, 2H), 2.11 (q, *J* = 7.4 2H), 1.41 (h, *J* = 7.3 Hz, 2H), 0.92 (t, *J* = 7.4 Hz, 3H).

**$^{13}$C NMR (126 MHz, CDCl$_3$) δ** 166.4, 164.7 (d, *J* = 251.8 Hz), 134.2, 130.7 (d, *J* = 3.3 Hz), 129.2 (d, *J* = 9.0 Hz), 124.9, 115.6 (d, *J* = 21.9 Hz), 37.3, 29.4, 22.6, 13.7.

**$^{19}$F NMR (470 MHz, CDCl$_3$)** δ -108.40.

**HRMS analysis (ESI):** calculated for [M+H]$^+$: C$_{13}$H$_{17}$FNO: 222.1294; Found: 222.1287
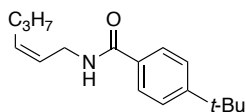


**I-70e**, (*Z*)-4-(*tert*-butyl)-*N*-(hex-2-en-1-yl)benzamide

**R$_f$:** 0.33 (20% EtOAC/Hex)

**$^1$H NMR (500 MHz, CDCl$_3$)** δ 7.71 (d, *J* = 8.5 Hz, 2H), 7.45 (d, *J* = 8.5 Hz, 2H), 5.99 (s, 1H), 5.63 (dtt, *J* = 10.4, 7.3, 1.4 Hz, 1H), 5.57 – 5.48 (m, 1H), 4.11 (t, *J* = 6.1 Hz, 2H), 2.13 (q, *J* = 7.6, 2H), 1.43 (h, *J* = 7.3 Hz, 2H), 1.34 (s, 9H), 0.94 (t, *J* = 7.3 Hz, 3H).

**$^{13}$C NMR (126 MHz, CDCl$_3$)** δ 167.3, 154.9, 134.1, 131.7, 126.7, 125.5, 125.2, 37.1, 34.9, 31.2, 29.4, 22.7, 13.7.

**HRMS analysis (ESI):** calculated for [M+H]$^+$: C$_{17}$H$_{26}$NO: 260.2014; Found: 260.2011

124
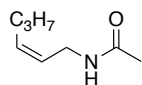
**I-70g**, (*Z*)-*N*-(hex-2-en-1-yl)acetamide

**R$_f$:** 0.23 (70% EtOAC/Hex)

**$^1$H NMR (500 MHz, CDCl$_3$)** δ 5.56 (dtt, *J* = 10.6, 7.5, 1.6 Hz, 1H), 5.46 (s, 1H), 5.40 (dtt, *J* = 10.8, 7.0, 1.6 Hz, 1H), 3.88 (t, *J* = 6.0 Hz, 2H), 2.04 (q, *J* = 7.6 Hz, 2H), 1.98 (s, 3H), 1.38 (h, *J* = 7.3 Hz, 2H), 0.90 (t, *J* = 7.4 Hz, 3H).

**$^{13}$C NMR (126 MHz, CDCl$_3$)** δ 169.9, 133.8, 125.1, 36.8, 29.3, 23.3, 22.6, 13.7.

**HRMS analysis (ESI):** calculated for [M+H]$^+$: C$_8$H$_{16}$NO: 142.1232; Found: 142.1229.
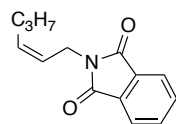


**I-70j**, (*Z*)-2-(hex-2-en-1-yl)isoindoline-1,3-dione

**R$_f$:** 0.17 (10% EtOAC/Hex)

**$^1$H NMR (500 MHz, CDCl$_3$)** δ 7.84 (dd, *J* = 5.4, 3.1 Hz, 2H), 7.70 (dd, *J* = 5.4, 3.0 Hz, 2H), 5.64 − 5.55 (m, 1H), 5.47 (dtd, *J* = 10.8, 7.0, 1.5 Hz, 1H), 4.32 (d, *J* = 7.0 Hz, 2H), 2.24 (q, *J* = 7.4 Hz, 2H), 1.44 (p, *J* = 7.3 Hz, 2H), 0.95 (t, *J* = 7.4 Hz, 3H).

**$^{13}$C NMR (126 MHz, CDCl$_3$)** δ 168.1, 134.4, 133.9, 132.3, 123.2, 123.0, 34.9, 29.3, 22.6, 13.8.

**HRMS analysis (ESI):** calculated for [M+H]$^+$: C$_{14}$H$_{16}$NO$_2$: 230.1181; Found: 230.1181
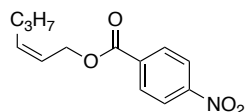


**I-70k**, (*Z*)-hex-2-en-1-yl 4-nitrobenzoate
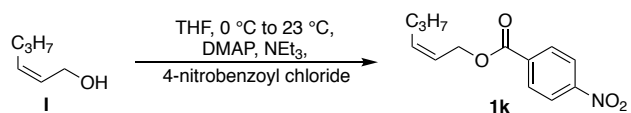
Alcohol **l** (400 mg, 4.0 mmol, 1.0 equiv) was placed in an oven-dried round bottom flask with stir bar under argon. THF (20 mL) and DMAP (12 mg, 0.1 mmol, 0.05 equiv) was added and the reaction was cooled to 0 °C, after which, 4-nitrobenzoyl chloride (814 mg, 4.4 mmol, 1.1 equiv) was added. Reaction progress was monitored by TLC and quenched at 2 h by the addition of water (5 mL). The reaction was concentrated in vacuo to remove THF. The aqueous phase was extracted with dichloromethane (3 x 10 mL). The combined organic layers were dried with anhydrous $Na_2SO_4$ and concentrated. Column chromatography ($SiO_2$/EtOAc–Hexanes gradient) provided **1j** in a 91% yield (909 mg).

**Rf:** 0.33 (10% EtOAC/Hex)

**¹H NMR (500 MHz, CDCl₃)** δ 8.29 (d, *J* = 9.1 Hz, 2H), 8.22 (d, *J* = 9.0 Hz, 2H), 5.75 (dtt, *J* = 11.0, 7.1, 1.0 Hz, 1H), 5.67 (dtt, *J* = 11.0, 6.9, 1.3 Hz, 1H), 4.92 (d, *J* = 6.4 Hz, 2H), 2.21 – 2.11 (m, 2H), 1.44 (h, *J* = 7.4 Hz, 2H), 0.93 (t, *J* = 7.4 Hz, 3H).

**¹³C NMR (126 MHz, CDCl₃)** δ 164.6, 150.5, 136.3, 135.7, 130.7, 123.5, 122.7, 61.7, 29.6, 22.5, 13.7.
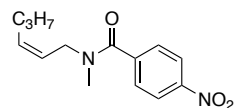


**I-70l**, (*Z*)-*N*-(hex-2-en-1-yl)-*N*-methyl-4-nitrobenzamide
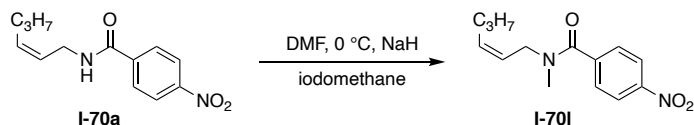
**I-70a** (124 mg, 0.5 mmol, 1.0 equiv) was added to a flame dried round bottom flask with stir bar under argon. Distilled DMF (5 mL) was added and the reaction was cooled to 0 °C. After stirring for 5 min, iodomethane (0.047 mL, 0.75 mmol, 1.5 equiv) was added via syringe and the reaction was slowly warmed to room temperature. The reaction was monitored by TLC and reached completion at 1 h. It was again cooled to 0 °C. Water (1 mL) was added dropwise to quench the reaction. After the exotherm was complete, water (10 mL) and dichloromethane (5 mL) were added, and the organic layer was separated. The organics were washed with water (3 x 5 mL) and then concentrated. Column chromatography (SiO$_2$/EtOAc–Hexanes gradient) provided **I-70l** in a 88% yield (121.8 mg).

**I-70l** exists as two rotamers in chloroform at room temperature in a ratio of 0.56:0.44.

*Major rotamer*: $^1$H NMR (500 MHz, CDCl$_3$) δ 8.27 (d, $J$ = 8.0 Hz, 2H), 7.58 (d, $J$ = 8.6 Hz, 2H), 5.61 (dd, $J$ = 12.5, 5.9 Hz, 1H), 5.37 (dt, $J$ = 11.0, 6.6 Hz, 1H), 3.83 (d, $J$ = 6.6 Hz, 2H), 3.08 (s, 3H), 1.85 (q, $J$ = 7.4 Hz, 2H), 1.33 (q, $J$ = 7.4 Hz, 2H), 0.84 (t, $J$ = 7.4 Hz, 3H).

*Minor rotamer*: $^1$H NMR (500 MHz, CDCl$_3$) δ 8.27 (d, $J$ = 8.0 Hz, 2H), 7.58 (d, $J$ = 8.6 Hz, 2H), 5.72 (q, $J$= 8.3 Hz, 1H), 5.47 (dd, $J$ = 10.0, 7.5 Hz, 1H), 4.23 (d, $J$ = 7.1 Hz, 2H), 2.87 (s, 3H), 2.14 (t, $J$ = 7.4 Hz, 2H), 1.44 (q, $J$ = 7.4 Hz, 2H), 0.94 (t, $J$ = 7.4 Hz, 3H).

Carbon NMR of the mixture is not reported since it was not possible to assign peaks to the major and minor components with confidence.

**HRMS analysis (ESI):** calculated for [M+H]$^+$: C$_{14}$H$_{20}$N$_2$O$_3$: 263.1396; Found: 263.1406
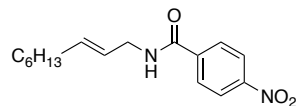
**I-70q,** (*E*)-4-nitro-*N*-(non-2-en-1-yl)benzamide

**R<sub>f</sub>:** 0.53 (40% EtOAc/Hex)

**¹H NMR (500 MHz, CDCl₃)** δ 8.30 (d, *J* = 8.8 Hz, 2H), 7.95 (d, *J* = 8.8 Hz, 2H), 6.15 (s, 1H), 5.78-5.71 (m, 1H), 5.60 − 5.51 (m, 1H), 4.06 (t, *J* = 6.6 Hz, 2H), 2.06 (q, *J* = 8.1, 7.5 Hz, 2H), 1.38 (q, *J* = 7.2, 6.7 Hz, 2H), 1.35 − 1.24 (m, 6H), 0.89 (t, *J* = 7.4 Hz, 3H)

**¹³C NMR (126 MHz, CDCl₃)** δ 165.1, 149.6, 140.2, 135.3, 128.1, 124.7, 123.9, 42.4, 32.3, 31.7, 29.0, 28.9, 22.6, 14.1.

**HRMS analysis (ESI):** calculated for [M+H]⁺: $C_{16}H_{23}N_2O_3$: 291.1709; Found: 291.1706.
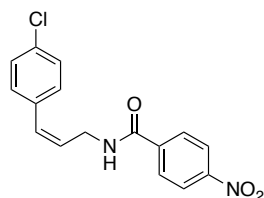


**1-70t**, (*Z*)-*N*-(3-(4-chlorophenyl)allyl)-4-nitrobenzamide

**R<sub>f</sub>:** 0.25 (30% EtOAC/Hex)

**¹H NMR (500 MHz, CDCl₃)** δ 8.29 (d, *J* = 8.8 Hz, 2H), 7.90 (d, *J* = 8.7 Hz, 2H), 7.34 (d, *J* = 8.5 Hz, 2H), 7.21 (d, *J* = 8.4 Hz, 2H), 6.62 (d, *J* = 11.5 Hz, 1H), 6.25 (s, 1H), 5.78 (dt, *J* = 11.5, 6.7 Hz, 1H), 4.36 (ddd, *J* = 7.0, 5.5, 1.9 Hz, 2H).

**¹³C NMR (126 MHz, CDCl₃)** δ 165.3, 149.7, 139.8, 134.4, 133.4, 131.3, 130.0, 128.7, 128.1, 127.6, 123.9, 38.6.

**HRMS analysis (ESI):** calculated for [M+H]⁺: $C_{16}H_{14}ClN_2O_3$: 317.0693; Found: 317.0693.
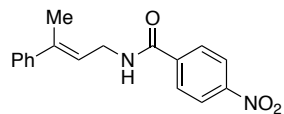
**I-70x**, (*E*)-4-nitro-*N*-(3-phenylbut-2-en-1-yl)benzamide

**R_f:** 0.43 (40% EtOAC/Hex)

**$^1$H NMR (500 MHz, CDCl$_3$)** δ 8.31 (d, *J* = 8.7 Hz, 2H), 7.96 (d, *J* = 8.8 Hz, 2H), 7.46 – 7.40 (m, 2H), 7.39 – 7.32 (m, 2H), 7.32 – 7.28 (m, 1H), 6.22 (s, 1H), 5.88 (td, *J* = 7.1, 1.5 Hz, 1H), 4.31 (t, *J*=6.3 2H), 2.18 (s, 3H).

**$^{13}$C NMR (126 MHz, CDCl$_3$)** δ 165.4, 149.6, 142.5, 140.1, 139.7, 128.4, 128.1, 127.6, 125.8, 123.9, 122.3, 38.9, 16.2.

**HRMS analysis (ESI):** calculated for [M+H]$^+$: C$_{17}$H$_{17}$N$_2$O$_3$: 297.1239; Found: 297.1238

# REFERENCES

# REFERENCES

1. Jacobsen, E. N.; Zhang, W.; Muci, A. R.; Ecker, J. R.; Deng, L., Highly Enantioselective Epoxidation Catalysts Derived from 1,2-Diaminocyclohexane. *J. Am. Chem. Soc.* **1991,** *113*, 7063-7064.

2. Katsuki, T.; Sharpless, K. B., The 1st Practical Method for Asymmetric Epoxidation. *J. Am. Chem. Soc.* **1980,** *102*, 5974-5976.

3. Wang, Z. X.; Tu, Y.; Frohn, M.; Zhang, J. R.; Shi, Y., An efficient catalytic asymmetric epoxidation method. *J. Am. Chem. Soc.* **1997,** *119*, 11224-11235.

4. Zhu, Y. G.; Wang, Q.; Cornwall, R. G.; Shi, Y., Organocatalytic Asymmetric Epoxidation and Aziridination of Olefins and Their Synthetic Applications. *Chem. Rev.* **2014,** *114*, 8199-8256.

5. Li, Z.; Conser, K. R.; Jacobsen, E. N., Asymmetric Alkene Aziridination with Readily Available Chiral Diimine-Based Catalysts. *J. Am. Chem. Soc.* **1993,** *115*, 5326-5327.

6. Kolb, H. C.; Vannieuwenhze, M. S.; Sharpless, K. B., Catalytic Asymmetric Dihydroxylation. *Chem. Rev.* **1994,** *94*, 2483-2547.

7. Bodkin, J. A.; McLeod, M. D., The Sharpless asymmetric aminohydroxylation. *Journal of the Chemical Society-Perkin Transactions 1* **2002**, 2733-2746.

8. Bruncko, M.; Schlingloff, G.; Sharpless, K. B., N-bromoacetamide - A new nitrogen source for the catalytic asymmetric aminohydroxylation of olefins. *Angewandte Chemie-International Edition in English* **1997,** *36*, 1483-1486.

9. Demko, Z. P.; Bartsch, M.; Sharpless, K. B., Primary amides. A general nitrogen source for catalytic asymmetric aminohydroxylation of olefins. *Org. Lett.* **2000,** *2*, 2221-2223.

10. Knowles, W. S., Asymmetric hydrogenations (Nobel lecture). *Angew Chem Int Edit* **2002,** *41*, 1999-2007.

11. Noyori, R., Asymmetric catalysis: Science and opportunities (Nobel lecture). *Angew Chem Int Edit* **2002,** *41*, 2008-2022.

12. Zhang, Z. Y.; Wang, J. X.; Li, J.; Yang, F.; Liu, G. D.; Tang, W. J.; He, W. W.; Fu, J. J.; Shen, Y. H.; Li, A.; Zhang, W. D., Total Synthesis and Stereochemical Assignment of Delavatine A: Rh-Catalyzed Asymmetric Hydrogenation of Indene-Type

Tetrasubstituted Olefins and Kinetic Resolution through Pd Catalyzed Triflamide-Directed C-H Olefination. *J. Am. Chem. Soc.* **2017,** *139*, 5558-5567.

13. Chung, W. J.; Vanderwal, C. D., Stereoselective Halogenation in Natural Product Synthesis. *Angew Chem Int Edit* **2016,** *55*, 4396-4434.

14. Zhang, Y. A.; Yaw, N.; Snyder, S. A., General Synthetic Approach for the Laurencia Family of Natural Products Empowered by a Potentially Biomimetic Ring Expansion. *J. Am. Chem. Soc.* **2019,** *141*, 7776-7788.

15. Shen, M. X.; Kretschmer, M.; Brill, Z. G.; Snyder, S. A., Strategies for the Total Synthesis of Diverse Bromo-Chamigrenes. *Org. Lett.* **2016,** *18*, 5018-5021.

16. Snyder, S. A.; Treitler, D. S.; Brucks, A. P.; Sattler, W., A General Strategy for the Stereocontrolled Preparation of Diverse 8- and 9-Membered Laurencia-Type Bromoethers. *J. Am. Chem. Soc.* **2011,** *133*, 15898-15901.

17. Burckle, A. J.; Gal, B.; Seidl, F. J.; Vasilev, V. H.; Burns, N. Z., Enantiospecific Solvolytic Functionalization of Bromochlorides. *J. Am. Chem. Soc.* **2017,** *139*, 13562-13569.

18. Neverov, A. A.; Brown, R. S., Br+ and I+ transfer from the halonium ions of adamantylideneadamantane to acceptor olefins. Halocyclization of 1,omega-alkenols and alkenoic acids proceeds via reversibly formed intermediates. *J. Org. Chem.* **1996,** *61*, 962-968.

19. Denmark, S. E.; Burk, M. T.; Hoover, A. J., On the absolute configurational stability of bromonium and chloronium ions. *J. Am. Chem. Soc.* **2010,** *132*, 1232-1233.

20. Olah, G. A.; Westerma.Pw; Melby, E. G.; Mo, Y. K., Onium Ions .10. Structural Study of Acyclic and Cyclic Halonium Ions by C-13 Nuclear Magnetic-Resonance Spectroscopy - Question of Intramolecular and Intermolecular Equilibration of Halonium Ions with Haloalkylcarbenium Ions. *J. Am. Chem. Soc.* **1974,** *96*, 3565-3573.

21. Ohta, B. K.; Hough, R. E.; Schubert, J. W., Evidence for beta-chlorocarbenium and beta-bromocarbenium ions. *Org. Lett.* **2007,** *9*, 2317-2320.

22. Ashtekar, K. D.; Marzijarani, N. S.; Jaganathan, A.; Holmes, D.; Jackson, J. E.; Borhan, B., A new tool to guide halofunctionalization reactions: the halenium affinity (HalA) scale. *J. Am. Chem. Soc.* **2014,** *136*, 13355-62.

23. Ashtekar, K. D.; Vetticatt, M.; Yousefi, R.; Jackson, J. E.; Borhan, B., Nucleophile-Assisted Alkene Activation: Olefins Alone Are Often Incompetent. *J. Am. Chem. Soc.* **2016,** *138*, 8114-9.

24. Whitehead, D. C.; Yousefi, R.; Jaganathan, A.; Borhan, B., An Organocatalytic Asymmetric Chlorolactonization. *J. Am. Chem. Soc.* **2010,** *132*, 3298.

25. Jaganathan, A.; Staples, R. J.; Borhan, B., Kinetic Resolution of Unsaturated Amides in a Chlorocyclization Reaction: Concomitant Enantiomer Differentiation and Face Selective Alkene Chlorination by a Single Catalyst. *J. Am. Chem. Soc.* **2013,** *135*, 14806-14813.

26. Jaganathan, A.; Garzan, A.; Whitehead, D. C.; Staples, R. J.; Borhan, B., A Catalytic Asymmetric Chlorocyclization of Unsaturated Amides. *Angew Chem Int Edit* **2011,** *50*, 2593-2596.

27. Soltanzadeh, B.; Jaganathan, A.; Staples, R. J.; Borhan, B., Highly Stereoselective Intermolecular Haloetherification and Haloesterification of Allyl Amides. *Angew. Chem. Int. Ed. Engl.* **2015,** *54*, 9517-22.

28. Soltanzadeh, B.; Jaganathan, A.; Yi, Y.; Yi, H.; Staples, R. J.; Borhan, B., Highly Regio- and Enantioselective Vicinal Dihalogenation of Allyl Amides. *J. Am. Chem. Soc.* **2017,** *139*, 2132-2135.

29. Zhou, L.; Chen, J.; Tan, C. K.; Yeung, Y. Y., Enantioselective Bromoaminocyclization Using Amino-Thiocarbamate Catalysts. *J. Am. Chem. Soc.* **2011,** *133*, 9164-9167.

30. Cheng, Y. A.; Yu, W. Z.; Yeung, Y. Y., Carbamate-catalyzed enantioselective bromolactamization. *Angew. Chem. Int. Ed. Engl.* **2015,** *54*, 12102-6.

31. Struble, T. J.; Lankswert, H. M.; Pink, M.; Johnston, J. N., Enantioselective Organocatalytic Amine-Isocyanate Capture-Cyclization: Regioselective Alkene Iodoamination for the Synthesis of Chiral Cyclic Ureas. *Acs Catalysis* **2018,** *8*, 11926-11931.

32. Alix, A.; Lalli, C.; Retailleau, P.; Masson, G., Highly enantioselective electrophilic alpha-bromination of enecarbamates: chiral phosphoric acid and calcium phosphate salt catalysts. *J. Am. Chem. Soc.* **2012,** *134*, 10389-92.

33. Lebee, C.; Blanchard, F.; Masson, G., Highly Enantioselective Intermolecular Iodo- and Chloroamination of Enecarbamates Catalyzed by Chiral Phosphoric Acids or Calcium Phosphate Salts. *Synlett* **2016,** *27*, 559-563.

34. Qi, J.; Fan, G. T.; Chen, J.; Sun, M. H.; Dong, Y. T.; Zhou, L., Catalytic enantioselective bromoamination of allylic alcohols. *Chem. Commun.* **2014,** *50*, 13841-13844.

35. Seidl, F. J.; Min, C.; Lopez, J. A.; Burns, N. Z., Catalytic Regio- and Enantioselective Haloazidation of Allylic Alcohols. *J. Am. Chem. Soc.* **2018,** *140*, 15646-15650.

36. Pemberton, R.; Hu, D.; Burns, N.; Tantillo, D., Catalytic, enantioselective dibromination of allylic alcohols: A computational perspective. *Abstr Pap Am Chem S* **2016,** *251*.

37. Landry, M. L.; Hu, D. X.; McKenna, G. M.; Burns, N. Z., Catalytic Enantioselective Dihalogenation and the Selective Synthesis of (-)-Deschloromytilipin A and (-)-Danicalipin A. *J. Am. Chem. Soc.* **2016,** *138*, 5150-5158.

38. Hu, D. X.; Seidl, F. J.; Bucher, C.; Burns, N. Z., Catalytic Chemo-, Regio-, and Enantioselective Bromochlorination of Allylic Alcohols. *J. Am. Chem. Soc.* **2015,** *137*, 3795-3798.

39. Hu, D. X.; Shibuya, G. M.; Burns, N. Z., Catalytic Enantioselective Dibromination of Allylic Alcohols. *J. Am. Chem. Soc.* **2013,** *135*, 12960-12963.

40. Caron, M.; Carlier, P. R.; Sharpless, K. B., Regioselective Azide Opening of 2,3-Epoxy Alcohols by [Ti(O-I-Pr)2(N3)2] - Synthesis of Alpha-Amino-Acids. *J. Org. Chem.* **1988,** *53*, 5185-5187.

41. Cai, Y.; Liu, X.; Jiang, J.; Chen, W.; Lin, L.; Feng, X., Catalytic asymmetric chloroamination reaction of alpha,beta-unsaturated gamma-keto esters and chalcones. *J. Am. Chem. Soc.* **2011,** *133*, 5636-9.

42. Cai, Y. F.; Liu, X. H.; Zhou, P. F.; Feng, X. M., Asymmetric Catalytic Halofunctionalization of alpha,beta-Unsaturated Carbonyl Compounds. *J. Org. Chem.* **2019,** *84*, 1-13.

43. Jiang, D. H.; He, T.; Ma, L.; Wang, Z. Y., Recent developments in Ritter reaction. *Rsc Advances* **2014,** *4*, 64936-64946.

44. Ritter, J. J.; Minieri, P. P., A New Reaction of Nitriles .1. Amides from Alkenes and Mononitriles. *J. Am. Chem. Soc.* **1948,** *70*, 4045-4048.

45. Lusskin, R. M.; Ritter, J. J., A New Reaction of Nitriles .5. Preparation of N-(2-Halo-1-Ethyl)-Amides. *J. Am. Chem. Soc.* **1950,** *72*, 5577-5578.

46. Cairns, T. L.; Graham, P. J.; Barrick, P. L.; Schreiber, R. S., A New Reaction of Olefins, Nitriles, and Halogens. *J. Org. Chem.* **1952,** *17*, 751-757.

47. Yeung, Y. Y.; Gao, X.; Corey, E. J., A general process for the haloamidation of olefins. Scope and mechanism. *J. Am. Chem. Soc.* **2006,** *128*, 9644-5.

48. Yeung, Y. Y.; Hong, S.; Corey, E. J., A short enantioselective pathway for the synthesis of the anti-influenza neuramidase inhibitor Oseltamivir from 1,3-butadiene and acrylic acid. *J. Am. Chem. Soc.* **2006,** *128*, 6310-6311.

49. Tay, D. W.; Tsoi, I. T.; Er, J. C.; Leung, G. Y. C.; Yeung, Y. Y., Lewis Basic Selenium Catalyzed Chloroamidation of Olefins Using Nitriles as the Nucleophiles. *Org. Lett.* **2013,** *15*, 1310-1313.

50. Lucchini, V.; Modena, G.; Pasquato, L., Enantiopure Thiosulfonium Salts in Asymmetric-Synthesis - Face Selectivity in Electrophilic Additions to Unfunctionalised Olefins. *Journal of the Chemical Society-Chemical Communications* **1994**, 1565-1566.

51. Guerinot, A.; Reymond, S.; Cossy, J., Ritter Reaction: Recent Catalytic Developments. *European Journal of Organic Chemistry* **2012,** *2012*, 19-28.

52. Arnold, A. M.; Pothig, A.; Drees, M.; Gulder, T., NXS, Morpholine, and HFIP: The Ideal Combination for Biomimetic Haliranium-Induced Polyene Cyclizations. *J. Am. Chem. Soc.* **2018,** *140*, 4344-4353.

53. Roth, A.; Denmark, S. E., Enantioselective, Lewis Base-Catalyzed, Intermolecular Sulfenoamination of Alkenes. *J. Am. Chem. Soc.* **2019,** *141*, 13767-13771.

54. Yousefi, R.; Sarkar, A.; Ashtekar, K. D.; Whitehead, D. C.; Kakeshpour, T.; Holmes, D.; Reed, P.; Jackson, J. E.; Borhan, B., Mechanistic Insights into the Origin of Stereoselectivity in an Asymmetric Chlorolactonization Catalyzed by (DHQD)(2)PHAL. *J. Am. Chem. Soc.* **2020,** *142*, 7179-7189.

55. Soltanzadeh, B.; Jaganathan, A.; Yi, Y.; Yi, H.; Staples, R. J.; Borhan, B., Highly Regio- and Enantioselective Vicinal Dihalogenation of Allyl Amides. *J. Am. Chem. Soc.* **2017,** *139*, 2132-2135.

56. Nicolaou, K. C.; Simmons, N. L.; Ying, Y. C.; Heretsch, P. M.; Chen, J. S., Enantioselective Dichlorination of Allylic Alcohols. *J. Am. Chem. Soc.* **2011,** *133*, 8134-8137.

57. Gadwood, R. C.; Kamdar, B. V.; Dubray, L. A. C.; Wolfe, M. L.; Smith, M. P.; Watt, W.; Mizsak, S. A.; Groppi, V. E., Synthesis and Biological-Activity of Spirocyclic

Benzopyran Imidazolone Potassium Channel Openers. *J. Med. Chem.* **1993,** *36*, 1480-1487.

58. Zhou, L.; Chen, J.; Zhou, J.; Yeung, Y. Y., N-Bromosuccinimide Promoted One-Pot Synthesis of Guanidine: Scope and Mechanism. *Org. Lett.* **2011,** *13*, 5804-5807

59. Booker-Milburn, K. I.; Guly, D. J.; Cox, B.; Procopiou, P. A., Ritter-type reactions of N-chlorosaccharin: a method for the electrophilic diamination of alkenes. *Org. Lett.* **2003,** *5*, 3313-5.

60. Tao, Z.; Gilbert, B. B.; Denmark, S. E., Catalytic, Enantioselective syn-Diamination of Alkenes. *J. Am. Chem. Soc.* **2019,** *141*, 19161-19170.

61. Muniz, K.; Barreiro, L.; Romero, R. M.; Martinez, C., Catalytic Asymmetric Diamination of Styrenes. *J. Am. Chem. Soc.* **2017,** *139*, 4354-4357.

62. Rajbongshi, K. K.; Saikia, I.; Chanu, L. D.; Roy, S.; Phukan, P., A Metal-Free Protocol for Aminofunctionalization of Olefins Using TsNBr2. *J. Org. Chem.* **2016,** *81*, 5423-32.

63. Lykke, L.; Carlsen, B. D.; Rambo, R. S.; Jorgensen, K. A., Catalytic asymmetric synthesis of 4-nitropyrazolidines: an access to optically active 1,2,3-triamines. *J. Am. Chem. Soc.* **2014,** *136*, 11296-9.

64. Ingalls, E. L.; Sibbald, P. A.; Kaminsky, W.; Michael, F. E., Enantioselective Palladium-Catalyzed Diamination of Alkenes Using N-Fluorobenzenesulfonimide. *J. Am. Chem. Soc.* **2013,** *135*, 8854-8856.

65. Cardona, F.; Goti, A., Metal-catalysed 1,2-diamination reactions. *Nat. Chem.* **2009,** *1*, 269-275.

66. Du, H. F.; Zhao, B. G.; Shi, Y., Catalytic asymmetric allylic and homoallylic diamination of terminal olefins via formal C-H activation. *J. Am. Chem. Soc.* **2008,** *130*, 8590.

67. Jiang, H.; Nielsen, J. B.; Nielsen, M.; Jorgensen, K. A., Organocatalysed asymmetric beta-amination and multicomponent syn-selective diamination of alpha,beta-unsaturated aldehydes. *Chemistry (Easton)* **2007,** *13*, 9068-9075.

68. Du, H. F.; Yuan, W. C.; Zhao, B. G.; Shi, Y. A., Catalytic asymmetric diamination of conjugated dienes and triene. *J. Am. Chem. Soc.* **2007,** *129*, 11688.

## Chapter II  Bromenium and Chlorenium Mechanistic Divergence

## II-1  Catalytic Bromenium and Chlorenium Induced Reactions

Halofunctionalization reactions serve as one of the early transformations introduced in sophomore organic chemistry. The mechanism of this family of reactions is often portrayed in a simplified manner that does not satisfy observed reactivity reflected in the dependence on both the halenium donor and the nucleophile; furthermore, little effort explored dissimilarities between different halenium ions, halenium sources, and nucleophiles in their roles in dictating reaction pathways. We were particularly drawn to dissecting differences between bromenium and chlorenium induced reactions with allyl amides when we discovered a divergent reaction with the chlorenium reagent providing the intermolecular chloroamide product and the analogous bromenium reagent yielding the bromocyclization product (Figure II-1). To the best of our knowledge, this is the first halenium dependent divergent reaction. Through investigation of nucleophile and electrophile reactivity, we were able to redirect the bromenium induced reactions to provide a strong preference for the intermolecular bromoamide product **II-14** (Table II-1). Mechanistic analysis through Eyring plots examine the enthalpic and entropic variables as a function of nitrile nucleophile and bromenium sources. Taken together, this hints at a concerted mechanism for intermolecular bromofunctionalizations.

## II-2  Bromenium Reaction Divergence

The stereodefined carbon bromine bond is a highly valuable functionality in organic chemistry. Recent advancements display its utility in downstream synthesis and its

increased ability to halogen bond is structurally significant and unique to chlorine. While chlorenium has served as the primary halogen electrophile in previous alkene halofunctionalizations, we were delighted that the intermolecular enantioselective halofunctionalizations previously developed within our laboratory were highly compatible with both chlorenium and bromenium induced reactions. This enabled the construction of stereodefined vicinal bromoethers (**II-5**)[1] and bromochlorides (**II-6**)[2] with efficiency similar to their chlorine analogs (Figure II-2). To our surprise, the extension of our halo-Ritter chemistry[3] is incompatible with dibromodimethyl hydantoin (DBDMH), the bromenium equivalent of DCDMH. Interestingly, this reaction condition cleanly provided oxazoline (**II-7**) in 75% enantiomeric excess with no trace of the Ritter product. The use of NBS, the bromenium source of choice for dihalogenation and bromoetherification reactions, provided only a trace of the intermolecular product (~2% intermolecular product). While background reactions for both bromo and chlorofunctionalization reactions can lead to cyclization, conditions for the bromoamidation yield the cyclization product in 75% *ee*; thus, under these conditions, the cyclization product is indeed a catalyzed process. To the best of our knowledge, this reaction is the first report of a halenium dependent divergent reaction. This focus of this section is to elucidate the origin of the observed divergence in catalytic halofunctionalization reaction.
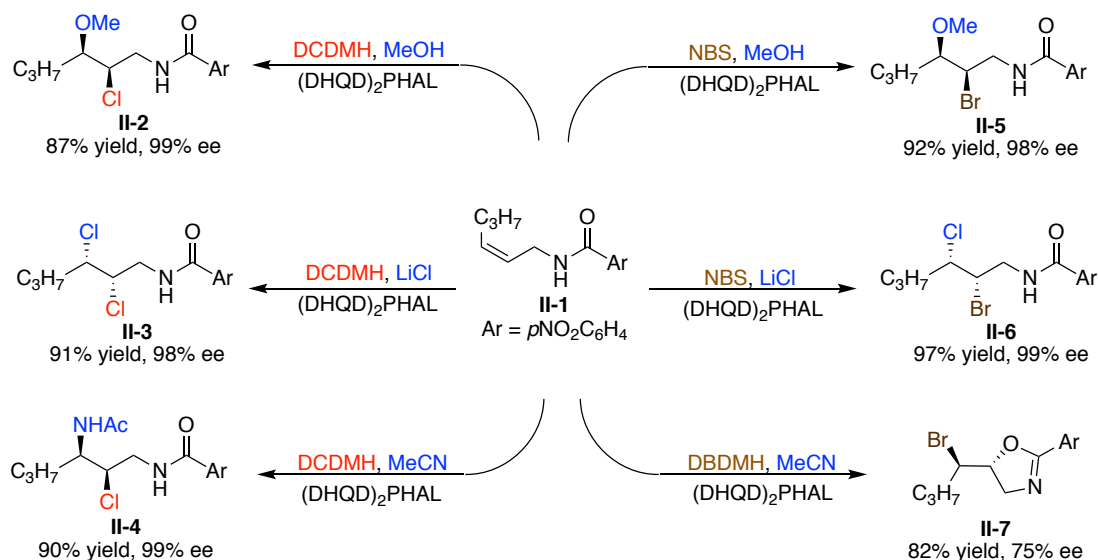
**Figure II-1:** Divergent reaction paths observed with chlorenium and bromenium reagents

## II-2-1  Kinetic     Competition     Studies     for     Catalyzed

## Halofunctionalizations
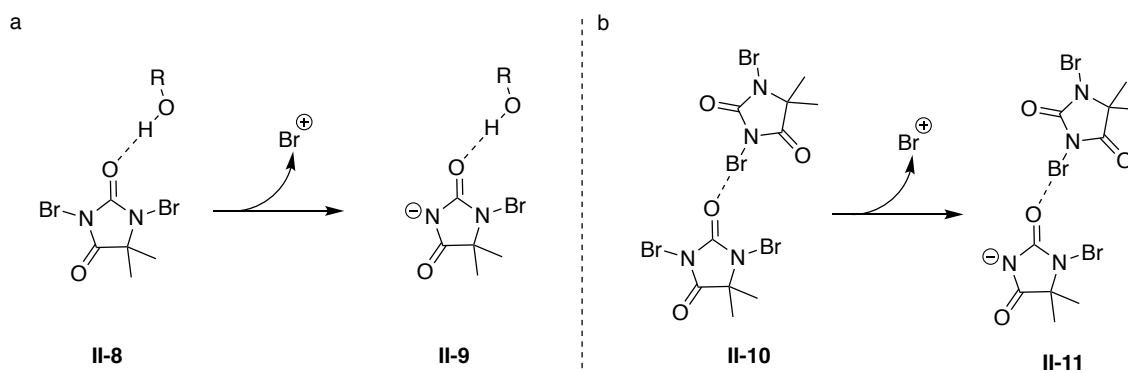


**Figure II-2:** (a) Hydrogen bond assisted bromenium transfer (b) Halogen bond assisted bromenium transfer

We performed comparative kinetic studies in a preliminary effort to probe the origin

of the observed reaction divergence for the bromenium and chlorenium induced reactions.

The competition reactions serve as a gauge of the relative reaction rates, as well as probe

hydrogen (Figure II-2a)[4] and/or halogen bond (Figure II-2b)[5-6] as the potential origin of

the reaction divergence. These studies lay the groundwork for the development of an enantioselective bromoamidation of alkenes.

## II-2-1-1   Nucleophile Dependent Kinetic Competition Study

The divergent reaction paths illustrated in Figure II-1 suggest that the nucleophile plays a role in the ultimate fate of the reaction. Acetonitrile, the weakest nucleophile tested, is the only one that failed to provide the intermolecular product. While nucleophilicity appears to function as the determining factor in the reaction pathway, each reaction is performed in a different protic medium. This is significant as proton donors are known to function in different roles for catalytic asymmetric halofunctionalization ranging from activation of halenium ion sources (Figure II-2a)[7-9] to modulating the confirmation of cinchona alkaloid catalysts.[10] Cognizant of the fact that different proton donors with different polarities have been employed as solvents in bromoetherification (methanol cosolvent) and bromochlorination (trifluoroethanol solvent), we sought to compare a successful nucleophile with an unsuccessful nucleophile in the same reaction medium. If nucleophilicity plays a role in dictating the product distribution, then there should be a preference for the stronger nucleophile to appear in the product. We viewed a 1:1 molar ratio of methanol with acetonitrile as the ideal medium to study as methanol reacts cleanly to provide the intermolecular product and acetonitrile only provides the cyclized product. We observed exclusive formation of **II-2** (Figure II-3a), hence displaying methanol's nucleophilic superiority.

To support the proposal that enhanced nucleophilicity modulates the reaction pathway as opposed to the nucleophile's ability to function as a hydrogen bond donor, we

employed a 1:1 molar concentration of acetonitrile and dimethylcyanamide (DMC) in dichloramine-T initiated chloroamidation (Figure II-3b). The dimethylcyanamide nucleophile outcompeted acetonitrile yielding an 8:1 ratio of the two corresponding products. This displays the ability of a stronger nitrile nucleophile to redirect the reaction.
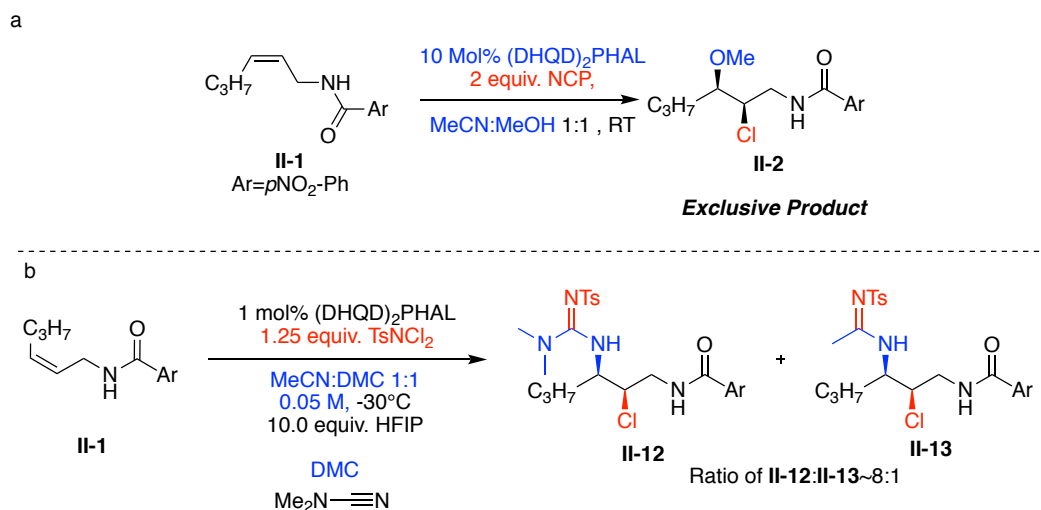


**Figure II-3:** Nucleophile dependent kinetic competition study

## II-2-1-2 Halenium Dependent Kinetic Competition Study

The use of competition reactions between analogous chlorenium and bromenium reagents probes the relative rates of chlorenium and bromenium induced halofunctionalizations and potential for halogen bonding (Figure II-2b) to redirect the reaction pathway.[5-6] Subjecting **II-1** to a solution of a 1:1 molar ratio of N-chlorophthalimide (NCP) and N-bromophthalimide (NBP) provided the bromocyclized product **II-7** with no trace of chlorofunctionalization or Ritter products (Figure II-4). This

result indicates the increased reaction rate for bromofunctionalizations relative to chlorofunctionalizations.
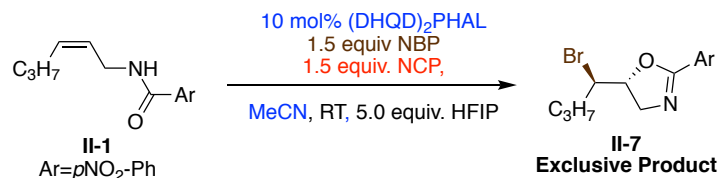


**Figure II-4**: Bromenium and chlorenium kinetic competition

The results of the nucleophile competition reactions prompted efforts to redirect the reaction pathway and provide a catalytic asymmetric bromo Ritter product. Comparing acetonitrile and methanol, methanol was significantly faster. The effect of nucleophilicity was also apparent in the competitive reaction between DMC and acetonitrile. Additionally, between analogous chlorenium (NCP) and bromenium (NBP) sources, bromenium reacted faster than chlorenium. The results of the studies suggest the use of a stronger nitrile nucleophile and a less potent (i.e., higher *HalA*) bromenium source could lead to a successful enantioselective bromo Ritter reaction.

## II-2-2  Catalytic Asymmetric Bromoamidation Optimization

With guiding principles discussed in Section II-2-1 in hand, we aspired to develop an intermolecular bromoamidation reaction. The optimization of this reaction is shown in Table II-1. As previously mentioned, we hypothesized that a stronger nitrile nucleophile could potentially outcompete the cyclization reaction and provide the bromo Ritter product. We viewed DMC's enhanced nucleophilicity as the ideal mode to test to this hypothesis having already displayed its nucleophilic superiority (Figure II-3b). Gratifyingly, the employment of DMC (entry 2) greatly improved the yield, providing a 39% yield of **II-8**. An

increase in hexafluoroisopropanol (HFIP) equivalents (entry 3) proved advantageous, further improving the yield of the intermolecular product. Next, we compared different bromonium sources and their ability to modulate the reaction pathway. The potent halenium donor N-bromosaccharine (*HalA* of 112.2 kcal/mol in polar solvent) completely reverted selectivity to produce the cyclization product **II-7** (entry 5). Additionally, under these conditions, **II-7** was racemic. Use of weaker bromenium sources (based on their *HalA* values) led to improved **II-7:II-14** ratios. For example, the use of N-bromophthalimide (*HalA* of 131.3 kcal/mol in polar solvent) offered improved selectivity favoring the Ritter product in preference to cyclization in roughly a ~ 4:1 ratio. Further optimization displayed that HFIP positively affects the reaction with 100 equivalents providing the optimal results.

**Table II-1:** Catalytic bromoamidation optimization



| Entry | Solvent | Temp °C | HFIP Equiv. | Br+ Source | Ratio **II-7:II-14**[a] | Yield (**II-14**)[b] | *ee* (**II-14**)[c] |
|---|---|---|---|---|---|---|---|
| 1 | ACN | -30 | 10 | DBDMH | 100:0[d] | 0[d] | NA |
| 2 | DMC | -40 | 10 | DBDMH | 45:55 | 39 | 99% |
| 3 | DMC | -40 | 20 | DBDMH | 42:58 | 47 | 99% |
| 4 | DMC | -40 | 20 | NBSAC | 100:0 | 0 | NA |
| 5 | DMC | -40 | 20 | N-Bromophthalimide | 19:81 | 69 | 99% |
| 6 | DMC | -40 | 100 | N-Bromophthalimide | 6:94 | 79 | 99% |

[a] Ratio determined by NMR of crude reaction mixture [b] NMR yield with triphenylmethane standard [c] enantiomeric excess determined by chiral HPLC. [d] There was no yield for the respective Ritter product

As indicated by the enantiomeric excess of both **II-7** and **II-14**, one can deduce that each reaction is efficiently catalyzed by (DHQD)$_2$PHAL, yet the selectivity can be inverted through the use of a large excess of HFIP. While the exact role of HFIP is uncertain at this time, protic additives are known to serve multiple roles in (DHQD)$_2$PHAL catalyzed halofunctionalizations. Two behaviors are particularly relevant to the divergent reactivity:

1) Protic additives are known to induce confirmational changes in (DHQD)$_2$PHAL upon protonation of the quinuclidine nitrogen atom. A modified catalyst conformation may catalyze one reaction in preference of the other.

2) While (DHQD)$_2$PHAL was employed as the catalyst in both halolactonization and intermolecular halofunctionalizations, mechanistic investigations suggest different roles for the quinuclidine nitrogen atom. In halolactonization reactions, the quinuclidine nitrogen atom acts as a base to enhance the nucleophilicity of the carboxylic acid. Conversely, in the case of haloetherification reactions, the polar protic solvent aids in the halogenation of the quinuclidine, which then transfers the halenium ion to the alkene. We speculate that HFIP might be playing a similar role in the divergent catalytic reactivity seen in Table II-2. The less of the protic additive used, the more likely the quinuclidine exists as a free base which can hydrogen bond with the amide; thus, enhancing the nucleophilicity for halocyclization (Figure II-5a, **II-15**). Additionally, HFIP functions as a
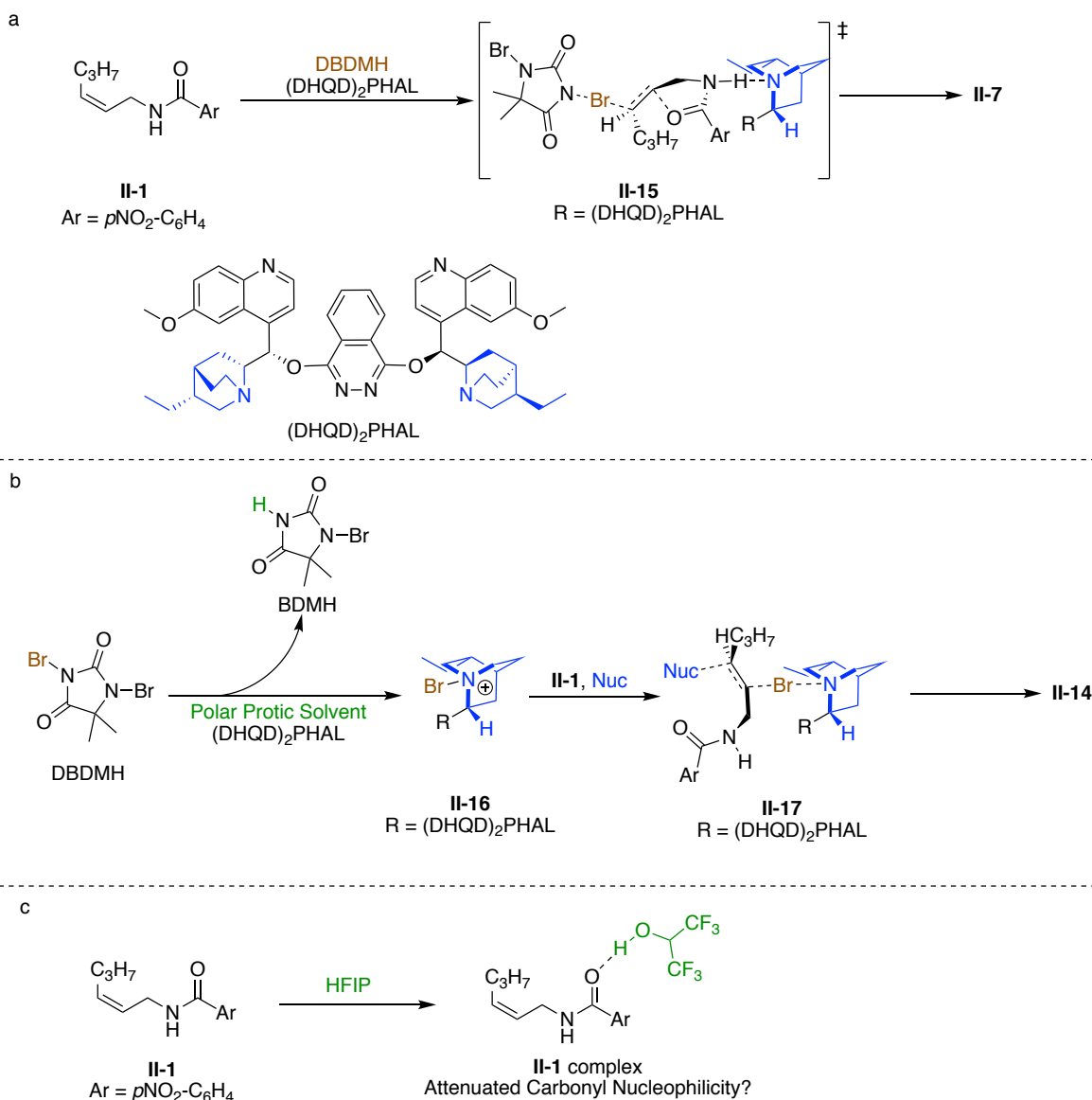
**Figure II-5:** Potential roles of HFIP in redirecting catalytic bromofunctionalizations. (a) Quinuclidine activating the amide providing **II-7** (b) Quinuclidine functioning as a Lewis base for chlorenium transfer (c) HFIP attenuating the nucleophilicity of the amide carbonyl

catalyst to lead to **II-16**, which has served as a key intermediate in intermolecular haloetherification reactions. It is reasonable to speculate that these two reactions are operating under different catalytic mechanisms with the same catalyst. One with less HFIP, that leads to the amide cyclization

through **II-15**, and an alternative mechanism with more HFIP that yields **II-16** leading to the intermolecular product.

It should also be noted that HFIP's ability to hydrogen bond may attenuate the nucleophilicity of the amide oxygen, leading to less **II-7**. (Figure II-5c).

## II-2-3 Nucleophile Assisted Alkene Activation in Catalytic Bromofunctionalization Reactions
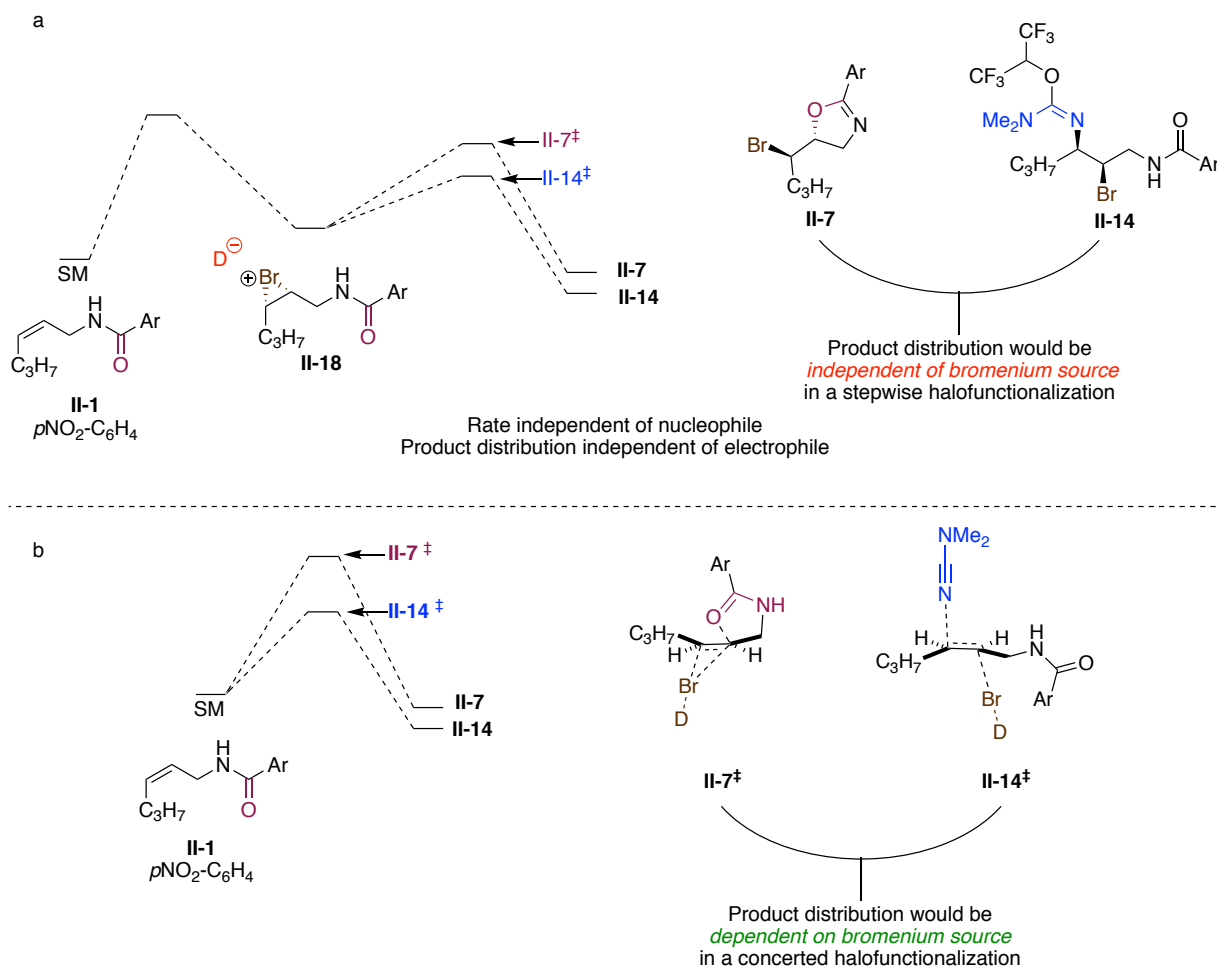


**Figure II-6:** (a) Classical reaction pathway which electrophile and nucleophile should have no influence on product distribution. (b) Mechanism with sensitivity to electrophile and nucleophile

The main challenge of bromoamidation optimization (Table II-1) was the improvement of the ratio of the intermolecular product **II-14** to the cyclization product **II-7**.

We discovered a high sensitivity to the bromenium donor with NBP providing a 4:1 ratio in preference of product **II-14** (entry 5) while N-bromosaccharine only provided the intramolecular product **II-7** (entry 3). This contradicts the classical reaction pathway (Figure II-6a) that proceeds through the formation of haliranium ion **II-18**, in which the selectivity determining step does not involve the bromenium donor's counteranion and therefore, product ratios should be independent of the donor. Alternatively, the dependence of the bromenium donor on product distribution suggests that it is involved in the selectivity determining step of the bromofunctionalization. This led us to the initial hypothesis that the intermolecular bromoamidation is a concerted addition of the bromenium and nucleophile to the alkene. The next set of experiments is focused on the relative entropic and enthalpic barriers to activation leading to products **II-7** and **II-14** and how a catalytic and concerted mechanism would affect those variables.

## II-2-4  Eyring Analysis of Competitive Reactions

We employed Eyring analysis to elucidate the mechanistic variables dictating the preference of **II-7** and **II-14** in terms of nucleophile and electrophile.[11] Considering that both intramolecular and intermolecular reactions are irreversible, the product ratios directly reflect the relative Gibbs free energies of the two selectivity determining step (or $\Delta\Delta G^{\ddagger}$). It is important to recognize that $\Delta G^{\ddagger}$ is comprised of enthalpy ($\Delta H^{\ddagger}$) and entropy ($\Delta S^{\ddagger}$) ($\Delta G^{\ddagger} = \Delta H^{\ddagger}-T\Delta S^{\ddagger}$), and therefore, the significance of the entropic barrier is scaled by temperature. This has enabled the elucidation of $\Delta H^{\ddagger}$ and $\Delta S^{\ddagger}$ by studying the effect of temperature on reaction rate. We sought to apply this in a comparative context between

**II-7** and **II-14** to probe the relative enthalpic and entropic factors leading each product to understand factors that lead to the divergent reaction behavior.

## II-2-4-1   Eyring Analysis of Varied Nucleophiles

The importance of nucleophilicity in delivering the intermolecular product is evident in entries 1 and 2 (Table II-1). We investigated the enthalpic and entropic differences between acetonitrile and DMC as nucleophiles, which required the use of alternative reaction conditions to provide a measurable quantity of bromo-Ritter product with acetonitrile. We were delighted to discover that with a large excess of HFIP (100 equiv.), a ~1:3 ratio of intermolecular acetonitrile bromo-Ritter product **II-19** to **II-7** was produced. This condition is similar to entry 6 (Table II-1), allowing for both Eyring analyses with DMC and acetonitrile to be completed under similar reaction conditions. This enables a fair comparison between the two Eyring analyses as they share **II-7** as a common internal clock, and acetonitrile and DMC have a similar dielectric constant (36.6 and 37.2, respectively).
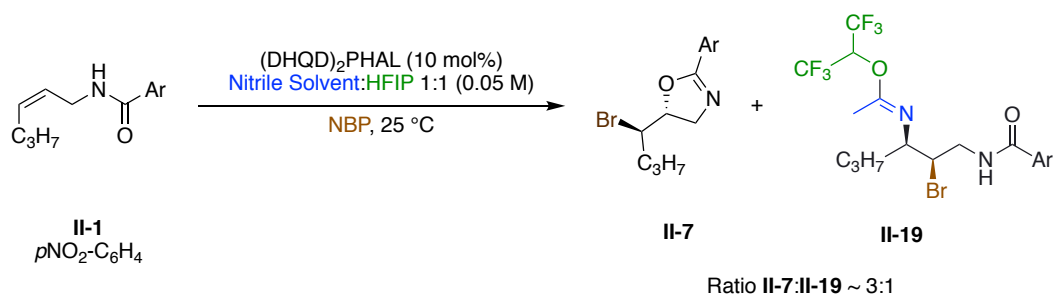


**Figure II-7:** Modified condition to yield Ritter product with acetonitrile

Competitive Eyring analysis of intermolecular reactions yielding **II-14** (Figure II-9a) and **II-19** (Figure II-8b) indicate lower enthalpic barrier (-3.9 and -2.6 kcal/mol, respectively) relative to the amide cyclization product **II-7.** The DMC's enhanced nucleophilicity provides a 1.3 kcal/mol lower enthalpic activation barrier for the intermolecular product, which helps redirect to favor the Ritter product. The relative entropic barriers favoring **II-7** relative to **II-14** and **II-19** indicate an increase in molecularity for the intermolecular reaction.

While these values only differ by 0.6 cal/molK, we were intrigued that acetonitrile, with its lower molecular weight and thus higher molarity relative to DMC (6.2 M for DMC, 9.6 M for acetonitrile), did not provide a lower entropic barrier than DMC (each reaction employed 0.5 mL of nucleophilic solvent and 0.5 mL of HFIP). This might be due to more pre-association of the DMC's higher energy HOMO with the alkene's LUMO.[12] At the moment, this is purely a speculative hypothesis, and more studies will continue; however, in terms of enthalpy, there is a clear correlation between nucleophile strength and a decreased enthalpy of activation.
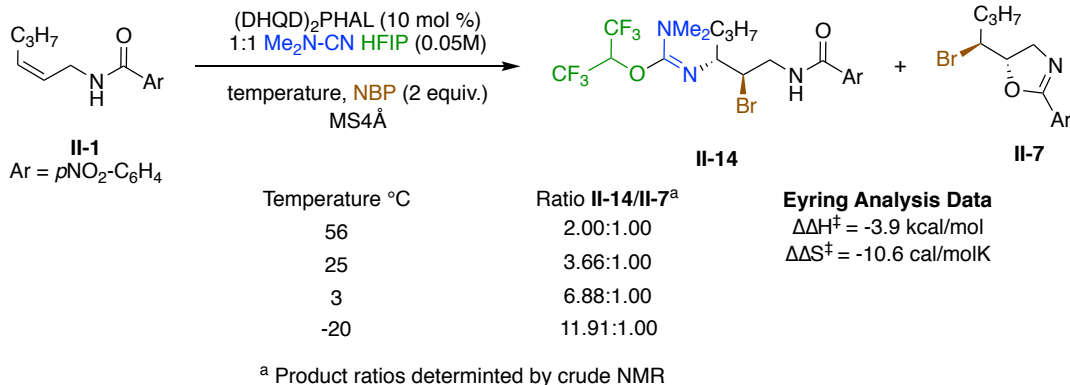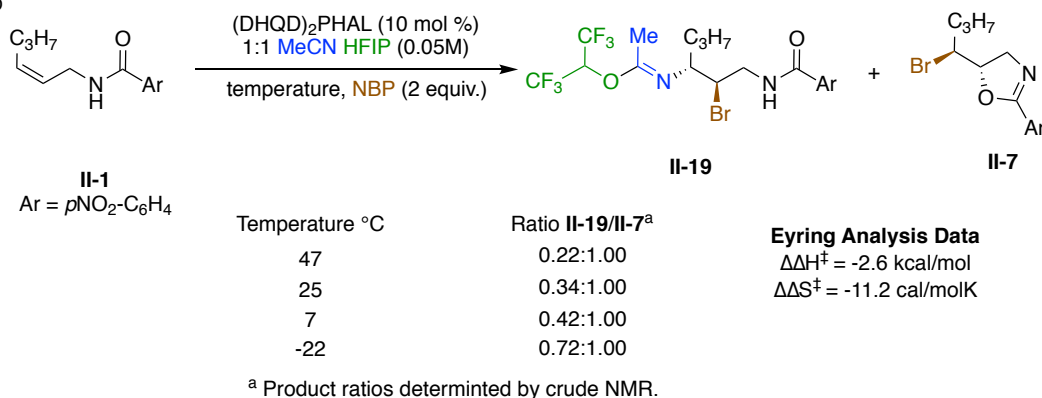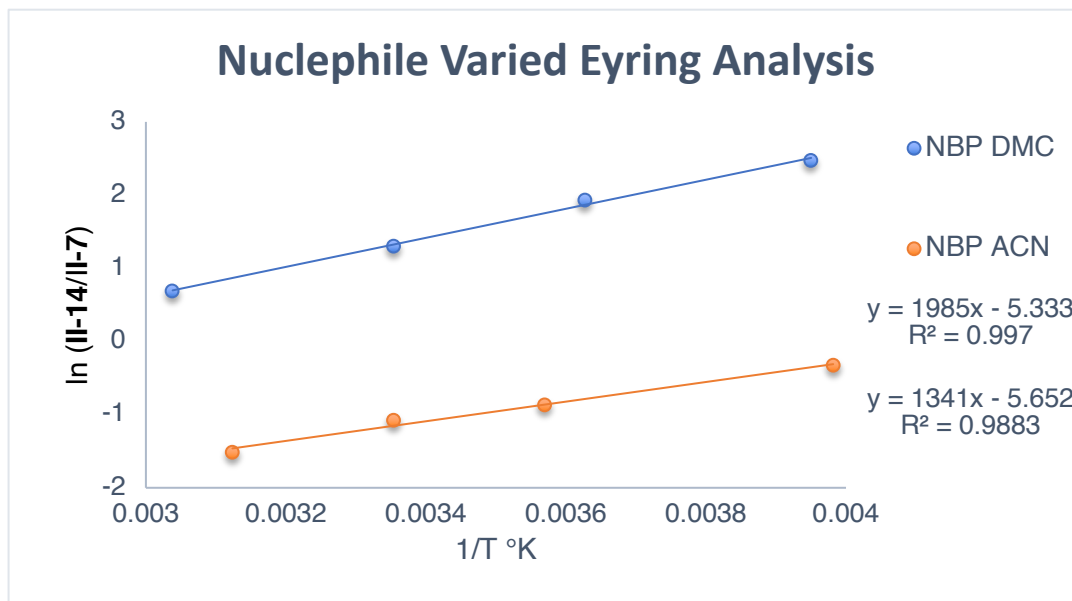
**Figure II-8:** (a) Eyring analysis with dimethylcyanamide. (b) Eyring analysis with acetonitrile. (c) Eyring Plots of data in (a) and (b)

## II-2-4-2  Eyring Analysis of Varied Bromenium Sources

Reaction screening indicated the importance of both the nucleophile and electrophile in product distribution. In an attempt to probe the role of the bromenium counter anion and relate it to the halenium affinity, and thus the potency of the bromenium source, we explored Eyring analysis for three brominating reagents with *HalAs* (B3LYP-6-31G* polar solvent) ranging from 131.3 kcal/mol in the case of NBP to 112.2 kcal/mol for N-bromosaccharine. The results of this study are summarized below in Figure II-9. While the nucleophilic strength affected the $\Delta\Delta H^{\ddagger}$ for both reaction paths, the bromenium source affected both the $\Delta\Delta H^{\ddagger}$ and $\Delta\Delta S^{\ddagger}$. The general trend bromenium strength shows that the more potent donor favors the intermolecular product **II-19** enthalpically but had the highest entropic penalty for the intermolecular product.

Our current hypothesis for the correlation between *HalA* and $\Delta\Delta H^{\ddagger}$ and $\Delta\Delta S^{\ddagger}$ is that since each reagent provides high *ee* for **II-19**, all are catalyzed. However, for more reactive bromenium sources, such as NBSac, the reaction to yield **II-7** is noncatalyzed as indicated by the 0% ee for **II-7** (Table II-1 entry 4, it is important to note that a reaction providing 0% *ee* can still be catalyzed process). This provides a significant difference between $\Delta\Delta H^{\ddagger}$ and $\Delta\Delta S^{\ddagger}$ as a catalyzed process is enthalpically favored but entropically disfavored. Alternatively, the *ee* obtained for both products with less reactive sources suggests that both pathways are at least partially catalyzed. This provides less of an

enthalpic and entropic barrier of the intermolecular reaction relative to the cyclization reaction.

(a)



| N-Bromopthalimide | |
|---|---|
| *HalA*: 131.3 kcal/mol | |
| $\Delta\Delta H^{\ddagger}$ = -2.6 kcal/mol | |
| $\Delta\Delta S^{\ddagger}$ = -10.6 cal/molK | |
| Temperature °C | Ratio **II-19:II-7** |
| 47 | 0.22:1.00 |
| 25 | 0.34:1.00 |
| 7 | 0.42:1.00 |
| -22 | 0.72:1.00 |

| Dibromodimethylhydantoin | |
|---|---|
| *HalA*: 123.8 kcal/mol | |
| $\Delta\Delta H^{\ddagger}$ = -3.6 kcal/mol | |
| $\Delta\Delta S^{\ddagger}$ = -16.6 cal/molK | |
| Temperature °C | Ratio **II-19:II-7** |
| 51 | 0.07:1.00 |
| 23 | 0.13:1.00 |
| 0 | 0.25:1.00 |
| -27 | 0.39:1.00 |

| N-Bromosaccharine | |
|---|---|
| *HalA*: 112.6 kcal/mol | |
| $\Delta\Delta H^{\ddagger}$ = -5.0 kcal/mol | |
| $\Delta\Delta S^{\ddagger}$ = -21.0 cal/molK | |
| Temperature °C | Ratio **II-19:II-7** |
| 51 | 0.07:1.00 |
| 23 | 0.10:1.00 |
| 0 | 0.39:1.00 |
| -27 | 0.70:1.00 |

(b)



**Figure II-9:** (a) Eyring analysis data for bromenium reagent temperature product ratio analysis. (b) Eyring plot of NBP, DBDMH and NBSac experiments

152

## II-2-5   Conclusion

Intrigued by an unprecedented divergent reactivity, which depends on the halenium ion (Figure II-1), we investigated the factors preferencing the intermolecular reaction relative to the intramolecular reaction. This led to the optimization of catalytic asymmetric bromo Ritter reaction via the use of a less reactive bromenium source and a stronger nitrile nucleophile. Though many aspects of the optimization of catalytic bromoamidation suggest that the reaction divergence could be operating under *NAAA*, Eyring analysis coupled with the enantioselectivity of halofunctionalization products indicated catalyst control of product distribution is likely with highly reactive bromenium sources such as N-bromosaccharine offering noncatalyzed pathways to **II-7**.

## II-3 Intermolecular Nucleophile Assisted Alkene Activation in Bromenium and Chlorenium Induced Halofunctionalizations

Introductory chemistry courses depict halofunctionalization reactions as a stepwise mechanism. This mechanism proceeds through the rate-determining formation of haliranium ion **II-21** that is subsequently opened by the nucleophile furnishing the difunctionalized product **II-22**. For this mechanistic picture to be true, the nucleophile should not affect the reaction rate and the halenium source should not affect product distribution. Our work examining the nucleophile's role in intramolecular reactions challenged the traditional mechanistic viewpoint and suggests a concerted addition of both nucleophile and halenium ion across the double bond for intramolecular halofunctionalizations.[12]

153

While nucleophile assisted halocyclization reactions have been studied in-depth, entropically challenged intermolecular halofunctionalizations have yet to see the same attention. A more complete understanding of this will enable control of reaction pathways via the selection of nucleophile and electrophile. Additionally, the ability to invoke a *NAAA* type concerted mechanism enables the potential to improve diastereoselectivity with electron rich alkenes that are prone to erosion of diastereoselectivity due to β-halocarbenium stability.
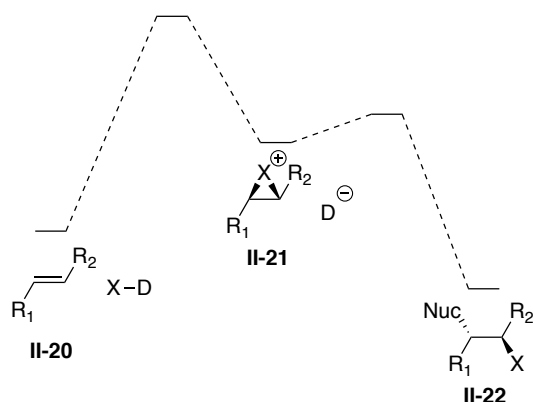


**Figure II-10:** Traditional mechanistic view of halofunctionalization

## II-3-1  Challenges Unique to Intermolecular Nucleophile Assisted Alkene Activation

Nucleophile assisted halofunctionalization for intramolecular transformations have been experimentally supported through KIE, spectroscopic, and competition studies (Section I-3-2). In the case of the chlorolactonization of 4-phenylpent-4-enoic acid, the *HalA* of the alkene computed for the traditional stepwise mechanism (Figure II-11a) 167.4 kcal/mol. Alternatively, the concerted mechanism (Figure II-11b), proceeding through transition state **II-28,** employs the tethered nucleophile to assist in transfer to the alkene,

154

raising the *HalA* of the alkene to 173.3 kcal/mol in conformer **II-29**. This example displays the lower enthalpic barrier for the concerted *NAAA* mechanism (Figure II-11c). Conceptually, the *intermolecular* adaptation of a concerted halofunctionalization (Figure II-11d) lowers the enthalpic reaction barrier for **II-33** relative to **II-31**, analogous to intramolecular transition states **II-28** and **II-24**. However, the increased entropic burden of a trimolecular transition state relative to the bimolecular stepwise mechanism renders the intermolecular adaptation of this reaction mechanism non-trivial.
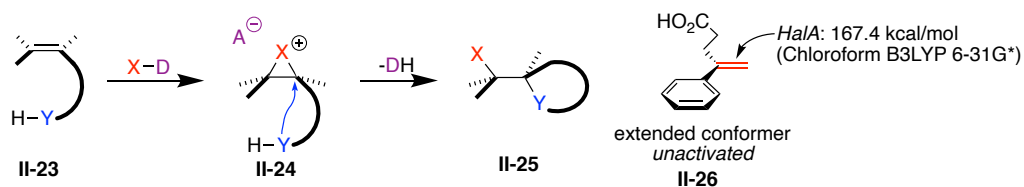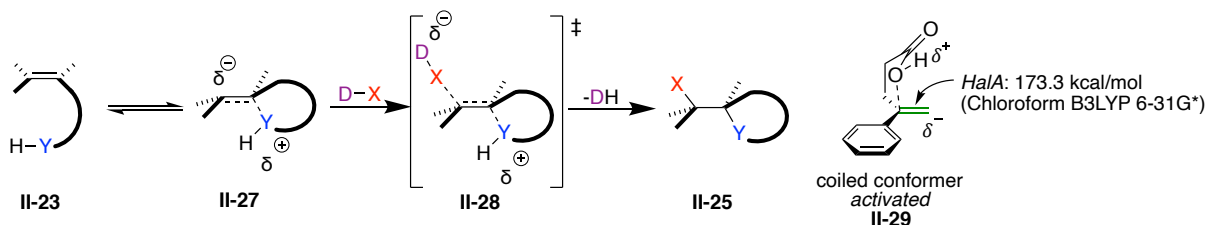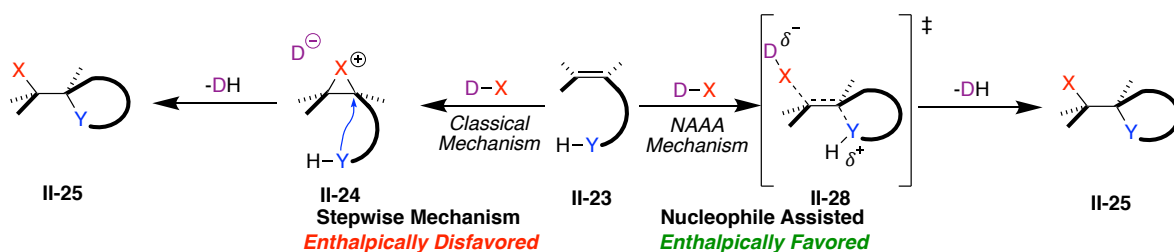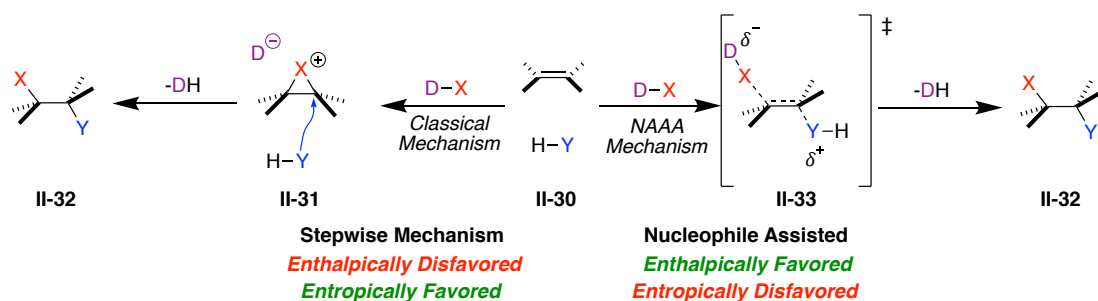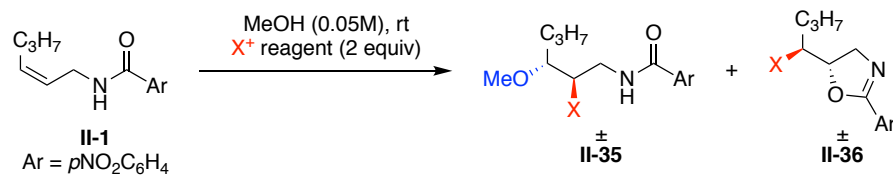
**Figure II-11:** (a) Stepwise intramolecular halofunctionalization. (b) Concerted Intramolecular . (c) Kinetic variables of stepwise vs. concerted intramolecular halofunctionalization. (d) Kinetic variables of stepwise vs. concerted intermolecular halofunctionalization

156

## II-3-2   Influence of Bromenium Donor *HalA* on Product Distribution

**Table II-2:** Influence of *HalA* on product distribution



| Entry | X⁺ reagent | *HalA* (Br)[a] | Ratio II-35:II-36[b] |
|-------|-----------|----------------|----------------------|
| 1 | NBSac | 112.2 | 2.20 : 1.0 |
| 2 | DBDMH | 123.8 | 0.53 : 1.0 |
| 3 | NBS | 133.8 | 0.47 : 1.0 |
| 4 | NBA | 150.3 | 0.40 : 1.0 |
| 5 | DCDMH | NA | 2.96 : 1.0 |

[a] HalA polar solvent. [b] Determined by crude NMR

We subjected Allyl-amide **II-1** to various bromenium reagents and a chlorenium reagent (DCDMH) in methanol (Table II-2). Under these conditions, the alkene can undergo two reactions: an intermolecular haloetherification to yield halo-ether **II-35**, or an amide cyclization to yield oxazoline **II-36**. If proceeding through the haliranium intermediate **II-34**, the counteranion of the halenium donor should have little effect on the product distribution. (Figure II-12) Interestingly, the product distribution for the two reaction pathways was sensitive to the halenium donor, following a trend of *HalA*[13] with the lower *HalA* donors favoring the intermolecular product (Table II-2). Additionally, the
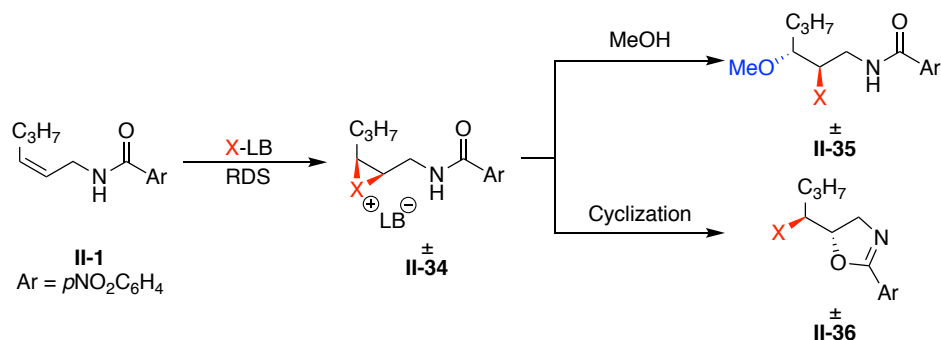


**Figure II-12:** Competitive reaction proceeding through a traditional stepwise mechanism

chlorenium donor DCDMH (entry 5) provides the highest preference for the intermolecular product **II-35**. The dependence on halenium counter-ion and product distributions leads to the interrogation of the traditional stepwise haliranium ion pathway that predicts the same product distribution regardless of the halenium counter anion.

**Table II-3:** Computational data for reaction divergence



| Entry | Halogenating Reagent | *HalA*(Br) kcal/mol | $\Delta H^{\ddagger}$ **II-38** (kcal/mol) | $\Delta H^{\ddagger}$ **II-39** (kcal/mol) | $\Delta\Delta H^{\ddagger}$ (kcal/mol) |
|-------|---------------------|---------------------|------------|------------|------------|
| 1 | DCDMH | NA | 9.3 | 16.4 | 7.1 |
| 2 | NBS | 133.8 | 17.3 | 20.9 | 3.6 |
| 3 | BCDMH | 123.2 | 12.4 | 16.8 | 4.4 |

## II-3-3  Computational Exploration of Product Distribution Relative to Halenium Reagent

Dr. Aritra Sarkar performed preliminary computational experiments (gas phase B3LYP-6-31G*) of the enthalpic energies of activation to probe the dependence of the halenium ion counteranion on the reaction pathway for allyl-amides (Table II-3). This study utilized allyl-amide **II-37** and calculated the $\Delta H^{\ddagger}$ for reaction pathways leading to the Ritter-product **II-38** and the halocyclization product **II-39**.  Three mechanistically significant findings were apparent:

> 1. No reactions proceed through a haliranium or β-halo carbenium pathway.
>
> 2. Chlorenium reagents provide more of an enthalpic bias to intermolecular transformations.

158

3. Halenium donors with a lower halenium affinity yield a higher enthalpic bias in favor of intermolecular product.

Each of these conclusions is in agreement with our previous publications or the experimental results of product distribution (Table II-2). The lower enthalpic barrier for the intermolecular product is due to the electron withdrawing nature of the amide biasing the etherification reaction due to the Markovnikov-like regiochemistry of **II-38**. This justifies the trend of $\Delta\Delta H^{\ddagger}$ correlating with the electrophilicity of the halenium source. Chlorenium reagents are more electrophilic than their bromenium counterparts, thus, they induce a larger positive charge on the alkene during halenium transfer. This scenario leads to more carbocationic character distal to the electron withdrawing group, the site at which acetonitrile adds. We propose a similar explanation for the correlation between the bromenium donor and the $\Delta\Delta H^{\ddagger}$ favoring the intermolecular product (entry 2 vs. 3). BCDMH is more electrophilic than NBS, thus it generates more of a partial positive on the alkene carbon which the distal carbon, leading to a higher preference for the intermolecular product **II-38**.

## II-3-4 Product Distribution with Electronically Unbiased Regiochemistry

We hypothesized that the electron withdrawing nature of the allyl-amide in substrate **II-1** generated a biased alkene. This enabled the production of **II-35** with Markovnikov like regiochemistry, and as the result the structural rigidity of Z alkenes, limited halocyclization to the 5-exo anti-Markovnikov selectivity. This results in the

159

sensitivity to bromenium sources observed in table II-2. The correlation between product and center of carbocationic character is depicted in Figure II-13a. The more electrophilic the bromenium source, the more carbocationic character induced on the alkene in the transition state. This justifies the transition state preference of **II-40** with more electrophilic halenium sources which provide carbocationic character distal to the electron withdrawing amide.

To confirm that the electronic bias plays a role in dictating in the reaction outcome,



a

b

**II-1**
Ar = $p$NO$_2$-C$_6$H$_4$

**II-42**
Ar = $p$NO$_2$-C$_6$H$_4$

**II-40**

**II-41**

**II-43**

**II-45**

±
**II-35**

±
**II-36**

±
**II-44**

±
**II-46**

*Partial Charges on Different Carbon Center*
*Electronic Bias Favors Intermolecular Product*

*Partial Charges on Same Carbon Center*
*No Electronic Bias in Alkene*
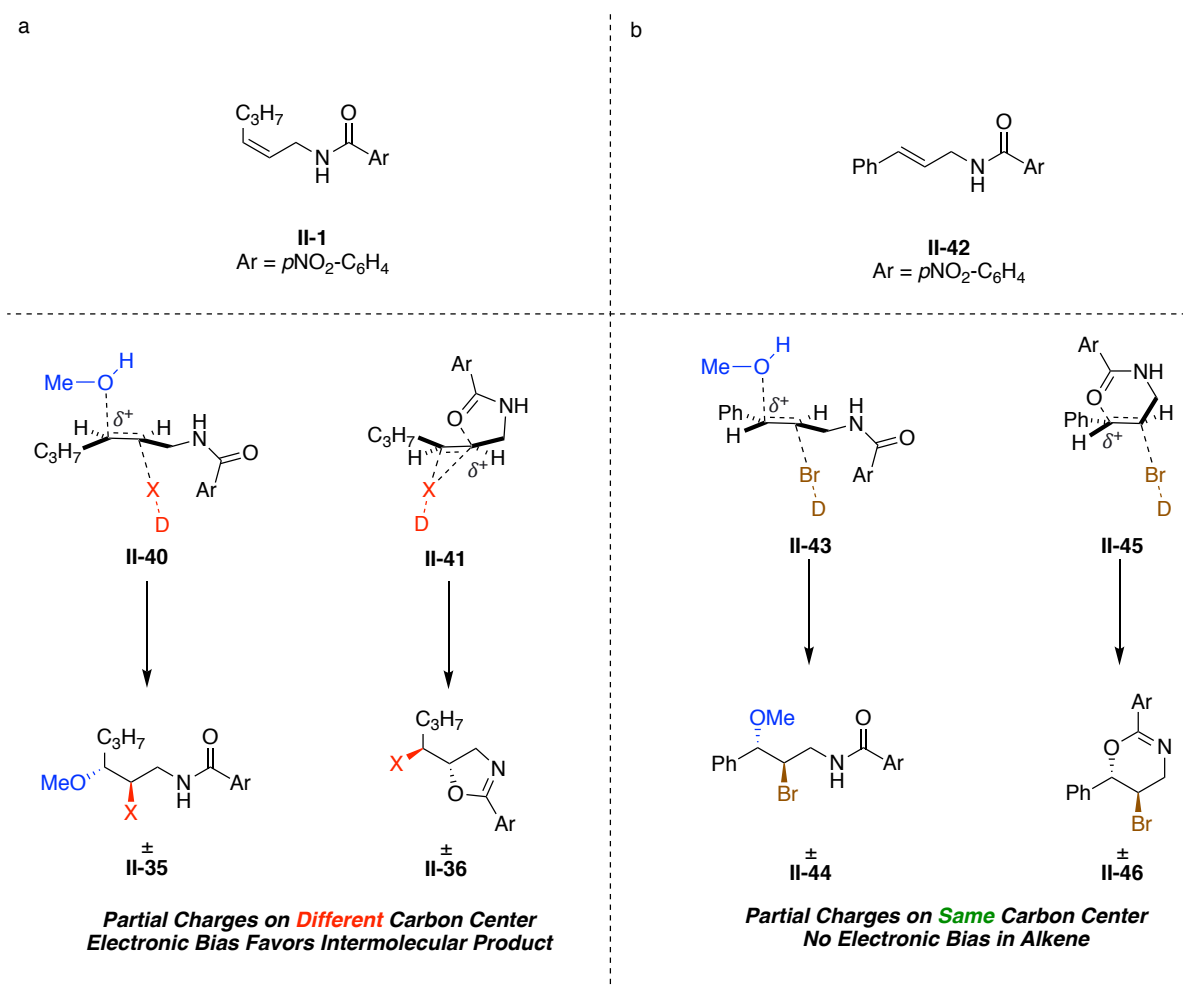
**Figure II-13**: (a) Transition state charges in electronically biased alkene **II-1** (b) Transition state charges in electronically unbiased alkene **II-42**

we selected alkene **II-42** (Figure II-13b) with E alkene geometry. This enables the 6-endo

**Table II-4:** Influence of bromenium source on product distribution with electronically unbiased regiochemistry
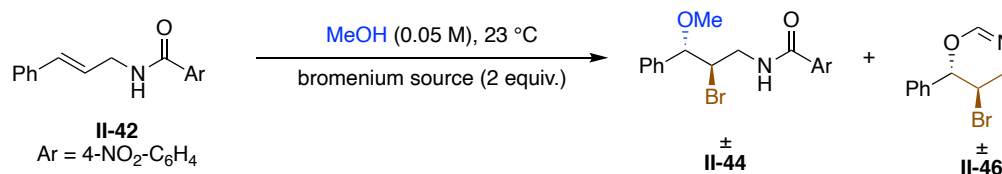


| Entry | Bromenium Source | *HalA*(Br)[a] | Ratio **II-44** : **II-46**[b] |
|-------|------------------|---------------|--------------------------------|
| 1 | NBS | 133.8 | 0.26 : 1.00 |
| 2 | NBP | 131.3 | 0.26 : 1.00 |
| 3 | DBDMH | 123.8 | 0.26 : 1.00 |
| 4 | NBSac | 112.2 | 1.00 : 1.00 |

[a]B3LYP/6-31G* polar solvent [b] Ratio determined by crude NMR

cyclization, allowing both intermolecular and intramolecular nucleophiles attack the same carbon center with Markovnikov like regiochemistry to provide products **II-44** and **II-46** (Figure II-13). This results in transition states (**II-43** and **II-45**) with the same carbocationic site. We hypothesized that alkene **II-42** would not possess any correlation between the *HalA* of the donor and product distribution. A sampling of bromenium sources (Table II-4) with a range of *HalA* provided the same ratio of intermolecular product **II-44** to intramolecular **II-46** with less reactive bromenium sources such as NBS, NBP, and DBDMH (entries 1-3). However, the more reactive N-bromosaccharine (entry 4) provided a 1.00 : 1.00 ratio of **II-44** and **II-46**. The identical product ratios provided by the three weaker halenium sources (Table II-4, entries 1-3) suggest that differences in product ratios (Table-II-2, entries 2-4) might be a result of the polarization of the alkene; however, the 1.00 : 1.00 ratio provided by N-bromosaccharine hints that there is a mechanistic break at some point between DBDMH and N-bromosaccharine that provides a stronger preference for the intermolecular product.

## II-3-5　Influence of Alkene Electronics on Product Distribution

　　We hypothesized that the regioselectivity and intermolecular bias observed with halenium reagents results from the amide's inductive effect. This notion was supported

**Table II-5:** Influence of alkene electronics on product distribution
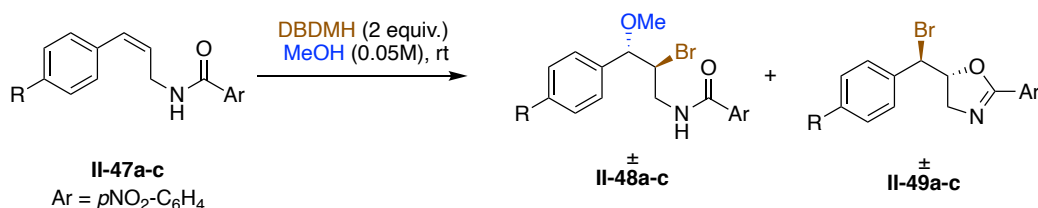


| Entry | Substrate | R | *HalA*(Br) kcal/mol[a] | Ratio **II-48:II-49**[b] |
|-------|-----------|------|------------------------|--------------------------|
| 1 | **II-47a** | H | 108.4 | 11.9 : 1 |
| 2 | **II-47b** | Cl | 106.8 | 7.1 : 1 |
| 3 | **II-47c** | CF$_3$ | 101.7 | 2.6 : 1 |

[a] *HalA* (polar solvent B3LYP 6-31G*) [b] Product ratio determined by crude NMR.

by the correlation of bromenium *HalA* and product distribution (Section II-3-2/II-3-4) and computational enthalpies of activation (Section II-3-3). We sought to more vigorously test this hypothesis by modulating the *HalA* of the alkene and measuring the subsequent effects on product distribution. If this hypothesis were to be functional, a more electron rich styrenyl alkene will prefer the transition state providing **II-48** due to the enhanced stability of the benzylic carbocation. Alternatively, a less electron rich styrenyl system would have contributions from **II-49** due to the decreased stability of the benzylic carbocation. We probed the effect of alkene *HalA* on product distribution by subjecting three alkenes of varied *HalA* to product distribution studies (Table II-5). The most electron donating substrate, **II-47a** (entry 1), provided the highest **II-48**:**11:49** ratio while the most electron withdrawing, substrate **II-47c** (entry 3), yielded the lowest **II-48**:**11-49** ratio. These results validate the olefin's polarization as a significant mode of control in the ratio of intermolecular haloetherifications and halocyclizations.

## II-3-6   Eyring Analysis of Various Bromenium Sources

Product distribution in kinetic competition studies and computational studies guided us towards a *HalA* dependent reaction divergence governed by the $\Delta\Delta H^\ddagger$ of different reaction paths. This thought originates from the idea that each bromenium source induces the same reaction mechanism and the inductive effect of the amide provides an increased enthalpic bias for the intermolecular product with more potent halenium donors. We performed Eyring analysis on the selectivity determining step by measuring the product ratios to probe the relative enthalpic barriers as a function of bromenium donor *HalA* (Figure II-14). To our surprise, Eyring analysis yielded a result contradictory to our initial hypothesis and computational data. N-Bromosaccharine (Entry 1), possessing the lowest *HalA* and the strongest preference for the intermolecular product **II-50**, counterintuitively had the smallest relative enthalpic barrier (-1.92 cal/molK) in favor of **II-50**. To compensate for this, N-Bromosaccharine had the lowest relative entropic barrier for **II-50** relative to **II-51,** thus posessing the highest preference for the intermolecular product. This study clearly demonstrates that increased *HalA* of the bromenium donor leads to larger relative entropic barrier to yield **II-50**.

Presumably, the observed correlation of $\Delta\Delta H^\ddagger$ and $\Delta\Delta S^\ddagger$ with *HalA* and its contradiction to computational transition state energies are evidence for intermolecular *NAAA* (Figure II-11d). Relative to the classical stepwise mechanism, intermolecular *NAAA* requires a more highly ordered transition state, which results in a higher entropic barrier. While more highly ordered, a concerted transition state raises the *HalA* of the alkene, thus decreasing the enthalpic activation barrier. This is displayed in the $\Delta\Delta H^\ddagger$ (-2.96 to -2.83 kcal/mol) and

163

$\Delta\Delta S^{\ddagger}$ (-15.1 to -14.6 cal/molK) for high *HalA* bromenium reagents (i.e., DBDMH and NBS) that require assistance via *NAAA* to enable bromenium transfer. Conversely, bromenium donors with a lower *HalA* such as N-bromosaccharine require less *NAAA,* exhibiting lower $\Delta\Delta H^{\ddagger}$ (-1.92) and $\Delta\Delta S^{\ddagger}$ (-6.77). Furthermore, only N-bromosaccharine initiated reaction provided traces of the Ritter product, displaying its tolerance to a less weaker nucleophile.

## II-3-7  Order of Methanol with Different Bromenium Sources

In the previous section there was a clear correlation between the *HalA* of the bromenium reagent and the relative entropy of activation leading to products **II-50** and **II-7**. This, coupled with the contradiction of the computationally predicted enthalpic

a



**II-1**
Ar = *p*NO$_2$-C$_6$H$_4$
HalA = 103.0 kcal/mol[a,b]

| Entry | Br$^+$ Reagent | *HalA* Br kcal/mol[a] | II-50:II-7 (-28 °C)[c] | II-50:II-7 (-7 °C)[c] | II-50:II-7 (25 °C)[c] | II-50:II-7 (51 °C)[c] | ΔΔH$^‡$ (kcal/mol) | ΔΔS$^‡$ (cal/mol °K) |
|-------|----------------|----------------------|------------------------|-----------------------|------------------------|------------------------|--------------------|---------------------|
| 1 | NBSac | 112.2 | 1.65 :1.00 | 1.35 :1.00 | 0.84 :1.00 | 0.65 :1.00 | -1.92 | -6.77 |
| 2 | DBDMH | 123.8 | 0.28 :1.00 | 0.16 :1.00 | 0.10 :1.00 | 0.06 :1.00 | -2.96 | -14.6 |
| 3 | NBS | 133.8 | 0.16 :1.00 | 0.11 :1.00 | 0.06 :1.00 | 0.04 :1.00 | -2.83 | -15.1 |

[a]B3LYP/6-31G* polar solvent [b]HalA calculated on alcohol analog [c]Ratio determined by crude NMR

b



**Figure II-14:** (a) Eyring Analysis of product ratios with varied bromenium donors. (b) Eyring Plot

activation energies, suggest a weaker bromenium reagent requires more *NAAA* and a stronger bromenium reagent is less reliant on *NAAA*. To further examine this mechanistic

possibility and rule out alternative pathways unrelated to methanol that could induce different entropic barriers, we studied the effect of methanol concentration on product distribution. Inspired by Hoye's study of HDDA reactions[14] and Dr. Soltanzadeh's studies of diastereoselectivity, we sought to elucidate the order of methanol with different bromenium reagents.

## II-3-8 Literature Precedent for Order Relative to an Internal Clock Reaction

In 2014 Hoye and coworkers disclosed a study elucidating the mechanistic divergence of benzyne trapping events with alcohols.[14] This study was spurred by the initial observation of a cyclohexanol concentration dependent divergent reaction. They

**Table II-6:** Competitive $H_2$ transfer and alcohol addition reactions
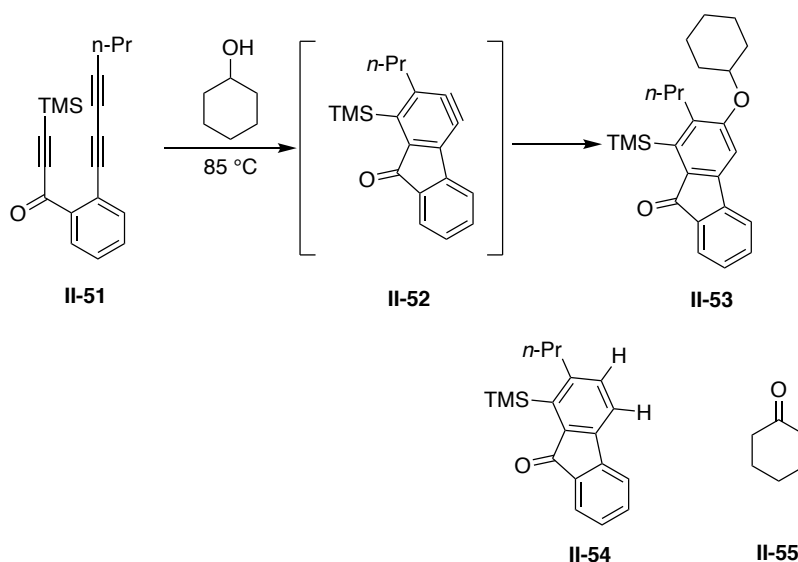
| Entry | [Cyclohexanol] | II-53:II-54 |
|-------|----------------|-------------|
| 1 | 9.5 M (neat) | 12:1 |
| 2 | 0.013 (in CDCl$_3$) | 1:17 |

noticed when **II-51** is subjected to hexadehydro Diels-Alder (HDDA) reaction conditions with high concentrations of cyclohexanol, they primarily obtained the aryl ether product **II-53** via oxygen trapping of the benzyne intermediate **II-52** (Table II-6 entry 1), and with low cyclohexanol concentrations they obtained **II-54** via transfer hydrogenation.

Considering both products **II-53** and **II-54** are the result of the alcoholic trapping of benzyne **II-52**, the authors were curious of the origin of the selectivity inversion of this post rate determining step. Suspicious that the concentration of alcohol played a role in the selectivity determining step, they cleverly designed substrate **II-56** which contains an aromatic ring functioning as an intramolecular benzyne trap of that is independent of alcohol concentration in product **II-58**. They subjected this substrate to HDDA conditions and measured the aryl ether (**II-59**) and hydrogenation product (**II-60**) ratios at different isopropanol concentrations relative to clock reaction product. The slopes of the ln[*i*-Pr] vs ln(**II-59/II-58**) or ln(**II-60/II-58**) provide the order of isopropanol for the respective products. This yielded an isopropanol order of two for **II-59** and one for **II-60**. Complementary computational experiments suggest that dimeric isopropanol functions as a nucleophile to react with the benzyne and yield the aryl ether product in a transition state similar to **II-61** while the hydrogenation is hydrogen transfer from the monomeric alcohol to the benzyne.
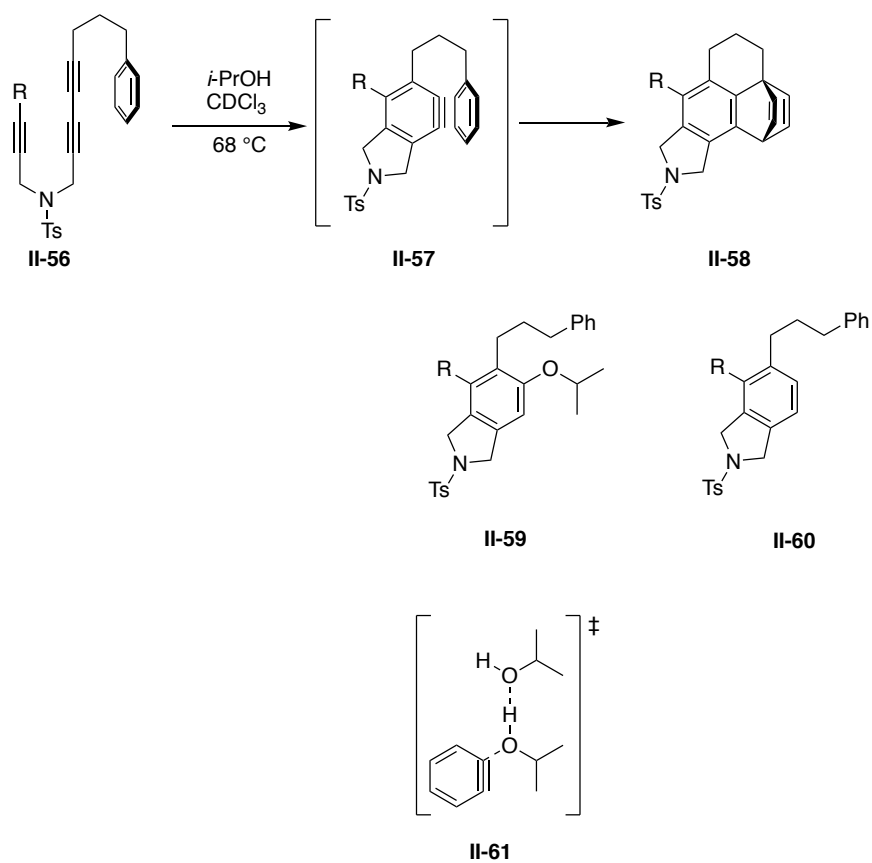
**Figure II-15:** Trapping experiment with benzyne intermediates

## II-3-8-1   Determination of Methanol Order with Different Bromenium Sources

Inspired by Hoye's technique,[14] we employed a similar clock method to determine the relative order of methanol for the formation. This method determines the order of methanol for **II-50** relative to clock reaction **II-7**, which is presumably independent of methanol concentration, by measuring the **II-50**:**II-7** ratio as a function of methanol concentration. The slope of the graph ln[MeOH] vs. ln(**II-50/II-7**) provides the order of

| [MeOH] | NBS Ratio (**II-50**:**II-7**)[a] | DBDMH Ratio (**II-50**:**II-7**)[a] | NBSac Ratio (**II-50**:**II-7**)[a] |
|---|---|---|---|
| 3.84 | 1.00 : 28.5 | 1.00 : 19.4 | 1.00 : 1.83 |
| 5.45 | 1.00 : 19.4 | 1.00 : 15.1 | 1.00 : 1.46 |
| 9.31 | 1.00 : 9.25 | 1.00 : 8.30 | 1.00 : 1.05 |
| 14.96 | 1.00 : 5.48 | 1.00 : 4.03 | 1.00 : 0.83 |

[a]Ratio determined by crude NMR
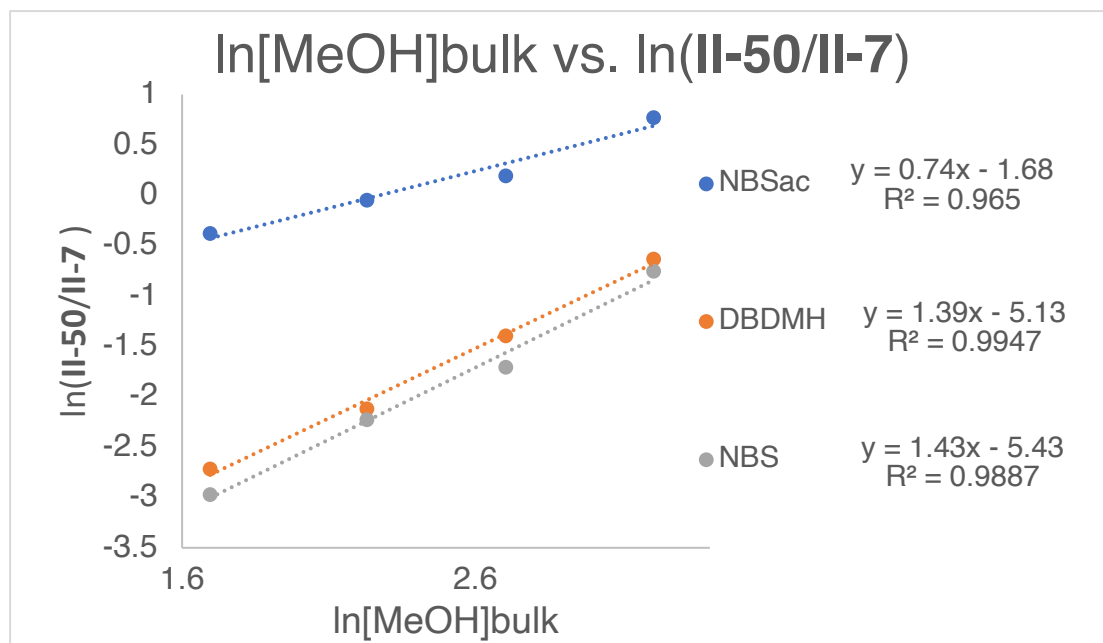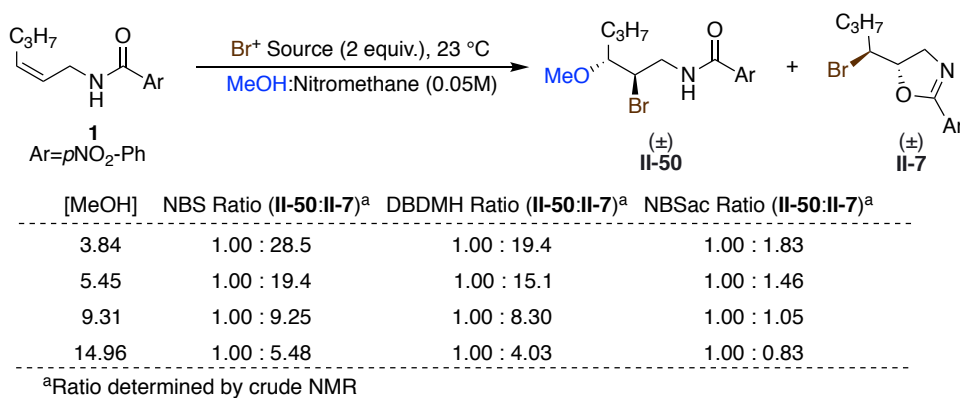
**Figure II-16:** Influence of methanol concentration on product distribution

methanol for **II-50** relative to **II-7**. As anticipated, there was a notable change in sensitivity

of methanol concentration with less reactive sources (NBS, DBDMH).

The aforementioned method provided a relative methanol order of about 1.4 for

NBS and DBDMH and 0.74 for the more reactive N-bromosaccharine. The higher order

of methanol for less reactive bromenium sources justifies the higher relative entropic

activation barrier displayed in Eyring analysis (Section II-3-6). The values of ~1.4 obtained

for the less reactive bromenium sources suggest a competitive reaction pathway that

employs two molecules of methanol to yield **II-50**. There are two potential explanations

for the requirement of two methanol molecules in a haloetherification reaction:

1. *Dimeric Methanol is functioning as a nucleophile.* Similar to what Hoye

    observed with **II-53** and **II-59**. Dimeric alcohol is more nucleophilic than the

    corresponding monomer. The enhanced nucleophilicity can more

    effectively assist the alkene in the abstraction of the bromenium ion from
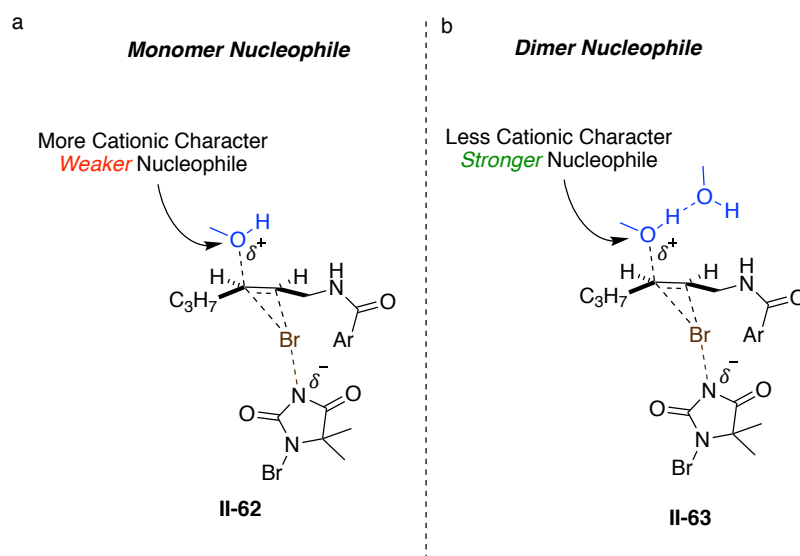


**Figure II-17:** Comparison of (a) monomer and (b) dimer
nucleophilicities

the weaker donor (Figure II-17). Similar phenomena have been observed

170

with intramolecular halofunctionalizations. (This will be explained in further detail in Section II-3-8.)

2. *Methanol is functioning as a protic activator of the bromenium source.* Hydrogen bonding is known to activate imide donors in electrophilic alkene difunctionalizations. The bromenium sources with lower *HalA* require the assistance of a proton donor to stabilize the formation of a negative charge on the donor in the transition state (Figure II-18). Alternatively, the more potent donors have a more stable counteranion and do not require the external bromenium source stabilization via a protic donor. (This will be explained in further detail in Section II-3-10.)
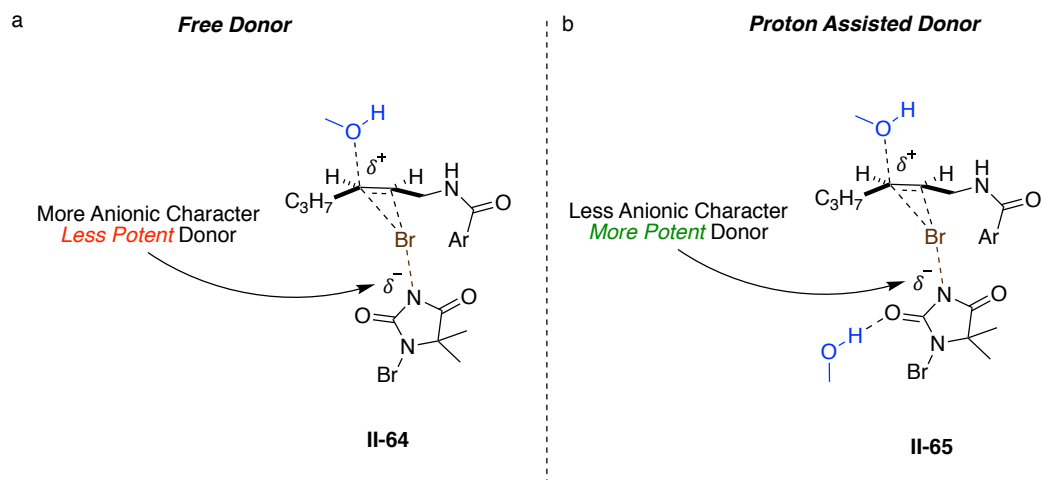


**Figure II-18:** Proton donor assisted bromenium source activation

The following sections are a deeper investigation to elucidate the role of the second equivalent of methanol.

171

## II-3-8-2   Literature Precedent for Hydrogen Bonding Nucleophilic Enhancement in Halofunctionalization

The enhancement of nucleophilicity via hydrogen bonding is a known mode of activation[14] and has been hypothesized to exist in the context of halofunctionalization. This behavior has been leveraged by our group in the quinuclidine catalyzed chlorolactonization of alkene **II-66** to yield **II-67** (Figure II-19a).[10] The employment of a quinuclidine base offers increased reaction rates relative to the free carboxylic acid **II-66** through enhancement of nucleophilicity via hydrogen bonding. The proposed transition state is displayed as **II-68.** The effect of the rate is substantial with the reaction reaching completion in 20 minutes with quinuclidine as opposed to 72 hours without. Brown observed similar behavior in the intramolecular bromoetherification of **II-69** to **II-70** (Figure II-18b).[15]   In this case, the reaction is *second order* with respect to **II-69**. With no clear mechanism for protic activation of the adamantylideneadamantane bromenium source **II-71**, the authors propose that a second molecule of **II-69** functions as a base in the reaction mechanism. The authors propose **II-72** and **II-73** as two possible junctions in which the alcohol could function as a base to catalyze the reaction. In **II-72**, the alcohol enhances the nucleophilicity of another molecule of alcohol leading to the opening of the bromiranium ion. Alternatively, in **II-73**, the alcohol functions as a base to deprotonate the oxonium ion and provide **II-70**.
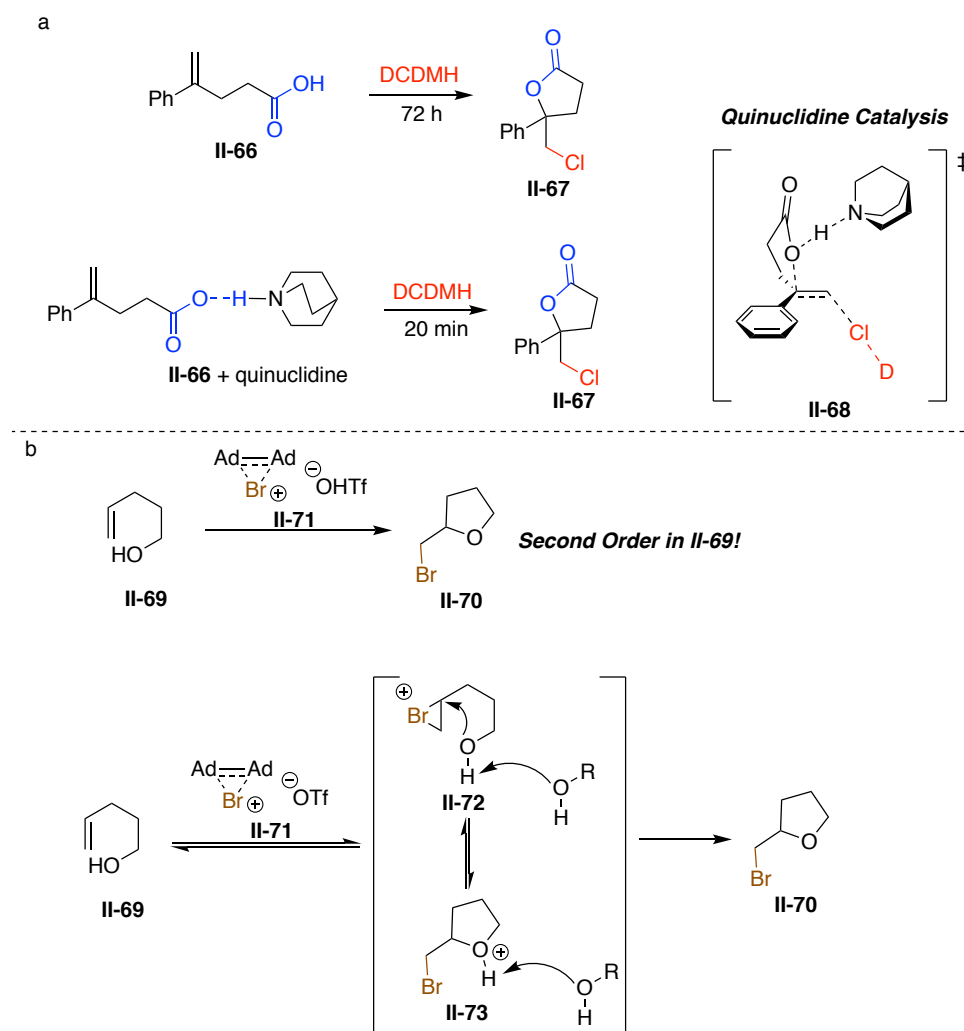
**Figure II-19:** Literature precedent for base assisted nucleophilic enhancement. (a) Chlorolactonizations (b) Bromoetherifications

## II-3-9   Influence of Sterics on Product Distribution

In the previous section, we proposed participation of methanol as a dimeric nucleophile for DBDMH initiated reactions and as a monomer for N-bromosaccharine initiated reactions. To further probe this hypothesis, we tested the steric influence of the alcohol on product distribution. The increase in steric interactions should disrupt the formation of the dimeric alcohol, and therefore, the proposed DBDMH transition state **II-74**, should be more sensitive to the sterics of the alcohol than N-bromosaccharine, which

presumably favors transition state **II-75** (Figure II-20a). The variation of nucleophile size has a significant effect on the product distribution for reactions utilizing DBDMH (Figure II-19b), with methanol providing a 1:6.5 ratio of **II-50** to **II-7** and isopropanol providing a 1.0:31 ratio of **II-50b** to **II-7**. Alternatively, the more reactive N-bromosaccharine is much less sensitive to the size of the alcohol nucleophile with the intermolecular to intramolecular ratio ranging only from 1.0:1.2 with methanol to 1.0:2.2 with isopropanol. The plot of alcohol size vs. ln(**II-50/II-7**) for DBDMH and N-bromosaccharine quantifies the relative magnitude of sensitivity to nucleophile size for each bromenium source with a slope of -0.31 for N-bromosaccharine and -0.78 for DBDMH. While the effect of alcohol size is clear for each reagent, the influence is greater with the less reactive DBDMH. We hypothesize that this is due to the necessity for alcohol dimerization to generate a stronger nucleophile required for the less reactive DBDMH, suggesting it proceeds through a transition state similar to **II-74,** while N-bromosaccharine proceeds through monomeric transition state **II-75** which is less sensitive to alcohol size. It should be noted that size

can affect an alcohol's ability to activate the bromenium source through hydrogen bonding

(Figure I-17). This possibility is explored in Section II-3-10.
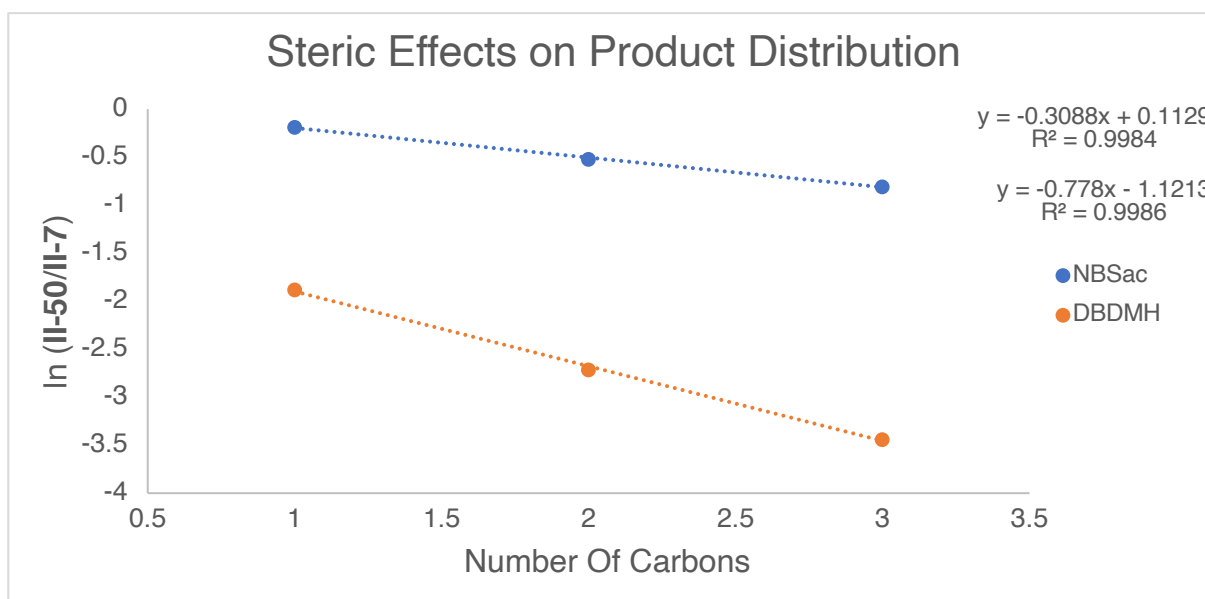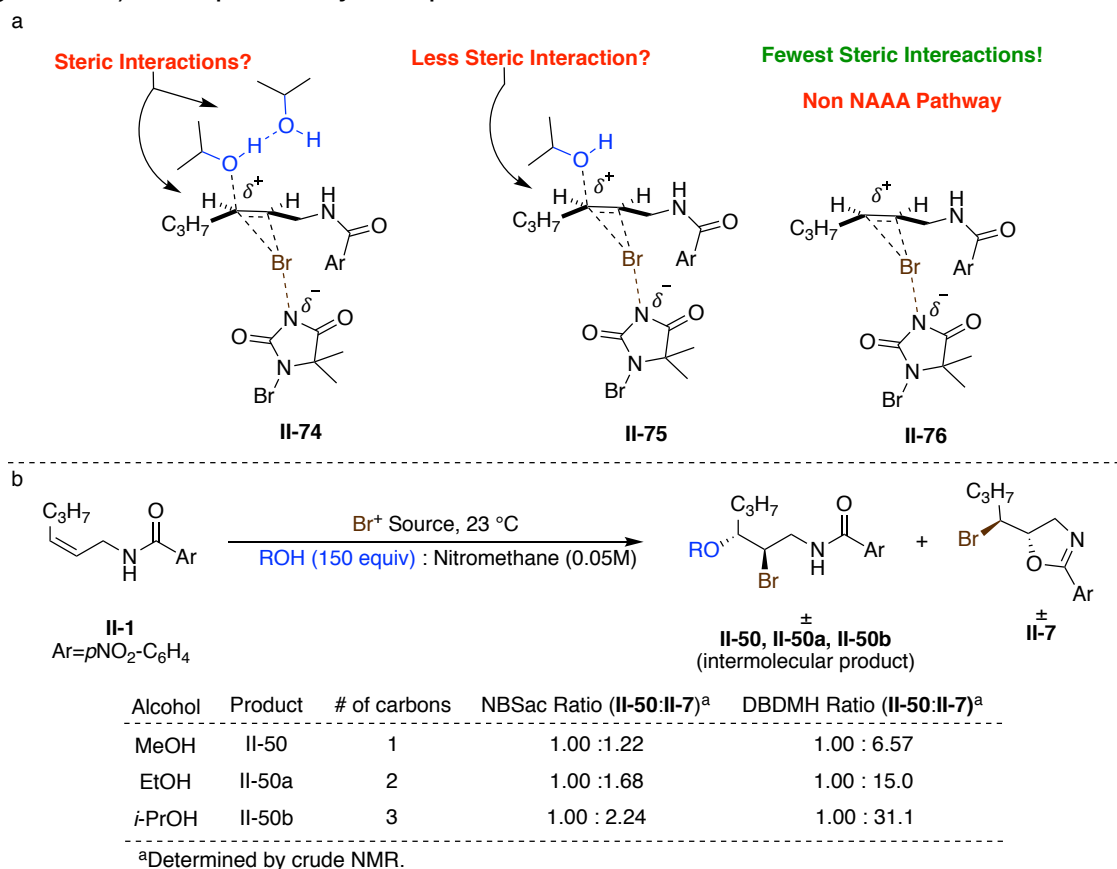


**Figure II-20:** Influence of alcohol size with different bromenium sources

## II-3-10 Influence of Acid Additives on Product Distribution

Hydrogen bond donors such as ureas and phosphoric acids are common catalysts in halofunctionalization reactions.[4, 16-17] They often function by stabilizing the halenium donor's counteranion, subsequently lowering *HalA* of the halenium donor. We sought to rule out the possibility that the higher order of methanol with DBDMH and NBS is the result of hydrogen bond activation of the bromenium donor. To examine this, we performed parallel reactions with common halofunctionalization protic additives hexafluoroisopropanol (HFIP) and trifluoroethanol (TFE) and measured their influence on



| Entry | Acid Additive | Ratio **II-50**:**II-7** |
|-------|---------------|--------------------------|
| 1 | None | 1.0:8.2 |
| 2 | TFE | 1.0:8.7 |
| 3 | HFIP | 1.0:7.6 |
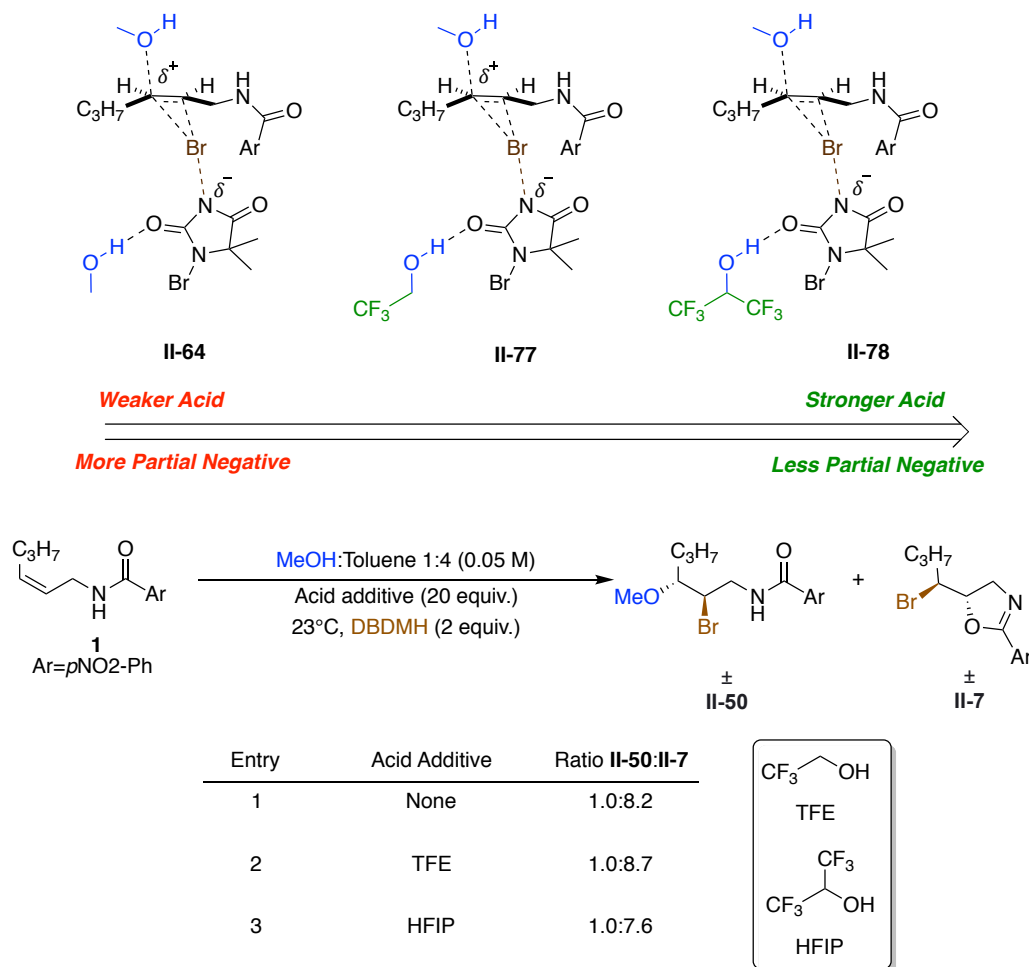
**Figure II-21:** Influence of protic additives on product distribution

product ratios. It is important to note that each of the acids, including methanol, can

behave as a proton donor and activate the bromenium source; however, methanol (pK$_a$ = 15.5) is a much weaker acid than HFIP (pK$_a$ = 9.3), and thus the methanol assisted transition state **II-64** a much less activated as compared to the HFIP assisted transition state **II-77** (Figure II-21). We anticipated that if the additional molecule of methanol functions as a proton donor to preference the intermolecular product **II-50**, then TFE and HFIP should be even more efficient at this than methanol and provide more **II-50**. These reactions were performed in toluene as a cosolvent to lessen the equivalents of methanol and lower the polarity of the solvent, which will enhance the need for a proton donor to stabilize a negative charge.[18-19]
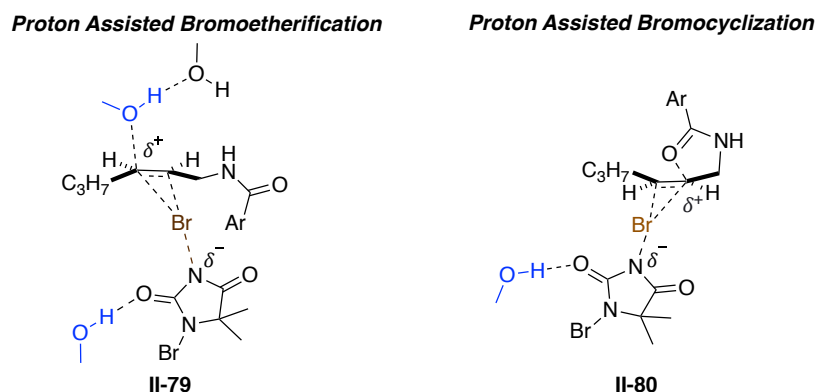


**Figure II-22:** Proton assisted pathways

We did not observe a strong correlation between acid strength and product distribution of **II-50** and **II-7 (**Figure II-21) with each condition providing similar ratios. This does not rule out the possibility that methanol is behaving as a proton donor; rather, it supports the fact that it does not account for the difference in the entropic barrier or order of the solvent between the two reaction pathways leading to products **II-50** and **II-7**. It is important to note that both the Eyring analysis (Section II-3-6) and the order of methanol (Section II-3-7) studies are relative to the cyclization reaction. Protic assistance for

halenium transfer to the alkene for inter and intramolecular pathways are likely present in both. For example, transition states depicted in Figure II-22 (**II-79** and **II-80**) are proton assisted; however, **II-79** has two additional molecules of methanol in the transition state.

## II-3-11 Divergent Reaction Pathways for DBDMH and N-Bromosaccharine

Preliminary studies exploring the effect of the *HalA* of the bromenium donor and product distribution with starting material **II-1** displayed a strong correlation between the bromenium donor and the **II-50**:**II-7** product ratios, with lower *HalA* donors yielding more **II-50**. This challenges the classical stepwise mechanism that suggests each reaction proceeding through a convergent bromiranium intermediate **II-18** (Figure II-6). This should yield similar product ratios regardless of the donor. Initially we hypothesized the possibility that a concerted mechanism is operational and the correlation between *HalA* and product distribution is the result of the inductive effect of the amide producing an enthalpic bias for **II-50** that generates carbocationic character distal to the withdrawing group in the transition state. Computational studies further support this hypothesis, suggesting that the bromenium sources with a lower *HalA* (i.e. N-bromosaccharine) will provide more of an enthalpic preference for product **II-50**. Contradictory to the hypothesis, Eyring analysis indicated that less reactive bromenium sources (DBDMH and NBS) provided a lower relative enthalpic barrier for **II-50** than lower *HalA* (less reactive) bromenium N-bromosaccharine. Additionally, Eyring analysis indicated the relative entropic barrier for intermolecular haloetherification product **II-50** was lower for N-bromosaccharine than DBDMH, hinting at differing mechanisms for **II-50** with different

bromenium sources. We further investigated methanol's role, elucidating a relative order of 1.4 for methanol with DBDMH and 0.74 for N-bromosaccharine, indicating a mechanistic switch is likely related to methanol. This led us to hypothesize that the reaction pathway yielding **II-50** with DBDMH is a dimeric in methanol, while a monomeric methanol is a sufficient nucleophile for N-bromosaccharine mediated reactions. Further studies exploring the relative effects of alcohol sterics and acid additives support this claim. The rationalization for this mechanistic switch is derived from the relative contribution of *NAAA* required for the transfer of the bromenium ion from the bromenium source to the alkene; an *NAAA* pathway lowers the enthalpic barrier but raises the entropic barrier, which is observed, shifting from N-bromosaccharine to DBDMH. Our current hypothesis is that the bromenium sources such as DBDMH that possess a higher *HalA* require "more *NAAA*". This decreased reactivity enables two competitive reaction pathways with DBDMH leading to **II-50**, an enthalpic dimeric nucleophile pathway through transition state **II-81** and an entropically favored monomeric pathway through transition state **II-82** (Figure II-23a). Alternatively, the more reactive N-bromosaccharine requires less nucleophilic assistance to transfer the bromenium ion to the alkene and primarily

proceeds through the monomeric pathway **II-83**, justifying the change in the relative

entropic activation barriers (Figure II-23b).
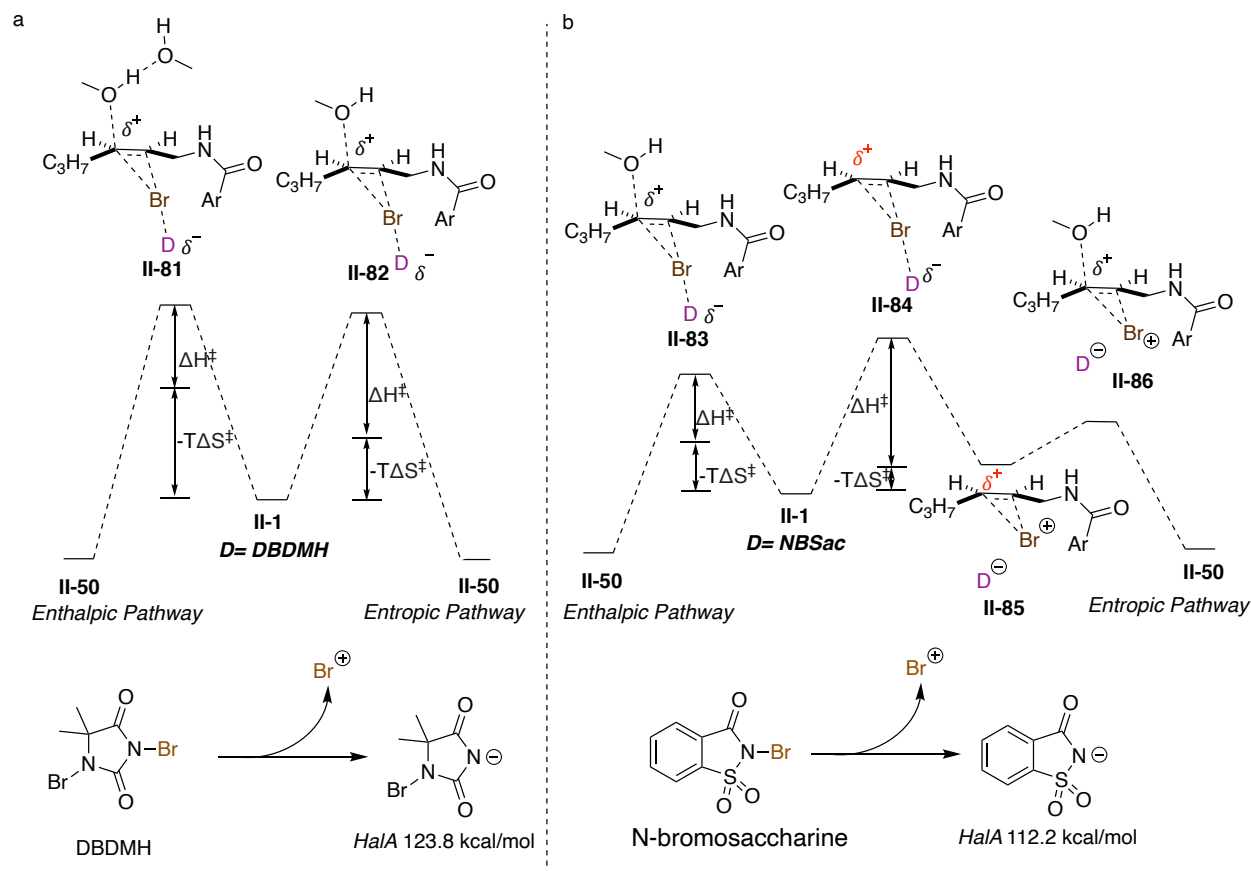


**Figure II-23:** Enthalpic and Entropic Pathways for bromoetherifications (a) DBDMH (b) N-bromosaccharine

## II-3-12 Modulation of Reaction Pathways via Alkene *HalA*

In previous sections, we observed an apparent change in mechanistic pathways via

the modulation of the bromenium donor's *HalA*. We hypothesized that when the HalA of

the bromenium donor became closer to the *HalA* of the alkene, less nucleophilic

assistance was required to transfer the bromenium ion to the alkene. We desired to

explore this hypothesis further by keeping the bromenium source constant but modulating

alkene *HalA*. We hypothesize that this should function in the same manner as bromenium

donor modulation; therefore, alkenes with higher *HalA* should require less nucleophile assistance than alkenes with lower *HalA*. We employed three styrenyl allyl amides (**II-47a-c**) with a range of alkene *HalA* (-101.7 to -108.4) in a comparative Eyring analysis study to test this hypothesis (Figure II-24). Eyring analysis exhibited that with alkenes with higher *HalA* yield lower relative enthalpic and entropic activation barriers for **II-48** products relative to intramolecular **II-49** products. The entropic variance ranging from -2.86 kcal/molK with **II-47a** to -7.84 kcal/molK with **II-47c** is rationalized by the relative *HalA* of the alkenes probed. **II-47a** possesses a higher *HalA* (-108.4 kcal/mol) than **II-47c** (-101.7 kcal/mol) therefore **II-47a** requires less assistance from an external nucleophile (methanol) to enable the transfer of bromenium from DBDMH to the alkene and provide **II-48a**. The

181

enthalpic variance favoring **II-48** follows the same trend, with **II-47a** providing the highest relative enthalpic barrier in favor of **II-48** (-2.31 kcal/mol) and **II-47c** the lowest enthalpically favoring of **II-48** (-1.78 kcal/mol). We rationalize **II-48a** proceeding with less *NAAA* (as measured by relative entropy of activation) than **II-47b,c** but a lower relative enthalpic barrier due to the stabilities of the benzylic carbocation in the respective



|  |  |  |  |  |  |
|---|---|---|---|---|---|
| **II-47a** R = H *HalA* = -108.4 kcal/mol | | **II-47b** R = Cl *HalA* = -106.8 kcal/mol | | **II-47c** R = CF$_3$ *HalA* = -101.7 kcal/mol | |
| $\Delta\Delta H^{\ddagger}$ = -2.31 kcal/mol $\Delta\Delta S^{\ddagger}$ = -2.86 cal/molK | | $\Delta\Delta H^{\ddagger}$ = -2.21 kcal/mol $\Delta\Delta S^{\ddagger}$ = -3.59 cal/molK | | $\Delta\Delta H^{\ddagger}$ = -1.78 kcal/mol $\Delta\Delta S^{\ddagger}$ = -7.84 cal/molK | |
| Temperature °C | Ratio **II-48c:II-49c** | Temperature °C | Ratio **II-48b:II-49b** | Temperature °C | Ratio **II-48a:II-49a** |
| -15 | 22.0 : 1.00 | -4 | 10.2 : 1.00 | 6 | 0.49 : 1.00 |
| 0 | 16.5 : 1.00 | 6 | 9.10 : 1.00 | 24 | 0.38 : 1.00 |
| 24 | 11.9 : 1.00 | 25 | 7.09 : 1.00 | 40 | 0.33 : 1.00 |
| 51 | 8.68 : 1.00 | 40 | 5.80 : 1.00 | 55 | 0.30 : 1.00 |
| | | 56 | 4.81 : 1.00 | | |
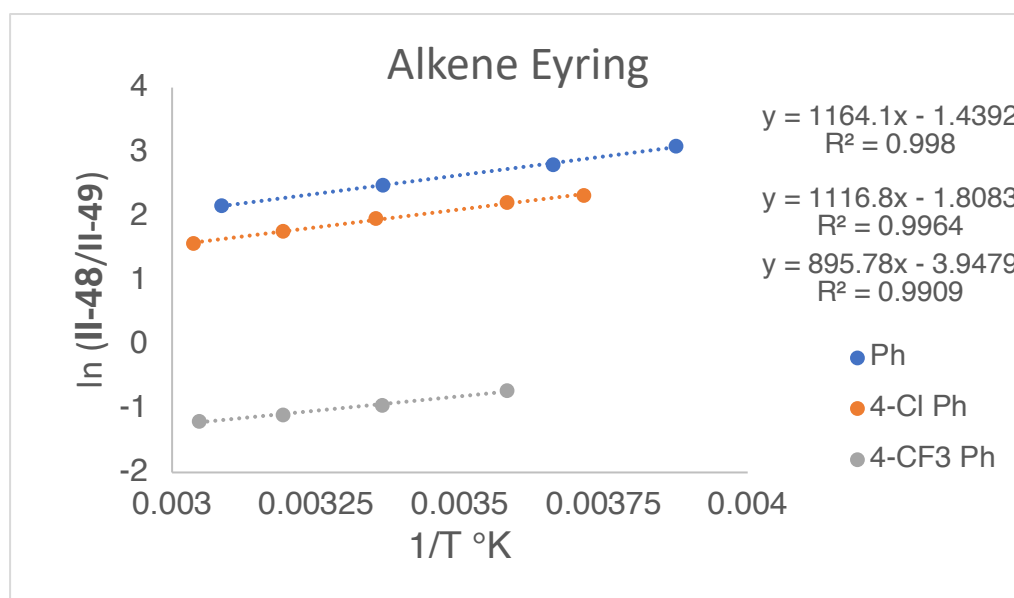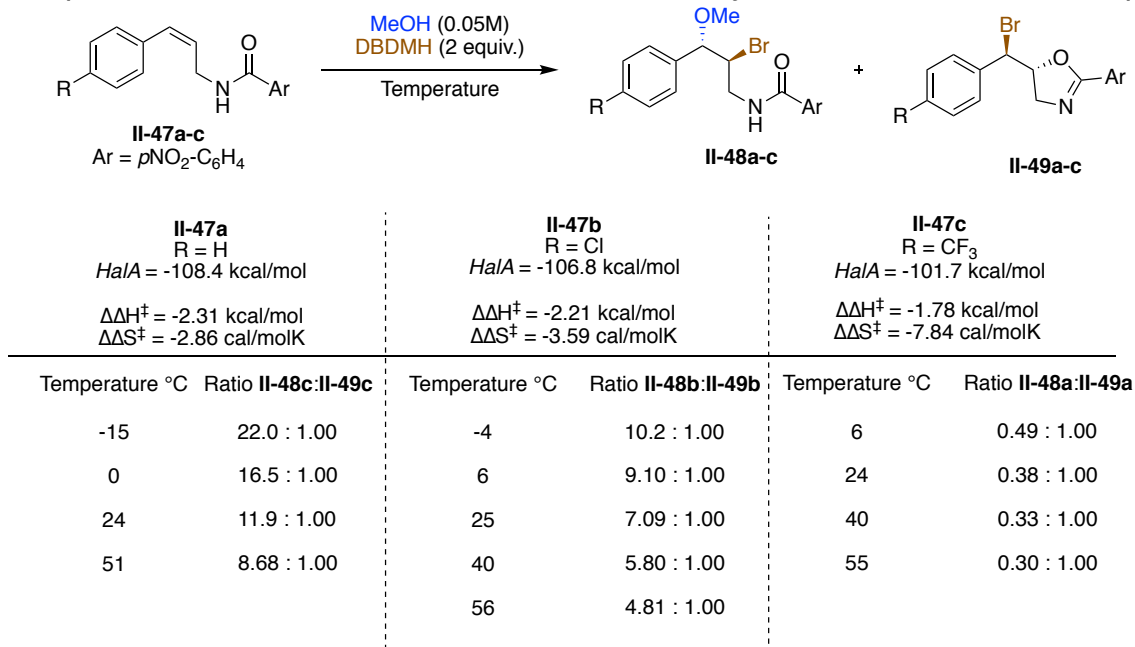


**Figure II-24:** Eyring analysis of varied alkenes

transition states. We envision a divergent mechanistic pathway for electron poor alkenes such as **II-47c**, requiring more nucleophile assistance and proceeding through more entropically challenged transition states **II-87** and **II-88**. Alternatively, electron rich alkenes such as **II-47a** require less *HalA* will proceed through less entropically challenged transition states such as **II-89** and **II-90** (Figure II-25).
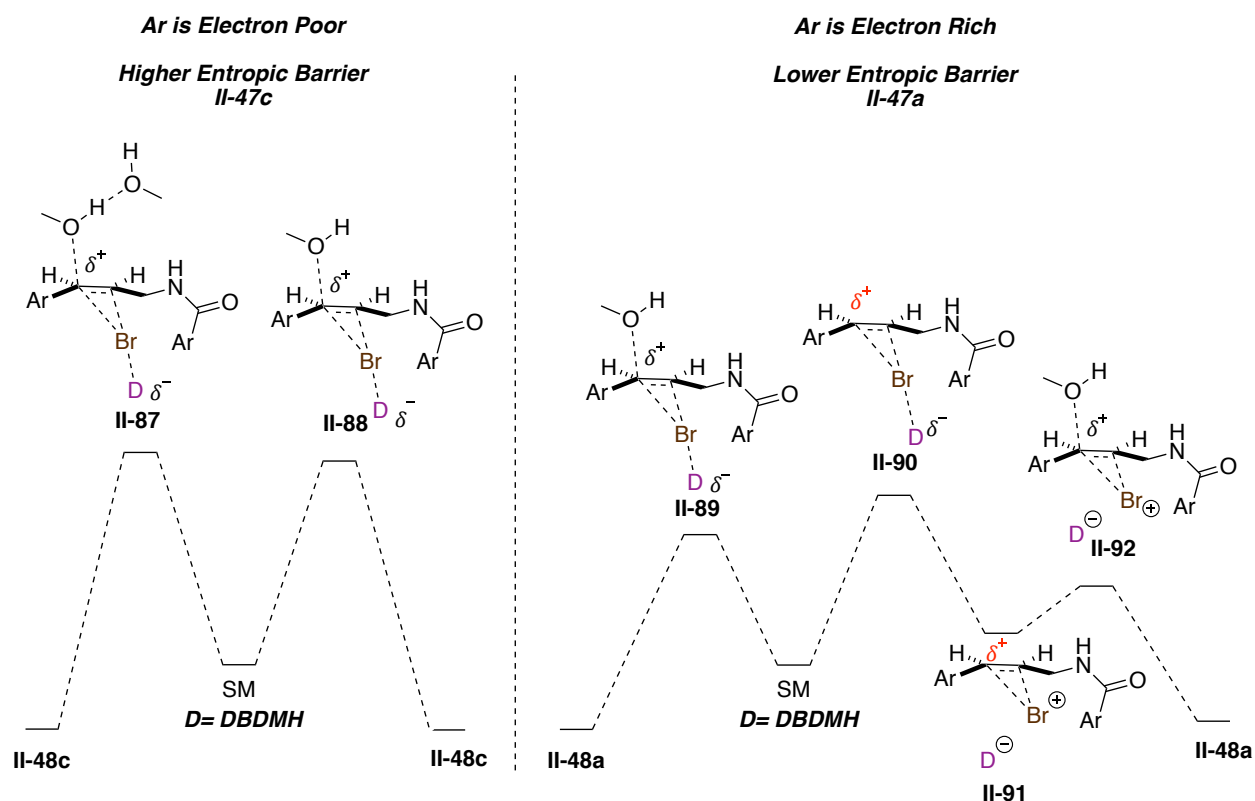


**Figure II-25:** Divergent bromoetherification molecularity with electron poor and electron rich alkenes

## II-4  Diastereoselectivity in Intermolecular Halofunctionalizations

Control of diastereoselectivity is a critical facet of alkene difunctionalizations. Generally, only one diastereomer is desired and thus any loss in diastereoselectivity results in a

reduced yield. Intermolecular halofunctionalizations are especially prone to erosion of diastereoselectivity. Classically, this is rationalized by the propensity for the haliranium ion intermediate **II-93** to open to the β-halocarbenium ion **II-94**, which as a carbocation, provides little stereocontrol leading to diastereomeric products (Figure II-26a). At first approximation, the β-halocarbenium ion pathway appears to be a reasonable justification for diastereoselectivity trend observed with chloroetherifications[1] and chloroamidations[3] of **II-47** (Figure II-26b**)**; however, deeper investigation into the structure the haliranium addition to styrenyl indicates a significant thermodynamic favoring of **II-94** in comparison to **II-93** with all styrenyl alkenes.[13] Additionally, the recent mechanistic reevaluation, *NAAA*, hints that the major diastereomer (anti addition) results from *NAAA* **II-99** and the minor diastereomer the result of the classical β-halocarbenium ion pathway **II-94** (Figure II-26c). The *NAAA* hypothesis for erosion of diastereoselectivity suggests that when the *HalA* of the alkene becomes closer to the *HalA* of the chlorenium donor DCDMH then non *NAAA* pathway **II-94** becomes operative. Utilizing the mechanistic observations obtained in Section II-3, we sought to improve diastereoselectivity for chloroetherifications by employing a chlorenium source with a higher *HalA* that will require more nucleophile assistance from methanol and lead to a stronger preference for the anti-product.
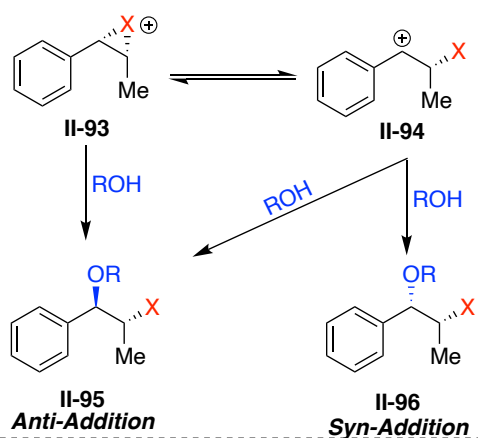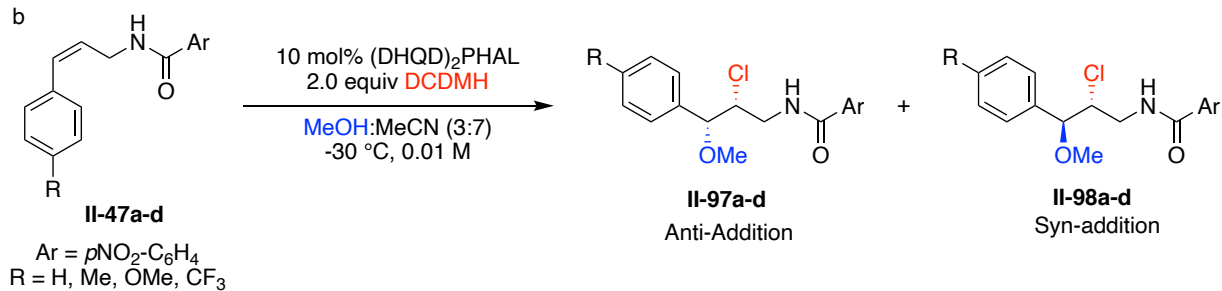
| Entry | Substrate | R | σ | $HalA^a$ | dr (II-97:II-98)[b] |
|-------|-----------|-----|-------|-------|---------|
| 1 | **II-48d** | OMe | -0.27 | 150.2 | 1:1 |
| 2 | **II-48a** | CH$_3$ | -0.14 | 142.8 | 1.3:1 |
| 3 | **II-48b** | H | 0 | 138.6 | 3.3:1 |
| 4 | **II-48c** | CF$_3$ | 0.53 | 131.5 | >20:1 |

a. HalA calculated with alcohol analog b.dr determined by crude NMR
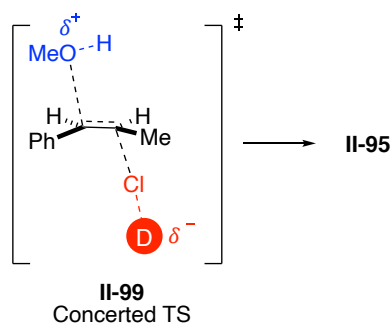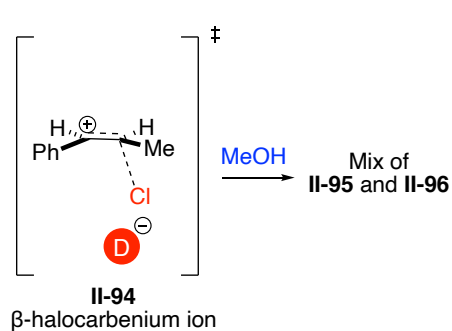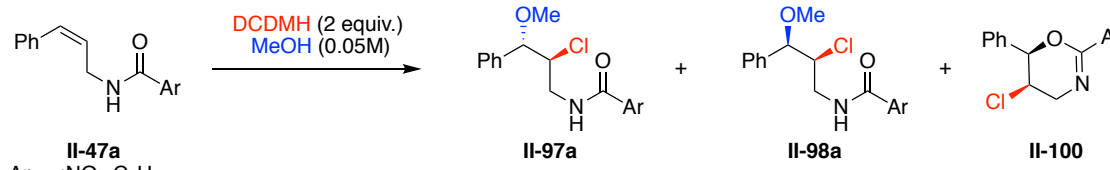
**Figure II-26:** (a) Traditional explanation for diastereoselectivity. (b) Diastereoselectivity in chloroetherifications (c) explanation for diastereoselectivity

## II-4-1 Eyring Analysis of Diastereoselectivity

The correlation between electronic perturbations of **II-47** and diastereoselectivity of haloetherification products has led to discussions on the origin of diastereoselectivity. We hypothesized that the major diastereomer **II-97** is the result of a nucleophile assisted transition state similar to **II-99** and the minor diastereomer **II-98** is the result of a stepwise



| Temperature (°C) | II-97a | II-98a | II-100 |
|---|---|---|---|
| 56 | 59.7 | 27.7 | 12.7 |
| 40 | 61.1 | 26.6 | 12.3 |
| 24 | 64.1 | 24.6 | 11.3 |
| 10 | 65.3 | 23.8 | 10.9 |

| | II-97a vs II-98a | II-97a vs. II-100 | II-98a vs. II-100 |
|---|---|---|---|
| $\Delta\Delta H^{\ddagger}$ Kcal/mol | -1.02 | -1.03 | -0.01 |
| $\Delta\Delta S^{\ddagger}$ cal/molK | -1.58 | -0.08 | 1.50 |
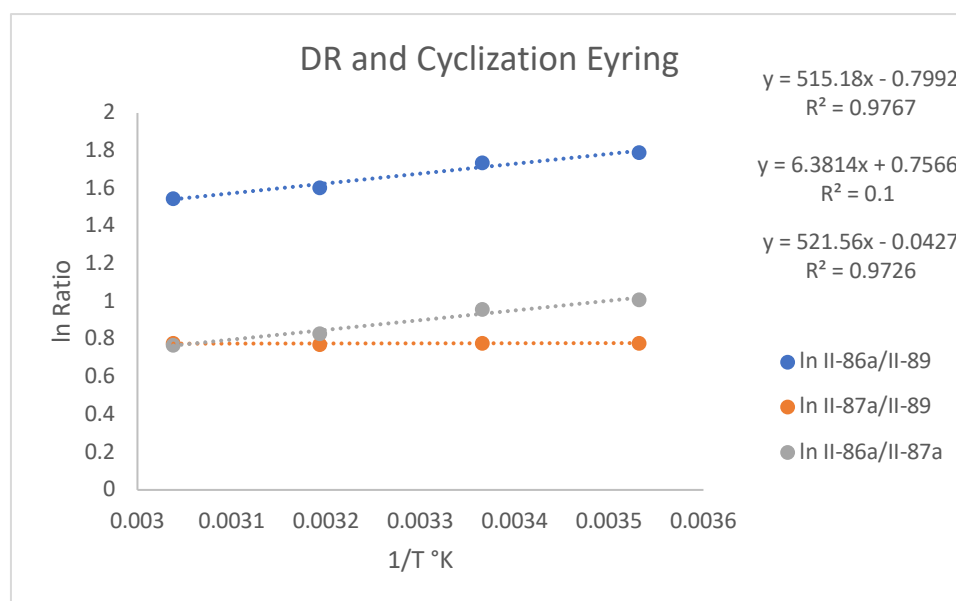


**Figure II-27:** Eyring analysis of diastereoselectivity

mechanism. We anticipated enthalpic and entropic consequences to these two reaction pathways, with *NAAA* like pathway **II-99** possessing a lower enthalpic barrier but a higher entropic barrier relative to stepwise pathway **II-94**. We sought to probe the entropic and enthalpic differences between both reaction pathways of the selectivity determining step via Eyring analysis in hopes of acquiring an improved comprehension of diastereoselectivity in intermolecular chloroetherifications.

As anticipated, the reaction pathway leading to the major diastereomer **II-97a** is enthalpically favored (by 1.02 kcal/mol) and entropically disfavored (by 1.58 cal/molK) relative to the minor diastereomer **II-98a** (Figure II-26), indicative of a nucleophile assisted transition state. Eyring analysis of both diastereomers relative to 6-endo chlorocyclization side product **II-100** led to peculiar relative entropic barriers to activation. To our surprise, we discovered that the relative entropy of activation for **II-97a** to **II-100** was relatively low (0.08 cal/molk) and the minor diastereomer **II-98a** was entropically favored relative to **II-100** by 1.50 cal/mol. This suggests that the reaction pathway leading to **II-100** has a moderate entropic barrier to activation, potentially via the adoption of a *NAAA* transition state. Regardless, we were intrigued to observe such a similar entropy of activation for the **II-97a** and **II-100** reaction pathways which is different than what was observed in Section II-3-12.

## II-4-2  Influence of Chlorenium Donor *HalA* on Diastereoselectivity

As previously discussed, diastereoselectivity is a pertinent issue in halofunctionalization. The correlation between alkene *HalA* and diastereoselectivity of the halofunctionalization product hints that the major diastereomer is the result of a concerted

*NAAA* like transition state and the minor diastereomer is the result of a non-*NAAA* β-halocarbenium ion pathway. We were curious as to whether the modulation of chlorenium donor to a lower *HalA* could increase the requirement for a nucleophile assisted transfer of chlorenium to the alkene, thus, mitigating the β-halocarbenium pathway and improving diastereoselectivity via reagent control (Figure II-27). This hypothesis was emboldened by Eyring analysis of bromofunctionalizations which displayed the ability to control the requisite for a *NAAA* concerted pathway by modulating the *HalA* of the bromenium donor or the alkene. Further Eyring studies related to the diastereoselectivities of chlorofunctionalizations of **II-47a** supported the hypothesis that the major diastereomer **II-97a** is the result of *NAAA* transition state **II-101** and the minor diastereomer **II-98a** is the result of a classical stepwise reaction through **II-102**.
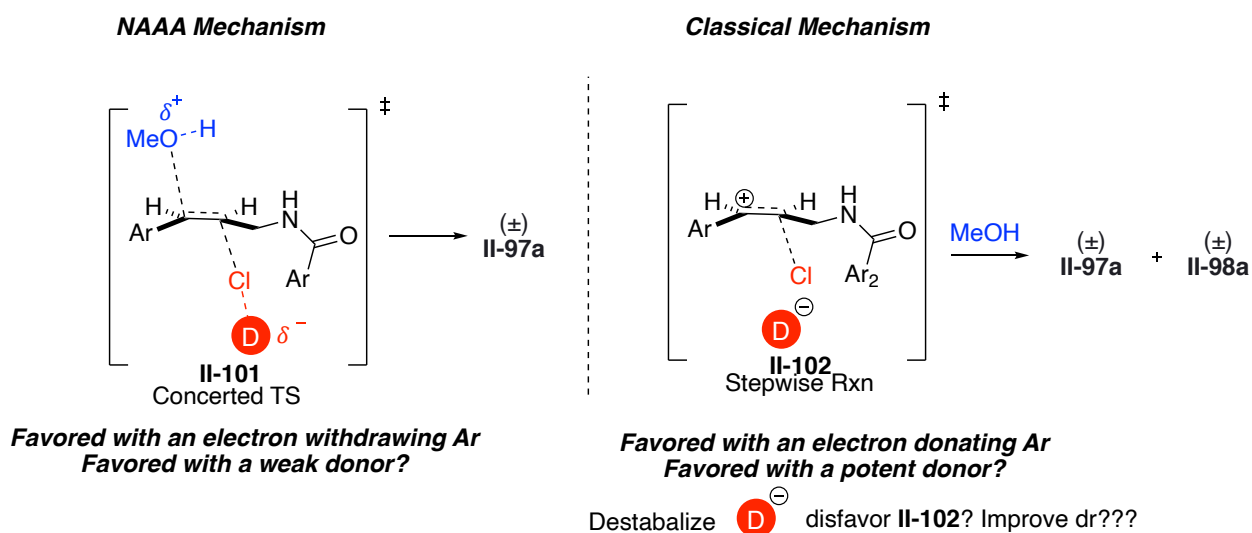


**Figure II-28:** Reagent controlled approach to improve diastereoselectivity

The summarization of diastereoselectivity studies with varied chlorenium sources is displayed in Table II-7. To our dismay, use of less reactive chlorenium sources did not improve diastereoselectivity (**II-97a:II-98a** ratio). The least reactive NCS (entry 1) and the

most reactive TCCA (entry 4) provided the same diastereoselectivities despite TCCA's *HalA* being lower 5.5 kcal/mol than of **II-47a** and NCS being 22.2 kcal/mol higher. While the independence of chlorenium donor *HalA* and diastereoselectivity insinuate that the reactions proceed through a stepwise intermediate, there are examples in the literature that propose a syn-concerted addition of the halenium ion and nucleophile to the alkene.[20-21]

**Table II-7:** Influence of *HalA* on diastereoselectivity in chloroetherifications
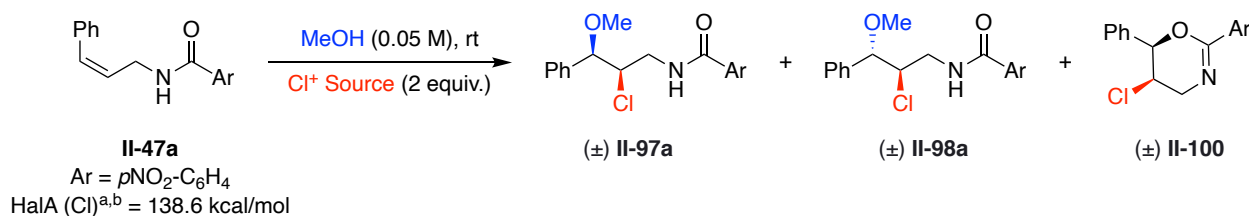


| Entry | Cl⁺ source | *HalA* (Cl) kcal/mol[a] | Ratio **II-97a:II-98a:II-100**[c] | dr[c] |
|-------|-----------|------------------------|----------------------------------|-------|
| 1 | NCS | 160.8 | 70 : 30 : 0 | 1:2.4 |
| 2 | DCDMH | 150.0 | 64 : 25 : 11 | 1:2.6 |
| 3 | NCSac | 138.7 | 64 : 27 : 9 | 1:2.4 |
| 4 | TCCA | 133.1 | 64 : 27 : 9 | 1:2.4 |

a. Calculated by B3LPY/6-31G* (polar solvent). b. HalA caclulation on alcohol analog c. Determined by crude NMR

## II-4-3  Influence of Bromenium Donor *HalA* on Diastereoselectivity

While we were surprised by the inability to improve diastereoselectivity by selecting a less reactive chlorenium source, we recognized that our Eyring studies detailing the relative entropies of activation with different halenium sources and alkenes all employed bromenium electrophiles. This led us to explore the possibility that bromenium and chlorenium induced are mechanistically distinct and perhaps there will be a correlation between bromenium donor *HalA* and diastereoselectivity. Gratifyingly we observed that highly reactive allyl-amide **II-47e**, the diastereoselectivity was sensitive to bromenium

donor *HalA* with DBDMH (entries 1 and 3), providing a higher *dr* than N-bromosaccharine (entries 2 and 4) (Table II-8).

**Table II-8:** Influence of bromenium donor *HalA* on bromoetherifications



II-47e
Ar = $p$NO$_2$C$_6$H$_4$
HalA (Br) = 112.2 kcal/mol[a,b]
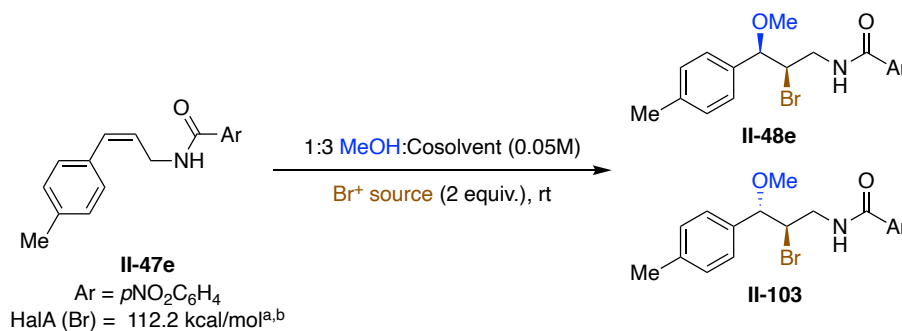
| Entry | Br$^+$ source | *HalA* (Br) kcal/mol[a] | Cosolvent | dr[c] |
|-------|---------------|-------------------------|-----------|-------|
| 1 | DBDMH | 123.7 | MeCN | 1:6.5 |
| 2 | NBSac | 112.2 | MeCN | 1:3.4 |
| 3 | DBDMH | 123.7 | None | 1:13.6 |
| 4 | NBSac | 112.2 | None | 1:8.4 |

a. *HalA* calculated in polar solvent (B3LYP/6-31G*) b. HalA of alcohol analog c. dr measured from crude NMR

The correlation between the *HalA* of the bromenium donor and diastereoselectivity suggests with low *HalA* donors such as N-bromosaccharine, **II-47e** requires less *NAAA* to transfer the bromenium ion and can potentially proceed through a β-halo carbenium intermediate leading to an erosion of diastereoselectivity. This pathway can be suppressed by selecting the less reactive bromenium source DBDMH which will provide a higher diastereoselectivity. We were curious as to why chlorenium induced halofunctionalizations display different *HalA* sensitivities than the bromenium analogs. This subject is addressed in future sections.

## II-5 Mechanistic Dissimilarities of Intermolecular Bromo and Chlorofunctionalizations

A multitude of studies suggested that bromenium induced haloetherifications proceed through a concerted nucleophile assisted mechanism. We observed that through the modulation of alkene and bromenium donor *HalA*, we can tune the requirement for nucleophile assistance. We hypothesized that we could improve diastereoselectivity for problematic chloroetherifications by employing a less reactive chlorenium source that would require nucleophile assistance to transfer the chlorenium ion to the alkene. To our surprise, we did not observe any correlation between the chlorenium donor *HalA* and diastereoselectivity; however, reinvestigation with bromenium reagents displayed *HalA* dependent reagent controlled diastereoselectivity for bromoetherifications. In an effort to elucidate the origin mechanistic divergence between bromenium and chlorenium reagents, we repeated many experiments in section II-3 with chlorenium analogs.

### II-5-1   Influence of Chlorenium Donor *HalA* on Product Distribution

The high sensitivity to the *HalA* of the bromenium donor and product distribution described in Section II-3-2 challenges the traditional stepwise mechanism that predicts minimal influence of bromenium donor on product distribution. Alternatively, a concerted intermolecular halofunctionalization reaction pathway was suggested as the explanation to these results (Figure II-29b). Reexamination of this experiment with various chlorenium sources yielded different results (Figure II-29a). We discovered that the product ratio is independent of the chlorenium source *HalA*, with NCP (entry 1, *HalA* = 158.2 kcal/mol) providing similar product ratios of **II-104** and **II-105** as TCCA (entry 5, *HalA* = 133.1

kcal/mol). This observation is in agreement with the diastereoselectivity observed for chloroetherifications (section II-4-2) that displays no correlation between donor *HalA* and product distribution. The lack of sensitivity for the chlorenium source for both of these reactions suggest that the selectivity determining step for chlorofunctionalization reactions is independent of the chlorenium donor; thus, chlorofunctionalizations could be proceeding through a common intermediate (Figure II-28c). Following the formation of the haliranium intermediate **II-109**, the selectivity determining step leading to products **II-104** and **II-105** occurs with no sensitivity for the counterion of the chlorenium donor.

## II-5-2 Competitive Eyring Analysis of Chlorofunctionalizations and Bromofunctionalizations

The observed divergent halenium source sensitivity for bromo and chlorofunctionalizations led to the hypothesis that bromofunctionalizations proceed through a nucleophile assisted transfer of bromenium (Figure II-29b) to the alkene and chlorofunctionalizations proceed through a stepwise mechanism involving a haliranium or β-halocarbenium intermediate (Figure II-29c). We anticipate that these mechanisms would have different enthalpic and entropic barriers to activation in the selectivity determining step. If proceeding through a nucleophile assisted concerted mechanism, the

**Figure II-29:** (a) Influence of chlorenium donor *HalA* on product distribution. (b) Potential mechanism for chlorofunctionalizations

intermolecular transition state **II-107** that yields bromoether **II-50** should possess a higher

entropy of activation relative to the transition state for cyclization **II-106**; however,

assisting the transfer of bromenium should lower the enthalpic barrier to activation relative

to **II-106**. Conversely, if chlorofunctionalizations proceed through a stepwise mechanism

with the formation of the highly reactive haliranium intermediate **II-109**, there will be smaller differences in enthalpic and entropic barriers in transition states **II-110** and **II-111**.

We viewed competitive Eyring analysis as the ideal tool to probe the proposed divergent reaction mechanisms. In this set of experiments, we were able to extract the relative enthalpic and entropic barriers of activation for the selectivity determining step. As predicated, N-chlorosaccharine provided a smaller relative enthalpic and entropic activation barriers (-0.68 kcal/mol for $\Delta\Delta H^\ddagger$ and -0.04 cal/molK for $\Delta\Delta S^\ddagger$) in comparison to N-bromosaccharine (-1.32 kcal/mol for $\Delta\Delta H^\ddagger$ and -2.94 cal/molK for $\Delta\Delta S^\ddagger$) (Figure II-29). This result, in conjunction with divergent results for bromenium and chlorenium related to the sensitivity of the halenium donor support alternative mechanisms for bromo and chlorofunctionalizations. If proceeding through a chloriranium ion, we would expect this highly reactive intermediate to have a low enthalpic barrier to open to the respective difunctionalized products.
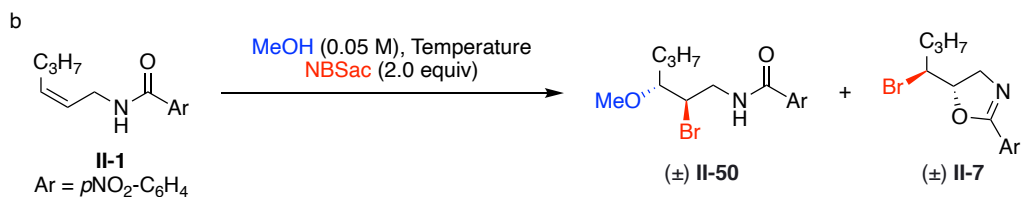
**Figure II-30:** Eyring analysis of bromo and chloroetherifications

## II-5-3  Influence of Sterics on Product Distribution with Bromo and Chlorofunctionalizations

Inspired by the sensitivity for the size of the alcohol with different bromenium reagents (section II-3-9), we examined the sensitivity to sterics with N-chlorosaccharine relative to its bromenium analog N-bromosaccharine. If the nucleophile plays less role in assisting the alkene to abstract the chlorenium ion (proposal based on results discussed in Sections II-3-2, II-4-1 and II-4-2), then we anticipate less sensitivity relative to the size of the alcohol with chlorofunctionalizations. Employing methanol, ethanol, and isopropanol we were able to test a range of steric effects on product distribution (II-Figure-31). As expected, the chlorenium reagent N-chlorosaccharine (Figure II-31b) was much less sensitive to the sterics of the nucleophile than N-bromosaccharine (Figure II-31a), supporting a different mechanistic pathway for bromo and chlorofunctionalizations. To gain a quantitative measurement of the sensitivity, the number of carbons vs ln(intermolecular/intramolecular) to get a sense of the relative sensitivity. This delivered a slope of -0.21 for chlorenium induced reactions and -0.31 for bromenium. This displays that with even N-bromosaccharine, the bromenium electrophile least sensitive to size, it is still more sensitive than N-chlorosaccharine and likely proceeds through more of a nucleophile assisted mechanism than its chlorenium counterpart. If proceeding through a chlorenium intermediate, a weaker and more sterically hindered nucleophile will be at less of a disadvantage.

**a**

| Alcohol | Product | # of carbons | Ratio (**II-50:II-7**)[a] |
|---------|---------|--------------|---------------------------|
| MeOH | **II-50** | 1 | 1.00 :1.22 |
| EtOH | **II-50a** | 2 | 1.00 :1.68 |
| *i*-PrOH | **II-50b** | 3 | 1.00 : 2.24 |

[a]Determined by crude NMR.

**b**

| Alcohol | Product | # of carbons | Ratio (**II-104:II-105**)[a] |
|---------|---------|--------------|------------------------------|
| MeOH | **II-93** | 1 | 1.00 :0.90 |
| EtOH | **II-93a** | 2 | 1.00 :1.11 |
| *i*-PrOH | **II-93b** | 3 | 1.00 : 1.37 |

[a]Determined by crude NMR.
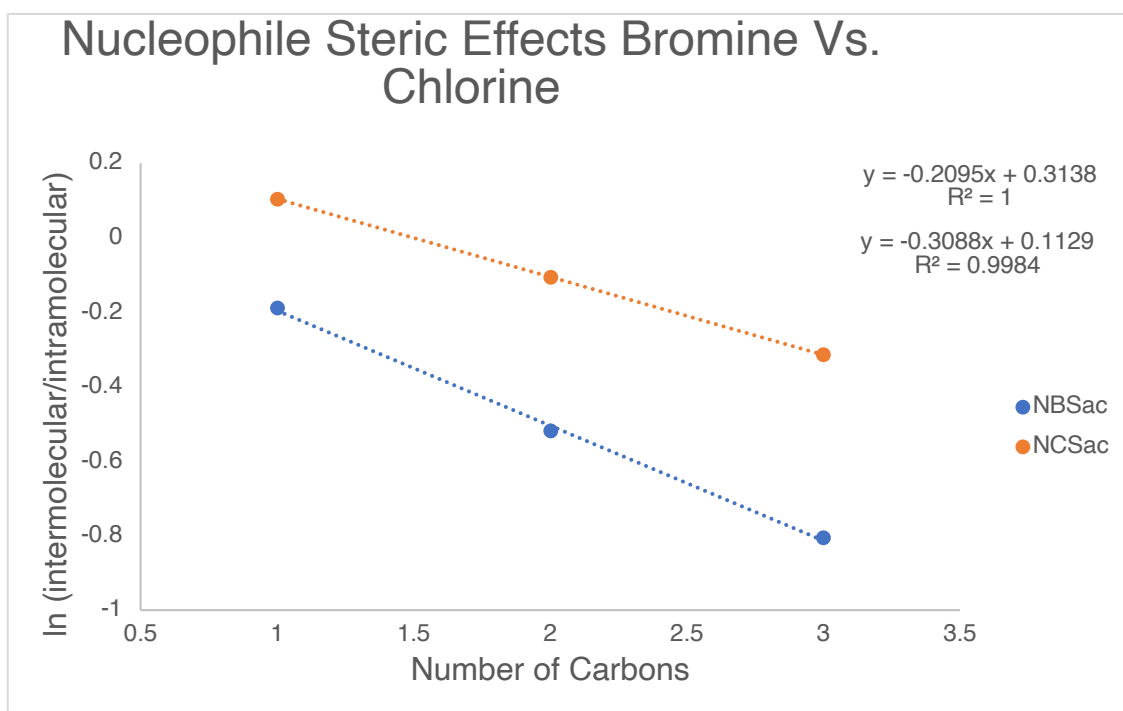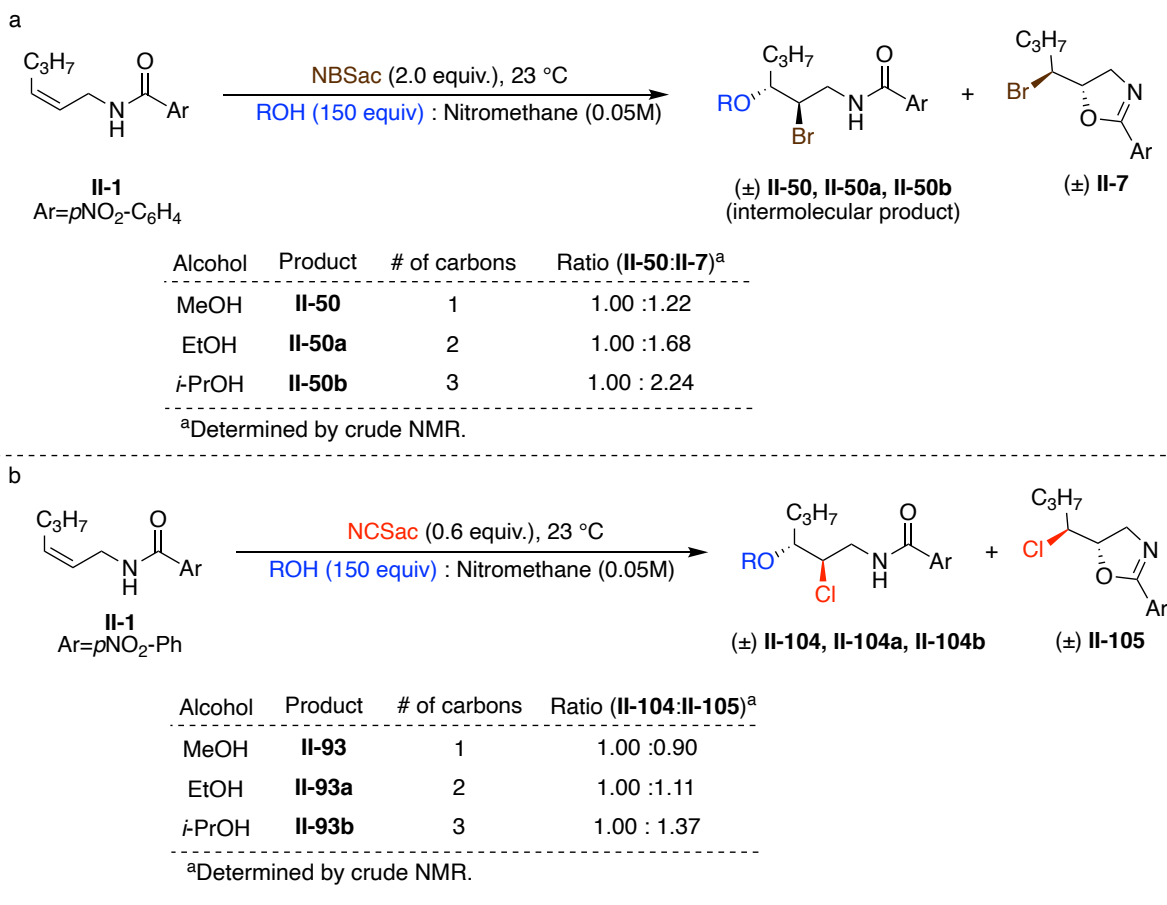
**Figure II-31:** Sensitivity to alcohol size for bromo and chloroetherifications

## II-5-4 Rationalization of Divergent Bromenium and Chlorenium Halofunctionalization Mechanisms

Considering the slower reaction rates of chlorofunctionalizations and decreased stabilities of chloriranium ions relative to their bromenium counterpart, we initially hypothesized that chlorenium induced halofunctionalizations were more likely to require an *NAAA* like concerted mechanism than bromenium induced halofunctionalization. We were surprised that mechanistic studies comparing the halenium donor's influence on product ratios and diastereoselectivity with allyl-amides suggested that bromenium induced reactions proceed through a concerted mechanism and chlorenium induced reactions through a stepwise pathway. This raises the obvious question as to why this mechanistic divergence is occurring. If the nucleophile-induced pre-polarization of the alkene (Figure I-9) occurs, we do not anticipate this reaction pathway to be present with in bromofunctionalizations and absent in chlorofunctionalizations. This provoked a reevaluation of this mechanistic hypothesis with allyl-amide **II-1** to consider bromine and chlorine atoms' varied properties and envision how they might modify reaction paths. This led us to contemplate the relative ability of bromenium and chlorenium reagents to halogen bond with Lewis bases as the divergent factor with these reactions. Halogen bonding is an intermolecular force that has been leveraged in crystal engineering, drug design, and catalysis.[6] This attractive force increases in strength with the polarizability of the halogen (I > Br > Cl > F) and thus is more viable activation mode with bromenium sources (**II-112**) than chlorenium sources (**II-113**) (Figure II-32a). We envision that bromofunctionalizations with **II-1** are initiated by reversible halogen bonding of the

bromenium donor with π-system of the alkene to generate **II-112**. The halogen bonding increases the electrophilicity of the alkene, thus activating it for attack by the nucleophile and subsequent cleavage of the bromine donor bond (Figure II-31b).[4, 22] The lower the HalA the bromenium donor, the less nucleophilic assistance to cleave the bond from the bromenium ion to the bromenium donor.[4] Chlorenium reagents do not possess the same aptitude for halogen bonding and cannot adequately activate the alkene while bound to the chlorenium donor. Thus, chlorenium donors must transfer the chlorenium ion to the alkene, forming the chloriranium ion **II-109**. This chloriranium ion pathway will be independent of the chlorenium donor in the selectivity determining step. It is also possible to envision that the "chloriranium ion" like intermediate **II-114** is still weakly bound to the donor, but not enough to modulate the electronics of the alkene and the subsequent reaction path. We believe that the common chloriranium ion intermediate hypothesis satisfies observations included in this chapter.

## II-6    Conclusion



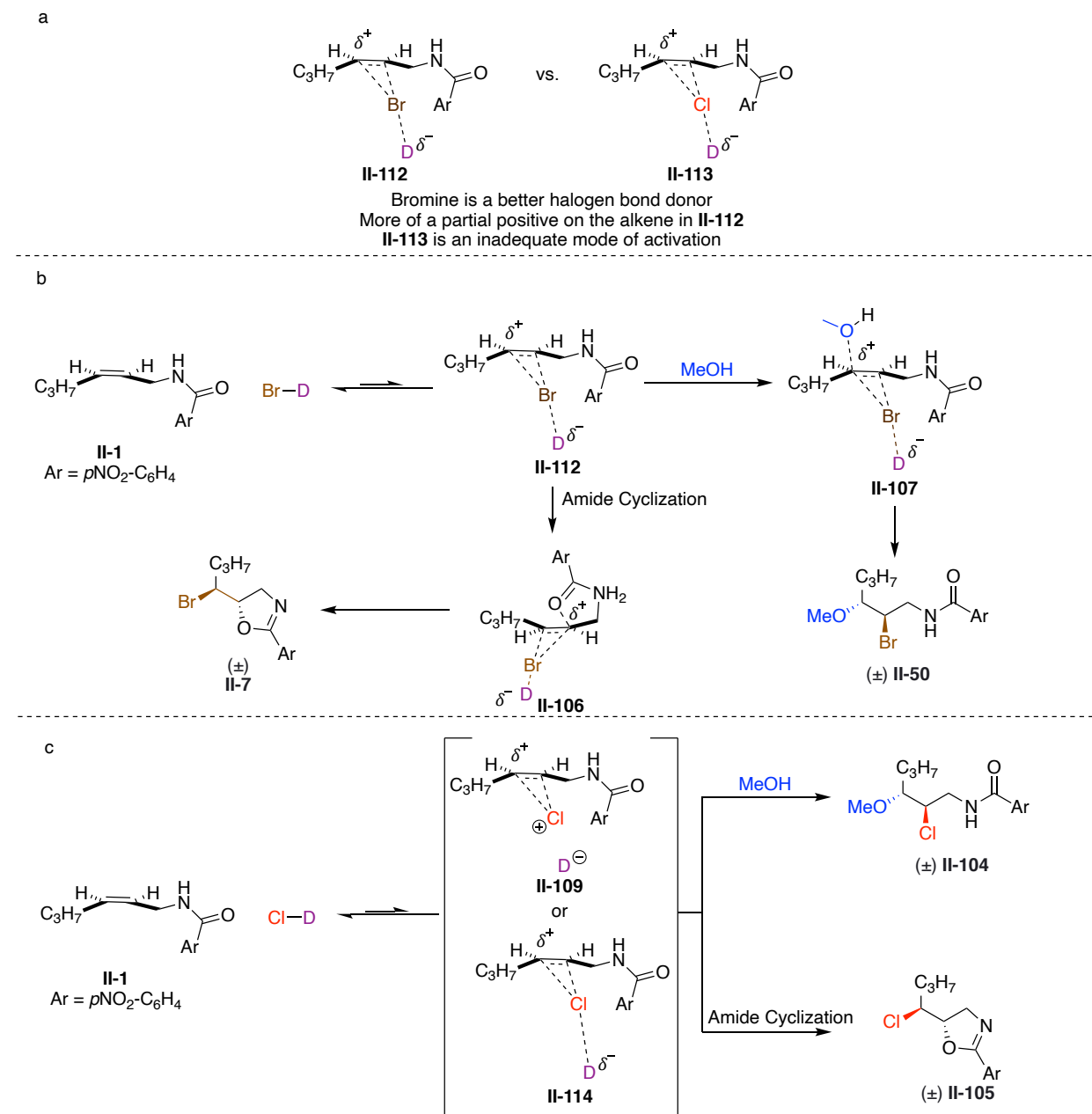**Figure II-32:** (a) Comparison of the bromine and chlorine halogen bond alkene activation (b) Proposed mechanism for bromofunctionalizations (c) Proposed mechanism for chlorofunctionalizations

Bromenium and chlorenium sources are often portrayed as mechanistically identical electrophiles regardless of the identity of the halenium ion or halenium donor. We were first enticed by the divergent nature of catalytic bromenium and chlorenium

induced reactions that provided a halocyclization with bromenium and intermolecular halo-Ritter reaction with chlorenium. We were delighted that with proper selection of bromenium reagent and nitrile nucleophile we were able to yield the bromo-Ritter product. Mechanistic studies hinted that the sensitivity to bromenium source might be the result of catalyst control. This led us to investigate the mechanistic divergence in the non-catalyzed haloetherifications. Multiple studies displayed a high sensitivity to bromenium donor as a determining factor in product distribution; however, analogous chlorofunctionalization studies displayed little or no dependence on the chlorenium donor. This initiated a mechanistic hypothesis that chlorenium induced difunctionalization reactions proceed through a stepwise mechanism and bromenium induced difunctionalization reactions proceed through a concerted addition of bromenium and nucleophile to the alkene. We hope this sparks appreciation to the complexity of halofunctionalization mechanisms and how one can leverage properties of an alkene, halenium ion, or halenium donor to induce an intended result. I hope people feel comfortable challenging my hypothesizes and look to explore this mechanism further.

## II-7  Experimental Section

### II-7-1  Materials and General Instrumentations

Commercially available reagents were purchased from Sigma-Aldrich, Alfa-Aesar, or TCI and used as received. Acetonitrile was freshly distilled over $CaH_2$ prior to use. All other solvents were used as purchased. NBS was purified by recrystallization in water. N-bromosaccharine was purchased from TCI and used without further purification.

Enantiomeric excess for all products was determined by HPLC analysis using DAICEL Chiralcel® OJ-H and OD-H or Chiralpak® IA, AD-H, and AS-H columns. Allyl amides **II-1**, **II-42**, **II-47a-c**, **II-47e**, were synthesized as reported previously and analytical data matched reported values.[1, 3] Spectral data for halofunctionalization products **II-7**, **II-50**, **II-97a**, **II-97b**, **II-104**, **II-104a**, **II-105** match reported values. Analytical data for the new substrates can be found below in Section **II-8.**

## II-7-2 General Procedure for the Screening of Catalytic Asymmetric Bromoamadination of II-1 to Yield Vicinal Bromoamadine II-14
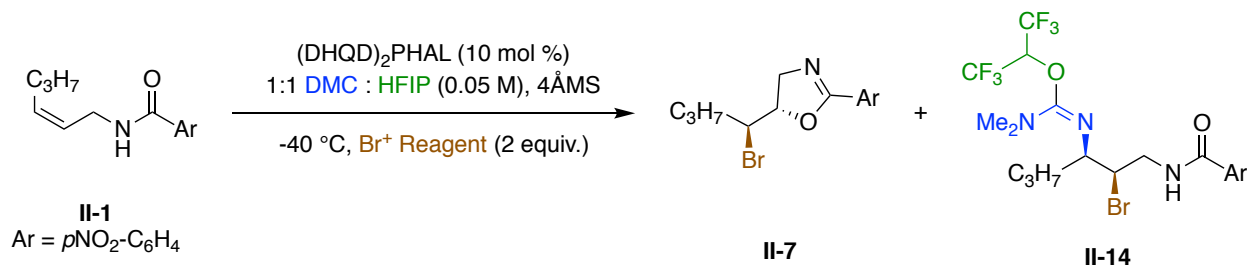


**Figure II-33:** General procedure for the screening of catalytic asymmetric bromoamadination of II-1 to yield vicinal bromoamadine **II-14**

The substrate **II-1** (12.4 mg, 0.1 mmol, 1.0 equiv) and (DHQD)$_2$PHAL (3.9 mg, 10 mol%) were suspended in dimethyl cyanamide (0.5 mL) in a test tube with a magnetic stir bar and capped with a rubber septa. HFIP (variable quantity) was added via syringe and 15mg of powder MS4Å was added. The resulting suspension was cooled to −40 °C in an immersion cooler. After stirring for 10 min, the bromenium reagent (0.1 mmol, 2 equiv) was added. Upon completion the reaction was quenched by the addition of saturated Na$_2$S$_2$O$_3$ (2 mL). The reaction was concentrated to remove acetonitrile and the resultant aqueous layer was extracted with DCM (3 x 5 mL). The combined organic layers were

dried with anhydrous Na$_2$SO$_4$ and concentrated. Yields were determined by crude NMR with 10 second relaxation delay and a triphenylmethane standard. Column chromatography (SiO$_2$/EtOAc–Hexanes gradient) provided the desired product (**II-14**).

## II-7-3 Procedure for the Eyring Analysis of the Catalytic Asymmetric Bromoamidation of II-1 With Acetonitrile



II-1
Ar = $p$NO$_2$-C$_6$H$_4$

**Figure II-34:** Procedure for the Eyring Analysis of the catalytic asymmetric bromoamidation of II-1 with acetonitrile

A stock solution of the substrate (**II-1**) (62.0 mg, 0.25 mmol, 1.0 equiv), (DHQD)$_2$PHAL (19.5 mg, 10 mol%), acetonitrile (2.5 mL), and HFIP (2.5 mL) were combined in a 20 mL vial. 1 mL aliquots were transferred via syringe to 10 mL test tubes with stir bars. Test tubes were heated (via oil bath) or cooled (via immersion cooler) to their respective temperature (47 °C, 25 °C, 7 °C, or -22 °C). After allowing 15 min to equilibrate, reactions were initiated by the addition of N-Bromophthalimide (22.6 mg, 0.1 mmol, 2 equiv.). Upon completion, the reaction was quenched by the addition of saturated Na$_2$S$_2$O$_3$ (2 mL). The reaction was concentrated to remove solvent and the resultant aqueous layer was extracted with DCM (3 x 5 mL). To the concentrated vial with a stir bar, acetonitrile (1 mL) and a solution of HCl (1 M, 0.2 mL) were added and stirred for 5 min. Water (3 mL) was added and the solution was concentrated in vacuo and extracted

with DCM (3 x 5 mL). The combined organic layers were dried with anhydrous $Na_2SO_4$ and concentrated. Yields and ratios were determined by crude NMR with 10 second relaxation delay and a triphenylmethane standard. Further analysis of product **II-19** was on the hydrolyzed product. Hydrolysis procedure is as follows: To the concentrated vial with a stir bar, acetonitrile (1 mL) and a solution of HCl (1 M, 0.2 mL) were added and stirred for 5 min. Water (3 mL) was added and the solution was concentrated in vacuo and extracted with DCM (3 x 5 mL). The combined organic layers were dried with anhydrous $Na_2SO_4$ and concentrated to provide amide xy.

## II-7-4 Procedure for the Eyring Analysis of the Catalytic Asymmetric Bromoamadination of II-1 With Dimethylcyanamide
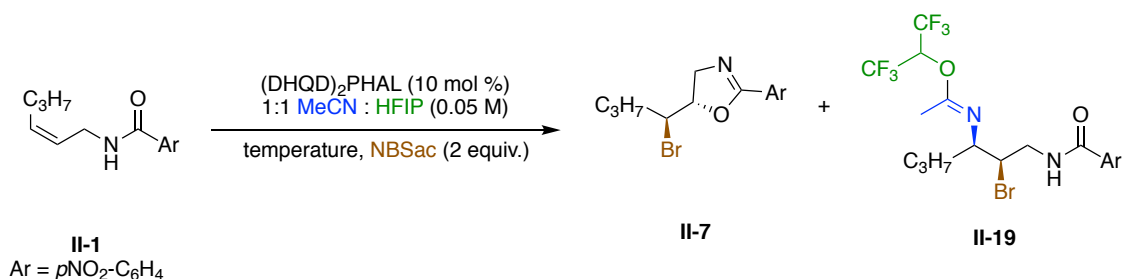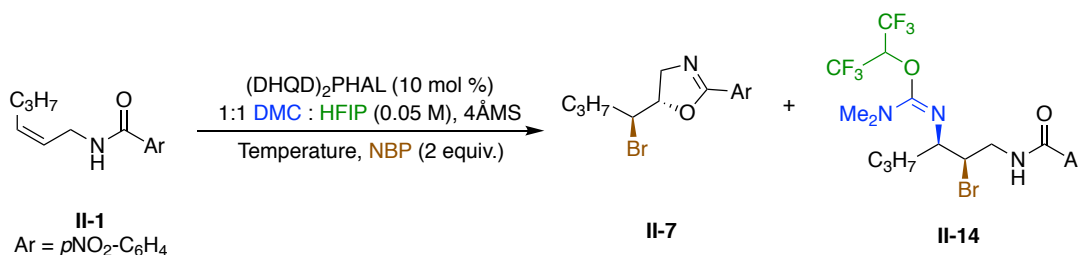


**Figure II-35:** Procedure for the Eyring Analysis of the catalytic asymmetric bromoamadination of **II-1** with dimethylcyanamide

A stock solution of the substrate (**II-1**) (62.0 mg, 0.25 mmol, 1.0 equiv), (DHQD)₂PHAL (19.5 mg, 10 mol%), acetonitrile (2.5 mL), and HFIP (2.5 mL) were combined in a 20 mL vial. 1 mL aliquots were transferred via syringe to 10 mL test tubes with stir bars. Test tubes were heated (via oil bath) or cooled (via immersion cooler) to their respective temperature (Figure II-9). After allowing 15 min to equilibrate, reactions were initiated by the addition of the bromenium reagent (0.1 mmol, 2 equiv.). Upon completion, the reaction

was quenched by the addition of saturated $Na_2S_2O_3$ (2 mL). The reaction was concentrated to remove solvent and the resultant aqueous layer was extracted with DCM (3 x 5 mL). The combined organic layers were dried with anhydrous $Na_2SO_4$ and concentrated. Ratios of **II-7** to **II-19** were determined by crude NMR with 10 second relaxation delay and a triphenylmethane standard.

## II-7-5 Procedure for Eyring Analysis of Haloetherification Reactions with Various Bromenium Reagents
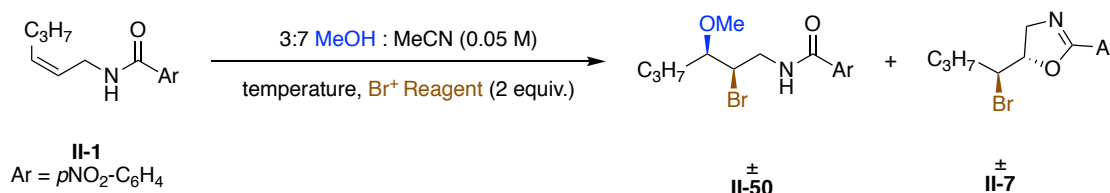


**Figure II-36:** Procedure for Eyring Analysis of haloetherification reactions with various bromenium reagents

A stock solution of the substrate (**II-1**) (161.4 mg, 0.65 mmol, 1.0 equiv.), acetonitrile (9.1 mL), and methanol (3.9 mL) were combined in a 20 mL vial. 1 mL aliquots were transferred via syringe to 10 mL test tubes with stir bars. Test tubes were heated (via oil bath) or cooled (via immersion cooler) to their respective temperature (51 °C, 25 °C, -7 °C, -28 °C) After allowing 15 min to equilibrate, reactions were initiated by the addition of the bromenium reagent (0.1 mmol, 2 equiv.). The reaction was monitored by TLC and upon completion was quenched by the addition of saturated $Na_2S_2O_3$ (2 mL). The reaction was concentrated to remove acetonitrile and the resultant aqueous layer was extracted with DCM (3 x 5 mL). The combined organic layers were dried with anhydrous $Na_2SO_4$ and concentrated. Product ratios (**II-50:II-7**) were determined by crude NMR with 10 second relaxation delay.

## II-7-6  Procedure for Product Ratio as a Function of Nucleophile Concentration



**Figure II-37:**  Procedure for product ratio as a function of nucleophile concentration

Stock solutions of methanol nitromethane mixtures were made providing methanol molar concentrations of 3.84, 5.45, 9.31, and 14.96. The substrate (**II-1**) (12.4 mg, 0.05 mmol, 1 equiv.) was added to a test tube with stir bar. 1 mL of the methanol nitromethane mixture was added to the test tube and it was allowed to stir for 5 minutes at room temperature. Reactions were initiated by the addition of the bromenium reagent (0.1 mmol, 2 equiv.). The reaction was monitored by TLC and upon completion was quenched by the addition of saturated $Na_2S_2O_3$ (2 mL). The reaction was concentrated to remove the solvent and the resultant aqueous layer was extracted with DCM (3 x 5 mL). The combined organic layers were dried with anhydrous $Na_2SO_4$ and concentrated. Product ratios were determined by crude NMR with 10 second relaxation delay.

## II-7-7  Procedure for Acid Additive Influence of Product Ratio



**Figure II-38:** Procedure for acid additive influence of product ratio

A stock solution of the substrate (**II-1**) (49.6 mg, 0.2 mmol, 1.0 equiv.), toluene (3.2 mL), and methanol (0.8 mL) were combined in a 20 mL vial. 1 mL aliquots were transferred via syringe to 10 mL test tubes with stir bars. Acid additives (TFE or HFIP) (0.8 mmol, 20 equiv.) were added to their respective test tube via glass syringe. After allowing 5 min to equilibrate, reactions were initiated by the addition of the DBDMH (28.5 mg, 0.1 mmol, 2 equiv.). The reaction was monitored by TLC and upon completion was quenched by the addition of saturated $Na_2S_2O_3$ (2 mL). The reaction was concentrated to remove the solvent and the resultant aqueous layer was extracted with DCM (3 x 5 mL). The combined organic layers were dried with anhydrous $Na_2SO_4$ and concentrated. Product ratios were determined by crude NMR with 10 second relaxation delay.

## II-7-8  Procedure for Product Ratio as a Function of Nucleophile Size



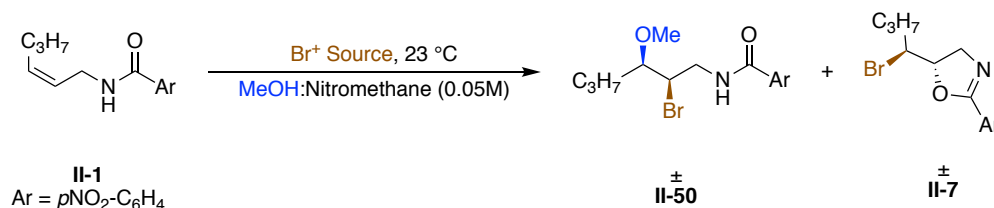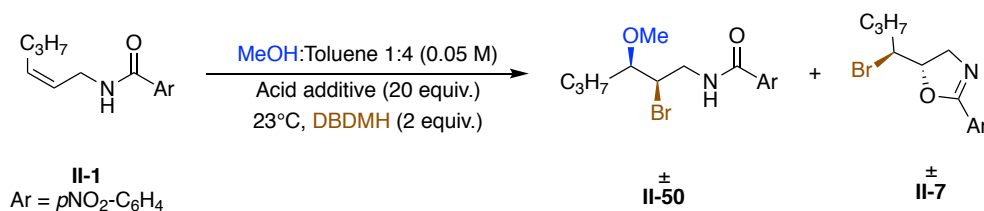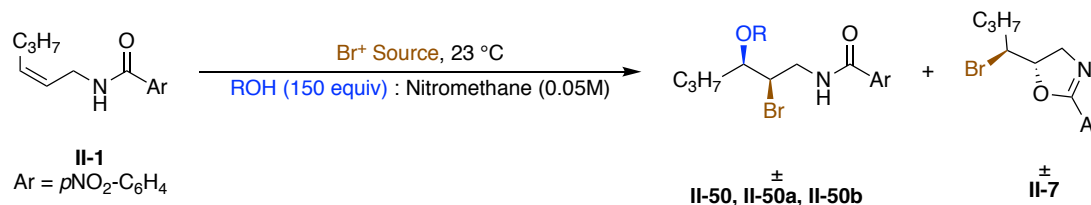**Figure II-39:** Procedure for product ratio as a function of nucleophile size

Stock Solutions of alcohol nucleophile (7.5 mmol, 150 equiv.) and nitromethane (supplemented to enable a 0.05M concentration of **II-1**). The substrate (**II-1**) (12.4 mg, 0.05 mmol, 1 equiv.) was added to a test tube with stir bar. 1 mL of the alcohol nitromethane mixture was added to the test tube and it was allowed to stir for 5 minutes at room temperature. Reactions were initiated by the addition of the bromenium reagent (0.1 mmol, 2 equiv.). Upon completion the reactions were quenched by the addition of

saturated Na$_2$S$_2$O$_3$ (2 mL). The reaction was concentrated to remove the alcohol/nitromethane solvent and the resultant aqueous layer was extracted with DCM (3 x 5 mL). The combined organic layers were dried with anhydrous Na$_2$SO$_4$ and concentrated. Product ratios were determined by crude NMR with 10 second relaxation delay.

## II-7-9   Procedure for Eyring Analysis With Alkenes of Varied Halenium Affinity
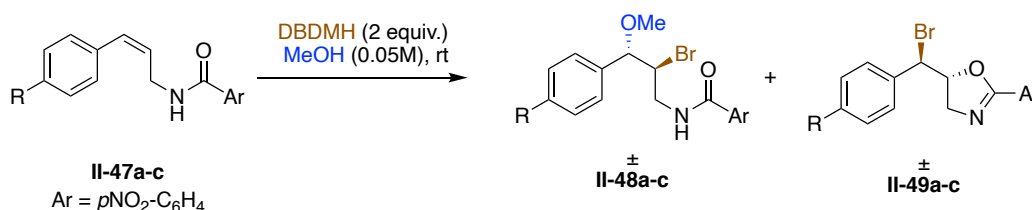


**Figure II-40:** Procedure for Eyring Analysis with alkenes of varied halenium affinity

A stock solution of the substrate (**II-47a**, **II-47b**, or **II-47c**) (0.25 mmol, 1.0 equiv.) and methanol (5 mL) were combined in a 20 mL vial. 1 mL aliquots were transferred via syringe to 10 mL test tubes with stir bars. Test tubes were heated (via oil bath) or cooled (via immersion cooler) to their respective temperature. After allowing 15 min to equilibrate, reactions were initiated by the addition of the DBDMH (28.5 mg, 0.1 mmol, 2 equiv.). The reaction was monitored by TLC and upon completion was quenched by the addition of saturated Na$_2$S$_2$O$_3$ (2 mL). The reaction was concentrated to remove methanol and the resultant aqueous layer was extracted with DCM (3 x 5 mL). The combined organic layers were dried with anhydrous Na$_2$SO$_4$ and concentrated. Product ratios of the intermolecular

product (**II-48**) to intramolecular product (**II-49**) were determined by crude NMR with 10 second relaxation delay.

## II-7-10 Procedure of Eyring Analysis of Diastereoselectivity in Chlorofunctionalization
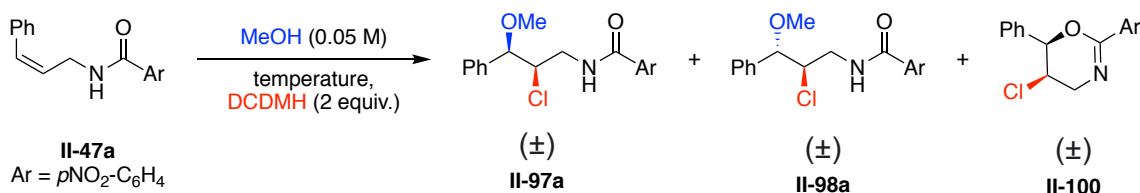


**Figure II-41:** Procedure of Eyring Analysis of diastereoselectivity in chlorofunctionalization

A stock solution of the substrate (**II-47a**) (70.5 mg, 0.25 mmol, 1.0 equiv.) and methanol (5 mL) were combined in a 20 mL vial. 1 mL aliquots were transferred via syringe to 10 mL test tubes with stir bars. Test tubes were heated (via oil bath) or cooled (via immersion cooler) to their respective temperature (56 °C, 40 °C, 24 °C, 10 °C) After allowing 15 min to equilibrate, reactions were initiated by the addition of the DBDMH (28.5 mg, 0.1 mmol, 2 equiv.). The reaction was monitored by TLC and upon completion was quenched by the addition of saturated $Na_2S_2O_3$ (2 mL). The reaction was concentrated to remove methanol and the resultant aqueous layer was extracted with DCM (3 x 5 mL). The combined organic layers were dried with anhydrous $Na_2SO_4$ and concentrated. Product ratios were determined by crude NMR with 10 second relaxation delay.

## II-7-11 Procedure for Halenium Affinity Diastereoselectivity Studies of Chlorofunctionalizations
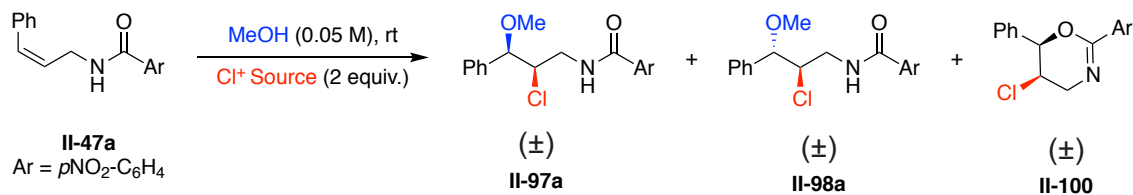
**Figure II-42:** Procedure for halenium affinity diastereoselectivity studies of chlorofunctionalizations

A stock solution of the substrate (**II-47a**) (70.5 mg, 0.25 mmol, 1.0 equiv.) and methanol (5 mL) were combined in a 20 mL vial. 1 mL aliquots were transferred via syringe to 10 mL test tubes with stir bars at room temperature. The reactions were initiated by the addition of the chlorinating reagent (0.1 mmol, 2 equiv.). The reaction was monitored by TLC and upon completion was quenched by the addition of saturated $Na_2S_2O_3$ (2 mL). The reaction was concentrated to remove methanol and the resultant aqueous layer was extracted with DCM (3 x 5 mL). The combined organic layers were dried with anhydrous $Na_2SO_4$ and concentrated. Product ratios were determined by crude NMR with 10 second relaxation delay.

## II-7-12 Procedure for the Study of the Influence of Chlorenium Donor *HalA* on Product Distribution
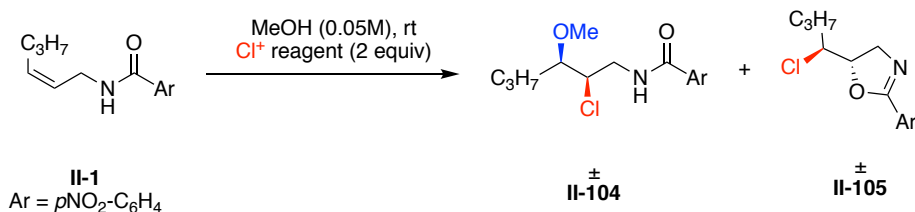


**Figure II-43:** Procedure for the study of the influence of chlorenium donor HalA on product distribution

A stock solution of the substrate (**II-1**) (74.4 mg, 0.3 mmol, 1.0 equiv.) and methanol (6 mL) were combined in a 20 mL vial. 1 mL aliquots were transferred via syringe to 10 mL

test tubes with stir bars at room temperature. The reactions were initiated by the addition of the chlorinating reagent (0.1 mmol, 2 equiv.). The reaction was monitored by TLC and upon completion was quenched by the addition of saturated $Na_2S_2O_3$ (2 mL). The reaction was concentrated to remove methanol and the resultant aqueous layer was extracted with DCM (3 x 5 mL). The combined organic layers were dried with anhydrous $Na_2SO_4$ and concentrated. Product ratios were determined by crude NMR with 10 second relaxation delay.

## II-7-13 Procedure for Eyring Analysis with N-Chlorosaccharine



**Figure II-44:** Procedure for Eyring Analysis with N-Chlorosaccharine

A stock solution of the substrate **II-1** (74.4 mg, 0.30 mmol, 1.0 equiv.) and methanol (6 mL) were combined in a 20 mL vial. 1 mL aliquots were transferred via syringe to 10 mL test tubes with stir bars. Test tubes were heated (via oil bath) or cooled (via immersion cooler) to their respective temperature (41 °C, 23 °C, 8 °C, -10 °C, -22 °C) After allowing 15 min to equilibrate, reactions were initiated by the addition of the NCSac (6.5 mg, 0.03 mmol, 0.6 equiv.). The reaction was quenched by the addition of saturated $Na_2S_2O_3$ (2 mL). The reaction was concentrated to remove methanol and the resultant aqueous layer was extracted with DCM (3 x 5 mL). The combined organic layers were dried with anhydrous $Na_2SO_4$ and concentrated. Product ratios were determined by crude NMR with 10 second relaxation delay.

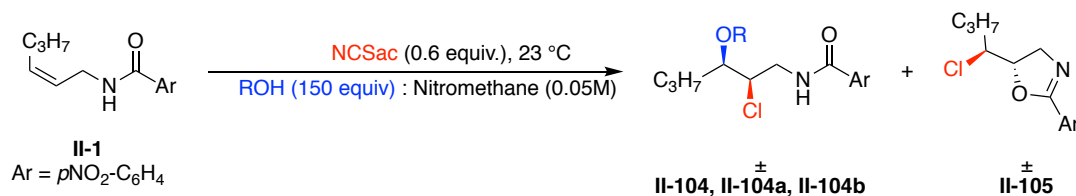## II-7-14 Procedure for Nucleophile Size Study with N-Chlorosaccharine



**Figure II-45:** Procedure for nucleophile size study with N-Chlorosaccharine

Stock Solutions of alcohol nucleophile (7.5 mmol, 150 equiv.) and nitromethane. The substrate (12.4 mg, 0.05 mmol, 1 equiv.) was added to a test tube with stir bar. 1 mL of the alcohol nitromethane mixture was added to the test tube and it was allowed to stir for 5 minutes at room temperature. Reactions were initiated by the addition of the bromenium reagent (0.1 mmol, 2 equiv.). The reaction was quenched with saturated $Na_2S_2O_3$ (2 mL). The reaction was concentrated to remove acetonitrile and the resultant aqueous layer was extracted with DCM (3 x 5 mL). The combined organic layers were dried with anhydrous $Na_2SO_4$ and concentrated. Product ratios were determined by crude NMR with 10 second relaxation delay.
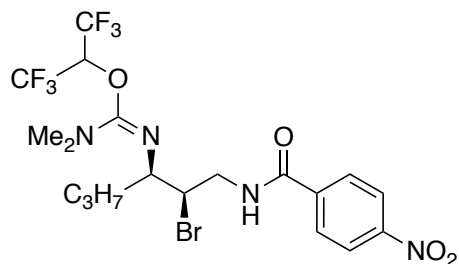
## II-8 Analytical Data
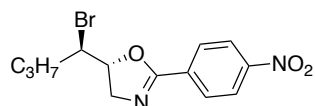


**II-7**, (*R*)-5-((*R*)-1-bromobutyl)-2-(4-nitrophenyl)-4,5-dihydrooxazole

¹H and ¹³C NMR data match previous publications

**Resolution of enantiomers:** DAICEL Chiralpak®, IA 98.5% IPA/Hexane 1ml/min, 254 nm, RT 1 (major)=21.8 min, RT 2 (minor) =24.4 min.
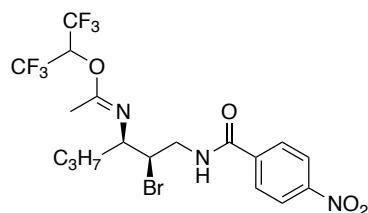
**II-14**, 1,1,1,3,3,3-hexafluoropropan-2-yl *N'*-((2*R*,3*R*)-2-bromo-1-(4-nitrobenzamido)hexan-3-yl)-*N*,*N*-dimethylcarbamimidate

**¹H NMR (500 MHz, CDCl₃)** δ 8.32 (d, *J* = 8.7 Hz, 2H), 7.95 (d, *J* = 8.8 Hz, 2H), 6.70 (s, 1H), 4.30 (dt, *J* = 9.5, 3.3 Hz, 1H), 4.12 (ddd, *J* = 14.4, 7.3, 3.5 Hz, 1H), 3.80 (td, *J* = 6.5, 2.8 Hz, 1H), 3.52 – 3.41 (m, 1H), 2.89 (s, 6H), 1.76 – 1.61 (m, 1H), 1.48 (ddt, *J* = 16.4, 14.3, 7.1 Hz, 1H), 1.36 – 1.28 (m, 2H), 0.95 (t, *J* = 7.3 Hz, 3H).

**¹³C NMR (126 MHz, CDCl₃)** δ 165.3, 150.2, 149.7, 139.7, 128.1, 123.9, 60.8, 57.0, 44.9, 39.6, 36.5, 18.9, 14.0.

**¹⁹F NMR (470 MHz, CDCl₃)** δ -73.06 (p, *J* = 8.2 Hz), -73.40.

**Resolution of enantiomers:** DAICEL Chiralpak®, IA 97.5% IPA/Hexane 1ml/min, 254 nm, RT 1 (minor)=18.9 min, RT 2 (major) =22.3 min.



**II-19**, 1,1,1,3,3,3-hexafluoropropan-2-yl *N*-((2*R*,3*R*)-1-(argioformamido)-2-bromohexan-3-yl)acetimidate

**R_f**: 0.32 (30% EtOAC/Hex)

**¹H NMR (500 MHz, CDCl₃)** δ 8.33 (d, *J* = 8.9 Hz, 2H), 7.96 (d, *J* = 8.9 Hz, 2H), 6.61 (s, 1H), 6.43 (hept, *J* = 6.5 Hz, 1H), 4.28 (ddd, *J* = 10.0, 4.4, 3.1 Hz, 1H), 4.15 (ddd, *J* = 14.4, 7.5, 2.9 Hz, 1H), 3.51 (dt, *J* = 8.7, 4.3 Hz, 1H), 3.32 (ddd, *J* = 14.4, 10.0, 4.4 Hz, 1H), 2.08 (s, 3H), 1.72 (dddd, *J* = 14.2, 10.4, 6.1, 4.5 Hz, 1H), 1.67 – 1.49 (m, 1H), 1.30 – 1.18 (m, 2H), 0.94 (t, *J* = 7.4 Hz, 3H).

**¹³C NMR (126 MHz, CDCl₃)** δ 165.5, 157.8, 149.8, 139.5, 128.2, 124.0, 60.8, 60.2, 44.5, 36.3, 19.0, 14.9, 13.9.

**¹⁹F NMR (470 MHz, CDCl₃)** δ -73.15 (p, *J* = 8.0 Hz), -73.35 (p, *J* = 8.1 Hz).

**Resolution of enantiomers:** DAICEL Chiralpak®, IA 96% IPA/Hexane 1ml/min, 254 nm, RT 1 (minor)=9.9 min, RT 2 (major) =10.7 min.
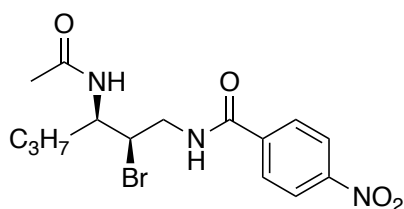


**II-19**-Hydrolyzed  *N*-((2*R*,3*R*)-3-acetamido-2-bromohexyl)-4-nitrobenzamide

**¹H NMR (500 MHz, CDCl₃)** δ 8.38 (dd, *J* = 7.9, 3.3 Hz, 1H), 8.32 (d, *J* = 8.8 Hz, 2H), 8.09 (d, *J* = 8.8 Hz, 2H), 5.58 (d, *J* = 9.3 Hz, 1H), 4.42 (ddd, *J* = 13.8, 8.8, 5.1 Hz, 1H), 4.22 (ddd, *J* = 11.3, 5.1, 1.8 Hz, 1H), 4.15 (tdd, *J* = 9.0, 5.4, 1.8 Hz, 1H), 3.05 (ddd, *J* = 13.7, 11.3, 4.3 Hz, 1H), 2.16 (s, 3H), 1.67 (dtd, *J* = 13.9, 8.5, 6.7 Hz, 1H), 1.58 – 1.49 (m, 1H), 1.40 – 1.33 (m, 2H), 0.91 (t, *J* = 7.3 Hz, 3H).

**¹³C NMR (126 MHz, CDCl₃)** δ 172.0, 164.7, 149.7, 139.2, 128.4, 123.9, 55.5, 49.0, 43.1, 36.3, 23.3, 19.2, 13.7.
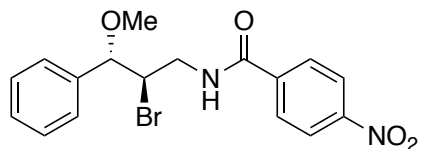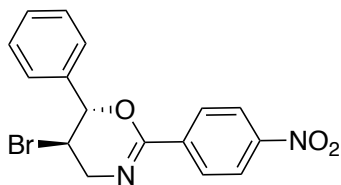
**II-44**, (±) *N*-((2*R*,3*S*)-2-bromo-3-methoxy-3-phenylpropyl)-4-nitrobenzamide

**R$_f$**: 0.28 (30% EtOAC/Hex)

**$^1$H NMR (500 MHz, CDCl$_3$)** δ 8.31 (d, *J* = 8.9 Hz, 2H), 7.92 (d, *J* = 9.0 Hz, 2H), 7.48 – 7.33 (m, 5H), 6.97 (s, 1H), 4.58 (d, *J* = 5.2 Hz, 1H), 4.36 (dd, *J* = 10.9, 5.0 Hz, 1H), 4.11 (ddd, *J* = 14.5, 6.5, 4.6 Hz, 1H), 3.71 (ddd, *J* = 14.6, 6.1, 4.5 Hz, 1H), 3.39 (s, 3H).

**$^{13}$C NMR (126 MHz, CDCl$_3$)** δ 165.2, 149.7, 139.9, 137.5, 128.8, 128.8, 128.2, 127.1, 123.9, 86.7, 58.2, 55.1, 42.7.
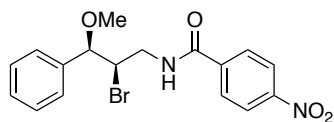


**II-46**, (±) (5*R*,6*S*)-5-bromo-2-(4-nitrophenyl)-6-phenyl-5,6-dihydro-4*H*-1,3-oxazine

**R$_f$**: 0.55 (30% EtOAC/Hex)

**$^1$H NMR (500 MHz, CDCl$_3$)** δ 8.23 (d, *J* = 9.0 Hz, 2H), 8.13 (d, *J* = 8.9 Hz, 2H), 7.48 – 7.41 (m, 3H), 7.42 – 7.36 (m, 2H), 5.37 (d, *J* = 8.0 Hz, 1H), 4.33 (td, *J* = 8.0, 4.8 Hz, 1H), 4.11 (dd, *J* = 17.6, 4.8 Hz, 1H), 3.96 (dd, *J* = 17.6, 8.1 Hz, 1H).

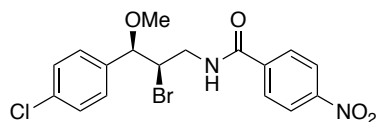**¹³C NMR (126 MHz, CDCl₃)** δ 153.6, 149.4, 138.4, 137.0, 129.4, 128.9, 128.3, 126.8, 123.4, 81.3, 50.6, 44.7.



**II-48a**, *N*-((2*R*,3*R*)-2-bromo-3-methoxy-3-phenylpropyl)-4-nitrobenzamide

**R_f**: 0.20 (30% EtOAC/Hex)

**¹H NMR (500 MHz, CDCl₃)** δ 8.29 (d, *J* = 8.9 Hz, 1H), 7.89 (d, *J* = 8.8 Hz, 1H), 7.45 – 7.32 (m, 5H), 6.66 (s, 1H), 4.44 (d, *J* = 5.0 Hz, 1H), 4.37 (ddd, *J* = 7.8, 5.0, 4.3 Hz, 1H), 3.35 (s, 3H)

**¹³C NMR (126 MHz, CDCl₃)** δ 165.3, 149.7, 139.6, 137.3, 128.8, 128.7, 128.2, 127.4, 123.9, 85.0, 57.4, 57.4, 44.3.
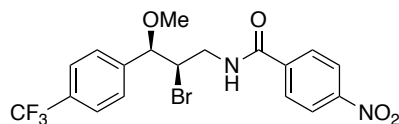


**II-48b**, (±) *N*-((2*R*,3*R*)-2-bromo-3-(4-chlorophenyl)-3-methoxypropyl)-4-nitrobenzamide

**R_f**: 0.18 (30% EtOAC/Hex)

**¹H NMR (500 MHz, CDCl₃)** δ 8.31 (d, *J* = 8.8 Hz, 2H), 7.91 (d, *J* = 8.8 Hz, 2H), 7.39 (d, *J* = 8.5 Hz, 2H), 7.31 (d, *J* = 8.5 Hz, 1H), 6.68 (t, *J* = 5.2 Hz, 1H), 4.43 (d, *J* = 4.5 Hz, 1H), 4.33 (dt, *J* = 8.4, 4.3 Hz, 1H), 4.08 (ddd, *J* = 14.5, 6.8, 4.1 Hz, 1H), 3.65 (ddd, *J* = 14.5, 8.1, 4.8 Hz, 1H), 3.34 (s, 3H).

**¹³C NMR (126 MHz, CDCl₃)** δ 165.4, 149.8, 139.5, 135.8, 134.7, 128.9, 128.7, 128.2, 124.0, 84.0, 57.5, 57.2, 44.3.
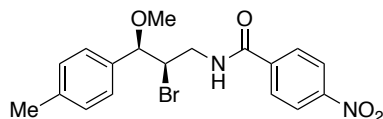


**II-48c**, (±) *N*-((2*R*,3*R*)-2-bromo-3-methoxy-3-(4-(trifluoromethyl)phenyl)propyl)-4-nitrobenzamide

**R_f**: 0.20 (30% EtOAC/Hex)

**¹H NMR (500 MHz, CDCl₃)** δ 8.31 (d, *J* = 8.8 Hz, 1H), 7.92 (d, *J* = 8.8 Hz, 1H), 7.68 (d, *J* = 8.5 Hz, 2H), 7.51 (d, *J* = 8.0 Hz, 2H), 4.53 (d, *J* = 4.0 Hz, 1H), 4.37 (dt, *J* = 8.1, 4.0 Hz, 1H), 4.15 (ddd, *J* = 14.4, 6.8, 4.0 Hz, 1H), 3.68 (ddd, *J* = 14.4, 8.2, 4.8 Hz, 1H), 3.38 (s, 3H).

**¹³C NMR (126 MHz, CDCl₃)** δ 165.5, 149.8, 141.4, 139.5, 130.9 (q, *J* = 32.5 Hz), 128.2, 127.8, 126.8 (q, *J* = 271.8 Hz), 125.6 (q, *J* = 3.8 Hz), 124.0, 83.9, 57.7, 57.0, 44.5.

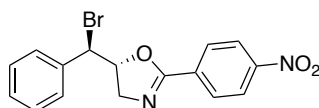**¹⁹F NMR (470 MHz, CDCl₃)** δ -62.63.



**II-48e**, (±) *N*-((2*R*,3*R*)-2-bromo-3-methoxy-3-(*p*-tolyl)propyl)-4-nitrobenzamide

**R_f:** 0.25 (30% EtOAC/Hex)

**¹H NMR (500 MHz, CDCl₃)** δ 8.30 (d, *J* = 8.8 Hz, 2H), 7.89 (d, *J* = 8.8 Hz, 2H), 7.27 – 7.20 (m, 4H), 6.61 (s, 1H), 4.40 (d, *J* = 5.3 Hz, 1H), 4.36 (dt, *J* = 7.5, 4.8 Hz, 1H), 4.00

(ddd, *J* = 14.4, 6.6, 4.4 Hz, 1H), 3.67 (ddd, *J* = 14.4, 7.6, 4.9 Hz, 1H), 3.34 (s, 3H), 2.38 (s, 3H).

**13C NMR (126 MHz, CDCl3)** δ 165.2, 149.7, 139.7, 138.8, 134.2, 129.4, 128.1, 127.3, 123.9, 85.0, 57.4, 57.3, 44.3, 21.3.
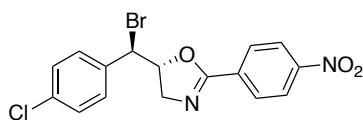


**II-49a**, (*R*)-5-((*R*)-bromo(phenyl)methyl)-2-(4-nitrophenyl)-4,5-dihydrooxazole

**Rf**: 0.23 (30% EtOAC/Hex)

**1H NMR (500 MHz, CDCl3)** δ 8.31 (d, *J* = 9.0 Hz, 1H), 8.18 (d, *J* = 8.8 Hz, 2H), 7.50 − 7.44 (m, 1H), 7.43 − 7.32 (m, 2H), 5.26 (dt, *J* = 9.9, 6.9 Hz, 1H), 5.02 (d, *J* = 6.6 Hz, 1H), 4.12 (dd, *J* = 15.8, 9.9 Hz, 1H), 3.88 (dd, *J* = 15.8, 7.0 Hz, 1H).

**13C NMR (126 MHz, CDCl3)** δ 162.1, 149.6, 137.1, 132.8, 129.4, 129.3, 129.1, 128.3, 123.6, 82.8, 58.8, 54.9. (Assisted by HSQC and HMBC NMR)



**II-49b**, (±) (*R*)-5-((*R*)-bromo(4-chlorophenyl)methyl)-2-(4-nitrophenyl)-4,5-dihydrooxazole

**1H NMR (500 MHz, CDCl3)** δ 8.31 (d, *J* = 9.0 Hz, 2H), 8.14 (d, *J* = 8.9 Hz, 2H), 7.43 (d, *J* = 8.6 Hz, 2H), 7.37 (d, *J* = 8.6 Hz, 2H), 5.18 (dt, *J* = 10.1, 6.6 Hz, 1H), 4.99 (d, *J* = 6.1 Hz, 1H), 4.14 (dd, *J* = 15.9, 9.9 Hz, 1H), 3.88 (dd, *J* = 15.8, 6.9 Hz, 1H).

**13C NMR (126 MHz, CDCl3)** δ 161.8, 149.8, 135.9, 135.1, 132.8, 129.6, 129.3, 129.2, 123.7, 82.4, 59.2, 51.7
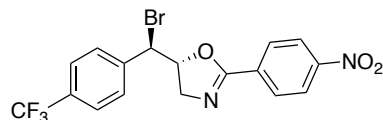
**II-49c**, (±) (*R*)-5-(((*R*)-bromo(4-(trifluoromethyl)phenyl)methyl)-2-(4-nitrophenyl)-4,5-dihydrooxazole

**R$_f$**: 0.24 (30% EtOAC/Hex)

**$^1$H NMR (500 MHz, CDCl$_3$)** δ 8.31 (d, *J* = 8.8 Hz, 2H), 8.14 (d, *J* = 8.8 Hz, 2H), 7.67 (d, *J* = 8.4 Hz, 2H), 7.63 (d, *J* = 8.3 Hz, 2H), 5.19 (ddd, *J* = 9.9, 6.9, 5.7 Hz, 1H), 5.05 (d, *J* = 5.7 Hz, 1H), 4.18 (dd, *J* = 15.8, 9.9 Hz, 1H), 3.92 (dd, *J* = 15.8, 6.9 Hz, 1H).

**$^{13}$C NMR (126 MHz, CDCl$_3$)** δ 161.8, 149.7, 141.3, 132.8, 131.3 (q, *J* = 32.9 Hz), 129.3, 128.8, 127.3 (q, *J* = 290.6 Hz), 126.0 (q, *J* = 3.8 Hz), 123.7, 82.1, 59.1, 53.6.
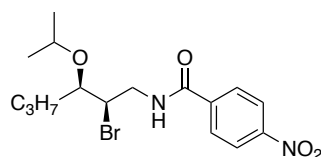
**$^{19}$F NMR (470 MHz, Chloroform-*d*)** δ -62.85.
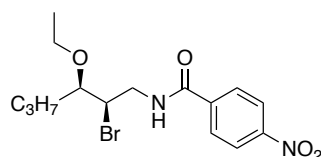


**II-50a**, (±) *N*-((2*R*,3*R*)-2-bromo-3-ethoxyhexyl)-4-nitrobenzamide

**R$_f$**: 0.36 (30% EtOAC/Hex)

**$^1$H NMR (500 MHz, CDCl$_3$)** δ 8.32 (d, *J* = 8.8 Hz, 2H), 7.96 (d, *J* = 8.8 Hz, 2H), 6.99 (s, 1H), 4.36 (ddd, *J* = 8.0, 5.1, 3.0 Hz, 1H), 4.17 (ddd, *J* = 14.3, 6.4, 5.1 Hz, 1H), 3.72 (ddd, *J* = 14.3, 7.7, 4.7 Hz, 1H), 3.65 (qd, *J* = 7.0, 2.3 Hz, 2H), 3.52 (ddd, *J* = 7.9, 5.0, 3.0 Hz, 1H), 1.81 − 1.71 (m, 1H), 1.68 − 1.59 (m, 1H), 1.51 − 1.34 (m, 2H), 1.23 (t, *J* = 7.0 Hz, 3H), 0.98 (t, *J* = 7.3 Hz, 3H).

**$^{13}$C NMR (126 MHz, Chloroform-*d*)** δ 165.2, 149.7, 139.8, 128.2, 123.9, 81.5, 66.0, 54.3, 44.1, 33.1, 19.1, 15.6, 14.0.
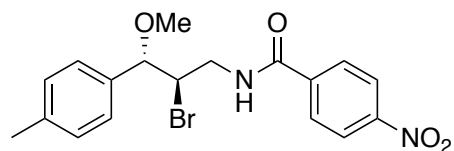
**II-50b**, (±) *N*-((2*R*,3*R*)-2-bromo-3-isopropoxyhexyl)-4-nitrobenzamide

**R_f**: 0.44 (30% EtOAC/Hex)

**¹H NMR (500 MHz, CDCl₃)** δ 8.32 (d, *J* = 8.7 Hz, 2H), 7.96 (d, *J* = 8.8 Hz, 2H), 7.05 (s, 1H), 4.33 (ddd, *J* = 8.4, 5.6, 3.0 Hz, 1H), 4.15 (dt, *J* = 14.2, 5.8 Hz, 1H), 3.79 – 3.67 (m, 2H), 3.62 (dt, *J* = 8.0, 4.0 Hz, 1H), 1.86 – 1.76 (m, 1H), 1.57 – 1.43 (m, 2H), 1.41 – 1.30 (m, 1H), 1.20 (t, *J* = 5.9 Hz, 6H), 0.98 (t, *J* = 7.3 Hz, 3H).

**¹³C NMR (126 MHz, Chloroform-*d*)** δ 165.1, 149.7, 139.8, 128.2, 123.9, 79.3, 71.3, 53.7, 43.7, 32.6, 23.0, 22.6, 19.2, 14.0.



**II-103**, (±) *N*-((2*R*,3*S*)-2-bromo-3-methoxy-3-(*p*-tolyl)propyl)-4-nitrobenzamide

**R_f:** 0.21 (30% EtOAC/Hex)

**¹H NMR (500 MHz, CDCl₃)** δ 8.31 (d, *J* = 8.8 Hz, 2H), 7.92 (d, *J* = 8.8 Hz, 2H), 7.27 – 7.19 (m, 4H), 6.97 (s, 1H), 4.55 (d, *J* = 5.2 Hz, 1H), 4.34 (q, *J* = 5.1 Hz, 1H), 4.10 (ddd, *J* = 14.7, 6.5, 4.7 Hz, 1H), 3.72 (ddd, *J* = 14.5, 5.9, 4.4 Hz, 1H), 3.37 (s, 3H), 2.37 (s, 3H).

**¹³C NMR (126 MHz, CDCl₃)** δ 165.1, 149.6, 140.0, 138.7, 134.5, 129.5, 128.1, 127.0, 123.9, 86.7, 58.1, 55.2, 42.7, 21.2.
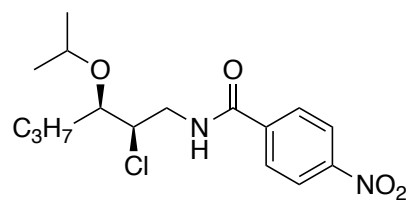
**II-104b**, (±) *N*-((2*R*,3*R*)-2-chloro-3-isopropoxyhexyl)-4-nitrobenzamide

**R_f:** 0.39 (30% EtOAC/Hex)

**¹H NMR (500 MHz, CDCl₃)** δ 8.32 (d, *J* = 8.8 Hz, 2H), 7.96 (d, *J* = 8.9 Hz, 2H), 7.00 (s, 1H), 4.23 (ddd, *J* = 8.2, 5.3, 3.2 Hz, 1H), 4.11 (ddd, *J* = 14.1, 6.2, 5.3 Hz, 1H), 3.75 (hept, *J* = 6.0 Hz, 1H), 3.66 – 3.58 (m, 2H), 1.83 – 1.64 (m, 1H), 1.55 – 1.45 (m, 2H), 1.43 – 1.30 (m, 1H), 1.20 (dd, *J* = 6.1, 3.5 Hz, 6H), 0.98 (t, *J* = 7.3 Hz, 3H).

**¹³C NMR (126 MHz, CDCl₃)** δ 165.3, 149.8, 139.9, 128.2, 123.9, 79.6, 71.4, 60.4, 43.4, 32.0, 22.7, 19.0, 14.0

# REFERENCES

# REFERENCES

1. Soltanzadeh, B.; Jaganathan, A.; Staples, R. J.; Borhan, B., Highly Stereoselective Intermolecular Haloetherification and Haloesterification of Allyl Amides. *Angew. Chem. Int. Ed. Engl.* **2015,** *54*, 9517-22.

2. Soltanzadeh, B.; Jaganathan, A.; Yi, Y.; Yi, H.; Staples, R. J.; Borhan, B., Highly Regio- and Enantioselective Vicinal Dihalogenation of Allyl Amides. *J. Am. Chem. Soc.* **2017,** *139*, 2132-2135.

3. Steigerwald, D. C.; Soltanzadeh, B.; Sarkar, A.; Morgenstern, C. C.; Staples, R. J.; Borhan, B., Ritter-enabled catalytic asymmetric chloroamidation of olefins. *Chemical Science* **2021,** *12*, 1834-1842.

4. Denmark, S. E.; Kuester, W. E.; Burk, M. T., Catalytic, Asymmetric Halofunctionalization of Alkenes-A Critical Perspective. *Angew Chem Int Edit* **2012,** *51*, 10938-10953.

5. Chan, Y. C.; Yeung, Y. Y., Halogen Bond Catalyzed Bromocarbocyclization. *Angew Chem Int Edit* **2018,** *57*, 3483-3487.

6. Cavallo, G.; Metrangolo, P.; Milani, R.; Pilati, T.; Priimagi, A.; Resnati, G.; Terraneo, G., The Halogen Bond. *Chem. Rev.* **2016,** *116*, 2478-2601.

7. Samanta, R. C.; Yamamoto, H., Catalytic Asymmetric Bromocyclization of Polyenes. *J. Am. Chem. Soc.* **2017,** *139*, 1460-1463.

8. Alix, A.; Lalli, C.; Retailleau, P.; Masson, G., Highly enantioselective electrophilic alpha-bromination of enecarbamates: chiral phosphoric acid and calcium phosphate salt catalysts. *J. Am. Chem. Soc.* **2012,** *134*, 10389-92.

9. Qi, J.; Fan, G. T.; Chen, J.; Sun, M. H.; Dong, Y. T.; Zhou, L., Catalytic enantioselective bromoamination of allylic alcohols. *Chem. Commun.* **2014,** *50*, 13841-13844.

10. Yousefi, R.; Sarkar, A.; Ashtekar, K. D.; Whitehead, D. C.; Kakeshpour, T.; Holmes, D.; Reed, P.; Jackson, J. E.; Borhan, B., Mechanistic Insights into the Origin of Stereoselectivity in an Asymmetric Chlorolactonization Catalyzed by (DHQD)(2)PHAL. *J. Am. Chem. Soc.* **2020,** *142*, 7179-7189.

11. Eyring, H., The activated complex in chemical reactions. *J. Chem. Phys.* **1935,** *3*, 107-115.

12. Ashtekar, K. D.; Vetticatt, M.; Yousefi, R.; Jackson, J. E.; Borhan, B., Nucleophile-Assisted Alkene Activation: Olefins Alone Are Often Incompetent. *J. Am. Chem. Soc.* **2016,** *138*, 8114-9.

13. Ashtekar, K. D.; Marzijarani, N. S.; Jaganathan, A.; Holmes, D.; Jackson, J. E.; Borhan, B., A new tool to guide halofunctionalization reactions: the halenium affinity (HalA) scale. *J. Am. Chem. Soc.* **2014,** *136*, 13355-62.

14. Willoughby, P. H.; Niu, D. W.; Wang, T.; Haj, M. K.; Cramer, C. J.; Hoye, T. R., Mechanism of the Reactions of Alcohols with o-Benzynes. *J. Am. Chem. Soc.* **2014,** *136*, 13657-13665.

15. Brown, R. S., Investigation of the early steps in electrophilic bromination through the study of the reaction with sterically encumbered olefins. *Acc. Chem. Res.* **1997,** *30*, 131-137.

16. Cheng, Y. A.; Yu, W. Z.; Yeung, Y. Y., Recent advances in asymmetric intra- and intermolecular halofunctionalizations of alkenes. *Org. Biomol. Chem.* **2014,** *12*, 2333-2343.

17. Chen, J.; Zhou, L., Recent Progress in the Asymmetric Intermolecular Halogenation of Alkenes. *Synthesis-Stuttgart* **2014,** *46*, 586-595.

18. Rombola, M.; Sumaria, C. S.; Montgomery, T. D.; Rawal, V. H., Development of Chiral, Bifunctional Thiosquaramides: Enantioselective Michael Additions of Barbituric Acids to Nitroalkenes. *J. Am. Chem. Soc.* **2017,** *139*, 5297-5300.

19. Banik, S. M.; Levina, A.; Hyde, A. M.; Jacobsen, E. N., Lewis acid enhancement by hydrogen-bond donors for asymmetric catalysis. *Science* **2017,** *358*, 761-764.

20. Marzijarani, N. S.; Yousefi, R.; Jaganathan, A.; Ashtekar, K. D.; Jackson, J. E.; Borhan, B., Absolute and relative facial selectivities in organocatalytic asymmetric chlorocyclization reactions. *Chemical Science* **2018,** *9*, 2898-2908.

21. Yousefi, R.; Ashtekar, K. D.; Whitehead, D. C.; Jackson, J. E.; Borhan, B., Dissecting the Stereocontrol Elements of a Catalytic Asymmetric Chlorolactonization: Syn Addition Obviates Bridging Chloronium. *J. Am. Chem. Soc.* **2013,** *135*, 14524-14527.

22. Qi, C. X.; Force, G.; Gandon, V.; Leboeuf, D., Hexafluoroisopropanol-Promoted Haloamidation and Halolactonization of Unactivated Alkenes. *Angew Chem Int Edit* **2021,** *60*, 946-953.